



HAL
open science

Contribution to ellipsoidal and zonotopic set-membership state estimation

Dory Merhy

► **To cite this version:**

Dory Merhy. Contribution to ellipsoidal and zonotopic set-membership state estimation. Automatic Control Engineering. Université Paris Saclay (COMUE), 2019. English. NNT : 2019SACLS362 . tel-02402347

HAL Id: tel-02402347

<https://theses.hal.science/tel-02402347>

Submitted on 10 Dec 2019

HAL is a multi-disciplinary open access archive for the deposit and dissemination of scientific research documents, whether they are published or not. The documents may come from teaching and research institutions in France or abroad, or from public or private research centers.

L'archive ouverte pluridisciplinaire **HAL**, est destinée au dépôt et à la diffusion de documents scientifiques de niveau recherche, publiés ou non, émanant des établissements d'enseignement et de recherche français ou étrangers, des laboratoires publics ou privés.



Contribution à l'estimation d'état par méthodes ensemblistes ellipsoïdales et zonotopiques

Thèse de doctorat de l'Université Paris-Saclay préparée à :

Université Paris-Sud

CentraleSupélec

École doctorale n° 580

Sciences et technologies de l'information et de la communication (STIC)

Spécialité de doctorat : Automatique

Thèse présentée et soutenue à Gif-sur-Yvette, le 24 octobre 2019 par :

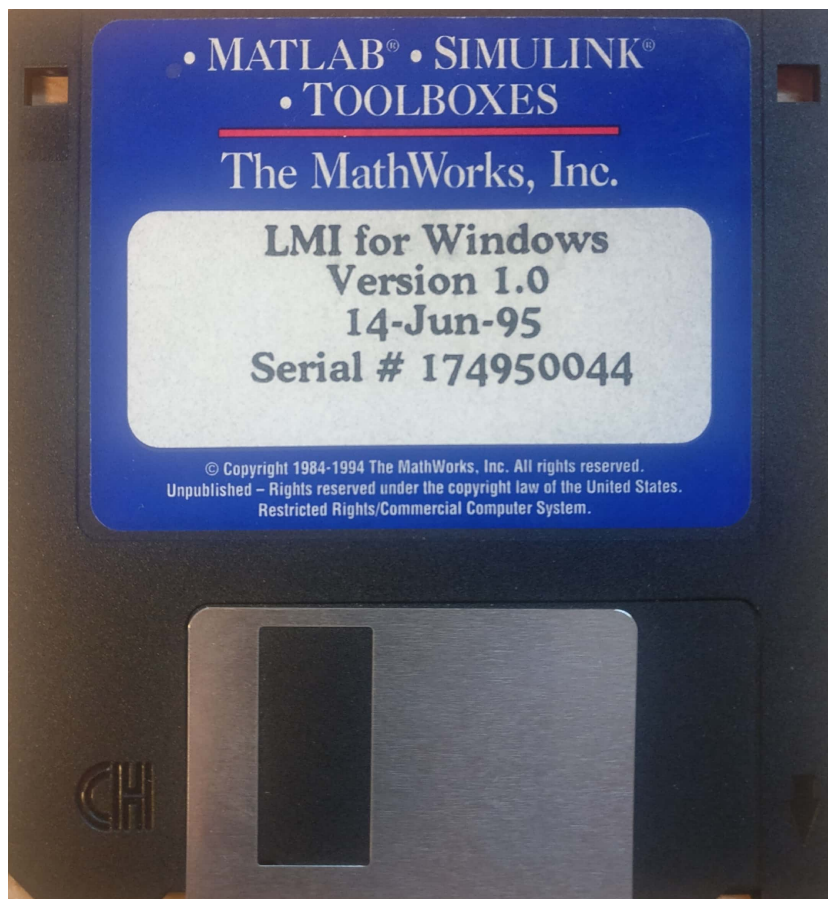
Dory Merhy

Composition du Jury :

| | |
|--|--------------------|
| Antoine Girard Directeur de recherche, L2S-CNRS | Président |
| José Manuel Bravo Caro Professeur, Université de Huelva, Espagne | Rapporteur |
| Nacim Ramdani Professeur, Université d'Orléans | Rapporteur |
| Dan Selişteanu Professeur, Université de Craiova, Roumanie | Rapporteur |
| Christophe Combastel Maître de Conférences, Université de Bordeaux 1 | Examineur |
| Cristina Stoica Maniu Professeur, CentraleSupélec/L2S | Directeur de thèse |
| Eduardo F. Camacho Professeur, Université de Séville, Espagne | Co-encadrant |
| Teodoro Alamo Professeur, Université de Séville, Espagne | Co-encadrant |

Sanity is not statistical

GEORGES ORWELL (1984)



Acknowledgments

It is thrilling to look back at my doctoral journey knowing that a chapter of my life has now come to an end; and since nothing worth having comes easy, I would like to take the time to acknowledge all of those who were there for me during this phase of personal growth.

I would like to start by thanking my PhD advisor Cristina Stoica Maniu for believing in me and trusting me. Her perfectionism and rigor taught me to strive for excellence in everything I do and this is indeed a life-lesson I'll always embrace. I feel privileged to be associated with her and words fail to express my deepest esteem to her.

It was a great honor to have prominent researchers like Teodoro Alamo and Eduardo F. Camacho as co-advisors for my thesis. I thank Teo for all the support and encouragement he gave me during my research visit to Universidad de Sevilla in Spain. His guidance and advice led to fruitful discussions on state estimation and convex optimization. With him, I learned how to transform a scientific idea into a well-conceived theorem. My appreciation equally goes to Eduardo who constantly gave me invaluable ideas and suggestions to improve my work. Thanks to them, I understood that humbleness is at the core of remarkable achievements in all circumstances.

I would also like extend my appreciation to my thesis committee members for all their propositions and feedback that have been invaluable. Their indispensable remarks, suggestions and challenging questions have contributed immensely in improving the quality of the final version of this manuscript.

I extend a word of thankfulness to all members of the department of Automatic Control at L2S. It was an extremely enriching experience to be around outstanding researchers and persons. I am also grateful to Israel Hinostroza from SONDRALaboratory for the fruitful collaboration and for all his beautiful explanations about the world of radar. I must also thank Sorin Olaru for the great opportunity he gave me to be part of the PHC SIAM project and to embark on a very exotic yet educational trip to Chulalongkorn University in Bangkok, Thailand. I also take this opportunity to thank Prof. Soorathep Kheawhom for the immense support during my sojourn there, and

Prof. Vladimir Polotski from ETS Montreal for his great interest in my work and his constructive feedback during IFAC.

The time I spent in L2S would not have been as pleasant without the company of my colleagues and friends. Special thanks go to Gauthier Rousseau and Fetra Rasoanarivo with whom I shared the office, great craziness and abundant laughs. I offer my heartiest recognition to Thomas Chevet for providing invaluable assistance to surmount all the LaTeX predicaments while writing this manuscript. I equally appreciate all our research collaborations and technical exchanges.

I am not only indebted to colleagues at work but also to many friends outside my academic circle. Their tremendous support and encouragement were an essential source of motivation and strength. As such, I am tremendously thankful to my close friends who bore my stressful days and panic attacks each in his and her own way and took the time to share the joy of the ceremony with me. On that account, my deepest gratitude goes to Elie Alsebaaly, Nadia Mouawad, Joseph Abdelnour, Tarek Chaiban, Elsa Abboud, Mark Baydoun, Nassif Bechara, Hadi Zaatiti, Ghida El Achkar, Chadi Boustani, Dona Kfoury, Ralph Doumit, Hiba Obeid, Dima Chammas, Maha Chebaro, Hanane Fadiaw, Joe Farjallah, Elmar Slikboer, Elias Thoumi and to all the others who made sure to send their greetings and to express their support and affection. Moreover, I must thank my childhood best friend Henry Jreij who flew all the way from the United States to share these rewarding moments with me. Obviously, I am extremely grateful to Elias Ghattas for all the support and to Tonya Houeiss for helping me with the presentation graphics.

I must also thank my cousin and friend Elias Merhy, his dear wife Maria and their cutest son, my beloved Maxime for all the assistance and encouragement they have consistently provided me in the past three years. They have been my family and my support system in France. I feel so lucky for having such amazing people in my life.

Last but foremost, none of my achievements would have seen the light had it not been for the support of my family. My mother's love and prayers accompanied me throughout my doctoral journey. My recognition extends to my father Farid, sisters Dalia and Dolly (and her husband) for all the affection. A special appreciation goes to my brother and idol Dany who has always placed my best interest above his, sacrificing some of his dreams only to see me fulfill mine. I extend my gratitude to my sister-in-law Layal for all her help and support.

Finally, I dedicate this thesis to my nephew Daniel-Farid and my niece Rita.

Contents

| | |
|---|-------------|
| List of Figures | viii |
| List of Tables | x |
| List of Symbols | xiv |
| List of Acronyms | xv |
| 1 Résumé en français | 1 |
| 1.1 Introduction | 2 |
| 1.2 Chapitre 3 : Outils pour l'estimation d'état ensembliste | 5 |
| 1.2.1 Définitions et propriétés | 5 |
| 1.2.2 Ensembles convexes pour l'estimation d'état | 6 |
| 1.2.2.1 ellipsoïdes | 6 |
| 1.2.2.2 Zonotopes | 7 |
| 1.2.3 Optimisation convexe | 7 |
| 1.3 Chapitre 4 : Estimation d'état ellipsoïdale pour les systèmes linéaires | 8 |
| 1.3.1 Formulation du problème d'estimation | 8 |
| 1.3.2 Technique d'estimation d'état fondée sur des ellipsoïdes | 10 |
| 1.3.3 Comparaison entre deux techniques d'estimation d'état pour les systèmes LTI | 11 |
| 1.3.4 Application à un modèle d'octorotor | 12 |
| 1.3.4.1 Modèle d'octorotor | 12 |
| 1.4 Chapitre 5 : Estimation d'état ellipsoïdale pour des systèmes descripteurs | 14 |
| 1.4.1 Formulation de problème | 14 |
| 1.4.2 Systèmes descripteurs linéaires invariants dans le temps | 15 |
| 1.4.2.1 <i>Méthode 1</i> | 15 |
| 1.4.2.2 <i>Méthode 2</i> | 16 |
| 1.4.2.3 <i>Méthode 3</i> | 16 |

| | | |
|----------|--|-----------|
| 1.4.3 | Systèmes descripteurs linéaires variant dans le temps . . . | 16 |
| 1.4.3.1 | <i>Méthode 4</i> | 17 |
| 1.4.3.2 | <i>Méthode 5</i> | 17 |
| 1.5 | Chapitre 6 : Estimation d'état zonotopique | 18 |
| 1.5.1 | Méthode d'estimation d'état zonotopique fondée sur un observateur de Luenberger | 18 |
| 1.5.2 | Estimation d'état à base de zonotopes pour les sys- tèmes affines par morceaux | 19 |
| 1.6 | Chapitre 7 : Filtre de Kalman à contraintes zonotopiques . . . | 20 |
| 1.6.1 | Filtre de Kalman zonotopique à contraintes zonotopiques (ZCKF) | 21 |
| 1.6.1.1 | Travail préliminaire | 21 |
| 1.6.1.2 | Solution algorithmique | 22 |
| 1.6.1.3 | Détails de calcul | 23 |
| 1.6.2 | Algorithme ISTA | 23 |
| 1.6.3 | FISTA | 24 |
| 1.6.4 | Extension du filtre de Kalman à contraintes zonotopiques (EZCKF) | 24 |
| 1.7 | Chapitre 8 : Conclusion et perspectives | 26 |
| 2 | Introduction | 29 |
| 2.1 | Context and motivations | 29 |
| 2.2 | Contribution | 32 |
| 2.3 | Publications | 37 |
| 3 | Mathematical tools for set-membership state estimation | 39 |
| 3.1 | Introduction | 39 |
| 3.2 | Matrices: definitions and properties | 41 |
| 3.3 | Set-theory preliminaries | 44 |
| 3.3.1 | Interval set | 46 |
| 3.3.2 | Ellipsoidal set | 48 |
| 3.3.3 | Polyhedral set | 50 |
| 3.3.4 | Zonotopic set | 53 |
| 3.4 | Convex optimization | 57 |
| 3.4.1 | Duality principle in convex optimization | 59 |
| 3.4.2 | Gradient-based methods for solving convex optimiza- tion problems | 60 |
| 3.5 | Conclusion | 61 |

| | | |
|-----------|--|------------|
| I | Ellipsoidal set-membership state estimation | 63 |
| 4 | Ellipsoidal state estimation for linear systems | 65 |
| 4.1 | Introduction | 65 |
| 4.2 | Overview of the classical Kalman filter | 67 |
| 4.3 | Problem formulation | 68 |
| 4.4 | Ellipsoidal state estimation technique | 70 |
| 4.5 | Comparison between two state estimation techniques for linear time-invariant systems | 74 |
| 4.6 | Application to an octorotor model | 77 |
| 4.6.1 | Octorotor modeling | 78 |
| 4.6.2 | Application to the design of SAR | 82 |
| 4.6.3 | Simulation results | 85 |
| 4.6.3.1 | Case 1: Circular trajectory | 87 |
| 4.6.3.2 | Case 2: Linear trajectory for a SAR application | 90 |
| 4.7 | Conclusion | 93 |
| 5 | Ellipsoidal state estimation for descriptor systems | 95 |
| 5.1 | Introduction | 96 |
| 5.2 | Overview of descriptor systems | 98 |
| 5.2.1 | Practical examples | 98 |
| 5.2.2 | Basic properties of descriptor systems | 99 |
| 5.3 | Problem formulation | 100 |
| 5.4 | Ellipsoidal state estimation technique for LTI descriptor systems | 102 |
| 5.4.1 | <i>Method 1</i> : Off-line state estimation approach with a constant observer gain | 102 |
| 5.4.2 | <i>Method 2</i> : Online ellipsoidal state estimation approach | 106 |
| 5.4.3 | <i>Method 3</i> : Online ellipsoidal state estimation approach with vector scaling technique | 107 |
| 5.5 | Ellipsoidal state estimation for LTV descriptor systems | 113 |
| 5.5.1 | Problem formulation | 113 |
| 5.5.2 | <i>Method 4</i> : Online flexible shape ellipsoidal state esti- mation approach | 114 |
| 5.5.3 | <i>Method 5</i> : Online flexible shape ellipsoidal state esti- mation approach with vector scaling technique | 117 |
| 5.6 | Conclusion | 121 |
| II | Zonotopic set-membership state estimation | 123 |
| 6 | Zonotopic set-membership state estimation | 125 |

| | | |
|----------|---|------------|
| 6.1 | Introduction | 125 |
| 6.2 | Zonotopic state estimation | 126 |
| 6.3 | Zonotopic set-membership estimation technique based on a Luenberger observer | 128 |
| 6.4 | Overview of piecewise affine systems | 133 |
| 6.4.1 | Practical example | 133 |
| 6.4.2 | State estimation for PWA systems | 134 |
| 6.5 | Zonotopic state estimation for PWA systems | 136 |
| 6.6 | Conclusion | 140 |
| 7 | Zonotopic constrained Kalman filter | 143 |
| 7.1 | Introduction | 143 |
| 7.2 | Constrained Kalman filter | 145 |
| 7.3 | Zonotopic Constrained Kalman Filter (ZCKF) | 147 |
| 7.3.1 | Preliminary work | 147 |
| 7.3.2 | Algorithmic solution for ZCKF | 149 |
| 7.3.3 | Computation details | 150 |
| 7.3.3.1 | Expression for $\mathbf{z}(\boldsymbol{\alpha}_j)$ | 150 |
| 7.3.3.2 | Expression for $\mathbf{w}(\boldsymbol{\alpha}_j)$ | 151 |
| 7.3.3.3 | Expression for $\Delta\boldsymbol{\alpha}_j$ | 151 |
| 7.3.4 | Iterative Shrinkage Thresholding Algorithm (ISTA) | 152 |
| 7.3.5 | Fast Iterative Shrinkage Thresholding Algorithm (FISTA) | 153 |
| 7.4 | Extended Zonotopic Constrained Kalman Filter (EZCKF) | 158 |
| 7.5 | Conclusion | 163 |
| 8 | Conclusion and perspectives | 165 |
| 8.1 | Conclusion | 165 |
| 8.2 | Future directions | 167 |

List of Figures

| | | |
|------|---|----|
| 1.1 | Différentes approches d'estimation d'état | 3 |
| 1.2 | Illustration de la méthode d'estimation d'état ensembliste . . . | 9 |
| 1.3 | Partitions de l'espace d'état | 20 |
| 2.1 | State estimation approaches | 31 |
| 2.2 | Roadmap for the thesis | 36 |
| 3.1 | Illustration of the definition of a convex function | 45 |
| 3.2 | Illustration of the convex hull of a convex set \mathcal{X} | 46 |
| 3.3 | Ellipsoidal set $\mathcal{E}(\mathbf{P}, \bar{\mathbf{x}})$ | 49 |
| 3.4 | Half-space representation of a polytope | 51 |
| 3.5 | Vertex representation of a polytope | 52 |
| 3.6 | Third order zonotope in a two-dimensional space | 54 |
| 3.7 | Ellipsoid related to the \mathbf{P} -radius of a zonotope | 56 |
| 4.1 | Illustration of the ellipsoidal state estimation method | 70 |
| 4.2 | Example 4.1: bounds of x_1 | 76 |
| 4.3 | Example 4.1: bounds of x_2 | 76 |
| 4.4 | Mikrokopter ARF representation and the associated drone's frame R | 78 |
| 4.5 | Representation of the drone and the scatterer | 83 |
| 4.6 | SAR image obtained in the ideal case allowing to correctly identify the scatterer position | 84 |
| 4.7 | SAR image obtained with an erroneous estimated position . . . | 84 |
| 4.8 | Estimation bounds of the altitude z | 86 |
| 4.9 | Drone's velocity on the z -axis | 86 |
| 4.10 | Circular reference trajectory | 88 |
| 4.11 | Circular trajectory: estimation bounds of the linear position x | 88 |
| 4.12 | Circular trajectory: drone's velocity on the x -axis | 89 |
| 4.13 | Circular trajectory: estimation bounds of the linear position y | 89 |
| 4.14 | Circular trajectory: drone's velocity on the y -axis | 90 |

| | | |
|------|---|-----|
| 4.15 | Linear proposed trajectory | 90 |
| 4.16 | Linear trajectory: estimation bounds of the linear position x . | 91 |
| 4.17 | Linear trajectory: drone's velocity on the x-axis | 92 |
| 4.18 | Linear trajectory: estimation bounds of the linear position y . | 92 |
| 4.19 | Distance errors | 93 |
| 5.1 | Electrical circuit | 98 |
| 5.2 | An overview of the five methods developed in this chapter . . | 102 |
| 5.3 | Example 5.1: bounds of x_1 | 111 |
| 5.4 | Example 5.1: bounds of x_2 | 111 |
| 5.5 | Example 5.1: bounds of x_3 | 112 |
| 5.6 | Example 5.2: bounds of x_1 | 119 |
| 5.7 | Example 5.2: bounds of x_2 | 120 |
| 5.8 | Example 5.2: bounds of x_3 | 120 |
| 6.1 | Linear proposed trajectory | 131 |
| 6.2 | Example 6.1: bounds of the linear position x | 132 |
| 6.3 | Example 6.1: bounds of the altitude z | 132 |
| 6.4 | Two-tank system | 134 |
| 6.5 | Partitions of the state-space | 137 |
| 6.6 | Example 6.2: bounds of x_1 | 139 |
| 6.7 | Example 6.2: bounds of x_2 | 140 |
| 7.1 | Illustration of the proposed zonotopic constrained algorithm . | 155 |
| 7.2 | Comparison of estimation errors obtained with ISTA and FISTA | 156 |
| 7.3 | Classical Kalman filter versus zonotopic constrained Kalman filter | 157 |
| 7.4 | Original setup | 162 |
| 7.5 | Example 7.4: first zonotope | 162 |
| 7.6 | Example 7.4: second zonotope | 163 |

List of Tables

| | | |
|-----|--|-----|
| 4.1 | SAR parameters | 83 |
| 4.2 | Drone parameters | 85 |
| 4.3 | SAR parameters considered for the linear trajectory | 92 |
| 5.1 | Example 5.1: total computation time | 112 |
| 5.2 | Example 5.1: volume of ellipsoidal sets at steady state | 113 |
| 7.1 | Computation time of the considered algorithms with large-scale zonotopes | 158 |

LIST OF TABLES

List of Symbols

Algebra

| | |
|--|---|
| $\text{conv}(\cdot)$ | Convex hull |
| \oplus | Minkowski sum |
| $\binom{n}{m}$ | n combination of m elements |
| $n!$ | Factorial of n |
| $\ \cdot\ _\infty$ | Infinity norm |
| $\ \cdot\ _1$ | 1-norm |
| $\ \cdot\ _{\mathbf{P}}$ | \mathbf{P} -norm |
| \triangleq | Equal by definition |
| $r \sim N(0, Q)$ | Random variable r having zero means, normal distribution |
| $\langle \mathbf{x}, \mathbf{y} \rangle$ | Dot product of the vectors \mathbf{x} and \mathbf{y} |
| $ \cdot $ | Absolute value |
| ∇f | Gradient of the function f |
| $\nabla^2 f$ | Hessian of the function f |
| $i = 1, \dots, n$ | Variable $i \in \mathbb{N}$ ranging from 1 to n |
| $\text{randn}(n, m)$ | n by m matrix of normally distributed random numbers |
| $\frac{1}{m}\text{randn}(n, m)$ | Normalized n by m matrix of normally distributed random numbers |

Matrices, vectors, scalars

| | |
|--------------------|--|
| \mathbf{A} | General notation for a matrix |
| \mathbf{a} | General notation for a vector |
| a | General notation for a scalar |
| $\mathbf{0}_{n,m}$ | Zeros matrix of dimensions $n \times m$ |
| $\mathbf{0}_n$ | Zeros matrix in $\mathbb{R}^{n \times n}$ |
| $\mathbf{I}_{n,m}$ | Identity matrix of dimensions $n \times m$ |
| \mathbf{I}_n | Identity matrix in $\mathbb{R}^{n \times n}$ |

| | |
|-----------------------------------|--|
| $\mathbb{1}_{n,m}$ | Matrix of dimensions $n \times m$ having all elements equal to 1 |
| $[\mathbf{A}]$ | General notation for an interval matrix |
| $mid[\mathbf{A}]$ | Center of the interval matrix \mathbf{A} |
| $rad[\mathbf{A}]$ | Radius of the interval matrix \mathbf{A} |
| $\mathcal{V}_{[\mathbf{A}]}$ | Vertices of the interval matrix \mathbf{A} |
| $diag(\sigma_1, \dots, \sigma_n)$ | Diagonal matrix of dimension n |
| * | Term required for the matrix symmetry |
| \mathbf{A}^\top | Transpose of matrix \mathbf{A} |
| \mathbf{A}^{-1} | Inverse of matrix \mathbf{A} |
| $det(\mathbf{A})$ | Determinant of matrix \mathbf{A} |
| $Tr(\mathbf{A})$ | Trace of matrix \mathbf{A} |
| $Im(\mathbf{A})$ | Image of matrix \mathbf{A} |
| $\mathbf{A} \succ 0$ | General notation for strictly positive definite matrix \mathbf{A} |
| $\mathbf{A} \succeq 0$ | General notation for positive definite matrix \mathbf{A} |
| $\mathbf{A} \prec 0$ | General notation for strictly negative definite matrix \mathbf{A} |
| $\mathbf{A} \preceq 0$ | General notation for negative definite matrix \mathbf{A} |
| $\mathcal{R}(\mathbf{A})$ | Range of the matrix \mathbf{A} |
| $\mathcal{N}(\mathbf{A})$ | Kernel of the matrix \mathbf{A} |
| $\hat{\mathbf{x}}_{k k-1}$ | Predicted state at time instant k knowing the state estimate at time instant $k - 1$ |

Sets

| | |
|---|--|
| \mathbb{R} | Set of real numbers |
| \mathbb{R}_+ | Set of positive real numbers |
| \mathbb{R}_+^* | Set of strictly positive real numbers |
| \mathbb{R}^n | Set of n -dimensional real vector |
| \mathbb{N}^* | Set of non-zero natural numbers |
| \mathbb{B}^n | Unitary box in \mathbb{R}^n |
| \mathcal{X} | General notation for a set |
| $Vol(\mathcal{X})$ | Volume of the set \mathcal{X} |
| $\mathcal{V}_{\mathcal{X}}$ | Vertices of the set \mathcal{X} |
| $\mathcal{Z} = \mathcal{Z}(\mathbf{p}; \mathbf{H}) = \mathbf{p} \oplus \mathbf{H}\mathbb{B}^m$ | General notation of a m -zonotope |
| $rs(\mathbf{H})$ | Round-sum of matrix \mathbf{H} |
| $box(\mathcal{Z})$ | Approximation of the zonotope \mathcal{Z} by a box |
| $\mathcal{E}(\mathbf{P}, \bar{\mathbf{x}}, \rho), \mathcal{E}(\mathbf{P}^{-1}, \bar{\mathbf{x}}, \rho)$ | General notation of an ellipsoid |
| $\mathcal{E}(\mathbf{P}, \bar{\mathbf{x}})$ | General notation of a normalized ellipsoid |
| $M(\mathcal{S})$ | Image of a set \mathcal{S} |

List of Acronyms

| | |
|-------|--|
| BMI | Bilinear Matrix Inequality |
| DAE | Differential Algebraic Equations |
| EZCKF | Extended Zonotopic Constrained Kalman Filter |
| LMI | Linear Matrix Inequality |
| LQI | Linear Quadratic Integral |
| LTI | Linear Time Invariant |
| LTV | Linear Time Variant |
| MHE | Moving Horizon Estimation |
| MPT | Multi Parametric Toolbox |
| PRF | Pulse Repetition Frequency |
| PWA | Piecewise Affine |
| OBE | Outer Bounding Ellipsoid |
| QP | Quadratic Programming |
| SAR | Synthetic Aperture Radar |
| SVD | Singular Value Decomposition |
| UAV | Unmanned Aerial Vehicle |
| ZCKF | Zonotopic Constrained Kalman Filter |
| ZGKF | Zonotopic Gaussian Kalman Filter |

Chapter 1

Résumé en français

Contents

| | | |
|------------|---|-----------|
| 1.1 | Introduction | 2 |
| 1.2 | Chapitre 3 : Outils pour l'estimation d'état ensembliste | 5 |
| 1.2.1 | Définitions et propriétés | 5 |
| 1.2.2 | Ensembles convexes pour l'estimation d'état | 6 |
| 1.2.3 | Optimisation convexe | 7 |
| 1.3 | Chapitre 4 : Estimation d'état ellipsoïdale pour les systèmes linéaires | 8 |
| 1.3.1 | Formulation du problème d'estimation | 8 |
| 1.3.2 | Technique d'estimation d'état fondée sur des ellipsoïdes | 10 |
| 1.3.3 | Comparaison entre deux techniques d'estimation d'état pour les systèmes LTI | 11 |
| 1.3.4 | Application à un modèle d'otorotor | 12 |
| 1.4 | Chapitre 5 : Estimation d'état ellipsoïdale pour des systèmes descripteurs | 14 |
| 1.4.1 | Formulation de problème | 14 |
| 1.4.2 | Systèmes descripteurs linéaires invariants dans le temps | 15 |
| 1.4.3 | Systèmes descripteurs linéaires variant dans le temps | 16 |
| 1.5 | Chapitre 6 : Estimation d'état zonotopique | 18 |
| 1.5.1 | Méthode d'estimation d'état zonotopique fondée sur un observateur de Luenberger | 18 |

| | | |
|------------|--|-----------|
| 1.5.2 | Estimation d'état à base de zonotopes pour les systèmes affines par morceaux | 19 |
| 1.6 | Chapitre 7 : Filtre de Kalman à contraintes zonotopiques | 20 |
| 1.6.1 | Filtre de Kalman zonotopique à contraintes zonotopiques (ZCKF) | 21 |
| 1.6.2 | Algorithme ISTA | 23 |
| 1.6.3 | FISTA | 24 |
| 1.6.4 | Extension du filtre de Kalman à contraintes zonotopiques (EZCKF) | 24 |
| 1.7 | Chapitre 8 : Conclusion et perspectives | 26 |

1.1 Introduction

Le progrès scientifique a pour but d'améliorer notre quotidien et nos conditions de vie en répondant aux besoins actuels. Du *mobile multifonction* au véhicule autonome en passant par l'intelligence artificielle, la détection des défauts, de même que la commande tolérante aux défauts des systèmes dynamiques, sont devenus des problèmes dont la résolution constitue des défis à relever par les chercheurs en Automatique.

En effet, les défauts doivent être pris en compte pour que le système puisse fonctionner de façon acceptable dans le but d'éviter son arrêt ou des conséquences potentiellement catastrophiques sur son état. Ceci est possible en considérant, par exemple, la commande par retour d'état qui, par définition, compare une valeur mesurée de l'état (s'il est connu) avec une valeur désirée pour changer l'entrée du système en conséquence. Si l'état n'est pas connu, il doit être *estimé*. C'est pour cette raison que l'estimation d'état est une étape primordiale avant l'élaboration d'une loi de commande.

Les variables d'état sont des grandeurs ayant une signification physique et qui peuvent entièrement décrire la dynamique du système. Ainsi, le *but* de cette thèse est de se concentrer sur les avancements dans le domaine de l'estimation d'état en Automatique.

L'estimation d'état n'est pas une discipline récente. Durant des siècles, les marins devaient par exemple estimer la position de leurs navires. Pour ce faire, des outils ont été progressivement inventés afin de mesurer la position, l'orientation, la latitude et la longitude des navires. Toutefois, ce n'est qu'au 19e siècle que Gauss introduit une nouvelle classe de techniques d'estimation d'état (approche stochastique) fondée sur l'hypothèse que les erreurs ont une

distribution statistique connue. Un siècle après, le filtre de Kalman classique est introduit pour des systèmes linéaires invariants dans le temps soumis à des perturbations et des bruits de mesure ayant une distribution gaussienne. Aussitôt, le filtre de Kalman devient la technique d'estimation la plus utilisée dans les mondes académique et industriel.

Alternativement, les approches déterministes considèrent des hypothèses plus réalistes : des perturbations et bruits de mesure inconnus mais bornés. Dans cette thèse, nous nous intéressons plus à ces approches d'estimation d'état ensembliste où l'état appartient à un ensemble géométrique tel qu'un polytope, les ellipsoïde, zonotope etc. La Figure 1.1 résume les différentes approches d'estimation d'état.

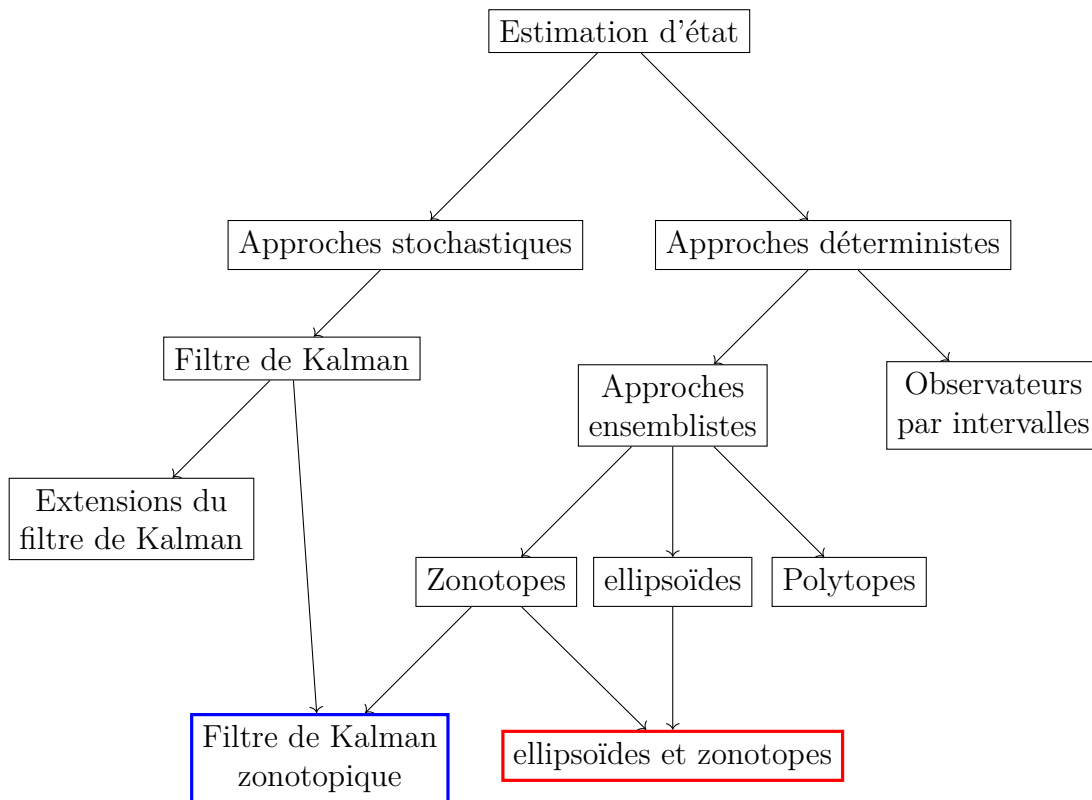


Figure 1.1 – Différentes approches d'estimation d'état

Dans cet esprit, les contributions de cette thèse se divisent en deux grandes parties :

- La première partie a comme point de départ une technique d'estimation d'état à base d'ellipsoïdes qui existe dans la littérature. Cette approche est appliquée à un modèle d'otorotor utilisé dans un contexte

d'imagerie radar. Ensuite, cette approche est étendue au cas des systèmes descripteurs.

- La deuxième partie propose une technique d'estimation d'état fondée sur la minimisation du \mathbf{P} -rayon d'un zonotope, appliquée au même modèle d'ocrotor. Cette technique est étendue par la suite pour traiter un cas particulier des systèmes affines par morceaux. Reprenant les techniques précédemment développées, un nouveau filtre de Kalman sous contraintes zonotopiques est ensuite proposé.

Cette thèse est structurée comme suit. Le Chapitre 2 introduit le contexte, les motivations, les contributions et les publications issues des résultats obtenus pendant cette thèse. Le Chapitre 3 présente les outils mathématiques nécessaires à la formulation des théorèmes présents dans ce mémoire, ainsi que la représentation des incertitudes dans le contexte des systèmes linéaires. Dans le Chapitre 4, une technique d'estimation d'état ellipsoïdale est étendue pour prendre en considération les entrées de commande, puis comparée au filtre de Kalman classique en termes de complexité et précision. La précision apportée par cette technique est utilisée pour estimer des bornes garanties pour la position d'un octorotor utilisé dans un contexte radar. Le Chapitre 5 propose cinq techniques ellipsoïdales pour des systèmes descripteurs linéaires. Les trois premières méthodes consistent à minimiser le "rayon" de l'ellipsoïde contenant l'état estimé pour des systèmes descripteurs linéaires invariants dans le temps, tandis que les méthodes 4 et 5 se concentrent sur les systèmes descripteurs linéaires variants dans le temps. Le Chapitre 6 porte sur l'estimation ensembliste fondée sur des zonotopes. Ce chapitre commence avec une technique d'estimation zonotopique fondée sur la minimisation du \mathbf{P} -rayon appliquée à un modèle d'ocrotor, puis étend cette méthode pour traiter le cas des systèmes affines par morceaux. Dans la continuité des approches précédentes, un nouveau filtre de Kalman sous contraintes zonotopiques (ZCKF) est proposé dans le Chapitre 7. En utilisant la forme duale d'un problème d'optimisation, l'algorithme ZCKF projette l'état sur l'ensemble des contraintes (auxquelles l'état est soumis) formant un zonotope. La complexité de l'algorithme est ensuite améliorée en réduisant le nombre de générateurs du zonotope initial.

Dans ce qui suit, le résumé de chaque chapitre est proposé.

1.2 Chapitre 3 : Outils pour l'estimation d'état ensembliste

Les systèmes dynamiques sont généralement représentés par un ensemble d'équations décrivant l'évolution du système. Cette représentation est utilisée pour la modélisation et l'élaboration des lois de commande en Automatique.

Dans cette thèse, nous considérons des systèmes standards, linéaires, variants ou invariants dans le temps, soumis à des perturbations, des bruits de mesure et des incertitudes inconnus, mais bornés. Toutefois, ces systèmes standards ne sont pas toujours suffisants pour donner une description complète du système à cause des simplifications considérées qui peuvent influencer la validité des modèles mathématiques ou négliger la signification physique du système. Les systèmes descripteurs, eux, combinent des équations différentielles et algébriques pour prendre en considération, par exemple, les lois de conservations de la physique (masse, volume, énergie etc.). Une autre classe de systèmes qui est détaillée dans cette thèse est celle des systèmes affines par morceaux. Ce système partitionne l'espace d'état en régions selon des contraintes linéaires et associe à chaque région une représentation linéaire du système.

En général, le modèle mathématique ne reprend pas exactement le comportement du système. Ainsi, nous considérons des incertitudes sur le système, des perturbations et des bruits de mesure. Deux approches existent dans la littérature pour modéliser les incertitudes :

- **Approche stochastique** : Les perturbations et les bruits de mesure ont une distribution stochastique (moyenne, covariance, etc.) supposée connue.
- **Approche déterministe** : Les perturbations et les bruits de mesure sont supposés inconnus, mais bornés par des ensembles convexes (ellipsoïdes, polytopes, zonotopes, intervalles etc.).

Ce chapitre présente des définitions et des propriétés nécessaires pour la compréhension des résultats proposés dans cette thèse et résume certains ensembles utilisés dans la littérature pour représenter les incertitudes.

1.2.1 Définitions et propriétés

Dans cette section, nous rappelons les définitions et les propriétés les plus importantes utilisées dans le Chapitre 3.

Définition 1.1. Une Inégalité Matricielle Linéaire (LMI) s'écrit sous la forme :

$$\mathbf{F}(\mathbf{x}) \triangleq \mathbf{F}_0 + \sum_{i=1}^n x_i \mathbf{F}_i \succ 0, \quad (1.1)$$

avec les matrices $\mathbf{F}_i = \mathbf{F}_i^\top \in \mathbb{R}^{m \times m}$, $i = 0, \dots, n$, et le vecteur de variables de décision $\mathbf{x} = [x_1 \ x_2 \ \dots \ x_n]^\top \in \mathbb{R}^n$, ayant comme composantes $x_i \in \mathbb{R}$, $i = 1, \dots, n$, les variables scalaires de décision.

Définition 1.2. *Complément de Schur.* [Boyd et al., 1994], [Scherer and Weiland, 2007] Soit la LMI suivante :

$$\begin{bmatrix} \mathbf{Q}(\mathbf{x}) & \mathbf{S}(\mathbf{x}) \\ \mathbf{S}^\top(\mathbf{x}) & \mathbf{R}(\mathbf{x}) \end{bmatrix} \succ 0, \quad (1.2)$$

avec $\mathbf{Q}(\mathbf{x})$, $\mathbf{R}(\mathbf{x})$ des matrices symétriques et $\mathbf{Q}(\mathbf{x})$, $\mathbf{R}(\mathbf{x})$ et $\mathbf{S}(\mathbf{x})$ affines en \mathbf{x} . Cette LMI est équivalente à :

$$\begin{cases} \mathbf{Q}(\mathbf{x}) \succ 0, \\ \mathbf{Q}(\mathbf{x}) - \mathbf{S}(\mathbf{x})\mathbf{R}^{-1}(\mathbf{x})\mathbf{S}^\top(\mathbf{x}) \succ 0, \end{cases} \quad (1.3)$$

ou

$$\begin{cases} \mathbf{R}(\mathbf{x}) \succ 0, \\ \mathbf{R}(\mathbf{x}) - \mathbf{S}^\top(\mathbf{x})\mathbf{Q}^{-1}(\mathbf{x})\mathbf{S}(\mathbf{x}) \succ 0. \end{cases} \quad (1.4)$$

1.2.2 Ensembles convexes pour l'estimation d'état

Dans la suite, les principaux ensembles convexes utilisés dans le domaine de l'estimation d'état ensembliste sont présentés. En fonction de la complexité et de la précision, l'ensemble pour représenter l'état est choisi parmi différentes formes géométriques : intervalle, ellipsoïde, polytope, paralléloptope ou zonotope. Les deux ensembles les plus utilisés dans cette thèse sont exposés dans la suite.

1.2.2.1 ellipsoïdes

De par leur simplicité, les ellipsoïdes sont largement utilisés dans plusieurs domaines de l'Automatique : l'identification, le diagnostic et surtout l'estimation ensembliste.

Définition 1.3. *ellipsoïde.* Soit une matrice strictement définie positive $\mathbf{P} = \mathbf{P}^\top \succ 0$, un vecteur réel $\bar{\mathbf{x}} \in \mathbb{R}^n$ et un scalaire strictement positif $\rho \in \mathbb{R}_+^*$. L'ellipsoïde $\mathcal{E}(\mathbf{P}, \bar{\mathbf{x}}, \rho)$ est défini par l'ensemble :

$$\mathcal{E}(\mathbf{P}, \bar{\mathbf{x}}, \rho) = \{\mathbf{x} \in \mathbb{R}^n : (\mathbf{x} - \bar{\mathbf{x}})^\top \mathbf{P}(\mathbf{x} - \bar{\mathbf{x}}) \leq \rho\}, \quad (1.5)$$

avec \mathbf{P} une matrice qui caractérise la taille et l'orientation de l'ellipsoïde, $\bar{\mathbf{x}}$ son centre et ρ son rayon.

1.2.2.2 Zonotopes

Grâce à la flexibilité et la simplicité de calcul qu'ils apportent, les zonotopes sont utilisés dans la deuxième partie de cette thèse. Le zonotope est un polytope symétrique et peut donc être représenté par des demi-espaces ou des sommets. De plus, il peut être représenté par ses générateurs ou par une transformation linéaire d'un hypercube. Cette dernière représentation est plus convenable dans le contexte de l'estimation d'état ensembliste et les approches proposées dans cette thèse. De ce fait, on la présente ici.

Définition 1.4. *Projection linéaire d'un hypercube.* Un zonotope d'ordre m dans \mathbb{R}^n ($m \geq n$) est la translation de centre $\mathbf{p} \in \mathbb{R}^n$ de l'image d'un hypercube unitaire de dimension m dans \mathbb{R}^n par une transformation linéaire. Soit une matrice $\mathbf{H} \in \mathbb{R}^{n \times m}$ représentant la transformation linéaire, le zonotope \mathcal{Z} est défini par :

$$\mathcal{Z} = (\mathbf{p}; \mathbf{H}) = \mathbf{p} \oplus \mathbf{H}\mathbb{B}^m. \quad (1.6)$$

Le \mathbf{P} -rayon d'un zonotope est défini comme suit :

Définition 1.5. Le \mathbf{P} -rayon d'un zonotope $\mathcal{Z} = \mathbf{p} \oplus \mathbf{H}\mathbb{B}^m$ peut s'écrire sous la forme :

$$r = \max_{\mathbf{z} \in \mathcal{Z}} (\|\mathbf{z} - \mathbf{p}\|_{\mathbf{P}}^2), \quad (1.7)$$

avec \mathbf{P} une matrice symétrique strictement définie positive $\mathbf{P} = \mathbf{P}^T \succ 0$.

Cette notation offre un critère pour évaluer la taille d'un zonotope, c'est-à-dire, pour une même valeur de la matrice \mathbf{P} , une valeur de \mathbf{P} -rayon élevée implique un zonotope de taille importante.

1.2.3 Optimisation convexe

Dans le contexte de l'estimation d'état, certaines informations sur l'état du système ne peuvent pas être intégrées directement dans le filtre de Kalman classique. Ces contraintes sont issues de la solution d'un problème d'optimisation convexe traité dans le Chapitre 7.

Dans cette thèse, nous considérons un problème d'optimisation de la forme :

$$\begin{aligned} \min_{\mathbf{u} \in \mathcal{U}, \mathbf{v} \in \mathbb{R}^m, \mathbf{s} \in \mathbb{R}^n} \quad & J_a(\mathbf{u}) + J_b(\mathbf{s}) + \frac{1}{2} \|\mathbf{u} - \mathbf{c}\|_{\mathbf{D}}^2 \\ \text{sous contraintes} \quad & \mathbf{A}\mathbf{v} = \mathbf{b}, \\ & \mathbf{R}\mathbf{v} = \mathbf{s}, \\ & \mathbf{u} = \mathbf{v}, \end{aligned}$$

avec $\mathbf{A} \in \mathbb{R}^{n \times m}$, $\mathbf{b} \in \mathbb{R}^n$, $\mathbf{c} \in \mathbb{R}^m$, $\mathbf{R} \in \mathbb{R}^{n \times m}$ et $\mathbf{D} \in \mathbb{R}^{m \times m}$.

La forme duale de ce problème est :

$$\max_{\mathbf{u} \in \mathcal{U}, \mathbf{v} \in \mathbb{R}^m, \mathbf{s} \in \mathbb{R}^n} \left\langle \mathbf{x}, \begin{bmatrix} \mathbf{R}\mathbf{v} - \mathbf{s} \\ \mathbf{A}\mathbf{v} - \mathbf{b} \\ \mathbf{v} - \mathbf{u} \end{bmatrix} \right\rangle - J_a(\mathbf{u}) - J_b(\mathbf{s}) - \frac{1}{2} \|\mathbf{u} - \mathbf{c}\|_{\mathbf{D}}^2.$$

Les problèmes d'optimisation convexe sont résolus en utilisant des méthodes standards comme les algorithmes du gradient [Fletcher, 1976], [Nesterov, 2013]. En particulier, l'algorithme du gradient à direction de descente est destiné à minimiser une fonction réelle différentiable. Cet algorithme est itératif et cherche à améliorer successivement l'objectif du problème. Ceci est fait en effectuant un déplacement dans la direction opposée au gradient, de manière à faire décroître la valeur de la fonction de coût.

1.3 Chapitre 4 : Estimation d'état ellipsoïdale pour les systèmes linéaires

Ce chapitre reprend des notions et des approches présentes dans la littérature pour étendre une technique d'estimation d'état ellipsoïdale [Ben Chabane et al., 2014b] en prenant en considération les entrées du système. La formulation du problème est présentée ci-dessous.

1.3.1 Formulation du problème d'estimation

Soit le système standard linéaire invariant dans le temps (LTI) suivant :

$$\begin{cases} \mathbf{x}_{k+1} = \mathbf{A}\mathbf{x}_k + \mathbf{B}\mathbf{u}_k + \mathbf{E}\boldsymbol{\omega}_k, \\ \mathbf{y}_k = \mathbf{C}\mathbf{x}_k + \mathbf{F}\boldsymbol{\omega}_k. \end{cases} \quad (1.8)$$

Nous supposons que l'état initial appartient à l'ensemble \mathcal{X}_0 supposé suffisamment grand par manque de connaissances précises sur le système. De plus, nous supposons que le vecteur $\boldsymbol{\omega}_k \in \mathbb{R}^{n_x+n_y}$ qui contient les perturbations d'état et de mesure est borné par une boîte unitaire $\mathbb{B}^{n_x+n_y}$.

Considérons qu'à l'instant k l'ensemble d'estimation d'état est $\hat{\mathcal{X}}_k$ (avec $x_k \in \hat{\mathcal{X}}_k$), l'objectif de l'estimation d'état est alors de trouver l'ensemble $\hat{\mathcal{X}}_{k+1}$ qui contient l'état x_{k+1} du système (1.8) à l'instant $k+1$. Dans la littérature, ce problème est traité en trois étapes :

- *Étape de prédiction* : L'ensemble de prédiction $\bar{\mathcal{X}}_{k+1}$ contenant l'état est donné par :

$$\bar{\mathcal{X}}_{k+1} \subseteq \mathbf{A}\hat{\mathcal{X}}_k \cup \mathbf{B}\mathbf{u}_k \cup \mathbf{E}\mathbb{B}^{n_x+n_y}. \quad (1.9)$$

Cet ensemble offre des bornes pour la trajectoire incertaine du système (1.8).

- *Étape de mesure* : L'ensemble des états cohérents avec les mesures $\mathcal{X}_{y_{k+1}}$ est donné par :

$$\mathcal{X}_{y_{k+1}} = \{\mathbf{x}_{k+1} \in \mathbb{R}^{n_x} : (\mathbf{y}_{k+1} - \mathbf{C}\mathbf{x}_{k+1}) \in \mathbf{F}\mathbb{B}^{n_x+n_y}\}. \quad (1.10)$$

- *Étape de correction* : L'ensemble d'estimation d'état garanti $\hat{\mathcal{X}}_{k+1}$ est une approximation extérieure de l'intersection entre l'ensemble prédit et l'ensemble cohérent avec les mesures. Il est donné par :

$$\hat{\mathcal{X}}_{k+1} \supseteq \bar{\mathcal{X}}_{k+1} \cap \mathcal{X}_{y_{k+1}}. \quad (1.11)$$

L'ensemble d'estimation d'état peut avoir plusieurs formes géométriques. La Figure 1.2 illustre les trois étapes nécessaires au calcul de l'ensemble d'estimation garanti en utilisant des ellipsoïdes.

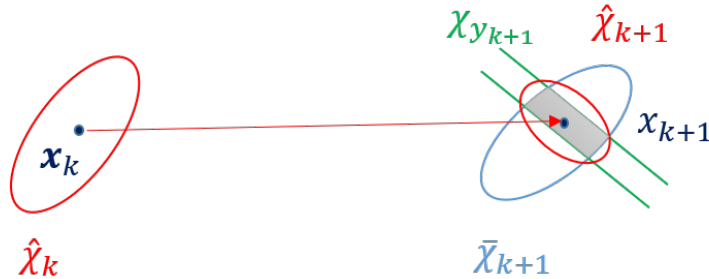


Figure 1.2 – Illustration de la méthode d'estimation d'état ensembliste

1.3.2 Technique d'estimation d'état fondée sur des ellipsoïdes

Cette partie décrit et améliore une technique d'estimation d'état ellipsoïdale présente dans la littérature [Ben Chabane, 2015]. Elle prend en considération le cas où les entrées du système ne sont pas connues. Considérons le système (1.8) et supposons qu'à l'instant k l'ellipsoïde contenant \mathbf{x}_k est noté $\mathcal{E}(\mathbf{P}, \bar{\mathbf{x}}_k, \rho_k)$, avec $\bar{\mathbf{x}}_k$ l'estimation nominale de l'état. L'objectif est de trouver un ellipsoïde de la forme $\mathcal{E}(\mathbf{P}, \bar{\mathbf{x}}_{k+1}, \rho_{k+1})$ contenant l'état \mathbf{x}_{k+1} à l'instant $k + 1$. L'état \mathbf{x}_{k+1} est garanti d'appartenir à l'ellipsoïde $\mathcal{E}(\mathbf{P}_{k+1}, \bar{\mathbf{x}}_{k+1}, \rho_{k+1})$ si, pour les matrices $\mathbf{Y}_{k+1} \in \mathbb{R}^{n_x \times n_y}$, $\mathbf{G}_{k+1} \in \mathbb{R}^{n_x \times n_x}$, le vecteur $\mathbf{g}_{k+1} \in \mathbb{R}^{n_x}$ et les scalaires $\beta_{k+1}, \rho_{k+1} > 0$, la LMI suivante ([Ben Chabane, 2015], page 113) est vérifiée :

$$\begin{aligned} & \min_{\beta_{k+1}, \mathbf{Y}_{k+1}, \mathbf{P}_{k+1}, \rho_{k+1}, \mathbf{G}_{k+1}, \mathbf{g}_{k+1}, \alpha, \gamma} \alpha \\ & \text{sous contraintes} \end{aligned}$$

$$\left\{ \begin{array}{l} \left[\begin{array}{ccc} \beta_{k+1} \mathbf{P}_k & * & * \\ \mathbf{0} & \rho_{k+1} - \beta_{k+1} \rho_k & * \\ \mathbf{P}_{k+1} \mathbf{A} - \mathbf{Y}_{k+1} \mathbf{C} & \boldsymbol{\tau}_{k+1} & \mathbf{P}_{k+1} \end{array} \right] \succ 0, \\ \mathbf{P}_{k+1} \geq \mathbf{P}_k, \\ \rho_{k+1} \leq \alpha \rho_k + \gamma, \\ 0 < \alpha < 1, \\ \gamma > 0, \\ \rho_{k+1} > 0, \end{array} \right. \quad (1.12)$$

pour tout $\boldsymbol{\omega}_k \in \mathbb{B}^{n_x+n_y}$, avec la matrice :

$$\mathbf{Y}_k = \mathbf{P}_k \mathbf{L}_k,$$

le vecteur :

$$\boldsymbol{\tau}_{k+1} = (\mathbf{P}_{k+1} \mathbf{A} - \mathbf{Y}_{k+1} \mathbf{C} - \mathbf{G}_{k+1}) \bar{\mathbf{x}}_k + (\mathbf{P}_{k+1} \mathbf{E} - \mathbf{Y}_{k+1} \mathbf{F}) \boldsymbol{\omega}_{k+1} - \mathbf{g}_{k+1} + \mathbf{B}(\mathbf{u}_k - \bar{\mathbf{u}}_k),$$

et l'état nominal estimé :

$$\bar{\mathbf{x}}_{k+1} = \mathbf{P}_{k+1}^{-1} (\mathbf{G}_{k+1} \bar{\mathbf{x}}_k + \mathbf{Y}_{k+1} \mathbf{y}_k + \mathbf{g}_{k+1}) + \mathbf{B} \bar{\mathbf{u}}_k,$$

où $\bar{\mathbf{u}}_k$ est la commande nominale. La contrainte :

$$\rho_{k+1} \leq \alpha \rho_k + \gamma,$$

avec $0 < \alpha < 1$ et $\gamma > 0$, borne le rayon de l'estimation ellipsoïdale $\mathcal{E}(\mathbf{P}_{k+1}, \bar{\mathbf{x}}_{k+1}, \rho_{k+1})$ à l'instant $k + 1$ pour diminuer la taille de l'ensemble.

De la même façon que dans [Ben Chabane, 2015], cette technique est améliorée en considérant des contraintes quadratiques sur la mesure et sur les perturbations à l'instant $k+1$. Dans ce contexte, en considérant l'estimation d'état à base d'ellipsoïdes $\mathcal{E}(\mathbf{P}, \bar{\mathbf{x}}_{k+1}, \rho_{k+1})$ donnée par le problème d'optimisation (1.12), un nouvel ensemble ellipsoïdal $\mathcal{E}'(\mathbf{P}', \bar{\mathbf{x}}'_{k+1}, \rho'_{k+1})$ est obtenu si le problème d'optimisation suivant ([Ben Chabane, 2015], page 118) est vérifié

$$\begin{aligned} & \min_{\rho'_{k+1}, \mathbf{P}', \mathbf{b}_{k+1}, \mathbf{H}, \theta, \mu_i, \alpha, \gamma} \alpha \\ & \text{sous contraintes} \end{aligned} \quad \left\{ \begin{array}{l} \left[\begin{array}{ccc} \boldsymbol{\eta}_1 & \boldsymbol{\eta}_2^\top & \mathbf{P}'_{k+1} \\ \boldsymbol{\eta}_2 & \eta_3 - \sum_{i=1}^{n_x+n_y} \mu_i & -\mathbf{b}_{k+1}^\top \\ \mathbf{P}'_{k+1} & -\mathbf{b}_{k+1} & \mathbf{P}'_{k+1} \end{array} \right] \succ 0, \\ \mathbf{P}' \succ 0, \\ \mathbf{F}^\top \mathbf{H} \mathbf{F} < \sum_{i=1}^{n_x+n_y} \mu_i \tilde{\mathbf{T}}_i, \\ \theta \geq 0, \\ \theta < 1, \\ \rho'_{k+1} > \theta \rho_{k+1}, \\ \mu_i \geq 0, \quad i = 1, \dots, n_x + n_y, \\ \mathbf{P}'_{k+1} \geq \mathbf{P}_{k+1}, \\ \rho_{k+1} \leq \alpha \rho_k + \gamma, \\ \gamma > 0, \end{array} \right. \quad (1.13)$$

avec :

$$\begin{aligned} \mathbf{b}_{k+1} &= \mathbf{P}'_{k+1} \bar{\mathbf{x}}_{k+1}, \\ \boldsymbol{\eta}_1 &= \theta \mathbf{P}_{k+1} + \mathbf{C}^\top \mathbf{H} \mathbf{C}, \\ \boldsymbol{\eta}_2 &= -\theta \bar{\mathbf{x}}_{k+1}^\top \mathbf{P}_{k+1} - \mathbf{y}_{k+1}^\top \mathbf{H} \mathbf{C} + \mathbf{u}_k^\top \mathbf{B}^\top \mathbf{C}^\top \mathbf{H} \mathbf{C}, \\ \eta_3 &= \rho'_{k+1} - \theta \rho_{k+1} + \theta \|\bar{\mathbf{x}}_{k+1}\|_{\mathbf{P}_{k+1}}^2 + \|\mathbf{y}_{k+1}\|_{\mathbf{H}}^2 + \|\mathbf{C} \mathbf{B} \mathbf{u}_k\|_{\mathbf{H}}^2 - 2 \mathbf{u}_k^\top \mathbf{B}^\top \mathbf{C}^\top \mathbf{H} \mathbf{y}_{k+1}. \end{aligned}$$

Le lecteur remarquera que les termes liés à la commande \mathbf{u}_k s'ajoutent à la formulation proposée par [Ben Chabane, 2015].

1.3.3 Comparaison entre deux techniques d'estimation d'état pour les systèmes LTI

La différence entre la technique d'estimation d'état ellipsoïdale présentée dans la Section 1.3.2 et le filtre de Kalman classique se trouve principalement au niveau des hypothèses considérées dans la modélisation du système. Le filtre de Kalman classique fonctionne pour des systèmes linéaires soumis à des

bruits ayant une distribution stochastique connue, tandis que la technique ellipsoïdale fonctionne pour des systèmes linéaires soumis à des perturbations et bruits de mesure inconnus, mais bornés. Toutefois, le filtre de Kalman offre une complexité réduite parce qu'il se base sur des opérations d'addition et de multiplication de matrices. La technique ellipsoïdale est fondée sur la résolution d'un problème d'optimisation convexe. Ainsi, la complexité de calcul est plus importante mais cette technique offre une plus grande précision. La comparaison entre les deux techniques a été publiée au 20ème congrès mondial de l'IFAC 2017.

1.3.4 Application à un modèle d'octorotor

Les drones peu coûteux ont donné aux utilisateurs et aux chercheurs un énorme potentiel pour tester leurs travaux dans divers domaines scientifiques, notamment en Automatique. Afin de profiter de la bonne précision que la technique d'estimation d'état ellipsoïdale fournit, celle-ci est appliquée dans cette thèse à un modèle d'octorotor utilisé dans un contexte d'imagerie radar. En utilisant le système radar intégré au drone, ainsi que les coordonnées estimées du drone, une application de reconstruction d'image est exposée. De plus, la distance réelle séparant le drone de la cible est garantie à l'intérieur des bornes calculées par la technique. Ensuite, l'erreur relative de l'estimation conduit au calcul de la fréquence de fonctionnement du radar. Le modèle de l'octorotor considéré est présenté par la suite.

1.3.4.1 Modèle d'octorotor

Partant d'une représentation d'état à temps continu avec 12 états :

- les coordonnées cartésiennes du centre de gravité du drone x , y et z ,
- l'orientation du drone ϕ , θ et ψ ,
- la vitesse linéaire du drone V_x , V_y et V_z ,
- la vitesse angulaire du drone ω_x , ω_y et ω_z ,

le système linéarisé et discrétisé est ensuite divisé en trois sous-systèmes pour réduire la complexité :

• **Sous-système 1 :**

$$\left\{ \begin{array}{l} \begin{bmatrix} z_{k+1} \\ \psi_{k+1} \\ V_{z_{k+1}} \\ \omega_{z_{k+1}} \end{bmatrix} = \mathbf{A} \begin{bmatrix} z_k \\ \psi_k \\ V_{z_k} \\ \omega_{z_k} \end{bmatrix} + \begin{bmatrix} 0 & 0 \\ 0 & 0 \\ \frac{T_e}{m} & 0 \\ 0 & \frac{T_e}{I_{zz}} \end{bmatrix} \begin{bmatrix} F_{z_k}^R \\ \tau_{z_k}^R \end{bmatrix} + \mathbf{E}_1 \boldsymbol{\omega}_k, \\ \\ \begin{bmatrix} z_k \\ \psi_k \end{bmatrix} = \mathbf{C} \begin{bmatrix} z_k \\ \psi_k \\ V_{z_k} \\ \omega_{z_k} \end{bmatrix} + \mathbf{F}_1 \boldsymbol{\omega}_k, \end{array} \right. \quad (1.14)$$

• **Sous-système 2 :**

$$\left\{ \begin{array}{l} \begin{bmatrix} \phi_{k+1} \\ \theta_{k+1} \\ \omega_{x_{k+1}} \\ \omega_{y_{k+1}} \end{bmatrix} = \mathbf{A} \begin{bmatrix} \phi_k \\ \theta_k \\ \omega_{x_k} \\ \omega_{y_k} \end{bmatrix} + \begin{bmatrix} 0 & 0 \\ 0 & 0 \\ \frac{T_e}{I_{xx}} & 0 \\ 0 & \frac{T_e}{I_{yy}} \end{bmatrix} \begin{bmatrix} \tau_{x_k}^R \\ \tau_{y_k}^R \end{bmatrix} + \mathbf{E}_2 \boldsymbol{\omega}_k, \\ \\ \begin{bmatrix} \phi_k \\ \theta \end{bmatrix} = \mathbf{C} \begin{bmatrix} \phi_k \\ \theta_k \\ \omega_{x_k} \\ \omega_{y_k} \end{bmatrix} + \mathbf{F}_2 \boldsymbol{\omega}_k, \end{array} \right. \quad (1.15)$$

• **Sous-système 3 :**

$$\left\{ \begin{array}{l} \begin{bmatrix} x_{k+1} \\ y_{k+1} \\ V_{x_{k+1}} \\ V_{y_{k+1}} \end{bmatrix} = \mathbf{A} \begin{bmatrix} x_k \\ y_k \\ V_{x_k} \\ V_{y_k} \end{bmatrix} + \begin{bmatrix} 0 & 0 \\ 0 & 0 \\ \frac{T_e}{m} & 0 \\ 0 & \frac{T_e}{m} \end{bmatrix} \begin{bmatrix} F_{x_k}^R \\ F_{y_k}^R \end{bmatrix} + \mathbf{E}_3 \boldsymbol{\omega}_k, \\ \\ \begin{bmatrix} x_k \\ y_k \end{bmatrix} = \mathbf{C} \begin{bmatrix} x_k \\ y_k \\ V_{x_k} \\ V_{y_k} \end{bmatrix} + \mathbf{F}_3 \boldsymbol{\omega}_k. \end{array} \right. \quad (1.16)$$

avec les mêmes matrices $\mathbf{A} = \begin{bmatrix} \mathbf{I}_2 & T_e \mathbf{I}_2 \\ \mathbf{0}_2 & \mathbf{I}_2 \end{bmatrix}$ et $\mathbf{C} = \begin{bmatrix} \mathbf{I}_2 & \mathbf{0}_2 \end{bmatrix}$ pour les trois sous-systèmes. Les perturbations et les bruits de mesure sont modélisés par le vecteur $\boldsymbol{\omega}_k$ borné par une boîte unitaire \mathbb{B}^6 et les matrices $\mathbf{E}_i = \epsilon_i \cdot \begin{bmatrix} \mathbf{I}_4 & \mathbf{0}_{4 \times 2} \end{bmatrix}$, $\mathbf{F}_i = \gamma_i \cdot \begin{bmatrix} \mathbf{0}_4 & \mathbf{I}_{4 \times 2} \end{bmatrix}$, pour $i \in \{1, 2, 3\}$. Les scalaires ϵ_i et γ_i représentent la précision fournie par les informations des capteurs. La méthode d'estimation

d'état ellipsoïdale est appliquée à l'octorotor utilisé pour la conception du SAR (Radar à synthèse d'ouverture). En testant deux trajectoires, la bonne précision de la technique ellipsoïdale est validée pour trouver la fréquence optimale de fonctionnement du radar. Ces résultats font partie d'un article de journal soumis à une édition spéciale "Interval estimation applied to diagnosis and control" de l'International Journal of Control.

1.4 Chapitre 5 : Estimation d'état ellipsoïdale pour des systèmes descripteurs

Un système descripteur est utilisé pour modéliser des systèmes physiques complexes. Il peut décrire des processus régis à la fois par des équations algébriques et différentielles d'où son avantage par rapport à un système standard. Dans ce chapitre, une extension de la technique d'estimation d'état ellipsoïdale au cas des systèmes descripteurs linéaires est proposée.

1.4.1 Formulation de problème

Soit le système descripteur à temps discret linéaire invariant dans le temps :

$$\begin{cases} \mathbf{E}_d \mathbf{x}_{k+1} &= \mathbf{A} \mathbf{x}_k + \mathbf{B} \mathbf{u}_k + \mathbf{E} \boldsymbol{\omega}_k, \\ \mathbf{y}_k &= \mathbf{C} \mathbf{x}_k + \mathbf{F} \boldsymbol{\omega}_k, \end{cases} \quad (1.17)$$

avec $\mathbf{x}_k \in \mathbb{R}^{n_x}$ le vecteur d'état, $\mathbf{u}_k \in \mathbb{R}^{n_u}$ le vecteur de commande et $\mathbf{y}_k \in \mathbb{R}^{n_y}$ le vecteur de sortie à chaque instant k . Les perturbations sont inconnues, mais bornées par des boîtes unitaires telles que $\boldsymbol{\omega}_k \in \mathbb{B}^{n_w}$. L'état initial appartient à l'ellipsoïde :

$$\mathcal{E}(\mathbf{P}_0, \bar{\mathbf{x}}_0, \rho_0) = \{\mathbf{x} \in \mathbb{R}^{n_x} : (\mathbf{x} - \bar{\mathbf{x}}_0)^\top \mathbf{P}_0 (\mathbf{x} - \bar{\mathbf{x}}_0) \leq \rho_0\}, \quad (1.18)$$

avec $\mathbf{P}_0 = \mathbf{P}_0^\top \succ 0$ la matrice de taille $n_x \times n_x$, $\bar{\mathbf{x}}_0$ le centre et ρ_0 le rayon de l'ellipsoïde $\mathcal{E}(\mathbf{P}_0, \bar{\mathbf{x}}_0, \rho_0)$. La matrice \mathbf{E}_d est une matrice singulière avec :

$$\text{rang}(\mathbf{E}_d) \leq n_x. \quad (1.19)$$

Pour garantir l'observabilité et la commandabilité du système, les conditions suivantes doivent être satisfaites :

$$\text{rang} \begin{bmatrix} \mathbf{E}_d \\ \mathbf{C} \end{bmatrix} = n_x, \quad (1.20)$$

$$\text{rang} \begin{bmatrix} \lambda \mathbf{E}_d - \mathbf{A} \\ \mathbf{C} \end{bmatrix} = n_x, \forall \lambda \in \mathbb{C}. \quad (1.21)$$

$$\text{rang} \begin{bmatrix} \mathbf{E}_d & \mathbf{B} \end{bmatrix} = n_x, \quad (1.22)$$

$$\text{rang} \begin{bmatrix} \lambda \mathbf{E}_d - \mathbf{A} & \mathbf{B} \end{bmatrix} = n_x, \forall \lambda \in \mathbb{C}. \quad (1.23)$$

Ceci permet de trouver deux matrices \mathbf{T} et \mathbf{N} telles que :

$$\mathbf{T}\mathbf{E}_d + \mathbf{N}\mathbf{C} = \mathbf{I}_{n_x}. \quad (1.24)$$

Cinq méthodes d'estimation d'état ellipsoïdales sont développées pour les systèmes descripteurs linéaires invariants ou variants dans le temps et sont résumées dans la suite.

1.4.2 Systèmes descripteurs linéaires invariants dans le temps

Ici, les matrices \mathbf{A} , \mathbf{B} , \mathbf{C} , \mathbf{D} , \mathbf{E} , \mathbf{E}_d et \mathbf{F} de (1.17) sont supposées constantes.

1.4.2.1 Méthode 1

L'estimation ellipsoïdale de l'état du système à chaque instant est donnée par le théorème qui suit.

Théorème 1.1. Soit l'état initial \mathbf{x}_0 et considérons que $\mathbf{x}_k \in \mathcal{E}(\mathbf{P}, \bar{\mathbf{x}}_k, \rho_k)$ à l'instant k . Étant donné un scalaire $\beta \in (0, 1)$, s'il existe une matrice symétrique strictement définie positive $\mathbf{P} = \mathbf{P}^\top \succ 0$ dans $\mathbb{R}^{n_x \times n_x}$, une matrice $\mathbf{Y} \in \mathbb{R}^{n_x \times n_y}$ et un scalaire $\sigma > 0$ pour lesquels l'inégalité matricielle linéaire (1.25) est vérifiée pour chaque $\boldsymbol{\omega}_k \in \mathcal{V}_{\mathbb{B}^{n_x+n_y}}$ (où $\mathcal{V}_{\mathbb{B}^{n_x+n_y}}$ représente les sommets de la boîte $\mathbb{B}^{n_x+n_y}$) :

$$\begin{bmatrix} \beta \mathbf{P} & * & * \\ \mathbf{0} & \sigma & * \\ \mathbf{P}\mathbf{T}\mathbf{A} - \mathbf{Y}\mathbf{C} & (\mathbf{P}\mathbf{T}\mathbf{E} - \mathbf{Y}\mathbf{F})\boldsymbol{\omega}_k - \mathbf{P}\mathbf{N}\mathbf{F}\boldsymbol{\omega}_{k+1} & \mathbf{P} \end{bmatrix} \succ 0, \quad (1.25)$$

alors l'état \mathbf{x}_{k+1} appartient à l'ellipsoïde $\mathbf{x}_{k+1} \in \mathcal{E}(\mathbf{P}, \bar{\mathbf{x}}_{k+1}, \rho_{k+1})$, avec $\mathbf{L} = \mathbf{P}^{-1}\mathbf{Y}$, la séquence $\bar{\mathbf{x}}_{k+1}$ et le scalaire ρ_{k+1} , calculés à partir des expressions récursives :

$$\bar{\mathbf{x}}_{k+1} = \mathbf{T}\mathbf{A}\bar{\mathbf{x}}_k + \mathbf{T}\mathbf{B}\mathbf{u}_k + \mathbf{N}\mathbf{y}_{k+1} + \mathbf{L}(\mathbf{y}_k - \mathbf{C}\bar{\mathbf{x}}_k), \quad (1.26)$$

$$\rho_{k+1} = \beta\rho_k + \sigma. \quad (1.27)$$

1.4.2.2 Méthode 2

Le problème d'optimisation (1.25) de la *Méthode 1* est résolu hors ligne. Une autre approche consiste à obtenir un gain \mathbf{L}_k mis à jour à chaque instant k , permettant d'améliorer la rapidité de la convergence de l'estimation. L'existence de \mathbf{P} , \mathbf{L} et β (calculés avec la *Méthode 1*) garantit l'existence de \mathbf{L}_k vérifiant les contraintes considérées. La LMI à résoudre minimise le rayon de l'ellipsoïde d'estimation ρ_{k+1} à chaque instant de sorte que :

$$\left\{ \begin{array}{l} \left[\begin{array}{ccc} \beta\mathbf{P} & * & * \\ \mathbf{0} & \rho_{k+1} - \beta\rho_k & * \\ \mathbf{P}\mathbf{T}\mathbf{A} - \mathbf{Y}_k\mathbf{C} & (\mathbf{P}\mathbf{T}\mathbf{E} - \mathbf{Y}_k\mathbf{F})\boldsymbol{\omega}_k - \mathbf{N}\mathbf{F}\boldsymbol{\omega}_{k+1} & \mathbf{P} \end{array} \right] \succ 0, \\ \rho_{k+1} \leq \beta\rho_k + \sigma \end{array} \right. \quad (1.28)$$

avec le centre de l'ellipsoïde :

$$\bar{\mathbf{x}}_{k+1} = \mathbf{T}\mathbf{A}\bar{\mathbf{x}}_k + \mathbf{T}\mathbf{B}\mathbf{u}_k + \mathbf{N}\mathbf{y}_{k+1} + \mathbf{L}_k(\mathbf{y}_k - \mathbf{C}\bar{\mathbf{x}}_k). \quad (1.29)$$

1.4.2.3 Méthode 3

Dans le but de réduire le temps de calcul en résolvant un problème d'optimisation à chaque instant, la *Méthode 3* évite l'énumération de tous les sommets de $\mathbb{B}^{n_x+n_y}$. Cette procédure se base sur une nouvelle *scaling technique* proposée par [Ben Chabane et al., 2014] pour les systèmes standards.

Si la contrainte LMI (1.28) est vérifiée, alors il existe un scalaire $\beta \in (0, 1)$ et une matrice $\mathbf{S} = \mathbf{S}^\top \succ 0$ de sorte que l'inégalité suivante est vérifiée :

$$\left[\begin{array}{ccc} \beta\mathbf{P} & * & * \\ \mathbf{P}\mathbf{T}\mathbf{A} - \mathbf{Y}_k\mathbf{C} & \mathbf{P} & * \\ \mathbf{0} & [\mathbf{P}\mathbf{T}\mathbf{E} - \mathbf{Y}_k\mathbf{F} \quad -\mathbf{P}\mathbf{N}\mathbf{F}]^\top & \mathbf{S} \end{array} \right] \succ 0. \quad (1.30)$$

La *Méthode 3* offre une meilleure précision d'estimation comparée à la *Méthode 1* avec un gain en termes de temps de calcul par rapport à la *Méthode 2*.

1.4.3 Systèmes descripteurs linéaires variant dans le temps

En général, il est important de prendre en considération les incertitudes dans le modèle. Le but de cette section est d'étendre l'approche d'estimation ellipsoïdale pour des systèmes descripteurs variant dans le temps (avec une matrice d'évolution \mathbf{A}_k variable).

1.4.3.1 Méthode 4

Cette méthode minimise le rayon de l'ellipsoïde contenant l'état du système à chaque instant k avec une matrice \mathbf{P}_k variable pour améliorer la précision de l'estimation. La solution à ce problème est formulée par le théorème suivant.

Théorème 1.2. Soit le système (1.17) avec une matrice intervalle variable dans le temps $\mathbf{A}_k \in [\mathbf{A}]$. Si les hypothèses suivantes sont vérifiées :

- L'état \mathbf{x}_k est contenu dans l'ellipsoïde $\mathcal{E}(\mathbf{P}_k, \bar{\mathbf{x}}_k, \rho_k)$;
- À l'instant k , les incertitudes sont bornées par un ensemble convexe Ω_k , i.e. $(\boldsymbol{\omega}_k, \mathbf{A}_k) \in \Omega_k$, avec \mathcal{V}_{Ω_k} l'ensemble des sommets de Ω_k ;
- Il existe deux matrices \mathbf{T} et \mathbf{N} vérifiant (1.24) ;
- Il existe des matrices $\mathbf{P}_{k+1} = \mathbf{P}_{k+1}^\top \succ 0$, avec $\mathbf{P}_{k+1} \in \mathbb{R}^{n_x \times n_x}$, $\mathbf{Y}_{k+1} \in \mathbb{R}^{n_x \times n_y}$, $\mathbf{G}_{k+1} \in \mathbb{R}^{n_x \times n_x}$, le vecteur $\mathbf{g}_{k+1} \in \mathbb{R}^{n_x}$ et les scalaires positifs $\beta_{k+1}, \rho_{k+1} > 0$ de sorte que la LMI suivante est vérifiée pour tout $(\boldsymbol{\omega}_k, \mathbf{A}_k) \in \mathcal{V}_{\Omega_k}$:

$$\begin{bmatrix} \beta_{k+1} \mathbf{P}_k & * & * \\ \mathbf{0} & \rho_{k+1} - \beta_{k+1} \rho_k & * \\ \mathbf{P}_{k+1} \mathbf{T} \mathbf{A}_k - \mathbf{Y}_{k+1} \mathbf{C} & \boldsymbol{\tau}_{k+1} & \mathbf{P}_{k+1} \end{bmatrix} \succ 0, \quad (1.31)$$

$$\text{avec } \boldsymbol{\tau}_{k+1} = (\mathbf{P}_{k+1} \mathbf{T}_k \mathbf{A}_k - \mathbf{Y}_{k+1} \mathbf{C} - \mathbf{G}_{k+1}) \bar{\mathbf{x}}_k + (\mathbf{P}_{k+1} \mathbf{T}_k \mathbf{E} - \mathbf{Y}_{k+1} \mathbf{F}) \boldsymbol{\omega}_k - \mathbf{g}_{k+1} + \mathbf{N}_k \mathbf{y}_{k+1} - \mathbf{N}_k \mathbf{F} \boldsymbol{\omega}_{k+1},$$

alors, à l'instant $k+1$, le vecteur d'état \mathbf{x}_{k+1} appartient à l'ellipsoïde $\mathcal{E}(\mathbf{P}_{k+1}, \bar{\mathbf{x}}_{k+1}, \rho_{k+1})$, avec $\bar{\mathbf{x}}_{k+1} = \mathbf{P}_{k+1}^{-1} (\mathbf{G}_{k+1} \bar{\mathbf{x}}_k + \mathbf{Y}_{k+1} \mathbf{y}_k + \mathbf{g}_{k+1})$.

Dans la section suivante, la *Méthode 4* est améliorée en ajoutant des contraintes quadratiques sur la mesure et sur les perturbations à l'instant $k+1$.

1.4.3.2 Méthode 5

Soit l'ellipsoïde $\mathcal{E}(\mathbf{P}_{k+1}, \bar{\mathbf{x}}_{k+1}, \rho_{k+1})$ contenant l'état estimé calculé à partir de (1.31). Le but de cette méthode est d'améliorer la précision de l'estimation en ajoutant des contraintes quadratiques en \mathbf{y}_{k+1} et $\boldsymbol{\omega}_{k+1}$. En effet, s'il existe une matrice $\mathbf{P}'_{k+1} = \mathbf{P}'_{k+1}{}^\top \succ 0$ dans $\mathbb{R}^{n_x \times n_x}$, une matrice $\mathbf{H} = \mathbf{H}^\top \succ 0$ dans $\mathbb{R}^{n_y \times n_y}$, un vecteur $\bar{\mathbf{x}}'_{k+1} \in \mathbb{R}^{n_x}$ et un scalaire positif réel $\rho'_{k+1} > 0$ de sorte

que les contraintes suivantes soient vérifiées:

$$\left\{ \begin{array}{l} \left[\begin{array}{ccc} \boldsymbol{\eta}_1 & * & * \\ \boldsymbol{\eta}_2 & \eta_3 - \sum_{i=1}^{n_x+n_y} \mu_i & * \\ \mathbf{P}'_{k+1} & -\mathbf{b}_{k+1} & \mathbf{P}'_{k+1} \end{array} \right] \succ 0, \\ \mathbf{F}^\top \mathbf{H} \mathbf{F} < \sum_{i=1}^{n_x+n_y} \mu_i \tilde{\mathbf{T}}_i, \\ \mathbf{P}' \succ 0, \mathbf{P}'_{k+1} \geq \mathbf{P}_{k+1}, \theta \geq 0, \theta < 1, \gamma > 0, \\ \rho'_{k+1} > \theta \rho_{k+1}, \rho_{k+1} \leq \alpha \rho_k + \gamma, \\ \mu_i \geq 0, \quad i = 1, \dots, n_x + n_y, \end{array} \right. \quad (1.32)$$

avec :

$$\left\{ \begin{array}{l} \mathbf{b}_{k+1} = \mathbf{P}'_{k+1} \bar{\mathbf{x}}'_{k+1}, \\ \boldsymbol{\eta}_1 = \theta \mathbf{P}_{k+1} + \mathbf{C}^\top \mathbf{H} \mathbf{C}, \\ \boldsymbol{\eta}_2 = -\theta \bar{\mathbf{x}}_{k+1}^\top \mathbf{P}_{k+1} - \mathbf{y}_{k+1}^\top \mathbf{H} \mathbf{C}, \\ \eta_3 = \rho'_{k+1} - \theta \rho_{k+1} + \theta \|\bar{\mathbf{x}}_{k+1}\|_{\mathbf{P}_{k+1}}^2 + \|\mathbf{y}_{k+1}\|_{\mathbf{H}}^2, \end{array} \right. \quad (1.33)$$

alors l'état se trouve dans l'ellipsoïde d'estimation $\mathcal{E}'(\mathbf{P}'_{k+1}, \bar{\mathbf{x}}'_{k+1}, \rho'_{k+1})$. Cette méthode donne une meilleure précision par rapport à la *Méthode 4* mais avec une complexité plus importante. La *Méthode 1* a été publiée à la 23ème International Conference on System Theory, Control and Computing, et les autres méthodes font partie d'un article qui sera soumis à Automatica.

1.5 Chapitre 6 : Estimation d'état zonotopique

Ce chapitre fait partie de la deuxième partie de la thèse qui traite de l'estimation d'état zonotopique. Ce choix est justifié par la bonne précision offerte par les zonotopes et par la définition de son \mathbf{P} -rayon donnant un critère pour évaluer la taille du zonotope.

1.5.1 Méthode d'estimation d'état zonotopique fondée sur un observateur de Luenberger

Considérons le système standard LTI suivant :

$$\left\{ \begin{array}{l} \mathbf{x}_{k+1} = \mathbf{A} \mathbf{x}_k + \mathbf{B} \mathbf{u}_k + \mathbf{E} \boldsymbol{\omega}_k \\ \mathbf{y}_k = \mathbf{C} \mathbf{x}_k + \mathbf{F} \boldsymbol{\omega}_k \end{array} \right. \quad (1.34)$$

Le vecteur $\boldsymbol{\omega}_k \in \mathbb{B}^{n_w}$ contient les perturbations d'état et les bruits de mesure. La méthode d'estimation d'état à base d'ensembles zonotopiques est formulée par le théorème suivant.

Théorème 1.3. (fondé sur l’approche proposé par [Wang et al., 2018]) Considérons que \mathbf{x}_0 est l’état initial et que l’état \mathbf{x}_k appartient au zonotope $\mathcal{Z}(\mathbf{p}_k, \mathbf{H}_k) = \mathbf{p}_k \oplus \mathbf{H}_k \mathbb{B}^m$. Etant donné un scalaire $\beta \in (0, 1)$, s’il existe une matrice $\mathbf{P} = \mathbf{P}^\top \succ 0$ dans $\mathbb{R}^{n_x \times n_x}$, une matrice $\mathbf{Y} \in \mathbb{R}^{n_x \times n_y}$ et un scalaire $\sigma > 0$ pour lesquels la LMI suivante est vérifiée :

$$\begin{bmatrix} \beta \mathbf{P} & \mathbf{0} & \mathbf{A}^\top \mathbf{P} - \mathbf{C}^\top \mathbf{Y}^\top \\ * & \Theta^\top \Theta & \mathbf{E}^\top \mathbf{P} - \mathbf{F}^\top \mathbf{Y}^\top \\ * & * & \mathbf{P} \end{bmatrix} \succeq 0, \quad (1.35)$$

alors il est garanti que l’état $\mathbf{x}_{k+1} \in \mathcal{Z}(\bar{\mathbf{x}}_{k+1}, \mathbf{H}_{k+1})$, $\forall \boldsymbol{\omega}_k \in \mathbb{B}^{n_x+n_y}$, avec :

$$\bar{\mathbf{x}}_{k+1} = \mathbf{A} \bar{\mathbf{x}}_k + \mathbf{B} \mathbf{u}_k + \mathbf{L}(\mathbf{y}_k - \mathbf{C} \bar{\mathbf{x}}_k), \quad (1.36)$$

$$\mathbf{H}_{k+1} = [\mathbf{A}_L \mathbf{H}_k \quad \boldsymbol{\eta}], \quad (1.37)$$

$$\mathbf{Y} = \mathbf{P} \mathbf{L}, \quad \mathbf{T} = [\mathbf{E}^\top \quad \mathbf{F}^\top]^\top, \quad \mathbf{A}_L = \mathbf{A} - \mathbf{L} \mathbf{C} \text{ et } \boldsymbol{\eta} = \mathbf{E} - \mathbf{L} \mathbf{F}.$$

Ce résultat a été publié au Summer Workshop on Interval Methods (SWIM), 2019.

1.5.2 Estimation d’état à base de zonotopes pour les systèmes affines par morceaux

Considérons le système bi-modal affine par morceaux :

$$\mathbf{x}_{k+1} = \begin{cases} \mathbf{A}_1 \mathbf{x}_k + \mathbf{B} \mathbf{u}_k + \mathbf{E} \boldsymbol{\omega}_k & \text{si } \mathbf{r}^\top \mathbf{x}_k \leq d, \\ \mathbf{A}_2 \mathbf{x}_k + \mathbf{B} \mathbf{u}_k + \mathbf{E} \boldsymbol{\omega}_k & \text{si } \mathbf{r}^\top \mathbf{x}_k > d, \end{cases} \quad (1.38a)$$

$$\mathbf{y}_k = \mathbf{C} \mathbf{x}_k + \mathbf{F} \boldsymbol{\omega}_k. \quad (1.38b)$$

L’hyperplan défini par la condition de commutation $\mathbf{r}^\top \mathbf{x}_k = d$ sépare l’espace d’état du système en deux demi-espaces, dans lesquels, à chaque instant k , une des deux dynamiques est active. Ceci est représenté sur la Figure 1.3. Nous distinguons deux matrices d’évolution \mathbf{A}_1 et \mathbf{A}_2 , avec les paires $(\mathbf{C}, \mathbf{A}_1)$ et $(\mathbf{C}, \mathbf{A}_2)$ détectables et les paires $(\mathbf{A}_1, \mathbf{B})$ et $(\mathbf{A}_2, \mathbf{B})$ stabilisables. L’état initial appartient au zonotope $\mathcal{Z}(\mathbf{p}_0, \mathbf{H}_0)$, avec \mathbf{p}_0 le centre du zonotope et \mathbf{H}_0 la matrice des générateurs.

Ayant une estimation zonotopique pour l’état \mathbf{x}_k de la forme $\mathcal{Z}(\mathbf{p}_k, \mathbf{H}_k)$, avec $\bar{\mathbf{x}}_k = \mathbf{p}_k$ l’état estimé, le but de cette technique est de donner une estimation zonotopique pour \mathbf{x}_{k+1} de la forme $\mathcal{Z}(\mathbf{p}_{k+1}, \mathbf{H}_{k+1})$. À partir d’un

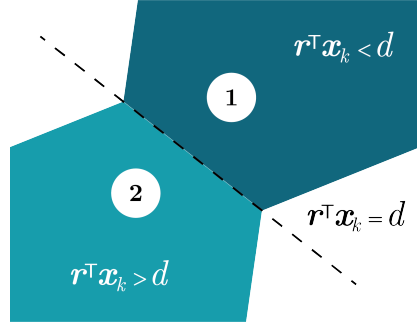


Figure 1.3 – Partitions de l'espace d'état

observateur de Luenberger pour le système (1.38), nous proposons la structure bi-modale suivante [Juloski et al., 2003] :

$$\bar{\mathbf{x}}_{k+1} = \begin{cases} \mathbf{A}_1 \bar{\mathbf{x}}_k + \mathbf{B} \mathbf{u}_k + \mathbf{L}_1 (\mathbf{y}_k - \mathbf{C} \bar{\mathbf{x}}_k) & \text{si } \mathbf{r}^\top \bar{\mathbf{x}} \leq d, \\ \mathbf{A}_2 \bar{\mathbf{x}}_k + \mathbf{B} \mathbf{u}_k + \mathbf{L}_2 (\mathbf{y}_k - \mathbf{C} \bar{\mathbf{x}}_k) & \text{si } \mathbf{r}^\top \bar{\mathbf{x}} > d. \end{cases} \quad (1.39)$$

L'observateur est déterminé pour que l'état estimé $\bar{\mathbf{x}}$ converge automatiquement vers \mathbf{x} . Le but est de trouver la même matrice $\mathbf{P} = \mathbf{P}^\top$ et les gains des observateurs \mathbf{L}_1 et \mathbf{L}_2 afin que les deux LMI représentant les deux conditions sur l'état réel soient vérifiées en même temps. En supposant connue la partition dans laquelle l'état réel se trouve et faisant l'hypothèse que l'état estimé se trouve dans cette même partition de l'espace d'état, les deux LMI suivantes doivent être vérifiées :

$$\begin{bmatrix} \beta \mathbf{P} & \mathbf{0} & \mathbf{A}_i^\top \mathbf{P} - \mathbf{C}^\top \mathbf{Y}_i^\top \\ * & \Theta^\top \Theta & \mathbf{E}^\top \mathbf{P} - \mathbf{F}^\top \mathbf{Y}_i^\top \\ * & * & \mathbf{P} \end{bmatrix} \succeq 0, \quad (1.40)$$

pour $i = 1, 2$.

1.6 Chapitre 7 : Filtre de Kalman à contraintes zonotopiques

Dans ce chapitre, le problème d'estimation d'état ensembliste est traité différemment. Nous proposons une nouvelle approche qui garantit que l'état, à chaque instant, se trouve dans un zonotope qui forme l'enveloppe de l'ensemble de contraintes appliquées sur l'état. Contrairement aux approches classiques, cette technique n'exige pas le calcul à chaque instant de l'intersection entre des ensembles. La nouveauté dans ce chapitre est l'introduction d'un algorithme dual efficace pour l'estimation d'état des systèmes dont l'état est potentiellement soumis à un grand nombre de contraintes.

1.6.1 Filtre de Kalman zonotopique à contraintes zonotopiques (ZCKF)

Considérons le système standard LTI suivant :

$$\begin{cases} \mathbf{x}_{k+1} = \mathbf{A}\mathbf{x}_k + \mathbf{B}\mathbf{u}_k + \mathbf{w}_k, \\ \mathbf{y}_k = \mathbf{C}\mathbf{x}_k + \mathbf{v}_k, \end{cases} \quad (1.41)$$

Ici, $\mathbf{w}_k \in \mathbb{R}^{n_x}$ et $\mathbf{v}_k \in \mathbb{R}^{n_y}$ sont des bruits blancs gaussiens avec zéro comme moyenne et respectivement, \mathbf{G}_w et \mathbf{G}_v comme covariances i.e. $\mathbf{w}_k \sim N(0, \mathbf{G}_w)$, $\mathbf{v}_k \sim N(0, \mathbf{G}_v)$. L'état est un vecteur Gaussien tel que l'état initial vérifie $\mathbf{x}_0 \sim N(\mathbf{x}_{0|-1}, \mathbf{G}_{0|-1})$. Toutefois, le filtre de Kalman classique ne peut pas prendre en considération les contraintes sur l'état. Nous supposons que l'état vérifie l'inégalité suivante :

$$\tilde{\mathbf{K}}\mathbf{x}_k \leq \tilde{\mathbf{c}}.$$

L'état final estimé est obtenu en résolvant le problème d'optimisation suivant:

$$\begin{aligned} \min_{\mathbf{x}_k \in \mathbb{R}^{n_x}} \quad & \|\mathbf{x}_k - \hat{\mathbf{x}}_{k|k}\|_{\mathbf{W}}^2 \\ \text{sous contraintes} \quad & \tilde{\mathbf{K}}\mathbf{x}_k \leq \tilde{\mathbf{c}}, \end{aligned} \quad (1.42)$$

avec \mathbf{W} une matrice symétrique définie positive. Dans la méthode présentée dans ce chapitre, l'état est projeté sur le zonotope formé par les contraintes auxquelles l'état est soumis.

Motivé par cette discussion, on rappelle qu'un zonotope est un polytope symétrique. De ce fait, résoudre un problème d'optimisation convexe contraint par un zonotope est équivalent à résoudre un problème d'optimisation soumis à des inégalités linéaires.

1.6.1.1 Travail préliminaire

Les problèmes d'optimisation peuvent être vus de deux perspectives, le problème primal ou le problème dual. Dans ce travail, nous considérons un problème d'optimisation de la forme :

$$\begin{aligned} J^* = \min_{\mathbf{u} \in \mathcal{U}} \quad & J_u(\mathbf{u}) \\ \text{s.c.} \quad & \mathbf{R}\mathbf{u} - \mathbf{p} = \mathbf{0}. \end{aligned} \quad (1.43)$$

La fonction duale [Nesterov, 2005] peut s'écrire :

$$f(\boldsymbol{\alpha}) = \max_{\mathbf{u} \in \mathcal{U}} \langle \boldsymbol{\alpha}, \mathbf{R}\mathbf{u} - \mathbf{p} \rangle - J_u(\mathbf{u}) \quad (1.44)$$

et

$$\mathbf{u}(\boldsymbol{\alpha}) = \arg \max_{\mathbf{u} \in \mathcal{U}} \langle \boldsymbol{\alpha}, \mathbf{R}\mathbf{u} - \mathbf{p} \rangle - J_u(\mathbf{u}). \quad (1.45)$$

Cette formulation nous permet d'utiliser la propriété suivante.

Propriété 1.1. [Nesterov, 2005] Supposons que $J_u(\cdot)$ est une fonction strictement convexe ayant pour matrice hessienne :

$$\frac{\partial^2 J_u(\mathbf{u})}{\partial \mathbf{u}^2} \succeq \mathbf{S} \succ 0 \quad (1.46)$$

et que \mathcal{U} est un ensemble convexe. Alors, en utilisant la notation :

$$\bar{\mathbf{u}} = \mathbf{u}(\bar{\boldsymbol{\alpha}}) = \arg \max_{\mathbf{u} \in \mathcal{U}} \langle \bar{\boldsymbol{\alpha}}, \mathbf{R}\mathbf{u} - \mathbf{p} \rangle - J_u(\mathbf{u}), \quad (1.47)$$

la relation suivante est vérifiée :

$$f(\boldsymbol{\alpha}) \leq f(\bar{\boldsymbol{\alpha}}) + \langle \mathbf{R}\bar{\mathbf{u}} - \mathbf{p}, \Delta\boldsymbol{\alpha} \rangle + \frac{1}{2} \Delta\boldsymbol{\alpha}^\top \mathbf{R}\mathbf{S}^{-1}\mathbf{R}^\top \Delta\boldsymbol{\alpha}, \quad (1.48)$$

avec $\Delta\boldsymbol{\alpha} = \boldsymbol{\alpha} - \bar{\boldsymbol{\alpha}}$.

1.6.1.2 Solution algorithmique

Le problème d'optimisation du filtre de Kalman contraint est :

$$\begin{aligned} \min_{\mathbf{z}, \mathbf{w}} \quad & J_{z,w}(\mathbf{z}, \mathbf{w}) \\ \text{s.c.} \quad & \mathbf{z} = \mathbf{p} + \mathbf{H}\mathbf{w}, \\ & \|\mathbf{w}\|_\infty \leq 1, \end{aligned} \quad (1.49)$$

avec la fonction de coût définie par :

$$\begin{aligned} J_{z,w}(\mathbf{z}, \mathbf{w}) &= J_z(\mathbf{z}) + \frac{\epsilon}{2} \mathbf{w}^\top \mathbf{w} \\ &= \frac{1}{2} \|\mathbf{z} - \hat{\mathbf{x}}_{k|k}\|_{\mathbf{G}_{k|k}^{-1}}^2 + \frac{\epsilon}{2} \mathbf{w}^\top \mathbf{w}. \end{aligned} \quad (1.50)$$

et la matrice hessienne :

$$\mathbf{S} = \text{diag}(\mathbf{G}_{k|k}^{-1}, \epsilon \mathbf{I}_m). \quad (1.51)$$

Le problème d'optimisation (1.49) peut être divisé en deux problèmes d'optimisation indépendants tels que :

$$u(\boldsymbol{\alpha}) = \begin{bmatrix} \mathbf{z}(\boldsymbol{\alpha}) \\ \mathbf{w}(\boldsymbol{\alpha}) \end{bmatrix} = \begin{bmatrix} \arg \max_{\mathbf{z} \in \mathbb{R}^{n_z}} \langle \boldsymbol{\alpha}, \mathbf{z} \rangle - J_z(\mathbf{z}) \\ \arg \max_{\|\mathbf{w}\|_\infty \leq 1} -\langle \boldsymbol{\alpha}, \mathbf{H}\mathbf{w} \rangle - \frac{\epsilon}{2} \mathbf{w}^\top \mathbf{w} \end{bmatrix}. \quad (1.52)$$

La variable \mathbf{z} soumise aux inégalités linéaires formant le zonotope en mode primal, appartient à l'ensemble des nombres réels en mode dual. En d'autres termes, le nombre de variables de décision ne dépend plus du nombre des contraintes, mais plutôt de la dimension de l'espace d'état qui est généralement plus petite.

1.6.1.3 Détails de calcul

En résolvant le premier problème d'optimisation du premier ordre de l'équation (1.52), nous obtenons :

$$\mathbf{z}_j = \mathbf{G}_{k|k} \boldsymbol{\alpha}_j + \hat{\mathbf{x}}_{k|k}. \quad (1.53)$$

De plus, nous considérons la notation suivante :

$$\mathbf{w}_j = \mathbf{w}(\boldsymbol{\alpha}_j) = \begin{bmatrix} w_j(1) & w_j(2) & \dots & w_j(m) \end{bmatrix}^\top. \quad (1.54)$$

En considérant la contrainte $|w_j(i)| \leq 1$ pour chaque composante de \mathbf{w} avec $i = 1, \dots, m$, nous avons :

$$w_j(i) = \begin{cases} -\frac{1}{\epsilon} \boldsymbol{\alpha}_j^\top \mathbf{h}_i, & \text{si } |\frac{1}{\epsilon} \boldsymbol{\alpha}_j^\top \mathbf{h}_i| \leq 1 \\ 1, & \text{si } -\frac{1}{\epsilon} \boldsymbol{\alpha}_j^\top \mathbf{h}_i > 1 \\ -1 & \text{si } -\frac{1}{\epsilon} \boldsymbol{\alpha}_j^\top \mathbf{h}_i < -1 \end{cases} \quad (1.55)$$

En utilisant la Propriété 1.1, la valeur de $\Delta \boldsymbol{\alpha}_j$ à chaque itération j est donnée par l'expression :

$$\Delta \boldsymbol{\alpha}_j = (\mathbf{R} \mathbf{S}^{-1} \mathbf{R}^\top)^{-1} (\mathbf{p} + \mathbf{H} \mathbf{w}_j - \mathbf{z}_j). \quad (1.56)$$

Cette norme fournit une condition de sortie pour l'algorithme. En effet, si la norme de $\mathbf{p} + \mathbf{H} \mathbf{w}_{j-1} - \mathbf{z}_{j-1}$ est petite, la paire $(\mathbf{w}_{j-1}, \mathbf{z}_{j-1})$ est proche de l'optimalité car le gradient au point $\boldsymbol{\alpha}_{j-1}$ est presque nul. Les équations (1.53)-(1.56) sont indispensables pour la conception des algorithmes du filtre de Kalman à contraintes zonotopiques.

1.6.2 Algorithme ISTA

La particularisation de l'algorithme Iterative Shrinkage Thresholding Algorithm (ISTA) pour le problème d'optimisation dual adapté dans ce chapitre est donnée ci-dessous.

Algorithme 1 ISTA appliqué à (1.49)

Entrée : $\hat{\mathbf{x}}_{k|k}, \mathbf{H}, \mathbf{p}$.

Sortie : $\mathbf{p} + \mathbf{H} \mathbf{w}_{j-1}$.

- 1: **Initialisation :** $j = 1, \boldsymbol{\alpha}_1 = \mathbf{0}, \mathbf{z}_0 = \hat{\mathbf{x}}_{k|k}, \mathbf{w}_0 = \mathbf{0}$.
 - 2: **Tant que** $\|\mathbf{z}_{j-1} - \mathbf{p} - \mathbf{H} \mathbf{w}_{j-1}\| > \mu$ **faire**
 - 3: Calcul de \mathbf{z}_j et \mathbf{w}_j , à partir de (1.53) et (1.55), respectivement.
 - 4: Calcul de $\Delta \boldsymbol{\alpha}_j$ à partir de (1.56).
 - 5: $\boldsymbol{\alpha}_{j+1} = \boldsymbol{\alpha}_j + \Delta \boldsymbol{\alpha}_j$.
 - 6: $j = j + 1$.
 - 7: **retourner** $\mathbf{p} + \mathbf{H} \mathbf{w}_{j-1}$.
-

L'avantage de cet algorithme est sa simplicité. Toutefois, il est reconnu dans la littérature comme étant lent.

1.6.3 FISTA

Fast Iterative Shrinkage Thresholding Algorithm (FISTA) est une version plus rapide de l'algorithme ISTA. Sa simplicité et sa rapidité font de lui un algorithme convenable pour les applications réelles en ligne. La différence entre les deux algorithmes se trouve au niveau du calcul du gradient de la fonction duale. Dans l'algorithme FISTA, α_{j+1} est calculé comme une combinaison linéaire entre deux valeurs d'une variable auxiliaire η_j [Beck and Teboulle, 2009]. De plus, la vitesse de convergence de l'algorithme ISTA est évaluée à $\mathcal{O}(\frac{1}{j})$ tandis que la vitesse de convergence de FISTA est $\mathcal{O}(\frac{1}{j^2})$ [Beck and Teboulle, 2009].

Algorithme 2 FISTA appliqué à (1.49)

Entrée : $\hat{\mathbf{x}}_{k|k}, \mathbf{H}, \mathbf{p}$.

Sortie : $\mathbf{p} + \mathbf{H}\mathbf{w}_{j-1}$.

- 1: **Initialisation :** $j = 1, \alpha_1 = \mathbf{0}, \mathbf{z}_0 = \hat{\mathbf{x}}_{k|k}, \mathbf{w}_0 = \mathbf{0}, \eta_0 = \mathbf{0}, t_j = 1$.
 - 2: **Tant que** $\|\mathbf{z}_{j-1} - \mathbf{p} - \mathbf{H}\mathbf{w}_{j-1}\| > \mu$ **faire**
 - 3: Calcul de \mathbf{z}_j et \mathbf{w}_j à partir de (1.53) et (1.55), respectivement.
 - 4: Calcul de $\Delta\alpha_j$ à partir de (1.56).
 - 5: $\eta_j = \alpha_j + \Delta\alpha_j$.
 - 6: $t_{j+1} = 0.5(1 + \sqrt{1 + 4t_j^2})$.
 - 7: $\alpha_{j+1} = \eta_j + \frac{t_j - 1}{t_{j+1}}(\eta_j - \eta_{j-1})$.
 - 8: $j = j + 1$.
 - 9: **retourner** $\mathbf{p} + \mathbf{H}\mathbf{w}_{j-1}$.
-

La vitesse de cet algorithme peut être améliorée en proposant une étape supplémentaire au ZCKF qui réduit la taille du zonotope initial. Cette étape supplémentaire est proposée dans l'extension du filtre de Kalman à contraintes zonotopiques.

1.6.4 Extension du filtre de Kalman à contraintes zonotopiques (EZCKF)

Quand le problème d'optimisation convexe (1.49) est appliqué sur un système de grande taille, le nombre de variables de décision sera grand. Le but de

cette méthode est de réduire le temps de calcul de l'algorithme présenté en utilisant au début un zonotope réduit, c'est à dire un zonotope avec un nombre réduit de générateurs. En effet, il est plus convenable pour le temps de calcul d'itérer l'algorithme sur un zonotope réduit que sur le zonotope initial.

Dans ce contexte, l'algorithme doit trouver un zonotope réduit que nous appelons par la suite *zonotope non fixe*. Par conséquent, on divise le zonotope en deux zonotopes indépendents selon une classification de sa matrice de générateurs \mathbf{H} . Le premier zonotope est un zonotope qui est fixe tandis que le deuxième est un zonotope non fixe sur lequel l'algorithme est appliqué. En détails, les générateurs de la matrice \mathbf{H} sont classés selon cet ordre :

$$\mathbf{H} = \begin{bmatrix} \mathbf{h}_1 & \mathbf{h}_2 & \dots & \mathbf{h}_m \end{bmatrix},$$

de sorte que :

$$\left| \frac{1}{\epsilon} \boldsymbol{\alpha}_j^\top \mathbf{h}_1 \right| \leq \left| \frac{1}{\epsilon} \boldsymbol{\alpha}_j^\top \mathbf{h}_2 \right| \leq \dots \leq \left| \frac{1}{\epsilon} \boldsymbol{\alpha}_j^\top \mathbf{h}_m \right|.$$

Le nouveau *zonotope non fixe* est $\mathcal{Z}(\mathbf{p}_{new}, \mathbf{H}_{nf})$ avec :

$$\mathbf{H}_{nf} = \begin{bmatrix} \mathbf{h}_1 & \mathbf{h}_2 & \dots & \mathbf{h}_l \end{bmatrix}, \quad (1.57)$$

$$\mathbf{w}_{nf} = \begin{bmatrix} \mathbf{w}_1 & \mathbf{w}_2 & \dots & \mathbf{w}_l \end{bmatrix}, \quad (1.58)$$

formé par les l premiers générateurs ($l < m$), avec un nouveau centre \mathbf{p}_{new} , obtenu par une simple translation de l'ancien centre du zonotope tel que :

$$\mathbf{p}_{new} = \mathbf{p} + \mathbf{H}_f \mathbf{w}_f, \quad (1.59)$$

avec :

$$\mathbf{H}_f = \begin{bmatrix} \mathbf{h}_{l+1} & \mathbf{h}_{l+2} & \dots & \mathbf{h}_m \end{bmatrix}, \quad (1.60)$$

$$\mathbf{w}_f = \begin{bmatrix} \mathbf{w}_{l+1} & \mathbf{w}_{l+2} & \dots & \mathbf{w}_m \end{bmatrix}. \quad (1.61)$$

Une fois le zonotope choisi, l'algorithme itère sur le nouveau zonotope $\mathcal{Z}(\mathbf{p}_{new}, \mathbf{H}_{nf})$ pour trouver une solution. L'algorithme devient :

Algorithme 3 FISTA réduit appliqué à (1.49)**Entrée** : $\mathbf{z}_{Kalman}, \mathbf{H}, \mathbf{p}$ **Sortie** : α_k

- 1: **Initialisation** : $k = 1, \alpha_1 = \mathbf{0}$
- 2: Décomposer le zonotope initial $\mathcal{Z}(\mathbf{p}, \mathbf{H})$ et trouver $\mathbf{H}_f, \mathbf{w}_f, \mathbf{H}_{nf}, \mathbf{w}_{nf}$, en utilisant (1.60), (1.61), (1.57), (1.58), respectivement.
- 3: **Si** \mathbf{H}_f n'est pas vide **alors**
- 4: $\mathbf{p}_{new} = \mathbf{p} + \mathbf{H}_f \mathbf{w}_f$
- 5: **Tant que** $\|\mathbf{z}_{j-1} - \mathbf{p}_{new} - \mathbf{H} \mathbf{w}_{j-1}\| > \mu$ **faire**
- 6: Calcul de \mathbf{z}_j et \mathbf{w}_j en utilisant (1.53) et (1.55), respectivement.
- 7: Calcul de $\Delta \alpha_j$ à partir de (1.56).
- 8: $\boldsymbol{\eta}_j = \alpha_j + \Delta \alpha_j$.
- 9: $t_{j+1} = 0.5(1 + \sqrt{1 + 4t_j^2})$.
- 10: $\alpha_{j+1} = \boldsymbol{\eta}_j + \frac{t_j - 1}{t_{j+1}}(\boldsymbol{\eta}_j - \boldsymbol{\eta}_{j-1})$.
- 11: $j = j + 1$.
- 12: **retourner** $\mathbf{p} + \mathbf{H} \mathbf{w}_{j-1}$.

Les algorithmes précédents ont été testés sur des systèmes académiques avec un nombre important de contraintes. Le ZCKF a été présenté à la 57ème Conférence on Decision and Control (CDC), 2018. L'extension du filtre de Kalman à contraintes zonotopiques fera partie d'un article de journal à soumettre à Automatica.

1.7 Chapitre 8 : Conclusion et perspectives

Dans cette thèse, le problème d'estimation d'état, en particulier l'estimation d'état ensembliste, est traité. Dans ce contexte, nous proposons de nouvelles approches ellipsoïdales et zonotopiques pour l'estimation d'état pour différentes classes de systèmes linéaires. Les principales contributions de cette thèse peuvent être divisées en deux parties :

- Dans la première partie, une extension d'une technique d'estimation d'état ellipsoïdale existant dans la littérature est proposée pour être appliquée sur modèle d'ocrotor dans un contexte radar. Une extension de cette approche ellipsoïdale d'estimation d'état est proposée pour des systèmes descripteurs.
- Dans la deuxième partie, une méthode fondée sur la minimisation du \mathbf{P} -rayon d'un zonotope est proposée, puis étendue pour traiter un cas

particulier des systèmes affines par morceaux. De plus, dans le dernier chapitre, le problème de l'estimation d'état ensembliste est traité différemment des approches classiques. Un nouveau filtre de Kalman à contraintes zonotopiques qui combine la bonne précision de l'estimation d'état zonotopique et la complexité réduite du filtre de Kalman classique est présenté. La complexité du filtre est ensuite améliorée en remplaçant le zonotope initial par un zonotope réduit.

Ce travail peut être étendu en considérant plusieurs propositions. Une perspective intéressante de la première partie sera de considérer que le vecteur de perturbations dans la première partie appartient à un ellipsoïde pour éviter l'énumération des sommets. Une deuxième perspective sera d'étendre la méthode zonotopique fondée sur un observateur de Luenberger pour une représentation générale des systèmes affines par morceaux. D'autre part, le filtre de Kalman à contraintes zonotopiques représente une étape initiale prometteuse pour l'estimation d'état des systèmes de grande taille. Il sera intéressant de valider les méthodes d'estimation et les algorithmes sur un système réel.

Chapter 2

Introduction

2.1 Context and motivations

Today, people have a better life thanks, in large part, to the advances in technology. The impact of new technologies in numerous fields is apparent in the way people lead their lives, understand the world and run their businesses. From smart-phones to smart houses and autonomous vehicles, the control of industrial processes became a need to increase reliability, efficiency, and security while reducing design and production's costs.

Tremendous scientific advances have been made in numerous directions including drones, rovers exploring Mars, smart houses, smartphones, artificial intelligence, etc. However, in most of these applications, common issues can occur in particular in *fault detection* and *control* related aspects. Indeed, malfunctions should be taken into account to avoid a potentially disastrous impact on the evolution of any system. This is done by finding a control law such that the system can operate in a tolerable way in such cases. By definition, a state feedback controller compares a measured value of a system state (when the entire state is available) with a desired value, and processes the resulting error signal to change the system's input, in such a way that the system maintains its set-point despite possible disturbances and measurement noises coming from different sources. If (part of) the system state is not measurable, then it has to be estimated. Thus, the process of state estimation becomes a primordial step before dealing with the control law. However, the importance and challenges of state estimation are often underrated in research and industry, therefore it is crucial to put it on an equal footing with control problems.

The state of a system is a set of quantities (e.g. position, velocity, and orientation) that, if known, fully describe the system's dynamics over time.

Therefore *the goal* of this thesis is to focus on the advancements done in the field of state estimation in control engineering.

The state estimation theory is not recent. Centuries ago, sailors were faced to the problem of estimating the ship's position while sailing. The advent of estimation tools later on, in particular the compass, allowed to have measurements for the sake of navigation. Gradually, instruments were invented to measure angles, latitudes and so on.

However, it was not until the nineteenth century that the German mathematician Gauss set the grounds for a new class of state estimation techniques [Sorenson, 1970]. Gauss proved that his least-squares technique [Gauss, 1857] is optimal under the assumption of normally distributed errors. Later on, in 1960, Kalman revolutionized the state estimation field by introducing a filter [Kalman, 1960] suitable for the state estimation of linear systems assuming the knowledge of the characteristics (i.e. Gaussian distribution) of perturbations and noises governing the state and the measurements. Due to its accuracy and easy implementation, the Kalman filter has been the main technique of estimation in various industrial fields suchlike navigation [Hoshino et al., 1996], finance [Manoliu and Tompaidis, 2002], pharmaceutical applications [Hassan et al., 1999], radar imaging [Chevet et al., 2017] and many more. It was used for the first time by the National Aeronautics and Space Administration (NASA), in its Apollo program for accurate position estimation above the lunar surface, taking into account possible disturbances and noisy radar measurements [Smith and Schmidt, 1961]. Many incremental improvements were then done on the classical Kalman filter to deal with real time systems, thus the introduction of the extended Kalman filter [Schmidt, 1966], [McElhoe, 1966], the unscented Kalman filter [Wan and Merwe, 2000], Bucy-Kalman filter [Kalman and Bucy, 1961] etc. These techniques belong to the class of stochastic approaches for state estimation, since they tend to assume the knowledge of the characteristics of noises and perturbations [Kalman, 1960].

Alternatively, the deterministic approaches [Schweppe, 1968] seem more realistic, by considering unknown but bounded perturbations and measurement noises. In this context, several approaches were elaborated, like interval observers [Efimov et al., 2013], [Raïssi et al., 2011], [Pourasghar et al., 2016] where the state estimation set is approximated by its interval hull. In these approaches, no statistical assumptions needed, the evolution of the system state is described by a set. Extensively, the set-membership state estimation approaches [Alamo et al., 2008a], [Bertsekas and Rhodes, 1971a] find at each time instant an estimated set containing all the possible states consistent with the model, the measurements, the possible perturbations and uncertainties that the system is subject to. Among the geometrical

sets used in the implementation of these approaches are parallelotopes [Koustousova, 2011], [Chisci et al., 1996], polytopes [Walter and Piet-Lahanier, 1989], [Barmish and Sankaran, 1979], zonotopes [Combastel, 2003], [Alamo et al., 2005], [Le et al., 2013b], [Combastel, 2006], ellipsoids [Kurzhanski and Vályi, 1996], [Durieu et al., 2001], [Polyak et al., 2004], [Daryin et al., 2006], [Daryin and Kurzhanski, 2012] and many more. Later on, to benefit from the set advantages, a combined technique between zonotopes and ellipsoids [Ben Chabane et al., 2014b] was proposed. Furthermore, a Gaussian and a zonotopic Kalman filters (ZGKF) are merged to have a robust state estimator for fault detection under noisy measurements that can be efficiently designed [Combastel, 2015b]. The non exhaustive workflow in Figure 2.1 summarizes the overall state estimation work in literature. It also highlights the major contributions made to combine the advantages of either two sets (i.e. the technique combining zonotopes and ellipsoids in red) or two approaches (i.e. the zonotopic Kalman filter (ZKF) merging between the stochastic and the deterministic approaches).

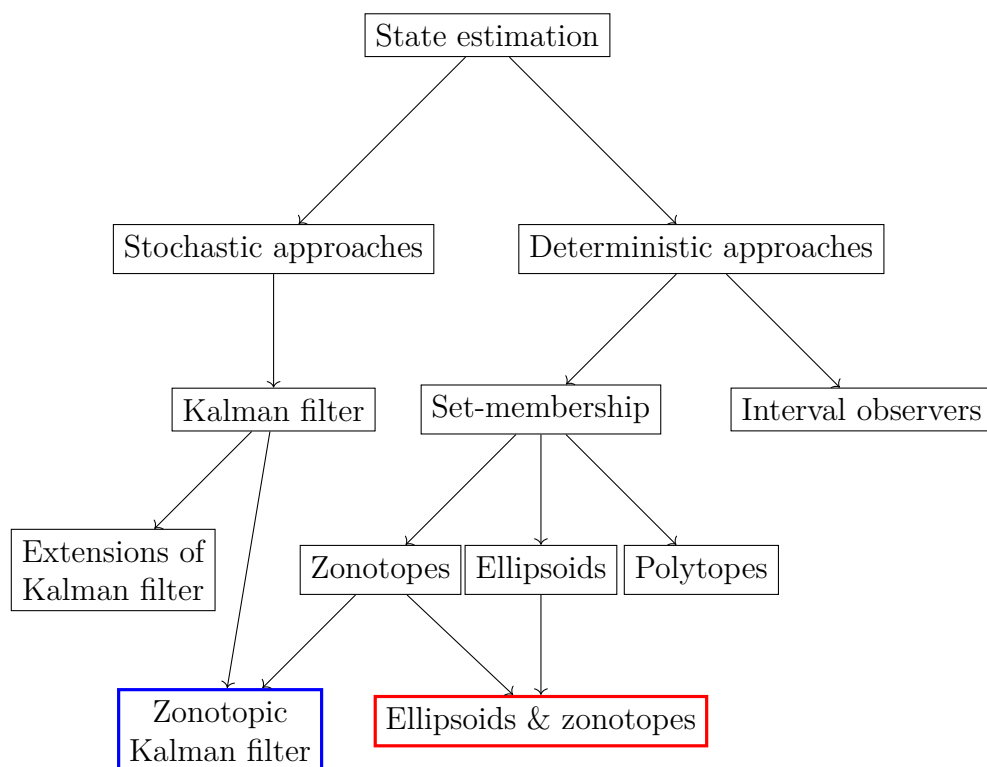


Figure 2.1 – State estimation approaches

The goal of this thesis is to answer to a significant problem in the auto-

matic control field: the state estimation for uncertain systems in the presence of perturbations, measurements noises and state constraints, based on the set-membership approach. Uncertainties acting on the system are considered unknown but bounded by known sets in particular zonotopes or ellipsoids.

This thesis builds upon previous results on the ellipsoidal [Ben Chabane, 2015] and zonotopic [Le et al., 2013a] set-membership state estimation techniques. Firstly, a comparison between two state estimation techniques in the literature in terms of accuracy and computation complexity is made: an ellipsoidal set-membership state estimation technique [Ben Chabane et al., 2014a] and the classical Kalman filter [Kalman, 1960]. Moreover, the ellipsoidal technique developed in [Ben Chabane, 2015] is further developed to consider the system inputs, then applied to a model of an octorotor used for radar applications [Makarov et al., 2015], [Makarov et al., 2016]. Then, a new class of systems is further analyzed. A new ellipsoidal approach, extended from previous work [Ben Chabane et al., 2014a], is proposed for linear time invariant descriptor systems where physical equality constraints are considered in the system's dynamics. Alternatively, the thesis details a new zonotopic set-membership state estimation technique for piecewise affine systems (PWA) with bounded perturbations and bounded measurement noises. Finally, a combined method between the stochastic approach and the deterministic approach is presented to highlight the advantages of both techniques. A zonotopic constrained Kalman filter is designed to guarantee that the state estimate belongs at each time instant to a defined zonotope. This zonotope is no other than the envelope of the set of inequality constraints applied on the system state at each time instant. To resume, the thesis deals with different class of systems (standard and descriptor systems) and two main sets used in state estimation (zonotopes and ellipsoids). Additionally, the set of equality/inequality constraints applied on the system state are treated in this thesis, either by considering descriptor systems or by using zonotopes as a form of envelope of these constraints.

2.2 Contribution

The thesis is made up of seven chapters in total illustrated in Figure 2.2. The main contributions of the remaining chapters are highlighted in this section.

- **Chapter 3:** This chapter starts with a brief summary of the deterministic and stochastic approaches in terms of uncertainties, disturbances and noises representations. Then, some basic definitions and properties needed to manipulate matrices and important operations for sets are given. Additionally, the chapter analyzes the most used convex sets

to represent uncertainties in deterministic approaches, with their main properties, advantages and limits. Due to their convenience, zonotopes and ellipsoids are used in this thesis. Finally, a brief summary of convex optimization techniques is presented along with some results of Nesterov that will be further employed in the thesis.

Part I

- **Chapter 4:** In this chapter, an existing ellipsoidal set-membership state estimation technique, along with the classical Kalman filter are summarized, then compared in terms of computational complexity, number of operations per iteration and accuracy. The main advantage of the Kalman filter is its simplicity and low complexity while the technique based on ellipsoids offers better estimation accuracy, with guaranteed bounds. This result has been published to the 20th IFAC World Congress 2017. That being exposed, the set-membership state estimation technique based on ellipsoids is extended and then applied on a model of an octorotor used for radar applications in collaboration with SONDRALABORATORY. Using ellipsoidal representations, the proposed technique computes the set of states that are consistent with the drone model in a first phase and with the measurements provided by the sensors in a second phase such that the drone's position is guaranteed to belong to this set. Using the accurate estimation, an image reconstruction of the target is done and the relative error is used to find the operating frequency of the considered Unmanned Aerial Vehicle (UAV). These results have been submitted to the special issue on "Interval estimation applied to diagnosis and control" of the International Journal of Control.
- **Chapter 5:** In this chapter, several guaranteed ellipsoidal set-membership state estimation techniques are proposed for descriptor systems with bounded perturbations and measurement noises. These methods extend previous ellipsoidal set-membership state estimation techniques for linear time invariant (LTI) standard systems. For this, four methods are derived. In the context of uncertain descriptor systems, the first technique considers a constant observer gain that can be found by solving one linear matrix inequality (LMI) problem. This result has been published in the proceedings of the 23rd International Conference on System Theory, Control and Computing (ICSTCC) 2019. The second technique updates the observer gain at each time instant by online solving a LMI. In the third technique, a trade-off between complexity and accuracy is done by considering a vector scaling technique. This allows

us to reduce the computation time while keeping a good estimation accuracy. Finally, a fourth technique is revisited for uncertain linear time invariant descriptor systems, where the model of the system is subject to bounded uncertainties. This technique is further improved by taking into consideration the measurement strip at the next time instant, and applying quadratic constraints on the perturbation vector. These results are currently ongoing work to be submitted to Automatica.

Part II

- **Chapter 6:** In this chapter, zonotopic sets will be used due to their flexibility and low-complexity. The chapter starts by proposing a zonotopic set-membership state estimation technique for linear time invariant systems subject to unknown but bounded perturbations and measurements noises. The technique builds upon previous results in the literature on state estimation based on a Luenberger observer for descriptor systems. The \mathbf{P} -radius of the estimated zonotopic set is minimized to guarantee its non-increasing at each time instant. Next, this technique is applied to the same model of the octorotor detailed in Chapter 4. This work has been presented to Summer Workshop on Interval Methods (SWIM) 2019. In a second part, the chapter proposes a new zonotopic set-membership state estimation technique for a particular class of piecewise affine systems (PWA). The considered PWA systems are defined by partitioning the state-space into regions via state conditions and associating with each region a different observer and/or state update equation. Assuming the knowledge of the partition in which the system state is located and considering the assumption that the state estimation belongs to the same partition as the real state, the state estimation technique ensures that the state is guaranteed to belong to a zonotopic set despite the existence of perturbations and measurement noises. This is done by solving two LMIs in the case of bi-modal PWA systems.
- **Chapter 7:** Building upon the contributions in the previous chapters and considering the advantages and weak points of the proposed techniques, this chapter treats the set-membership state estimation approaches from a different perspective. A new zonotopic constrained Kalman filter (ZCKF) is proposed to guarantee that the state estimation belongs to a zonotope, which is no other than the envelope of the constraints applied on the system state. This filter combines the advantages of the stochastic and the deterministic approaches. It is different from the classical deterministic approaches because it doesn't

require the intersection between sets that usually causes high complexity. The new filter relies on an efficient optimization strategy that takes advantage of the special structure of the problem. The developed algorithm finds a better solution at each iteration, by advancing a step in the direction of the gradient of the dual function of the original optimization problem. The algorithm is a particularization of the iterative shrinkage-thresholding algorithm (ISTA). A faster version of the ISTA algorithm called FISTA is then used to reduce the simulation time which can be practical in large scale systems, when the system state is constrained by a large number of constraints. This work has been presented to the 57th IEEE Conference on Decision and Control (CDC) 2018. Next, a new step is introduced to reach faster convergence leading to an Extended Zonotopic Constrained Kalman Filter (EZCKF). Indeed, in the proposed EZCKF technique, the complexity reduction step leads to approximate the given zonotope by a lower order one, by limiting the number of generators at each time instant. Compared to classical optimization techniques and deterministic approaches, the proposed algorithm is faster and simpler to implement on large scale systems and real applications. This is the object of current work that will be submitted to *Automatica*.

- **Chapter 8:** Conclusion and future perspectives are presented in this chapter.

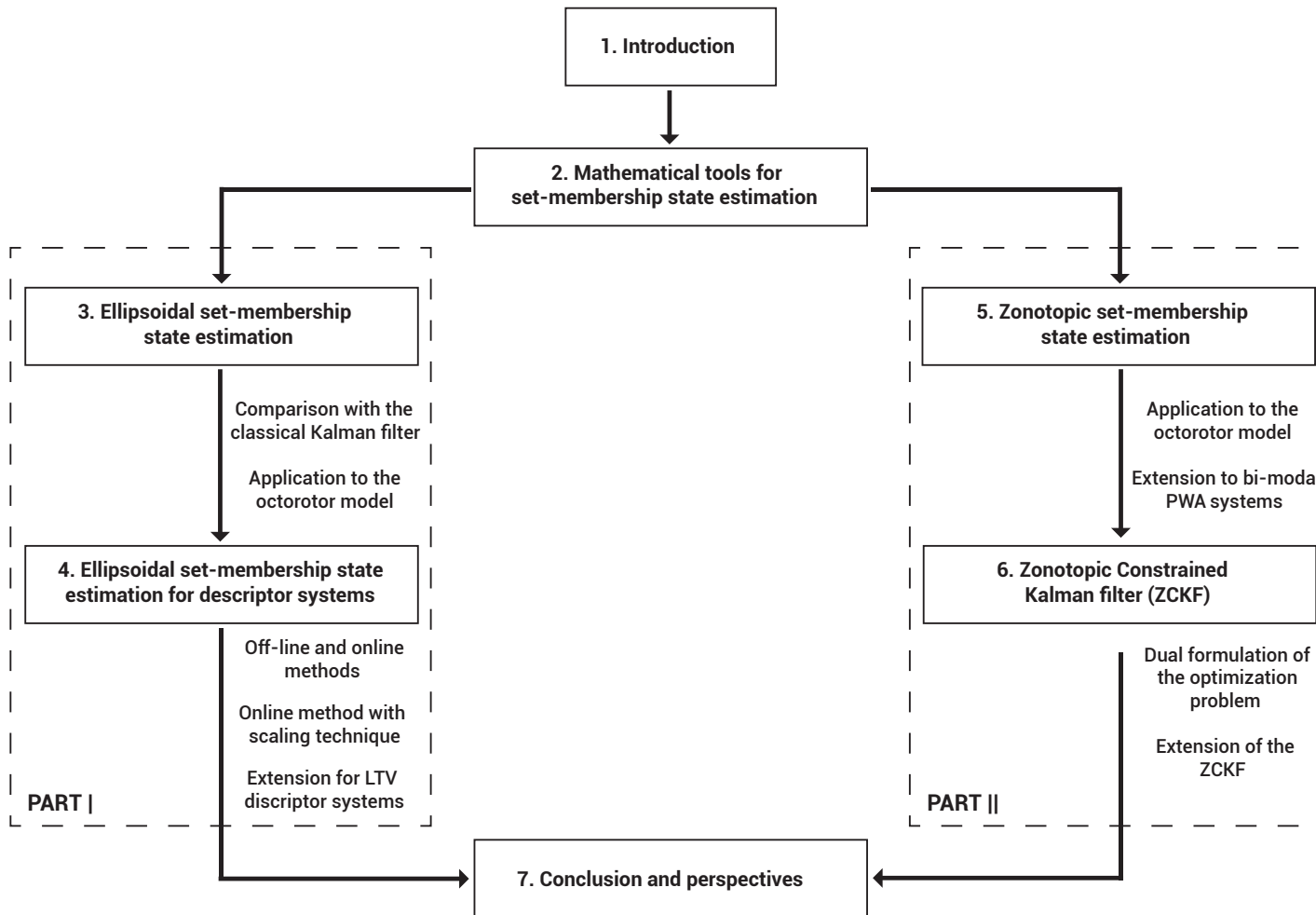


Figure 2.2 – Roadmap for the thesis

2.3 Publications

The thesis contributions resulted in several accepted/submitted/in progress publications to prestigious international conferences and journals.

Journal paper:

- **D. Merhy**, C. Stoica Maniu, T. Alamo, E. F. Camacho, S. Ben Chabane, T. Chevet, M. Makarov, and I. Hinostroza. Guaranteed set-membership state estimation of an octorotor's position for radar applications. *2nd submission to International Journal of Control*, special issue on "Interval estimation applied to diagnosis and control", 2019.

Conference and workshop papers:

- **D. Merhy**, C. Stoica Maniu, T. Alamo, E. F. Camacho and S. Ben Chabane. Comparison between two state estimation techniques for linear systems. *Preprints of the 20th World Congress of the International Federation of Automatic Control, Toulouse, France, pp. 4855-4859, July 9-14, 2017.*
- **D. Merhy**, T. Alamo, C. Stoica Maniu and E. F. Camacho. Zonotopic constrained Kalman filter based on a dual formulation. *Proceedings of the 57th IEEE Conference on Decision and Control, Miami, Florida, USA, pp. 6396-6401, December 17-19, 2018.*
- **D. Merhy**, C. Stoica Maniu, T. Alamo, E. F. Camacho, T. Chevet, M. Makarov, and I. Hinostroza. Zonotopic set-membership state estimation applied to an octorotor model. *Proceedings of the 12th Summer Workshop on Interval Methods, ENSTA Paristech, Palaiseau, France, July 23-26, 2019.*
- **D. Merhy**, C. Stoica Maniu, T. Alamo and E. F. Camacho. Ellipsoidal set-membership state estimation for descriptor systems. *Proceedings of the 23rd International Conference on System Theory, Control and Computing, Sinaia, Romania, October 9-11, 2019, Best Paper Award.*

Oral presentations:

- **D. Merhy**, C. Stoica Maniu, T. Alamo and E. F. Camacho. Estimation d'état à base d'un nouveau filtre de Kalman sous contraintes zonotopiques, *Journées de l'Automatique du GdR MACS, Nantes, France, November 15-16, 2018.*

- **D. Merhy**, C. Stoica Maniu, T. Alamo, E. F. Camacho, S. Ben Chabane, T. Chevet, M. Makarov, and I. Hinostroza. Set-membership state estimation of an octorotor applied to radar imaging, *Colloque de Recherche Inter-Ecoles Centrales*, Nantes, France, June 26, 2018.

Work in progress:

- **D. Merhy**, C. Stoica Maniu, T. Alamo and E. F. Camacho. Zonotopic constrained Kalman filter for large-scale systems. *to be submitted to Automatica*.
- **D. Merhy**, C. Stoica Maniu, T. Alamo and E. F. Camacho. Ellipsoidal set-membership state estimation for descriptor systems. *to be submitted to Automatica*.
- S. Ben Chabane, **D. Merhy**, C. Stoica Maniu, T. Alamo and E. F. Camacho. Guaranteed ellipsoidal set-membership state estimation for linear time-variant systems. *to be submitted to Systems & Control Letters*.
- **D. Merhy**, C. Stoica Maniu, T. Alamo and E. F. Camacho. Zonotopic set-membership state estimation for piecewise affine systems. *to be submitted as a journal paper*.

Chapter 3

Mathematical tools for set-membership state estimation

Contents

| | | |
|------------|---|-----------|
| 3.1 | Introduction | 39 |
| 3.2 | Matrices: definitions and properties | 41 |
| 3.3 | Set-theory preliminaries | 44 |
| 3.3.1 | Interval set | 46 |
| 3.3.2 | Ellipsoidal set | 48 |
| 3.3.3 | Polyhedral set | 50 |
| 3.3.4 | Zonotopic set | 53 |
| 3.4 | Convex optimization | 57 |
| 3.4.1 | Duality principle in convex optimization | 59 |
| 3.4.2 | Gradient-based methods for solving convex optimization problems | 60 |
| 3.5 | Conclusion | 61 |

3.1 Introduction

Dynamical systems are usually represented with a set of mathematical equations that represents the dynamics of the system as properly as possible. Based on the basic Physics laws, these models are used for analysis and

design of control systems. When modeling a system, a trade-off between the accuracy of the results of the analysis and the simplicity of the model is necessary.

In general, it is recommended to build a simplified model of a new system to get a general feeling of the solution when solving a new problem. Therefore, in this thesis, we mainly address systems belonging to the class of linear, finite dimensional, deterministic, multivariable, time-variant and time-invariant systems. Even though this class of systems seems restricted, it can model a large number of real time systems that we encounter in our daily life. Therefore, linearization techniques and identification procedures attracted more research attention from the scientific community to achieve good results, in simpler ways. However, sometimes standard linear systems are not enough to provide a complete representation of the linear system since for many physical systems, conservation laws (mass, volume, energy etc.) should be taken into account. This is done by employing a combination of differential and algebraic equations. In this thesis, we will refer to these systems by descriptor systems, that we will be detailing later. Another class of linear systems that will be detailed throughout this thesis is the piecewise affine systems (PWA). This category of systems partitions the state-space into regions using linear constraints and associates to each region a different linear (more generally affine) system.

No matter what type of linear model is chosen, the crucial problem is that the ideal mathematical model of the system does not match the behavior of the real system due to several reasons. In this context, one of the possible approaches on how to overcome this challenge is the use uncertain models. Uncertainties have been a central theme in the development of the automatic control field. Two ways exist in the literature to represent uncertainties: stochastic (statistical) approaches and deterministic approaches.

Stochastic approach: Uncertainties are represented by a random process assuming the knowledge of the statistical characteristics such as average, covariance, etc. [Kalman, 1960]. This applies to a large number of scientific fields like economy [Manoliu and Tompaidis, 2002], chemistry [Hassan et al., 1999], engineering [Chevet et al., 2017], [De Marina et al., 2011], [Salameh et al., 2018] and many more. However, for real systems, these assumptions tend to be sometimes unrealistic since the probability distribution of uncertain variables can not be known.

Deterministic approach: Uncertainties are assumed to be unknown but bounded. In general, they can be represented by convex sets: ellipsoids, polytopes, zonotopes, intervals and many more. The choice between the different families of classical sets depends on the accuracy and the complexity needed for each specific application. In this thesis, we only consider convex

sets because of their advantages in the theory of optimization, which we will briefly discuss in this chapter.

In the following parts, some of the useful tools for the deterministic estimation framework are detailed. First, some matrix and set related operations which are used in this thesis are introduced in the next section. Additionally, Section 3.3 highlights some popular convex sets in state estimation with their advantages and weaknesses. Section 3.4 presents some preliminaries for convex optimization. Finally, the last section draws the conclusion of the chapter.

3.2 Matrices: definitions and properties

Before going into the work details, we present in this section some of the basic matrix definitions and properties that will be used along the thesis in the design and development of set-membership state estimation techniques.

Definition 3.1. A *singular matrix* \mathbf{P} is a square matrix that does not have an inverse. In other terms, a matrix is singular if and only if its determinant is equal to 0.

Definition 3.2. A matrix $\mathbf{P} = \mathbf{P}^\top \in \mathbb{R}^{n \times n}$ is called a *strictly negative definite matrix* (respectively *strictly positive definite matrix*), denoted by $\mathbf{P} \prec 0$ (resp. $\mathbf{P} \succ 0$), if $\mathbf{z}^\top \mathbf{P} \mathbf{z} < 0$ (resp. $\mathbf{z}^\top \mathbf{P} \mathbf{z} > 0$) for all non-zero vectors \mathbf{z} with real entries ($\mathbf{z} \in \mathbb{R}^n \setminus \{\mathbf{0}_n\}$).

Definition 3.3. A matrix $\mathbf{P} = \mathbf{P}^\top \in \mathbb{R}^{n \times n}$ is called a *negative definite matrix* (respectively *positive definite matrix*), denoted by $\mathbf{P} \preceq 0$ (resp. $\mathbf{P} \succeq 0$), if $\mathbf{z}^\top \mathbf{P} \mathbf{z} \leq 0$ (resp. $\mathbf{z}^\top \mathbf{P} \mathbf{z} \geq 0$) for all non-zero vectors \mathbf{z} with real entries ($\mathbf{z} \in \mathbb{R}^n \setminus \{\mathbf{0}_n\}$).

Definition 3.4. The *Euclidean norm* denoted by $\|\mathbf{x}\|_{\mathbf{P}}^2$ is defined to be the quantity $\mathbf{x}^\top \mathbf{P} \mathbf{x}$, with $\mathbf{x} \in \mathbb{R}^n$, $\mathbf{P} \in \mathbb{R}^{n \times n}$ and $\mathbf{P} = \mathbf{P}^\top \succ 0$.

Definition 3.5. A *Linear Matrix Inequality* (LMI) is defined by the following formulation:

$$\mathbf{F}(\mathbf{x}) \triangleq \mathbf{F}_0 + \sum_{i=1}^n x_i \mathbf{F}_i \succ 0, \quad (3.1)$$

with the given matrices $\mathbf{F}_i = \mathbf{F}_i^\top \in \mathbb{R}^{m \times m}$, $i = 0, \dots, n$, and the *vector of decision variables* $\mathbf{x} = [x_1 \ x_2 \ \dots \ x_n]^\top \in \mathbb{R}^n$. The components x_i , $i = 1, \dots, n$, of this vector are called *scalar decision variables*.

Remark 3.1. The LMI $\mathbf{F}(\mathbf{x}) \succ 0$ can be rewritten as a set of scalar linear inequalities when the matrices \mathbf{F}_i , with $i = 0, \dots, m$, are diagonal.

Remark 3.2. The vector \mathbf{x} is constrained by the convex LMI (3.1), which means that the set $\{\mathbf{x} \in \mathbb{R}^n : \mathbf{F}(\mathbf{x}) \succ 0\}$ is convex (see *Definition 3.7* of convexity).

Two main problems related to LMIs are considered in this thesis:

1. *Feasibility problem:* Does a solution $\mathbf{x} \in \mathbb{R}^n$ exist such that the LMI $\mathbf{F}(\mathbf{x}) \succ 0$ is feasible?
2. *Eigenvalue optimization problem:* It consists on minimizing the maximum eigenvalue of a matrix that depends on a variable in an affine way, subject to LMI constraints:

$$\begin{aligned} \min_{\mathbf{x}, \lambda} \lambda \\ \text{subject to } \lambda \mathbf{I}_n - \mathbf{A}(\mathbf{x}) \succ 0, \\ \mathbf{B}(\mathbf{x}) \succ 0, \end{aligned} \quad (3.2)$$

where $\mathbf{A} \in \mathbb{R}^{n \times n}$ and $\mathbf{B} \in \mathbb{R}^{n \times n}$ are two symmetric matrices affinely dependent on the optimization variable \mathbf{x} . This problem can be rewritten in an equivalent form:

$$\begin{aligned} \min_{\mathbf{x}, \lambda} \lambda \\ \text{subject to } \mathbf{C}(\mathbf{x}, \lambda) \succ 0, \end{aligned} \quad (3.3)$$

where \mathbf{C} is affine both in \mathbf{x} and λ . The problem (3.3) is a LMI optimization problem.

Remark 3.3. Any LMI problem can be solved numerically by using the appropriate LMI solver. The Matlab/Robust Control ToolboxTM software has a special computational engine for LMI with two main solvers: `feasp` for feasibility problems and `mincx` for general optimization problems. On the market there exist several modeling tools for optimization problems among which CVX [Grant and Boyd, 2014] and YALMIP [Lofberg, 2004]. Among the toolboxes relying on YALMIP is the Multi-Parametric Toolbox (MPT), an open source toolbox that can be used for parametric optimization. The latter toolbox contains also a modeling of dynamical systems module, that features a powerful geometric library used in various problems from estimation to control [Herceg et al., 2013].

Property 3.1. *Schur complement.* [Boyd et al., 1994], [Scherer and Weiland, 2007] Consider the following LMI:

$$\begin{bmatrix} \mathbf{Q}(\mathbf{x}) & \mathbf{S}(\mathbf{x}) \\ \mathbf{S}^\top(\mathbf{x}) & \mathbf{R}(\mathbf{x}) \end{bmatrix} \succ 0, \quad (3.4)$$

where $\mathbf{Q}(\mathbf{x})$, $\mathbf{R}(\mathbf{x})$ are symmetric matrices and $\mathbf{Q}(\mathbf{x})$, $\mathbf{R}(\mathbf{x})$ and $\mathbf{S}(\mathbf{x})$ are affine in \mathbf{x} . Then this LMI is equivalent to:

$$\begin{cases} \mathbf{Q}(\mathbf{x}) \succ 0, \\ \mathbf{Q}(\mathbf{x}) - \mathbf{S}(\mathbf{x})\mathbf{R}^{-1}(\mathbf{x})\mathbf{S}^\top(\mathbf{x}) \succ 0, \end{cases} \quad (3.5)$$

or

$$\begin{cases} \mathbf{R}(\mathbf{x}) \succ 0, \\ \mathbf{R}(\mathbf{x}) - \mathbf{S}^\top(\mathbf{x})\mathbf{Q}^{-1}(\mathbf{x})\mathbf{S}(\mathbf{x}) \succ 0. \end{cases} \quad (3.6)$$

Definition 3.6. A *Bilinear Matrix Inequality* (BMI) is defined by the following expression:

$$\mathbf{F}(\mathbf{x}) = \mathbf{F}_0 + \sum_{i=1}^n x_i \mathbf{F}_i + \sum_{i=1}^n \sum_{j=1}^l x_i x_j \mathbf{F}_{ij} \succ 0, \quad (3.7)$$

where \mathbf{x} is the vector of decision variables and \mathbf{F}_0 , \mathbf{F}_i , $\mathbf{F}_{ij} \in \mathbb{R}^{l \times l}$, with $i = 1, \dots, n$ and $j = 1, \dots, l$, are given symmetric matrices.

Remark 3.4. When it comes to solving BMIs, the computational complexity grows in an ascending order when the bilinearity concerns the product between:

1. two scalar decision variables;
2. a scalar decision variable and a matrix decision variable;
3. two matrices decision variables.

Remark 3.5. A BMI can be solved numerically by calling the solver `penbmi` of PENOPT. Together with the YALMIP parser, `penbmi` provides an efficient tool for solving many problems of optimal control. The first two cases of the previous remark can be solved easily with Matlab, however for the third case the `penbmi` solver is needed. Despite the efficiency of these solvers, more powerful BMI solvers are still needed in research.

Remark 3.6. With the definition of the Schur complement, the nonlinear matrix inequalities (3.5) or (3.6) can be converted to a LMI problem (3.4). This is then one of the techniques making the conversion of BMIs to LMIs possible.

Property 3.2. *S-procedure.* [Boyd et al., 1994] Let F_0, \dots, F_p be quadratic functions of variable $\zeta \in \mathbb{R}^n$:

$$F_i(\zeta) \triangleq \zeta^\top \mathbf{T}_i \zeta + 2\boldsymbol{\mu}_i^\top \zeta + v_i,$$

with $i = 0, \dots, p$, $v_i \in \mathbb{R}$ and $\mathbf{T}_i = \mathbf{T}_i^\top \in \mathbb{R}^{n \times n}$. If

$$\exists \tau_i \geq 0, i = 1, \dots, p, \text{ such that } F_0(\zeta) - \sum_{i=1}^p \tau_i F_i(\zeta) \geq 0 \quad (3.8)$$

then

$$F_0(\zeta) \geq 0 \text{ for all } \zeta \text{ such that } F_i(\zeta) \geq 0, i = 1, \dots, p. \quad (3.9)$$

When $p = 1$, there exists a ζ_0 such that $F_0(\zeta_0) \geq 0$.

If the functions F_i are affine in ζ , then (3.9) and (3.8) are equivalent (see the affine form of the Farkas lemma [Haar, 1924]). In the following chapters, the S-procedure will be used to formulate the LMI problems in the set-membership state estimation techniques proposed.

Remark 3.7. In general, the S-procedure expresses some quadratic constraints as LMIs. In some cases, these LMIs can be more conservative than the initial constraints but some useful approximations can be done.

3.3 Set-theory preliminaries

Research on set-based state estimation has been quite active for the last decades. The different approaches can be classified according to which type of set they choose to represent uncertainties. Since the main contributions of this thesis fall in the category of set-membership state estimation, it is important to discuss the most used sets in the literature and their main properties. Among the sets used are intervals, polytopes, zonotopes, parallelotopes and ellipsoids. Before detailing these sets, we start by introducing some basic set definitions and operations.

Definition 3.7. A set $\mathcal{S} \subset \mathbb{R}^n$ is called a *convex set* if for any element $x_1, x_2, \dots, x_k \in \mathcal{S}$, with $k \geq 2$, and any $\alpha_1, \alpha_2, \dots, \alpha_k \in \mathbb{R}^+$ such that $\sum_{i=1}^k \alpha_i = 1$, the element $\sum_{i=1}^k \alpha_i x_i$ belong to \mathcal{S} .

Definition 3.8. A function f is called a *convex function* if it is defined in a convex set \mathcal{S} and for all $x, y \in \mathcal{S}$ and all $\lambda \in [0, 1]$ the following property holds:

$$f(\lambda x + (1 - \lambda)y) \leq \lambda f(x) + (1 - \lambda)f(y).$$

This definition is illustrated in Figure 3.1.

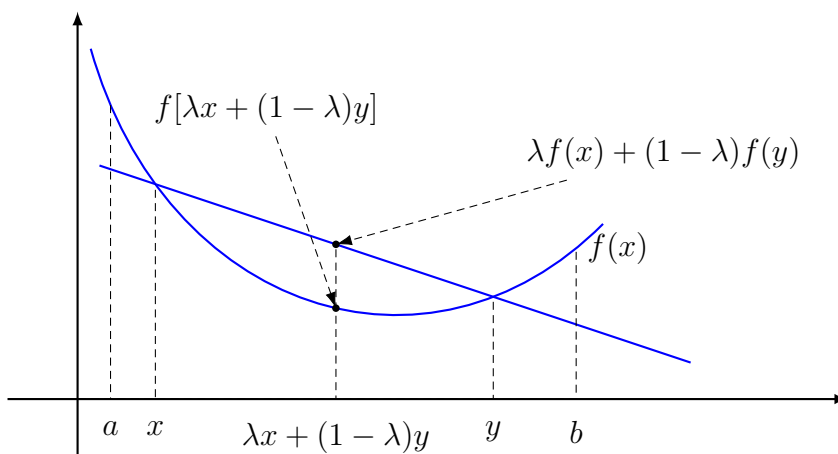


Figure 3.1 – Illustration of the definition of a convex function

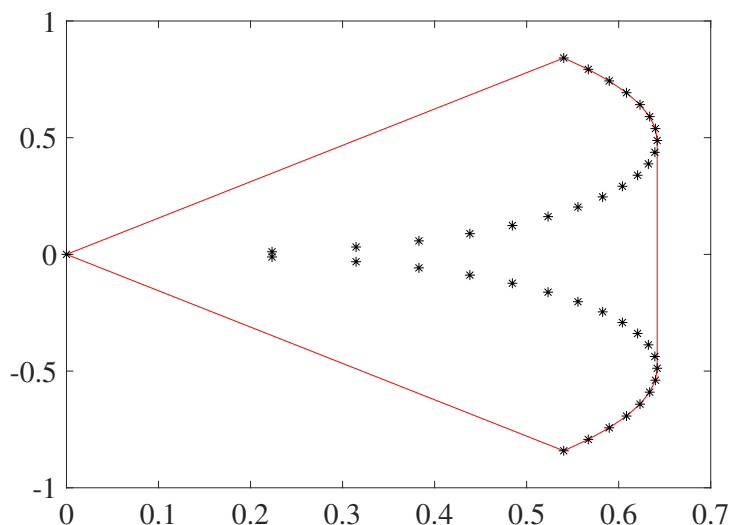
Definition 3.9. Given a set \mathcal{S} , the *convex hull* of \mathcal{S} , denoted by $\text{conv}(\mathcal{S})$ is the smallest convex set containing \mathcal{S} .

Definition 3.10. A set \mathcal{X} is included in a set \mathcal{Y} , i.e. $\mathcal{X} \subseteq \mathcal{Y}$, if and only if $x \in \mathcal{Y}, \forall x \in \mathcal{X}$. In others terms, \mathcal{X} is a subset of \mathcal{Y} .

Definition 3.11. The intersection of two sets \mathcal{X} and \mathcal{Y} is defined as $\mathcal{X} \cap \mathcal{Y} = \{z : z \in \mathcal{X} \text{ and } z \in \mathcal{Y}\}$.

Definition 3.12. The *Minkowski sum* of two sets \mathcal{X} and \mathcal{Y} is defined by $\mathcal{X} \oplus \mathcal{Y} = \{x + y : x \in \mathcal{X}, y \in \mathcal{Y}\}$.

Example 3.1. Figure 3.2 illustrates the convex hull (in red lines) of the convex set \mathcal{X} formed by the black dots.

Figure 3.2 – Illustration of the convex hull of a convex set \mathcal{X}

3.3.1 Interval set

A trivial way to define uncertainties when no distribution is known is using *interval sets*. The idea is to enclose numerical errors into an interval by setting an upper and a lower bound. Simplifying most of the standard operations [Hansen, 1965], the interval analysis became famous and widely used since its appearance in a book of Moore [Moore, 1966] back in 1966.

Definition 3.13. An *interval* denoted by $[a, b]$ is the set $\{x \in \mathbb{R} : a \leq x \leq b\}$.

Definition 3.14. A *unitary interval* is defined as $\mathbb{B} = [-1, 1]$.

Definition 3.15. The *center* of an interval $\mathcal{I} = [a, b]$ is defined as $\text{mid}(\mathcal{I}) = \frac{a+b}{2}$, its *radius* as $\text{rad}(\mathcal{I}) = \frac{b-a}{2}$.

Definition 3.16. An *interval vector* is a *box* $([a_1, b_1], \dots, [a_n, b_n])^\top$, with $a_i \leq b_i$ for $i = 1, \dots, n$.

Definition 3.17. A *unitary box* \mathbb{B}^n is composed by n unitary intervals given by $\{\mathbf{x} \in ([a_1, b_1], \dots, [a_n, b_n])^\top : a_i = -1, b_i = 1, i = 1, \dots, n\} \subset \mathbb{R}^n$.

Definition 3.18. An *interval matrix* $[\mathbf{M}]$ is a matrix whose elements are intervals. The notations $\text{mid}([\mathbf{M}])_{ij} = \frac{a_{ij}+b_{ij}}{2}$ and $\text{rad}([\mathbf{M}])_{ij} = \frac{b_{ij}-a_{ij}}{2}$ define the center and the radius of the interval matrix $[\mathbf{M}]$, respectively with $a_{ij} \leq m_{ij} \leq b_{ij}$, $i = 1, \dots, n$, and $j = 1, \dots, m$.

Definition 3.19. In the matrix space, the interval matrix is a hyper-rectangle and hence a convex set. A set $\mathcal{V}_{[\mathbf{M}]}$ defines the *set of all vertices* of the interval matrix $[\mathbf{M}]$.

The interval matrix $[\mathbf{M}]$ can be rewritten as:

$$[\mathbf{M}] = \text{mid}[\mathbf{M}] + \Delta\mathbf{M}, \quad (3.10)$$

$\Delta\mathbf{M}$ being the uncertain part of the interval matrix $[\mathbf{M}]$. Consider n_δ to be the number of the uncertain scalar terms δ_i of $\Delta\mathbf{M}$, with $\delta_i \in \mathbb{B}$, then $\Delta\mathbf{M}$ can be decomposed as:

$$\Delta\mathbf{M} = \sum_{i=1}^{n_\delta} \mathbf{M}_{\delta_i} \delta_i \quad (3.11)$$

where the matrices \mathbf{M}_{δ_i} , $i = 1, \dots, n_\delta$, have only one non-zero element corresponding to the coefficient of δ_i . Example 3.2 illustrates this decomposition

Example 3.2. Consider the interval matrix $[\mathbf{M}] = \begin{bmatrix} 3 & -1 + 0.4\delta_1 \\ 1 + 0.3\delta_2 & -4 \end{bmatrix}$,
 with $\delta_1, \delta_2 \in [-1, 1]$. Then, we compute $\text{mid}[\mathbf{M}] = \begin{bmatrix} 3 & -1 \\ 1 & -4 \end{bmatrix}$, $\Delta\mathbf{M} = \begin{bmatrix} 0 & 0.4\delta_1 \\ 0.3\delta_2 & 0 \end{bmatrix}$,
 $\mathbf{M}_{\delta_1} = \begin{bmatrix} 0 & 0.4 \\ 0 & 0 \end{bmatrix}$, $\mathbf{M}_{\delta_2} = \begin{bmatrix} 0 & 0 \\ 0.3 & 0 \end{bmatrix}$.

Given two intervals $[x] = [\underline{x}, \bar{x}]$ and $[y] = [\underline{y}, \bar{y}]$. An operation \circ between the two intervals $[x]$ and $[y]$ can be formalized as:

$$[x] \circ [y] = \{x \circ y : x \in [x], y \in [y]\}. \quad (3.12)$$

The four basic operations of interval analysis [Moore, 1979] can be defined as follows:

1. $[x] + [y] = [\underline{x} + \underline{y}, \bar{x} + \bar{y}]$,
2. $[x] - [y] = [\underline{x} - \bar{y}, \bar{x} - \underline{y}]$,
3. $[x] * [y] = [\min(\underline{x} \cdot \underline{y}, \underline{x} \cdot \bar{y}, \bar{x} \cdot \underline{y}, \bar{x} \cdot \bar{y}), \max(\underline{x} \cdot \underline{y}, \underline{x} \cdot \bar{y}, \bar{x} \cdot \underline{y}, \bar{x} \cdot \bar{y})]$,
4. $[x]/[y] = [x] * [1/\bar{y}, 1/\underline{y}]$, if $0 \notin [y]$.

Definition 3.20. A *strip* is defined by the following set

$$\mathcal{S}(y, \mathbf{d}, \sigma) = \{\mathbf{x} \in \mathbb{R}^n : |y - \mathbf{d}^\top \mathbf{x}| \leq \sigma\}, \quad (3.13)$$

where $y \in \mathbb{R}$, $\mathbf{d} \in \mathbb{R}^n$ and $\sigma \in \mathbb{R}_+^*$.

Despite its efficiency and simplicity, two main drawbacks of interval arithmetic can be mentioned: *the dependency effect* in which a variable that occurs more than once in the same function is treated independently, and the *wrapping effect* that overestimates the image of an interval vector at each sampling time [Moore, 1966], [Kühn, 1998], [Jaulin et al., 2001]. Next, the ellipsoidal sets are detailed. The presented properties will be further used along this thesis to develop ellipsoidal state estimation techniques.

3.3.2 Ellipsoidal set

Ellipsoids are popular sets widely used in control system applications due to their low complexity [Schweppe, 1968] and the resulting estimation stability properties [Hu and Lin, 2003]. For instance, they are used in identification [Polyak et al., 2004], [Norton, 1987], diagnosis [Durieu et al., 2001], [Chernousko, 1994], [Kurzahanskiy and Varaiya, 2007] etc. In particular, the ellipsoidal set knows an immense success in the field of set-membership state estimation. It is one of the main sets used in this thesis, thus in this section several useful properties and definitions will be detailed.

Definition 3.21. *Ellipsoidal set.* Given a strictly positive symmetric definite matrix $\mathbf{P} = \mathbf{P}^\top \succ 0$, a real vector $\bar{\mathbf{x}} \in \mathbb{R}^n$ and a strictly positive real scalar $\rho \in \mathbb{R}_+^*$, the bounded *ellipsoid* $\mathcal{E}(\mathbf{P}, \bar{\mathbf{x}}, \rho)$ is defined by the set:

$$\mathcal{E}(\mathbf{P}, \bar{\mathbf{x}}, \rho) = \{\mathbf{x} \in \mathbb{R}^n : (\mathbf{x} - \bar{\mathbf{x}})^\top \mathbf{P}(\mathbf{x} - \bar{\mathbf{x}}) \leq \rho\}, \quad (3.14)$$

where \mathbf{P} is the *shape matrix* of the ellipsoid, $\bar{\mathbf{x}}$ its *center* and ρ its so called *radius*.

Remark 3.8. A *normalized ellipsoid* is defined by:

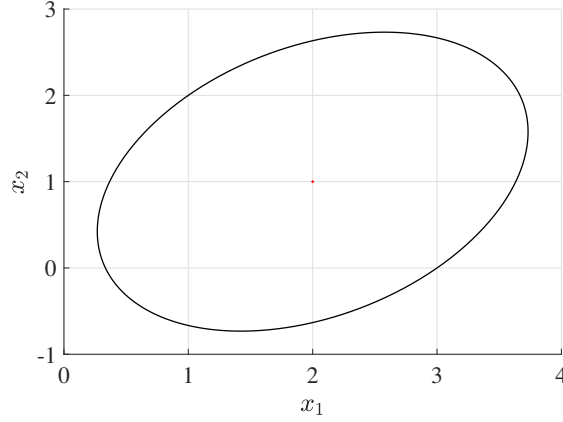
$$\mathcal{E}(\mathbf{P}, \bar{\mathbf{x}}, 1) = \mathcal{E}(\mathbf{P}, \bar{\mathbf{x}}) = \{\mathbf{x} \in \mathbb{R}^n : (\mathbf{x} - \bar{\mathbf{x}})^\top \mathbf{P}(\mathbf{x} - \bar{\mathbf{x}}) \leq 1\}, \quad (3.15)$$

where the matrix $\mathbf{P} = \mathbf{P}^\top \succ 0$ denotes its shape and size and $\bar{\mathbf{x}}$ its center.

Notice that for the normalized ellipsoid, the radius $\rho = 1$ can be omitted from the notation leading to a simplified notation $\mathcal{E}(\mathbf{P}, \bar{\mathbf{x}})$. Thus, the normalized ellipsoid $\mathcal{E}(\mathbf{P}^{-1}, \bar{\mathbf{x}})$, which is used largely in literature, has the following form:

$$\mathcal{E}(\mathbf{P}^{-1}, \bar{\mathbf{x}}) = \{\mathbf{x} \in \mathbb{R}^n : (\mathbf{x} - \bar{\mathbf{x}})^\top \mathbf{P}^{-1}(\mathbf{x} - \bar{\mathbf{x}}) \leq 1\}. \quad (3.16)$$

Example 3.3. Figure 3.3 proposes an example of an ellipsoidal set in a two-dimensional space with $\text{bitx} = [2 \ 1]^\top$, $\mathbf{P} = \begin{bmatrix} 3 & 1 \\ 1 & 3 \end{bmatrix}$ and $\rho = 1$.


 Figure 3.3 – Ellipsoidal set $\mathcal{E}(\mathbf{P}, \bar{\mathbf{x}})$

To keep a simplified formulation, all the following properties are given to the normalized representation of an ellipsoid (3.16) but they can be extended to the generalized form.

Definition 3.22. The *support function of the ellipsoid* $\mathcal{E}(\mathbf{P}^{-1}, \bar{\mathbf{x}})$ in a direction \mathbf{l} is $\mathcal{F}(\mathcal{E}(\mathbf{P}^{-1}, \bar{\mathbf{x}})|\mathbf{l})$ given by:

$$\begin{cases} \mathcal{F}(\mathcal{E}(\mathbf{P}^{-1}, \bar{\mathbf{x}})|\mathbf{l})_{upper} = \langle \mathbf{l}, \bar{\mathbf{x}} \rangle + \langle \mathbf{l}, \mathbf{P}^{-1}\mathbf{l} \rangle^{\frac{1}{2}}, \\ \mathcal{F}(\mathcal{E}(\mathbf{P}^{-1}, \bar{\mathbf{x}})|\mathbf{l})_{lower} = \langle \mathbf{l}, \bar{\mathbf{x}} \rangle - \langle \mathbf{l}, \mathbf{P}^{-1}\mathbf{l} \rangle^{\frac{1}{2}}, \end{cases} \quad (3.17)$$

where $\mathcal{F}(\mathcal{E}(\mathbf{P}^{-1}, \bar{\mathbf{x}})|\mathbf{l})_{upper}$ and $\mathcal{F}(\mathcal{E}(\mathbf{P}^{-1}, \bar{\mathbf{x}})|\mathbf{l})_{lower}$ are the upper and the lower bounds, respectively.

Property 3.3. *Affine transformation of an ellipsoid.* Given a normalized ellipsoidal set $\mathcal{E}(\mathbf{P}^{-1}, \bar{\mathbf{x}}) \subseteq \mathbb{R}^n$, a matrix $\mathbf{A} \in \mathbb{R}^{n \times n}$ and a vector $\mathbf{b} \in \mathbb{R}^n$, the affine transformation of this ellipsoid by the matrix \mathbf{A} and the vector \mathbf{b} is defined by:

$$\mathbf{A}\mathcal{E}(\mathbf{P}^{-1}, \bar{\mathbf{x}}) + \mathbf{b} = \mathcal{E}((\mathbf{A}\mathbf{P}\mathbf{A}^\top)^{-1}, \mathbf{A}\bar{\mathbf{x}} + \mathbf{b}). \quad (3.18)$$

Property 3.4. *Outer ellipsoidal approximation of the union of two ellipsoids.* [Durieu et al., 2001] Given two normalized ellipsoids $\mathcal{E}_1(\mathbf{P}_1^{-1}, \bar{\mathbf{x}}_1)$, $\mathcal{E}_2(\mathbf{P}_2^{-1}, \bar{\mathbf{x}}_2)$ and a vector $\phi \in \mathbb{R}^2$, with $\phi = [\phi_1 \ \phi_2]^\top$ and $\phi_1 + \phi_2 = 1$, then the following expression holds:

$$\mathcal{E}_1(\mathbf{P}_1^{-1}, \bar{\mathbf{x}}_1) \cup \mathcal{E}_2(\mathbf{P}_2^{-1}, \bar{\mathbf{x}}_2) \subseteq \mathcal{E}(\mathbf{P}^{-1}, \bar{\mathbf{x}}), \quad (3.19)$$

with $\bar{\mathbf{x}} = \phi_1\bar{\mathbf{x}}_1 + \phi_2\bar{\mathbf{x}}_2$ and $\mathbf{P} = \phi_1^{-1}\mathbf{P}_1 + \phi_2^{-1}\mathbf{P}_2$.

Property 3.5. *Intersection between an ellipsoid and a strip.* [Fogel and Huang, 1982] Given a normalized ellipsoid $\mathcal{E}(\mathbf{P}^{-1}, \bar{\mathbf{x}})$ and a normalized strip $\mathcal{S}(y, \mathbf{d}, 1) = \mathcal{S}(y, \mathbf{d})$, then the intersection between $\mathcal{E}(\mathbf{P}^{-1}, \bar{\mathbf{x}})$ and $\mathcal{S}(y, \mathbf{d})$ is outer bounded by the following ellipsoid:

$$\mathcal{E}(\mathbf{P}^{-1}, \bar{\mathbf{x}}) \cap \mathcal{S}(y, \mathbf{d}) \subseteq \mathcal{E}'(\mathbf{P}'^{-1}, \bar{\mathbf{x}}'), \quad (3.20)$$

with

$$\left\{ \begin{array}{l} \mathcal{E}'(\mathbf{P}'^{-1}, \bar{\mathbf{x}}') = \{\mathbf{x} \in \mathbb{R}^n : (\mathbf{x} - \bar{\mathbf{x}}')^\top \mathbf{P}'^{-1} (\mathbf{x} - \bar{\mathbf{x}}') \leq 1\}, \\ \bar{\mathbf{x}}' = \bar{\mathbf{x}} + \frac{\psi \delta}{1 + \psi g} \mathbf{P} \mathbf{d}, \\ \mathbf{P}' = \left(1 + \psi - \frac{\psi \delta^2}{1 + \psi g}\right) \left(\mathbf{P} - \frac{\psi}{1 + \psi g} \mathbf{P} \mathbf{d} \mathbf{d}^\top \mathbf{P}\right), \\ \psi \geq 0, \\ g = \mathbf{d}^\top \mathbf{P} \mathbf{d}, \\ \delta = y - \mathbf{d}^\top \bar{\mathbf{x}}. \end{array} \right. \quad (3.21)$$

In set-membership state estimation techniques, the main goal is to find the smallest guaranteed estimation set containing the state at each time instant. To minimize the size of an ellipsoidal set $\mathcal{E}(\mathbf{P}^{-1}, \mathbf{c})$ two criteria [Durieu et al., 2001] are mainly used in the open literature:

- the minimization of the volume of the ellipsoid that leads to the minimization of the determinant of the shape matrix \mathbf{P} ,
- the minimization of the sum of the semi-axes that leads to the minimization of the trace of the size matrix \mathbf{P} .

Next, we present the polyhedral set which is widely used in literature to represent uncertainties.

3.3.3 Polyhedral set

Polyhedral sets represent one of the most popular form of geometrical sets used in optimization and control. They appear for instance when linear constraints are applied on the state of a system. It can be defined as the intersection of finitely many closed half-spaces [Bronstein, 2008] in a finite dimensional euclidean space. Several representations and their related properties are further discussed.

Definition 3.23. *Half-space representation or H-representation.* A polyhedral set $\mathcal{P} \in \mathbb{R}^n$ in a finite-dimensional euclidean space is the intersection of a finite number of closed half-spaces as follows:

$$\mathcal{P} = \{\mathbf{x} \in \mathbb{R}^n : \mathbf{A}\mathbf{x} \leq \mathbf{b}\}, \quad (3.22)$$

with $\mathbf{A} \in \mathbb{R}^{m \times n}$ and $\mathbf{b} \in \mathbb{R}^m$.

Moreover, a specific widely used form of polyhedral set in automatic control is a *polytope*.

Definition 3.24. A *polytope* is a bounded polyhedral set.

Example 3.4. Figure 3.4 shows the half-space representation of a polytope with $\mathbf{A} = \begin{bmatrix} -1 & 0 & 1 & -2 & 0.5 \\ 1 & 1 & 0 & -1 & -1 \end{bmatrix}^\top$ and $\mathbf{b} = [0 \quad -5 \quad -12 \quad 6 \quad 11]^\top$.

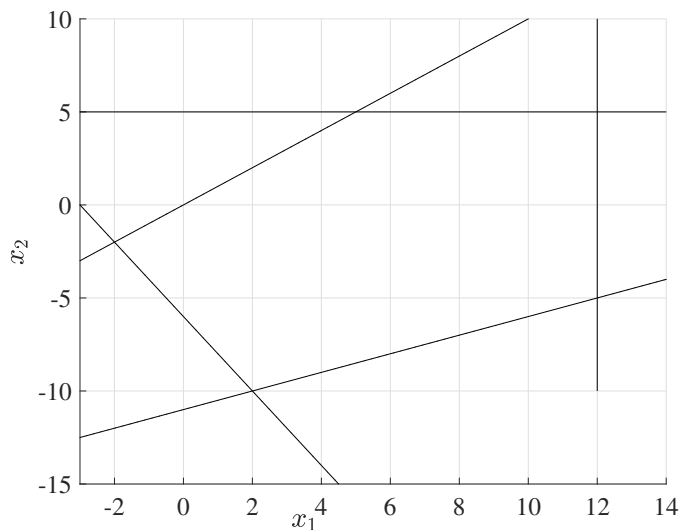


Figure 3.4 – Half-space representation of a polytope

Polytopes offer flexibility, thus they provide a good approximation of any convex set. Additionally, they are closed under some operations such as Minkowski sum, inclusion and intersection. Another main advantage of polytopes are their dual representation. Indeed, beside the half-space representation defined by Definition 3.23, polytopes can be represented in a vertex representation which allows us to choose the most suitable form for any particular problem.

Definition 3.25. (*Vertex representation or V-polytope*) For a finite set of points $\mathcal{V} = \{v_1, v_2, \dots, v_m\} \in \mathbb{R}^n$, a polytope \mathcal{P} can be defined as the convex hull of the set \mathcal{V} :

$$\mathcal{P} = \text{conv}(\mathcal{V}) = \left\{ \alpha_1 v_1 + \alpha_2 v_2 + \dots + \alpha_m v_m : \alpha_i \in \mathbb{R}^+, \sum_{i=1}^m \alpha_i = 1 \right\} \quad (3.23)$$

Example 3.5. Figure 3.5 shows the vertex representation of a polytope with $\mathcal{V} = \left\{ \begin{bmatrix} -2 \\ -2 \end{bmatrix}, \begin{bmatrix} 5 \\ 5 \end{bmatrix}, \begin{bmatrix} 12 \\ 5 \end{bmatrix}, \begin{bmatrix} 12 \\ -5 \end{bmatrix}, \begin{bmatrix} 2 \\ -10 \end{bmatrix} \right\}$.

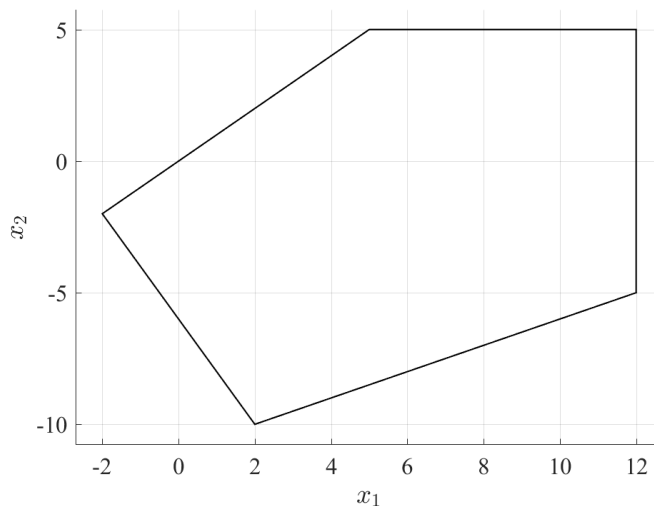


Figure 3.5 – Vertex representation of a polytope

The following theorem shows the equivalence between the representations of a polytope detailed in Definition 3.23 and Definition 3.25.

Theorem 3.1. *Equivalence of the two polytopic representations.* [Ziegler, 1995] A subset $\mathcal{P} \in \mathbb{R}^n$ is the convex hull of a finite point set (a *V*-polytope) if and only if it is a bounded intersection of half-spaces (a *H*-polytope).

Remark 3.9. The **H**-representation in Figure 3.4, and the **V**-representation in Figure 3.5 are two different representations for the same polytope.

In other terms, any polytope represented in **H**-representation can be transformed to the **V**-representation and vice versa. The transformations are well known in the literature as the *facet enumeration problem* for the

transformation of a \mathbf{H} -polytope to a \mathbf{V} -polytope, and the *vertex enumeration problem* for the transformation to a \mathbf{H} -polytope. The existing algorithms to do the transformations can be time consuming [Dantzig, 1972], [Fukuda, 1997], however they permit to choose a suitable representation depending on the problem. For instance, it is trivial to use the \mathbf{V} -representation when proving that the polytopic set is closed under the Minkowski addition. Nevertheless, the critical disadvantage of polytopes are their complexity that depends on the number of vertices and not on the space dimension. Therefore, even in low space dimension, the complexity of the polytope, approximating the convex set accurately, can quickly increase. In this context, another special class of convex polytopes are presented to offer a good trade-off between complexity and flexibility.

3.3.4 Zonotopic set

Due to their flexibility and simplicity in computation, zonotopes will be further used in this thesis. *Zonotopes* are a particular class of convex polytopes which exhibit symmetry with respect to their center. Similar to polytopes, zonotopes can be represented by the half-space representation and the vertex representation. Additionally, zonotopes can be also defined by the generator representation and the hypercube linear transformation.

Definition 3.26. *Generators representation.* Given a vector $\mathbf{p} \in \mathbb{R}^n$ and a set of vectors $\mathcal{G} = \{\mathbf{g}_1, \mathbf{g}_2, \dots, \mathbf{g}_m\} \subset \mathbb{R}^n$, with $m \geq n$, a *zonotope* \mathcal{Z} of order m (also called *m-zonotope*) is defined as follows:

$$\mathcal{Z} = (\mathbf{p}; \mathbf{g}_1, \mathbf{g}_2, \dots, \mathbf{g}_m) = \left\{ \mathbf{x} \in \mathbb{R}^n : \mathbf{x} = \mathbf{p} + \sum_{i=1}^m \alpha_i \mathbf{g}_i; |\alpha_i| \leq 1 \right\}. \quad (3.24)$$

The vector \mathbf{p} is the *center* of the zonotope \mathcal{Z} . The set of vectors $\mathcal{G} = \{\mathbf{g}_1, \mathbf{g}_2, \dots, \mathbf{g}_m\}$ are the generators. The *order* of a zonotope is defined by the number of its generators (m in this case). This definition is equivalent to the definition of zonotopes by the Minkowski sum of a finite number of line segments defined by:

$$\mathcal{Z} = (\mathbf{p}; \mathbf{g}_1, \mathbf{g}_2, \dots, \mathbf{g}_m) = \mathbf{p} \oplus \mathbf{g}_1 \mathbb{B}^1 \oplus \dots \oplus \mathbf{g}_m \mathbb{B}^1. \quad (3.25)$$

The following alternative definition of a zonotope is more convenient for the estimation approaches proposed in the thesis.

Definition 3.27. *Hypercube linear projection representation.* A zonotope of order m in \mathbb{R}^n ($m \geq n$) is the translation by the center $\mathbf{p} \in \mathbb{R}^n$ of the

image of an unitary hypercube of dimension m in \mathbb{R}^n under a linear transformation. Given a matrix $\mathbf{H} \in \mathbb{R}^{n \times m}$ representing the linear transformation, the zonotope \mathcal{Z} is defined by:

$$\mathcal{Z} = (\mathbf{p}; \mathbf{H}) = \mathbf{p} \oplus \mathbf{H}\mathbb{B}^m. \quad (3.26)$$

Remark 3.10. Both of the definitions of the zonotope 3.26 and 3.27 are equivalent if the matrix $\mathbf{H} = [\mathbf{g}_1 \ \mathbf{g}_2 \ \dots \ \mathbf{g}_m]$.

From now on, the zonotope \mathcal{Z} will be described by $\mathcal{Z}(\mathbf{p}; \mathbf{H})$, to simplify the manuscript, with \mathbf{p} being the center of the zonotope and \mathbf{H} its matrix of generators.

Example 3.6. Using the notation $\mathcal{Z}(\mathbf{p}; \mathbf{H})$, with $\mathbf{p} = [0 \ 0]^\top$ and $\mathbf{H} = \begin{bmatrix} 4 & 7 & 1 \\ 1 & 5 & 3 \end{bmatrix}$, we can plot the zonotope of order 3 in Figure 3.6. In this context, each vertex of the zonotope $\mathbf{v}_{\mathcal{Z}_i} \in \mathcal{V}_{\mathcal{Z}}$, with $i = 1, \dots, 2^3$ can be found by this formula $\mathbf{v}_{\mathcal{Z}_i} = \mathbf{p} + \mathbf{H}\mathbf{v}_i$ such that $\mathbf{v}_i \in \mathcal{V}_{\mathbb{B}^3}$ (i.e. $\mathbf{v}_i \in \{[\pm 1 \ \pm 1 \ \pm 1]^\top\}$).

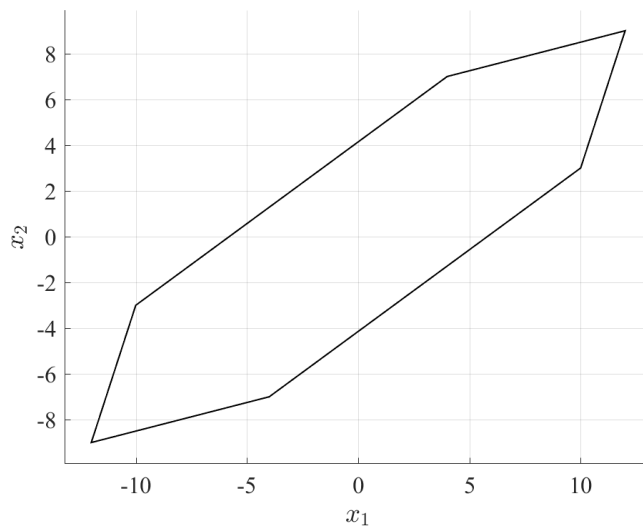


Figure 3.6 – Third order zonotope in a two-dimensional space

Remark 3.11. There exist conversion algorithms between different zonotopic representations: generator representation, \mathbf{H} -representation and \mathbf{V} -representation [Gritzmann and Sturmfels, 1993], [Seymour, 1994], [Fukuda, 2004], [Schön and Kutterer, 2005], [Althoff et al., 2010].

Remark 3.12. A significant advantage of the hypercube linear projection representation of a zonotope in a set-membership state estimation context is the ability to represent a zonotope using one vector and a matrix, or a matrix in the case of a centered zonotope (i.e. the $\mathbf{p} = \mathbf{0}_{n \times 1}$).

Definition 3.28. The \mathbf{P} -radius of a zonotope $\mathcal{Z} = \mathbf{p} \oplus \mathbf{H}\mathbb{B}^m$ is defined by the following expression:

$$r = \max_{z \in \mathcal{Z}} (\|z - \mathbf{p}\|_{\mathbf{P}}^2), \quad (3.27)$$

where \mathbf{P} is a strictly symmetric and positive definite matrix $\mathbf{P} = \mathbf{P}^T \succ 0$.

This notation provides a criterion to evaluate the size of a zonotope. For the same value of the matrix \mathbf{P} , a larger value of the \mathbf{P} -radius leads to a larger zonotope.

Example 3.7. The \mathbf{P} -radius definition is illustrated in Figure 3.7. In red the ellipsoid (see Definition 3.21) related to the \mathbf{P} -radius of the zonotope $\mathcal{Z} = \mathbf{p} \oplus \mathbf{H}\mathbb{B}^m$ with $\mathbf{p} = [0 \ 0]^\top$, $\mathbf{H} = \begin{bmatrix} 4 & 7 & 1 \\ 1 & 5 & 3 \end{bmatrix}$ and $\mathbf{P} = \mathbf{I}_2$. The \mathbf{P} -radius is $r_1 = 225$. In blue, the ellipsoid related to the \mathbf{P} -radius of the zonotope $\mathcal{Z} = \mathbf{p} \oplus \mathbf{H}\mathbb{B}^m$ with $\mathbf{p} = [0 \ 0]^\top$, $\mathbf{H} = \begin{bmatrix} 4 & 7 & 1 \\ 1 & 5 & 3 \end{bmatrix}$ and $\mathbf{P} = 0.2 \cdot \mathbf{I}_2$. The \mathbf{P} -radius is $r_2 = 45$.

This criterion will be used in Chapter 6 to present a new zonotopic set-membership state estimation technique based on the Luenberger observer for piecewise affine systems.

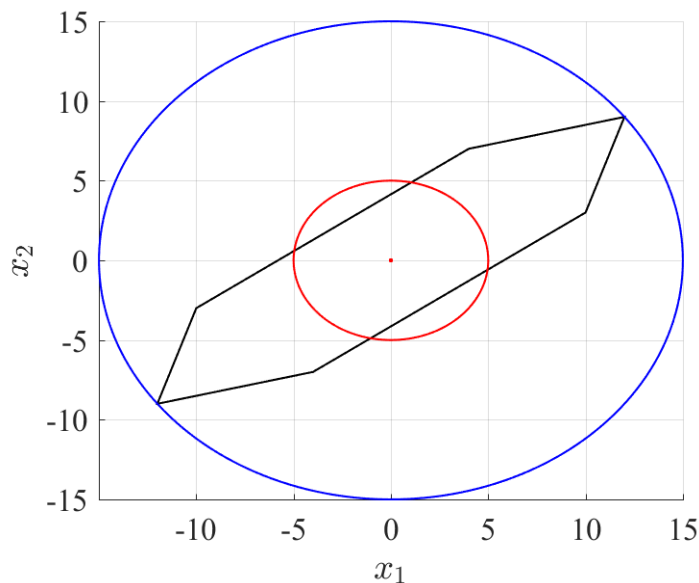
In what follows, several important properties of zonotopes [Le, 2012] that will be further used in this this, are synthesized below.

Property 3.6. *Sum of two zonotopes.* Given two zonotopes $\mathcal{Z}_1 = \mathbf{p}_1 \oplus \mathbf{H}_1\mathbb{B}^{m_1} \in \mathbb{R}^n$ and $\mathcal{Z}_2 = \mathbf{p}_2 \oplus \mathbf{H}_2\mathbb{B}^{m_2} \in \mathbb{R}^n$, the Minkowski sum of two zonotopes is also a zonotope defined by:

$$\mathcal{Z} = \mathcal{Z}_1 \oplus \mathcal{Z}_2 = (\mathbf{p}_1 + \mathbf{p}_2) \oplus \begin{bmatrix} \mathbf{H}_1 & \mathbf{H}_2 \end{bmatrix} \mathbb{B}^{m_1+m_2}. \quad (3.28)$$

Property 3.7. *Affine transformation of a zonotope.* Given a zonotope $\mathcal{Z} = \mathbf{p} \oplus \mathbf{H}\mathbb{B}^m$ and a matrix $\mathbf{A} \in \mathbb{R}^{n \times n}$, the linear transformation of \mathcal{Z} by the matrix \mathbf{A} is:

$$\mathbf{A} \cdot \mathcal{Z} = (\mathbf{A} \cdot \mathbf{p}) \oplus (\mathbf{A} \cdot \mathbf{H})\mathbb{B}^m. \quad (3.29)$$


 Figure 3.7 – Ellipsoid related to the \mathbf{P} -radius of a zonotope

The following properties discuss few of the techniques employed in literature to reduce the complexity of a zonotope. It is well known that when a problem of a set-membership state estimation is addressed using m -zonotopes, the complexity of the zonotope grows up due to the computation of linear transformation or the Minkowski sum operation for example. The goal of any reduction technique is to approximate a high order zonotope by a lower order one.

Property 3.8. *Interval hull method.* [Kühn, 1998] Considering a zonotope $\mathcal{Z} = \mathbf{p} \oplus \mathbf{H}\mathbb{B}^m \in \mathbb{R}^n$, the smallest box containing this zonotope is computed by:

$$\text{box}(\mathcal{Z}) = \mathbf{p} \oplus rs(\mathbf{H})\mathbb{B}^n, \quad (3.30)$$

with $rs(\mathbf{H})$ a diagonal matrix such that $rs(\mathbf{H})_{ii} = \sum_{j=1}^m |\mathbf{H}_{ij}|$, $i = 1, \dots, n$.

Property 3.9. *Criterion-based reduction.* [Combastel, 2003], [Alamo et al., 2005] Given a zonotope $\mathcal{Z} = \mathbf{p} \oplus \mathbf{H}\mathbb{B}^m$, an integer s , with $n < s < m$, and denote by $\hat{\mathbf{H}} = [\hat{\mathbf{h}}_1 \ \hat{\mathbf{h}}_2 \ \dots \ \hat{\mathbf{h}}_m]$ the matrix resulting from the reordering of the columns of \mathbf{H} in decreasing order of the euclidean norm which is equivalent to reordering the segments of zonotope from the longest to the shortest. The following expression holds:

$$\mathcal{Z} \subseteq \mathbf{p} \oplus [\hat{\mathbf{H}}_T \ \mathbf{Q}] \mathbb{B}^s, \quad (3.31)$$

where $\hat{\mathbf{H}}_T$ is composed by the first $s - n$ columns of the matrix $\hat{\mathbf{H}}$ and $\mathbf{Q} \in \mathbb{R}^{n \times n}$ is a diagonal matrix satisfying $\mathbf{Q}_{ii} = \sum_{j=s-n+1}^m |\hat{\mathbf{H}}_{ij}|$, with $i = 1, \dots, n$.

The quality of approximation mainly depends on the value of s that limits the complexity, or the criterion used to split the zonotope \mathcal{Z} or the approximation method used. In Chapter 7, a criterion based reduction technique will be detailed to limit the complexity of a zonotope incorporating the linear constraints applied on the system state.

The notations presented thus far in this chapter cover the definition and the properties of some of the convex sets in literature along with convex functions. In the next section, we use these notations to discuss a particular class of optimization problems called *convex optimization*. The section will give some basic definitions along with a famous standard technique to solve convex optimization problems that will be further used and extended in Chapter 7 of the thesis.

3.4 Convex optimization

State estimators are a key enabler for process control. An unreliable estimate can lead to poor system performance. As mentioned earlier, state estimation techniques fall under two main categories. In particular, the Kalman filter became a standard technique widely used in industry. However, some prior information are impossible to incorporate in the classical filter framework. Some of these information, known as constraints, can be considered as convex optimization problems to solve. This problem is treated in Chapter 7 of this thesis. In this section, a very brief introduction to convex optimization is given along with some of the preliminaries and main properties that will be further used in the following chapters.

Definition 3.29. A *convex optimization problem* is a problem consisting of minimizing a convex function over a convex set.

Definition 3.30. A general convex optimization problem has the form:

$$\begin{aligned} & \underset{\mathbf{x}}{\text{minimize}} && f_0(\mathbf{x}) \\ & \text{subject to} && f_i(\mathbf{x}) \leq 0, \quad i = 1, \dots, m, \\ & && l_j(\mathbf{x}) = 0, \quad j = 1, \dots, r, \end{aligned} \tag{3.32}$$

where the vector $\mathbf{x} \in \mathbb{R}^n$ is called the *decision variable* of the problem, f_0 is the objective or cost convex function, the convex functions f_i with $i = 1, \dots, m$, (see Definition 3.8) designate inequality constraints while the convex function l_j , with $j = 1, \dots, r$ designate equality constraints.

Definition 3.31. An *optimal solution* denoted by \mathbf{x}^* of the convex optimization problem has the smallest objective value among all vectors that satisfy the constraints.

Remark 3.13. If there are no constraints $m = 0$ and $r = 0$, the optimization problem (3.32) is said unconstrained.

Definition 3.32. A function f defined on an interval \mathcal{I} is called *Lipschitz continuous* if there exists a positive constant c such that:

$$|f(x_1) - f(x_2)| \leq c|x_1 - x_2|, \text{ for all } x_1, x_2 \in \mathcal{I}. \quad (3.33)$$

Definition 3.33. A function f is defined as *strictly convex* if for all $\mathbf{x}, \mathbf{y} \in \mathcal{S}$ and all $\lambda \in [0, 1]$ the following property holds:

$$f(\lambda\mathbf{x} + (1 - \lambda)\mathbf{y}) < \lambda f(\mathbf{x}) + (1 - \lambda)f(\mathbf{y}). \quad (3.34)$$

Equivalently, a function f is also strictly convex if it is twice continuously differentiable such that:

$$\nabla^2 f(\mathbf{x}) \succ 0. \quad (3.35)$$

Definition 3.34. A function f is defined as *strongly convex* if for all $\mathbf{x}, \mathbf{y} \in \mathcal{S}$, there exists a scalar $d > 0$ for which:

$$\langle \nabla f(\mathbf{x}) - \nabla f(\mathbf{y}), \mathbf{x} - \mathbf{y} \rangle \geq d \|\mathbf{x} - \mathbf{y}\|_2^2 \quad (3.36)$$

Equivalently, a function f is also strongly convex if it is twice continuously differentiable such that

$$\nabla^2 f(\mathbf{x}) \succeq d\mathbf{I} \quad (3.37)$$

Remark 3.14. Strong convexity implies strict convexity which implies convexity. However, the converse of neither implication is true.

Definition 3.35. A function f is called *smooth function* if it has derivatives of all orders everywhere in its domain.

Example 3.8. Consider the function $f : \mathbb{R} \rightarrow \mathbb{R}$, with $f(x) = 4x$ defined in \mathbb{R} . The function f is continuous and its first derivative $f'(x) = 4$ is also a continuous function. Differentiating the first derivative we get that $f^{(n)}(x) = 0$ for $n > 1$, with $f^{(n)}$ the n -th derivative of the function f . Thus, the function f is a smooth function.

3.4.1 Duality principle in convex optimization

In mathematical optimization theory, optimization problems can be seen from two perspectives, the primal and the dual problem (duality principle). The solution to both problems are interconnected. Generally, the term *dual problem* refers to the *Lagrangian dual problem* but other dual problems exist and are used in the literature [Boyd and Vandenberghe, 2004], [Nesterov, 2018].

Definition 3.36. Given the primal problem (3.32), we define its *Lagrangian* as:

$$L(\mathbf{x}, \mathbf{u}, \mathbf{v}) = f(\mathbf{x}) + \sum_{i=1}^m u_i f_i(\mathbf{x}) + \sum_{j=1}^r v_j l_j(\mathbf{x}), \quad (3.38)$$

where $\mathbf{u} \in \mathbb{R}^m$, $\mathbf{v} \in \mathbb{R}^r$, and $\mathbf{u} \geq 0$.

Definition 3.37. Given the Definition 3.36, a *Lagrange dual function* is defined as:

$$g(\mathbf{u}, \mathbf{v}) = \underset{\mathbf{x} \in \mathbb{R}^n}{\text{minimize}} \quad L(\mathbf{x}, \mathbf{u}, \mathbf{v}). \quad (3.39)$$

Definition 3.38. Given primal problem (3.32), we define its *Lagrange dual problem* as:

$$\begin{aligned} & \underset{\mathbf{u}, \mathbf{v}}{\text{maximize}} \quad g(\mathbf{u}, \mathbf{v}) \\ & \text{subject to} \quad \mathbf{u} \geq 0. \end{aligned} \quad (3.40)$$

Remark 3.15. The dual problem is a convex optimization problem since the function g is always concave even if the primal problem is not convex.

Property 3.10. The primal and dual optimal values always satisfy weak duality:

$$f^* \geq g^*, \quad (3.41)$$

with f^* the optimal solution of the primal problem (3.32) and g^* the optimal solution of the dual problem (3.40).

Property 3.11. Slater's condition. For the constrained convex primal optimization problem (3.32), if there exists a vector \mathbf{x} such that $f_1(\mathbf{x}) < 0, \dots, f_m(\mathbf{x}) < 0$ and $l_1(\mathbf{x}) = 0, \dots, l_r(\mathbf{x}) = 0$, then strong duality holds:

$$f_0^* = g^*. \quad (3.42)$$

In this thesis, we consider an optimization problem of the form:

$$\begin{aligned} & \underset{\mathbf{u} \in U}{\text{minimize}} \quad J_a(\mathbf{u}) + J_b(\mathbf{R}\mathbf{u}) + \frac{1}{2} \|\mathbf{u} - \mathbf{c}\|_{\mathbf{D}}^2 \\ & \text{subject to} \quad \mathbf{A}\mathbf{u} = \mathbf{b}. \end{aligned} \quad (3.43)$$

with $\mathbf{A} \in \mathbb{R}^{n \times m}$, $\mathbf{b} \in \mathbb{R}^n$, $\mathbf{c} \in \mathbb{R}^m$, $\mathbf{R} \in \mathbb{R}^{n \times m}$, under the following assumption.

Assumption 3.1. Assume that:

1. $J_a : \mathbb{R}^m \rightarrow \mathbb{R}$ is a separable strictly convex function,
2. $J_b : \mathbb{R}^r \rightarrow \mathbb{R}$ is a separable strictly convex function,
3. $\mathbf{D} \in \mathbb{R}^{m \times m}$ is a diagonal definite positive matrix,
4. $\mathcal{U} \subset \mathbb{R}^m$ is a closed convex set containing \mathbf{u} .

The considered problem (3.43) can be rewritten as:

$$\begin{aligned}
 & \underset{\mathbf{u} \in \mathcal{U}, \mathbf{v} \in \mathbb{R}^m, \mathbf{s} \in \mathbb{R}^n}{\text{minimize}} && J_a(\mathbf{u}) + J_b(\mathbf{s}) + \frac{1}{2} \|\mathbf{u} - \mathbf{c}\|_{\mathbf{D}}^2 \\
 & \text{subject to} && \mathbf{A}\mathbf{v} = \mathbf{b} \\
 & && \mathbf{R}\mathbf{v} = \mathbf{s} \\
 & && \mathbf{u} = \mathbf{v}
 \end{aligned} \tag{3.44}$$

The dual formulation of this problem consists in solving the following optimization problem:

$$\underset{\mathbf{u} \in \mathcal{U}, \mathbf{v} \in \mathbb{R}^m, \mathbf{s} \in \mathbb{R}^n}{\text{maximize}} \quad \left\langle \mathbf{x}, \begin{bmatrix} \mathbf{R}\mathbf{v} - \mathbf{s} \\ \mathbf{A}\mathbf{v} - \mathbf{b} \\ \mathbf{v} - \mathbf{u} \end{bmatrix} \right\rangle - J_a(\mathbf{u}) - J_b(\mathbf{s}) - \frac{1}{2} \|\mathbf{u} - \mathbf{c}\|_{\mathbf{D}}^2. \tag{3.45}$$

A particular form of the optimization problem (3.45) will be further used in Chapter 7 of this thesis. Convex optimization problems can be efficiently solved using standard methods such as gradient descent algorithms [Fletcher, 1976], [Nesterov, 2013].

3.4.2 Gradient-based methods for solving convex optimization problems

In this section we present the gradient descent algorithm for minimizing an unconstrained convex function of the form:

$$\underset{\mathbf{x}}{\text{minimize}} \quad f(\mathbf{x}). \tag{3.46}$$

The gradient descent method [Cauchy, 1847] is one of the oldest techniques for convex optimization problems. It starts at an initial point and then repeatedly takes a step opposite to the gradient direction of the function at the current point. The gradient descent algorithm to minimize a function $f(\mathbf{x})$ and at each iteration the following inequality holds:

$$f(\mathbf{x}_{k+1}) < f(\mathbf{x}_k), \tag{3.47}$$

until the optimum value \mathbf{x}^* is reached. This is where the name *descent* from the algorithm comes from. Given the description of the algorithm, several choices have to be made in the implementation phase: the initial point \mathbf{x}_0 , the step size t_k , and the exit condition. Ideally, \mathbf{x}_0 is close to the minimum, however it is not trivial to make such a guess. The stopping criterion is generally $\nabla f(\mathbf{x}_k) < \epsilon$ where ϵ is a small positive value. For the choice of the step size t_k , two possible approaches can be found in the literature: a fixed value for t_k at each time instant k , or an adaptively adjusted step size on each iteration.

An entire family of gradient descent algorithms exists, following the same methodology with different technical details. Among them some concepts will be covered in later chapters.

3.5 Conclusion

This chapter presented a general representation of uncertainties that will be used in the next chapters in the context of uncertain linear standard and descriptor systems. Interval sets are simple and widely used to deal with uncertainties. However, their applications can be limited due to the dependency and wrapping effects. Polytopes are a strong tool for state estimation due to their high accuracy, but they can lead to high complexity when a large number of vertices is considered. Due to their simplicity and interesting properties detailed above, ellipsoids and zonotopes are the most popular sets in set-membership state estimation. Therefore, both of these geometric shapes will be employed in this thesis, depending on the considered system and the required specifications. The remainder of this thesis is divided into main parts. All the set-membership state estimation techniques presented in the first part are based on ellipsoids, while those presented in the second part are based on zonotopes.

In the next chapter, an ellipsoidal set-membership state estimation technique is compared in terms of accuracy and complexity to the classical Kalman filter before extending the technique to apply it on a model of an octorotor.

Part I

Ellipsoidal set-membership state estimation

Chapter 4

Ellipsoidal state estimation for linear systems

Contents

| | | |
|------------|---|-----------|
| 4.1 | Introduction | 65 |
| 4.2 | Overview of the classical Kalman filter | 67 |
| 4.3 | Problem formulation | 68 |
| 4.4 | Ellipsoidal state estimation technique | 70 |
| 4.5 | Comparison between two state estimation techniques for linear time-invariant systems | 74 |
| 4.6 | Application to an octorotor model | 77 |
| 4.6.1 | Octorotor modeling | 78 |
| 4.6.2 | Application to the design of SAR | 82 |
| 4.6.3 | Simulation results | 85 |
| 4.7 | Conclusion | 93 |

4.1 Introduction

Generally, process control requires accurate information about the plant. However, the measured variables do not totally describe the behavior of the system. Therefore, the entire system state is not always accessible. This could be possibly due to the difficulty of adding sensors into the plant because of the topology of the system, the expensive costs or some safety precautions. This is why it is important to get access to the unknown information using available data/knowledge. Various methods for state estimation

are suggested in the literature and they can be divided into two categories like mentioned in Section 3.1. Stochastic approaches such as the Kalman Filter (see [Kalman, 1960]) assume the prior knowledge of the distribution of the perturbations and the measurement noises (in general Gaussian distribution) taking into account certain characteristics like the mean and the covariance. This assumption can be sometimes unrealistic. Thus deterministic approaches [Bertsekas and Rhodes, 1971b], [Fogel and Huang, 1982]) that considers unknown but bounded perturbations and bounded noises have been elaborated. There are several deterministic approaches used for state estimation, like set-membership state estimation [Schweppe, 1968], interval observers [Pourasghar et al., 2016], [Petre et al., 2015] or robust filtering methods [El Ghaoui and Calafiore, 2001]. In the implementation of set-based deterministic estimation methods, various sets are used: polytopes [Walter and Piet-Lahanier, 1989], zonotopes [Combastel, 2003], [Alamo et al., 2005], [Le et al., 2013b], parallelotopes [Chisci et al., 1996], ellipsoids [Kurzahanski and Vályi, 1996], [Durieu et al., 2001], [Polyak et al., 2004], [Daryin et al., 2006], [Chernousko, 1994]. The low complexity of ellipsoids makes them widely used compared to polytopes which offer better accuracy of the estimation. [Combastel, 2015a] proposed a combination between stochastic and deterministic approaches, more exactly a zonotopic Kalman filter.

Despite the theoretical development of deterministic approaches, there is an obvious gap between theory and practice, and thus the need to apply more accurate recent state estimation techniques on real systems. In this context, the wide use of Unmanned Aerial Vehicles (UAVs) in resource monitoring [Laliberte and Rango, 2009], oil and gas [Hausamann et al., 2005], mapping [Nex and Remondino, 2014] or even for emergencies like forest fire surveillance [Casbeer et al., 2005] attracted more research attention from the scientific community. More specifically, studies related to the need of an accurate knowledge of linear and angular positions of drones are often conducted [Kingston and Beard, 2004]. Within this framework, several approaches have been adopted for the state estimation of a drone. The linear Kalman filter, as well as its extensions to non-linear systems have been widely used in industry to estimate the position of UAVs [Kada et al., 2016], [De Marina et al., 2011], [Teixeira et al., 2011]. Alternatively, attempts have been made to bridge the gap between set-membership state estimation theory and practice. For instance, a Zonotopic Extended Kalman Filter (ZEKF) applied to a quadrotor helicopter is presented in [Wang and Puig, 2016]. Moreover, in [Garcia et al., 2015], the results of an interval arithmetic based estimation technique applied to a quadrotor are compared with the results of a set-membership state estimation technique based on zonotopes. With the

proliferation of moderately low cost UAVs, radar-based techniques can now be tested on small drones. However, perturbations might cause the deviation of the drones from their planned trajectories leading to erroneous formation of radar images. Thereby, the use of set-membership state-estimation approaches arises from the need of guaranteed estimates of the system state in the presence of bounded measurement noises and perturbations.

In this chapter, a comparison in terms of accuracy and computation complexity is made between two estimation techniques studied in the literature: an ellipsoidal set-membership state estimation ([Ben Chabane et al., 2014], [Ben Chabane et al., 2014a]) and a classical Kalman filter. These results have been published to the 20th IFAC World Congress 2017. Additionally, we extend the ellipsoidal estimation technique to deal with system control signals, and then apply it to a linearized system of an Unmanned Aerial Vehicle (UAV) with eight rotors used for radar applications. This is one of the contributions of the thesis and was submitted to the special issue on "Interval estimation applied to diagnosis and control" of the International Journal of Control.

The remainder of the chapter is organized as follows. Section 4.3 formulates the state estimation problem for linear time invariant systems. Section 4.4 briefly presents ellipsoidal set-membership state estimation techniques existing in the literature with a focus on the technique that we will be extending. Section 4.2 reminds the state estimation problem using the classical Kalman Filter. Section 4.5 exposes the comparison between the two techniques. Then, Section 4.6 details the application of the ellipsoidal technique on a model of an octorotor used for radar applications along with the simulation results. Finally, conclusions of this chapter are drawn in Section 4.7.

4.2 Overview of the classical Kalman filter

Let us consider the following discrete-time linear time-invariant (LTI) system

$$\begin{cases} \mathbf{x}_{k+1} = \mathbf{A}\mathbf{x}_k + \mathbf{B}\mathbf{u}_k + \mathbf{E}_w\mathbf{w}_k, \\ \mathbf{y}_k = \mathbf{C}\mathbf{x}_k + \mathbf{F}_v\mathbf{v}_k, \end{cases} \quad (4.1)$$

where $\mathbf{x}_k \in \mathbb{R}^{n_x}$ is the state vector of the system, $\mathbf{u}_k \in \mathbb{R}^{n_u}$ is the input vector, and $\mathbf{y}_k \in \mathbb{R}^{n_y}$ is the measured output vector at sample time k with the matrices $\mathbf{A} \in \mathbb{R}^{n_x \times n_x}$, $\mathbf{B} \in \mathbb{R}^{n_x \times n_u}$, $\mathbf{C} \in \mathbb{R}^{n_y \times n_x}$, $\mathbf{E}_w \in \mathbb{R}^{n_x \times n_x}$ and $\mathbf{F}_v \in \mathbb{R}^{n_y \times n_y}$. We consider the assumptions that the pairs (\mathbf{A}, \mathbf{B}) and (\mathbf{A}, \mathbf{C}) are stabilizable and detectable, respectively. For the Kalman filter, the vectors $\mathbf{w}_k \in \mathbb{R}^{n_x}$ and $\mathbf{v}_k \in \mathbb{R}^{n_y}$ are random, independent white Gaussian noises, with the covariance matrices denoted by \mathbf{G}_w and \mathbf{G}_v , respectively, i.e. $\mathbf{w}_k \sim N(0, \mathbf{G}_w)$

and $\mathbf{v}_k \sim N(0, \mathbf{G}_v)$. Notice that the state is a random Gaussian vector and particularly the initial state is represented by $\mathbf{x}_0 \sim N(\mathbf{x}_{0|-1}, \mathbf{G}_{0|-1})$. The Kalman filter design is divided into two steps:

- *Prediction.* A previously estimated state $\hat{\mathbf{x}}_{k-1|k-1}$ and the linear nominal model (without any perturbation) are used to predict the value of the next estimated state $\hat{\mathbf{x}}_{k|k-1}$ as well as the state estimate covariance $\mathbf{G}_{k|k-1}$:

$$\hat{\mathbf{x}}_{k|k-1} = \mathbf{A}\hat{\mathbf{x}}_{k-1|k-1} + \mathbf{B}\mathbf{u}_{k-1}, \quad (4.2)$$

$$\mathbf{G}_{k|k-1} = \mathbf{A}\mathbf{G}_{k-1|k-1}\mathbf{A}^\top + \mathbf{E}_w\mathbf{G}_w\mathbf{E}_w^\top. \quad (4.3)$$

- *Correction.* The current output measurements and the statistical properties of the model are used to correct the state estimation, leading to compute the state estimate covariance:

$$\mathbf{S}_k = \mathbf{C}\mathbf{G}_{k|k-1}\mathbf{C}^\top + \mathbf{F}_v\mathbf{G}_v\mathbf{F}_v^\top, \quad (4.4)$$

$$\mathbf{K}_k = \mathbf{G}_{k|k-1}\mathbf{C}^\top\mathbf{S}_k^{-1}, \quad (4.5)$$

$$\hat{\mathbf{x}}_{k|k} = \hat{\mathbf{x}}_{k|k-1} + \mathbf{K}_k(\mathbf{y}_k - \mathbf{C}\hat{\mathbf{x}}_{k|k-1}), \quad (4.6)$$

$$\mathbf{G}_{k|k} = (\mathbf{I} - \mathbf{K}_k\mathbf{C})\mathbf{G}_{k|k-1}, \quad (4.7)$$

with \mathbf{K}_k the Kalman gain and \mathbf{S}_k the innovation covariance at time instant k .

4.3 Problem formulation

The aim of this section is to illustrate the problem formulation of a guaranteed state estimation set in set-membership state estimation technique. In this context, considering the system (4.1) with a state perturbation vector \mathbf{w}_k and a measurement perturbation vector (noise, offset, etc.) \mathbf{v}_k .

Combining \mathbf{w}_k and \mathbf{v}_k in a single vector $\boldsymbol{\omega}_k = [\mathbf{w}_k^\top \ \mathbf{v}_k^\top]^\top \in \mathbb{R}^{n_x+n_y}$, the system (4.1) can be rewritten in an equivalent form:

$$\begin{cases} \mathbf{x}_{k+1} &= \mathbf{A}\mathbf{x}_k + \mathbf{B}\mathbf{u}_k + \mathbf{E}\boldsymbol{\omega}_k, \\ \mathbf{y}_k &= \mathbf{C}\mathbf{x}_k + \mathbf{F}\boldsymbol{\omega}_k, \end{cases} \quad (4.8)$$

with the matrices $\mathbf{E} = [\mathbf{E}_w \ \mathbf{0}_{n_x, n_y}] \in \mathbb{R}^{n_x \times (n_x+n_y)}$ and $\mathbf{F} = [\mathbf{0}_{n_y, n_x} \ \mathbf{F}_v] \in \mathbb{R}^{n_y \times (n_x+n_y)}$. This form is useful in the comparison section between this filter and the ellipsoidal technique. The initial state is assumed to belong to a

compact set $\mathbf{x}_0 \in \mathcal{X}_0$ which can be chosen large enough due to the lack of knowledge on the system. Additionally, we assume that the vector $\boldsymbol{\omega}_k$ containing the state and the measurement perturbations is bounded by the unitary box $\mathbb{B}^{n_x+n_y}$.

Given an initial state set \mathcal{X}_0 (with $\mathbf{x}_0 \in \mathcal{X}_0$) and considering that at time k the state estimation set is $\hat{\mathcal{X}}_k$ (with $\mathbf{x}_k \in \hat{\mathcal{X}}_k$), the objective is to find the state estimation set $\hat{\mathcal{X}}_{k+1}$ that guarantees to contain the state \mathbf{x}_{k+1} of the system (4.8) at time $k+1$.

To solve this problem, three main steps are considered:

- *Prediction step*: The predicted state set is consistent with the evolution equation of the system (4.8). It offers bounds for the uncertain trajectory of the system. Therefore, $\bar{\mathcal{X}}_{k+1}$ is given by:

$$\bar{\mathcal{X}}_{k+1} \subseteq \mathbf{A}\hat{\mathcal{X}}_k \cup \mathbf{B}\mathbf{u}_k \cup \mathbf{E}\mathbb{B}^{n_x+n_y}. \quad (4.9)$$

- *Measurement step*: The consistent state set with the measurements $\mathcal{X}_{y_{k+1}}$ is given by:

$$\mathcal{X}_{y_{k+1}} = \{\mathbf{x}_{k+1} \in \mathbb{R}^{n_x} : (\mathbf{y}_{k+1} - \mathbf{C}\mathbf{x}_{k+1}) \in \mathbf{F}\mathbb{B}^{n_x+n_y}\}. \quad (4.10)$$

- *Correction step*: The guaranteed state estimation set $\hat{\mathcal{X}}_{k+1}$ at time instant $k+1$ is computed as an outer approximation of the intersection between the predicted state set $\bar{\mathcal{X}}_{k+1}$ and the measurement strip $\mathcal{X}_{y_{k+1}}$. Thus, the following expression is verified:

$$\hat{\mathcal{X}}_{k+1} \supseteq \bar{\mathcal{X}}_{k+1} \cap \mathcal{X}_{y_{k+1}}. \quad (4.11)$$

This methodology is generally applied to set-membership state estimation techniques. In particular, the set \mathcal{X} can have different geometric forms. In this chapter, ellipsoids are used for their simplicity of formulation [Durieu et al., 2001], [Polyak et al., 2004]. Figure 4.1 shows an example of the set-membership state estimation algorithm implemented with ellipsoids. The blue ellipsoid represents the predicted estimate at time instant $k+1$, and the green strip represents the measurements. The exact state estimation set that contains the real state is the intersection between these two sets. Nevertheless, the intersection has (in general) an arbitrary shape (the grey part), thus the need of outer-approximating it by an ellipsoid for simplicity reasons. For this, the Outer Bounding Ellipsoid (OBE) algorithm [Fogel and Huang, 1982] can be used.

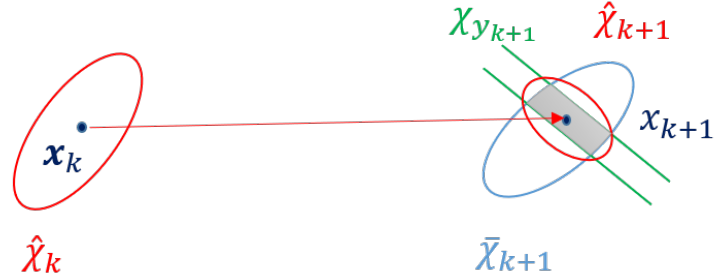


Figure 4.1 – Illustration of the ellipsoidal state estimation method

In the next section, we introduce an improvement of a previously developed ellipsoidal set-membership state estimation technique [Ben Chabane, 2015]. Considering the system (4.8), we assume that:

- The pairs (\mathbf{A}, \mathbf{B}) and (\mathbf{A}, \mathbf{C}) are respectively stabilizable and detectable,
- The matrices \mathbf{E} and \mathbf{F} represent weights for the normalized noises $\omega_k \in \mathbb{B}^{n_x+n_y}$,
- The initial state belongs to the ellipsoid:

$$\mathcal{E}(\mathbf{P}_0, \bar{\mathbf{x}}_0, \rho_0) = \{\mathbf{x}_0 \in \mathbb{R}^{n_x} : (\mathbf{x}_0 - \bar{\mathbf{x}}_0)^\top \mathbf{P}_0 (\mathbf{x}_0 - \bar{\mathbf{x}}_0) \leq \rho_0\}, \quad (4.12)$$

with $\mathbf{P}_0 = \mathbf{P}_0^\top \succ 0$ being the shape matrix, $\bar{\mathbf{x}}_0$ the center and ρ_0 the so-called radius [Ben Chabane, 2015].

Goal: Given an ellipsoidal state estimation set $\mathcal{E}(\mathbf{P}, \bar{\mathbf{x}}_k, \rho_k)$ for the state vector \mathbf{x}_k at time instant k , with $\bar{\mathbf{x}}_k$ the nominal estimated state, the goal of the following technique is to provide a state estimation set of the form $\mathcal{E}(\mathbf{P}, \bar{\mathbf{x}}_{k+1}, \rho_{k+1})$ for the state \mathbf{x}_{k+1} at time instant $k + 1$.

4.4 Ellipsoidal state estimation technique

This section briefly describes and improves the ellipsoidal guaranteed state estimation technique [Ben Chabane, 2015] based on the minimization of the radius of the ellipsoidal estimation at each sample time k by solving an optimization problem. Considering the system (4.8), the technique [Ben Chabane, 2015] was improved by considering input signals in this section. The dynamics of the state at each time instant \mathbf{x}_k is now governed by the initial state \mathbf{x}_0 and the control signal \mathbf{u}_k . This leads to some modifications in the initial theorem [Ben Chabane, 2015], that we will be detailing here.

The system state \mathbf{x}_{k+1} is guaranteed to belong to the following ellipsoid $\mathcal{E}(\mathbf{P}_{k+1}, \bar{\mathbf{x}}_{k+1}, \rho_{k+1})$ if, for the matrices $\mathbf{Y}_{k+1} \in \mathbb{R}^{n_x \times n_y}$, $\mathbf{G}_{k+1} \in \mathbb{R}^{n_x \times n_x}$, the vector $\mathbf{g}_{k+1} \in \mathbb{R}^{n_x}$ and the scalars $\beta_{k+1}, \rho_{k+1} > 0$, the following Linear Matrix Inequality (LMI) ([Ben Chabane, 2015], page 113) is satisfied:

$$\begin{aligned} & \min_{\beta_{k+1}, \mathbf{Y}_{k+1}, \mathbf{P}_{k+1}, \rho_{k+1}, \mathbf{G}_{k+1}, \mathbf{g}_{k+1}, \alpha, \gamma} \alpha \\ & \text{subject to} \end{aligned} \quad \left\{ \begin{array}{l} \left[\begin{array}{ccc} \beta_{k+1} \mathbf{P}_k & * & * \\ \mathbf{0} & \rho_{k+1} - \beta_{k+1} \rho_k & * \\ \mathbf{P}_{k+1} \mathbf{A} - \mathbf{Y}_{k+1} \mathbf{C} & \boldsymbol{\tau}_{k+1} & \mathbf{P}_{k+1} \end{array} \right] \succ 0, \\ \mathbf{P}_{k+1} \geq \mathbf{P}_k, \\ \rho_{k+1} \leq \alpha \rho_k + \gamma, \\ 0 < \alpha < 1, \\ \gamma > 0, \\ \rho_{k+1} > 0, \end{array} \right. \quad (4.13)$$

for all $\boldsymbol{\omega}_k$ belonging to the vertices set of the box $\mathbb{B}^{n_x+n_y}$, with the matrix:

$$\mathbf{Y}_k = \mathbf{P}_k \mathbf{L}_k,$$

the vector:

$$\boldsymbol{\tau}_{k+1} = (\mathbf{P}_{k+1} \mathbf{A} - \mathbf{Y}_{k+1} \mathbf{C} - \mathbf{G}_{k+1}) \bar{\mathbf{x}}_k + (\mathbf{P}_{k+1} \mathbf{E} - \mathbf{Y}_{k+1} \mathbf{F}) \boldsymbol{\omega}_{k+1} - \mathbf{g}_{k+1} + \mathbf{B}(\mathbf{u}_k - \bar{\mathbf{u}}_k),$$

and the nominal estimated state:

$$\bar{\mathbf{x}}_{k+1} = \mathbf{P}_{k+1}^{-1} (\mathbf{G}_{k+1} \bar{\mathbf{x}}_k + \mathbf{Y}_{k+1} \mathbf{y}_k + \mathbf{g}_{k+1}) + \mathbf{B} \bar{\mathbf{u}}_k,$$

with $\bar{\mathbf{u}}_k$ the nominal control signal¹. The constraint:

$$\rho_{k+1} \leq \alpha \rho_k + \gamma,$$

with $0 < \alpha < 1$ and γ a strictly positive scalar serving to bound the so-called radius of the ellipsoidal estimation $\mathcal{E}(\mathbf{P}_{k+1}, \bar{\mathbf{x}}_{k+1}, \rho_{k+1})$ in order to decrease the estimation set. The scalar γ bounds the effect of any additive terms.

The proof of this result is similar to the proof provided by [Ben Chabane, 2015] with the additional terms $\mathbf{B} \bar{\mathbf{u}}_k$ in $\boldsymbol{\tau}_{k+1}$ and $\bar{\mathbf{x}}_{k+1}$. Indeed, denoting by:

$$\mathbf{z}_k = \mathbf{x}_k - \bar{\mathbf{x}}_k,$$

¹By considering a nominal control signal, we assume that the technique can work with unknown control inputs.

the error between the real state and the nominal estimated state at time k , the goal is to prove that the following expression holds at each time instant k , based on the results proposed in [Ben Chabane, 2015]:

$$\mathbf{z}_k^\top \mathbf{P}_k \mathbf{z}_k \leq \rho_k \Rightarrow \mathbf{z}_{k+1}^\top \mathbf{P}_{k+1} \mathbf{z}_{k+1} \leq \rho_{k+1}.$$

At the time instant $k + 1$, the error is computed such that:

$$\mathbf{z}_{k+1} = (\mathbf{A} - \mathbf{L}_{k+1} \mathbf{C}) \mathbf{z}_k + (\mathbf{A} - \mathbf{L}_{k+1} \mathbf{C}) \bar{\mathbf{x}}_k + (\mathbf{E} - \mathbf{L}_{k+1} \mathbf{F}) \boldsymbol{\omega}_k - \mathbf{P}_{k+1}^{-1} (\mathbf{G}_{k+1} \bar{\mathbf{x}}_k + \mathbf{g}_{k+1}).$$

Notice that the evolution of the error \mathbf{z}_{k+1} relies on the eigenvalues of the matrix $\mathbf{A} - \mathbf{L}_{k+1} \mathbf{C}$. Additionally, the computation of the matrix \mathbf{G}_{k+1} and the vector \mathbf{g}_{k+1} guarantees a faster convergence of the error to zero. In this context, the observer (which is similar to the structure of the Luenberger observer) is stable since \mathbf{z}_k converges to zero. Besides minimizing the size of the estimation set by solving the LMI problem (4.13), this method also reduces the conservativeness of the estimation by allowing the adjustment of the ellipsoid shape. Indeed, considering the matrix \mathbf{P}_{k+1} as a decision variable can modify the shape of the ellipsoid at time instant $k + 1$ compared to the ellipsoid at the previous time instant.

The advantage of this method lies in the trade-off between its good accuracy and reduced complexity [Ben Chabane, 2015] compared to other techniques in the literature. Indeed, the proposed ellipsoidal state estimation method offers better accuracy than the P -radius based zonotopic state estimation technique [Le et al., 2013b] and the three ellipsoidal-based state estimation techniques presented in [Ben Chabane et al., 2014]. The ellipsoidal set-membership state estimation technique takes into consideration the measurements at time instant k , when computing the estimated ellipsoidal set $\mathcal{E}(\mathbf{P}_{k+1}, \bar{\mathbf{x}}_{k+1}, \rho_{k+1})$ at time instant $k + 1$. However, the estimation accuracy can be improved by considering additional quadratic constraints on the output measurements [Ben Chabane, 2015]:

$$\mathbf{y}_{k+1} = \mathbf{C} \mathbf{x}_{k+1} + \mathbf{F} \boldsymbol{\omega}_{k+1}$$

and on the perturbations vector at time instant $k + 1$ such that:

$$\boldsymbol{\omega}_{k+1}^\top \tilde{\mathbf{T}}_i \boldsymbol{\omega}_{k+1} \leq 1,$$

with $i = 1, \dots, n_x + n_y$ and $\tilde{\mathbf{T}}_i = \mathbf{e}_i \mathbf{e}_i^\top$ the matrix having only the element (i, i) equal to 1. The updated method, improves the accuracy of the estimation by decreasing the size of the ellipsoid $\hat{\mathcal{E}}_{k+1}$ at each iteration. In this context, considering the ellipsoidal state estimation set $\mathcal{E}(\mathbf{P}, \bar{\mathbf{x}}_{k+1}, \rho_{k+1})$ obtained by solving the previous LMI (4.13), an updated set $\mathcal{E}'(\mathbf{P}', \bar{\mathbf{x}}'_{k+1}, \rho'_{k+1})$

can be found if the following LMI problem ([Ben Chabane, 2015], page 118) is verified:

$$\begin{aligned}
 & \min_{\rho'_{k+1}, \mathbf{P}', \mathbf{b}_{k+1}, \mathbf{H}, \theta, \mu_i, \alpha, \gamma} \alpha \\
 & \text{subject to} \\
 & \left\{ \begin{array}{l} \left[\begin{array}{ccc} \boldsymbol{\eta}_1 & \boldsymbol{\eta}_2^\top & \mathbf{P}'_{k+1} \\ \boldsymbol{\eta}_2 & \eta_3 - \sum_{i=1}^{n_x+n_y} \mu_i & -\mathbf{b}_{k+1}^\top \\ \mathbf{P}'_{k+1} & -\mathbf{b}_{k+1} & \mathbf{P}'_{k+1} \end{array} \right] \succ 0, \\ \mathbf{P}' \succ 0, \\ \mathbf{F}^\top \mathbf{H} \mathbf{F} < \sum_{i=1}^{n_x+n_y} \mu_i \tilde{\mathbf{T}}_i, \\ \theta \geq 0, \\ \theta < 1, \\ \rho'_{k+1} > \theta \rho_{k+1}, \\ \mu_i \geq 0, \quad i = 1, \dots, n_x + n_y, \\ \mathbf{P}'_{k+1} \geq \mathbf{P}_{k+1}, \\ \rho_{k+1} \leq \alpha \rho_k + \gamma, \\ \gamma > 0, \end{array} \right. \quad (4.14)
 \end{aligned}$$

with:

$$\begin{aligned}
 \mathbf{b}_{k+1} &= \mathbf{P}'_{k+1} \bar{\mathbf{x}}_{k+1}, \\
 \boldsymbol{\eta}_1 &= \theta \mathbf{P}_{k+1} + \mathbf{C}^\top \mathbf{H} \mathbf{C}, \\
 \boldsymbol{\eta}_2 &= -\theta \bar{\mathbf{x}}_{k+1}^\top \mathbf{P}_{k+1} - \mathbf{y}_{k+1}^\top \mathbf{H} \mathbf{C} + \mathbf{u}_k^\top \mathbf{B}^\top \mathbf{C}^\top \mathbf{H} \mathbf{C}, \\
 \eta_3 &= \rho'_{k+1} - \theta \rho_{k+1} + \theta \|\bar{\mathbf{x}}_{k+1}\|_{\mathbf{P}_{k+1}}^2 + \|\mathbf{y}_{k+1}\|_{\mathbf{H}}^2 + \|\mathbf{C} \mathbf{B} \mathbf{u}_k\|_{\mathbf{H}}^2 - 2 \mathbf{u}_k^\top \mathbf{B}^\top \mathbf{C}^\top \mathbf{H} \mathbf{y}_{k+1}.
 \end{aligned}$$

The proof of this result is similar to [Ben Chabane, 2015], with the additional terms related to the control signal in η_2 and η_3 . Exhaustively, supposing that $\mathbf{x}_{k+1} \in \mathcal{E}(\mathbf{P}, \bar{\mathbf{x}}_{k+1}, \rho_{k+1})$, the expression (4.14) offers an improved ellipsoidal state estimation set $\mathcal{E}'(\mathbf{P}', \bar{\mathbf{x}}'_{k+1}, \rho'_{k+1})$. Due to the fact that this estimation method changes both the shape and the radius at each iteration k , the computational complexity can be high even though it offers a very good accuracy estimation wise. This accuracy in addition to complexity will be further exploited where the technique is compared to the classical Kalman filter in the next section.

Remark 4.1. Notice that this technique can also be applied on linear time varying systems with interval uncertainties [Ben Chabane, 2015]. Even though it is considered to be an important advantage of this method, this characteristic will not be tested in this chapter.

4.5 Comparison between two state estimation techniques for linear time-invariant systems

The main difference between the approaches presented in Sections 4.2 and 4.4 can be mainly spotted in terms of assumptions considered for the system modeling. The ellipsoidal set-membership state estimation guarantees the estimated bounds of the state within an ellipsoid for any LTI system, while certain requirements should be met in order to efficiently run the classical Kalman filter. The Kalman filter (well known for its implementation facility) works properly when the LTI model matrices are fixed and do not present parametric uncertainties. The set-membership state estimation offers guaranteed bounds for the state estimation despite the presence of possible bounded perturbations, measurement noises and even interval uncertainties on the evolution matrix \mathbf{A} of the system (4.8) [Ben Chabane, 2015].

However, the Kalman filter offers a reduced computation complexity with respect to the considered set-membership estimation method. In fact, the Kalman equations are based on basic matrix operations and the computational complexity can be approximated by the number of multiplications per loop. Using the expressions (4.2)-(4.7) and considering the worst case scenario (i.e. full matrices) we can approximate the filter computational complexity to $\mathcal{O}(N^3)$, with $N = \max(n_x, n_y)$.

The computational complexity of the ellipsoidal state estimation method relies on solving a LMI optimization problem. The `mincx` solver of the Matlab Robust Control Toolbox is based on the interior point method which is an iterative technique solving a least square problem at each iteration [Nesterov and Nemirovski, 1994]. The complexity of the method in the worst case scenario can be approximated to $\mathcal{O}(o^{2.75}l^{1.5})$ with o the number of scalar decision variables and l the number of constraints [Vandenberghe and Boyd, 1994]. Notice that $o = (n_x + n_y)^2 + n_x n_y + 2$ and $l = 2^{n_x + n_y} + 3$ for the optimization problem (4.13) and $o = 0.5(n_x^2 + n_y^2) + 2.5n_x + 1.5n_y + 2$ and $l = n_x + n_y + 6$ for the optimization problem (4.14).

The comparison allows us to conclude that the Kalman filter offers us a better result in terms of complexity, thus faster computations. In terms of accuracy, and for each iteration, the ellipsoidal method computes an ellipsoidal set to which the real state is guaranteed to belong. The set-membership estimation setup offers the possibility to use correlated/uncorrelated perturbations and measurement noises, however the choice of the perturbation bounds needs good knowledge of the plant. The Kalman filter uses the assumption of Gaussian noises, which can be difficult to verify for some real

plants.

A numerical example is considered to illustrate the comparison of the presented state estimation techniques.

Example 4.1. Consider the following stable LTI system:

$$\begin{cases} \mathbf{x}_{k+1} = \begin{bmatrix} -0.8 & 0.2 \\ -0.3 & 0.1 \end{bmatrix} \mathbf{x}_k + \begin{bmatrix} -0.12 \\ 0.02 \end{bmatrix} w_k \\ y_k = \begin{bmatrix} -2 & 1 \end{bmatrix} \mathbf{x}_k + 0.2v_k \end{cases} \quad (4.15)$$

In this example, we present the results obtained by the improved guaranteed ellipsoidal set-membership state estimation (4.14) compared to the results obtained by Kalman filter. In order to make a valid comparison between these two techniques, appropriate assumptions should be taken regarding the initial state and noises. In fact, the following assumptions were made for the Kalman filter:

- $\mathbf{x}_0 \sim N(\mathbf{x}_{0|-1}, \mathbf{G}_{0|-1})$, with $\mathbf{x}_{0|-1} = [5 \ 5]^\top$ and $\mathbf{G}_{0|-1} = \mathbf{I}_2$,
- $w_k \sim N(0, 1)$, $v_k \sim N(0, 1)$.

Simultaneously, the following assumptions were made for the ellipsoidal set-membership state estimation approach:

- $\mathbf{x}_0 \in \mathcal{E}(\mathbf{P}_0, \mathbf{x}_{0|-1}, \rho_0)$, with $\mathbf{P}_0 = \mathbf{I}_2$ and $\rho_0 = 20$,
- $\boldsymbol{\omega}_k = [\mathbf{w}_k^\top \ \mathbf{v}_k^\top]^\top \in \mathbb{B}^{n_x+n_y}$ leading to $|w_k| \leq 1$ and $|v_k| \leq 1$.

Indeed, the covariance matrix of the initial state $\mathbf{G}_{0|-1}$ is chosen such that the initial probabilistic confidence ellipsoid has the same shape as the initial ellipsoid in the ellipsoidal technique with the matrix shape \mathbf{P}_0 . Additionally, the noise generated in both cases are bounded by unitary boxes and generated with the `rand` function of Matlab.

Figures 4.2 and 4.3 show the bounds of x_1 and x_2 , respectively, after 10 iterations obtained by the ellipsoidal set-membership state estimation method (4.14) and the Kalman filter. The real state (red asterisk) is always inside the guaranteed bounds (in dashed blue) calculated by the ellipsoidal set-membership method (4.14). It can be noticed that, in this example, the state estimated with the Kalman filter (black asterisk) has a slower convergence and it is not always inside the guaranteed bounds obtained with the improved set-membership method.

When it comes to the computational complexity, the Kalman filter takes around 0.21ms per iteration, while the set-membership estimation technique

(LMIs (4.13) and (4.14)) spends around 10ms to determine the estimation bounds.

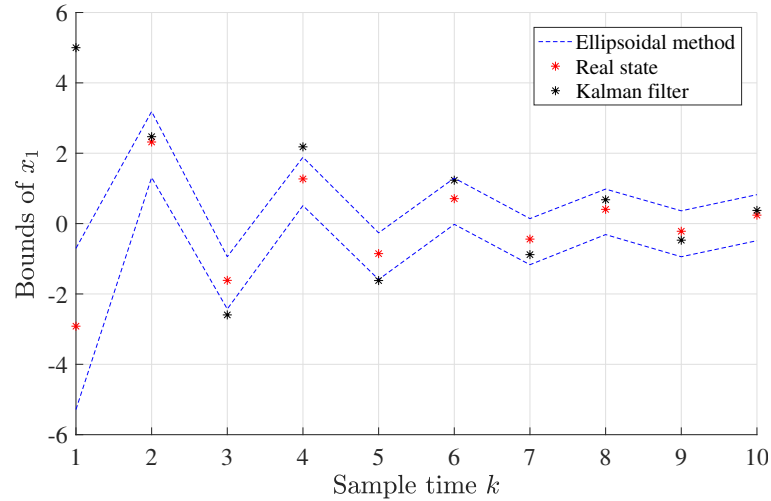


Figure 4.2 – Example 4.1: bounds of x_1

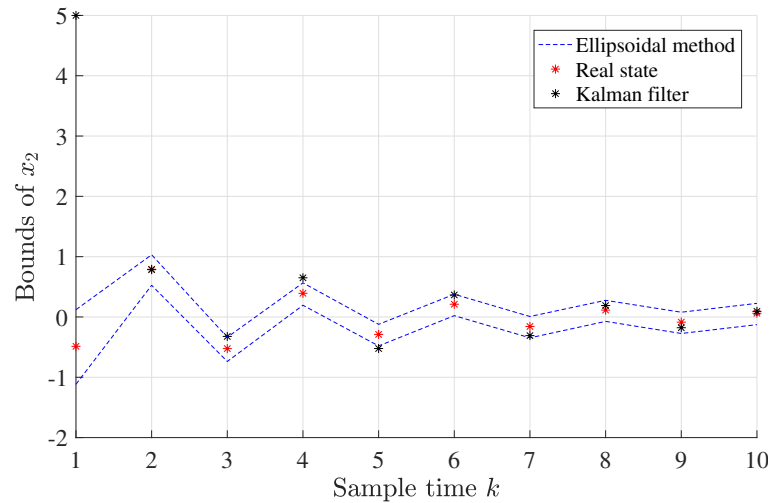


Figure 4.3 – Example 4.1: bounds of x_2

To take advantage of the ellipsoidal technique, it will be further exploited in the next section to the case of a linear octorotor model used in the context of radar applications.

4.6 Application to an octorotor model

Low cost UAVs gave the users and researchers an enormous potential to test their work in various fields of science, notably automatic control. Recently, control strategies are being tested and mounted on various type of drones like quadrotors or octorotors. In some applications, a precise estimation of the state of the UAV is needed because perturbations leads to a deviation of the drones from their planned trajectories which might cause, in a radar context for example, an erroneous formation of radar images. In order to take advantage of its high accuracy, the guaranteed ellipsoidal set-membership state estimation technique exposed in the previous Sections 4.4 and 4.5 and inspired from [Ben Chabane, 2015] is applied in this section on an octorotor. The goal is to guarantee the drone's position when bounded perturbations and measurement noises are considered. Using ellipsoidal representations, the proposed technique computes the set of states that are consistent with the model in a first phase and with the measurements in second phase such that the system's real state is guaranteed to belong to this set. The advantage of this method lies in its good accuracy and reduced complexity [Ben Chabane, 2015]. Using the radar system embedded in the UAV, as well as the estimated coordinates of the drone, an image reconstruction application is exposed to value the efficiency of the set-membership state estimation technique. Furthermore, the real distance separating the drone from the target is guaranteed to be inside the computed bounds. The relative error done by the estimation leads to the calculation of the operating frequency of the radar.

As an experimental platform, the Mikrokopter ARF Okto-XL drone (Figure 4.4) is used in this paper. The higher payload capacity and the motor redundancy make this octorotor more advantageous over traditional quadrotor aircraft for radar applications. In this context, the UAV is equipped with radar sensors in order to scan large areas and provide high resolution images, thus there is a need for an accurate estimation of the drone's position (which is also the radar's position²) and guaranteed limits for perturbations. The challenge of this estimation problem resides in the model complexity and the possible uncertainties coming from various sources (e.g. measurement noises, perturbations).

²For simplicity reasons, we assume that SAR sensor position and the octorotor position are identical.

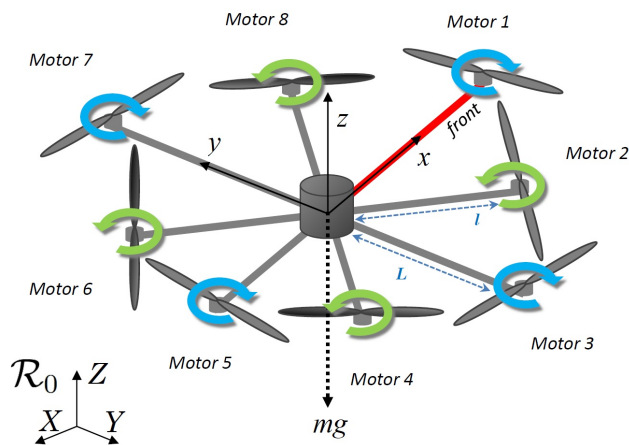


Figure 4.4 – Mikrokopter ARF representation and the associated drone’s frame R

4.6.1 Octorotor modeling

The Mikrokopter ARF Okto-XL (Figure 4.4) is equipped with an inertial measurement unit (IMU), an altimeter, a GPS and a magnetometer. The drone’s microcontroller provides fused and filtered data on its position coordinates (both linear and angular). The measurement data are transferred to the PC through the microcontroller’s serial port for off-line data processing. The octorotor’s motion in a state-space representation can be obtained using twelve states (see Figure 4.4):

- the drone’s position in the Earth’s frame x , y and z ,
- the drone’s orientation in the Earth’s frame ϕ , θ and ψ ,
- the drone’s speed in the same frame V_x , V_y and V_z ,
- the drone’s rotational speed in its own frame ω_x , ω_y and ω_z .

This leads to the following state vector:

$$\mathbf{x} = [x \ y \ z \ \phi \ \theta \ \psi \ V_x \ V_y \ V_z \ \omega_x \ \omega_y \ \omega_z]^\top. \quad (4.16)$$

The nonlinear continuous-time dynamical model of the drone used to simulate its behavior is presented in [Makarov et al., 2015]. However, while this nonlinear model can be useful to evaluate the drone performances in simulation, a simplified linear model will be used for the development of linear control laws based on estimation techniques. The model is linearized

around the static hovering equilibrium with null translational and rotational velocities and null roll, pitch and yaw angles. The linear continuous-time state-space equation can be denoted by:

$$\dot{\mathbf{x}}(t) = \mathbf{A}_c \mathbf{x}(t) + \mathbf{B}_c \mathbf{u}(t), \quad (4.17)$$

with the state vector $\mathbf{x} \in \mathbb{R}^{12}$, the control vector:

$$\mathbf{u} = \left[F_x^R \quad F_y^R \quad F_z^R \quad \tau_x^R \quad \tau_y^R \quad \tau_z^R \right]^\top \in \mathbb{R}^6,$$

where F_x^R , F_y^R and F_z^R are the components of the resulting propeller's force and τ_x^R , τ_y^R and τ_z^R are the components of the resulting propeller's torque expressed in the drone's frame denoted by the superscript R . The matrices $\mathbf{A}_c \in \mathbb{R}^{12 \times 12}$ and $\mathbf{B}_c \in \mathbb{R}^{12 \times 6}$ are provided in [Makarov et al., 2015]. The thrust force and drag torque generated by the i -th propeller are assumed to be proportional to the squared propeller's speed Ω_i , with $i = \{1, 2, \dots, 8\}$. The new reduced control vector in this case can be expressed as a linear combination of the rotational speeds of the motor Ω_i denoted by the matrix \mathbf{M}_u , leading to $\mathbf{u}(t) = \mathbf{M}_u \boldsymbol{\Omega}$, with $\boldsymbol{\Omega} = [\Omega_1 \quad \Omega_2 \quad \dots \quad \Omega_8]^\top$.

In order to avoid the high computation complexity of the ellipsoidal state estimation method, the 12-state linearized model is decoupled into three double integrator subsystems detailed below. In fact, decoupling the 12-state octorotor model into 3 subsystems (4.21)-(4.23) allows us to reduce the number of LMI constraints in (4.13) from $2^{3(n_x+n_y)}$ to $3 \cdot 2^{n_x+n_y}$.

- **Continuous-time subsystem 1 (altitude and yaw dynamics)** It describes the altitude dynamics expressed by the altitude z and the velocity V_z of the drone on this axis as well as the movement of the drone around the vertical axis that changes the direction the drone is pointing to:

$$\begin{cases} \dot{z}(t) &= V_z(t), \\ \dot{\psi}(t) &= \omega_z(t), \\ \dot{V}_z(t) &= \frac{1}{m} F_z^R(t), \\ \dot{\omega}_z(t) &= \frac{1}{I_{zz}} \tau_z^R(t), \end{cases} \quad (4.18)$$

with m the octorotor's mass and I_{zz} the UAV's inertia component around z-axis.

- **Continuous-time subsystem 2 (roll and pitch dynamics)** It describes the movement of the drone around the roll axis (front-to-back)

and the pitch (side-to-side) axis:

$$\left\{ \begin{array}{l} \dot{\phi}(t) = \omega_x(t), \\ \dot{\theta}(t) = \omega_y(t), \\ \dot{\omega}_x(t) = \frac{1}{I_{xx}}\tau_x^R(t), \\ \dot{\omega}_y(t) = \frac{1}{I_{yy}}\tau_y^R(t), \end{array} \right. \quad (4.19)$$

with I_{xx} and I_{yy} the UAV's inertia components around the x -axis and the y -axis respectively.

- **Continuous-time subsystem 3 (longitudinal dynamics)** It refers to the motion of the drone across the longitudinal axis denoted by the linear coordinates (x and y) with the corresponding velocities on the two axes (V_x and V_y , respectively):

$$\left\{ \begin{array}{l} \dot{x}(t) = V_x(t), \\ \dot{y}(t) = V_y(t), \\ \dot{V}_x(t) = \frac{1}{m}F_x^R(t), \\ \dot{V}_y(t) = \frac{1}{m}F_y^R(t). \end{array} \right. \quad (4.20)$$

However, simplifying conditions should be met for the obtained decoupled model to hold. Indeed, the rotational angles (i.e. roll, pitch and yaw) should be as small as possible and maintained as close as possible to zero. To quantify this constraint, the change in these angles should not exceed 0.2618rad or 15° [Abdolhosseini et al., 2013], which is the case in the considered radar application.

The subsystems 1 and 2 describe the angular behavior of the drone, in addition to its altitude, while the subsystem 3 describes the linear movement on both of the x -axis and the y -axis. These subsystems are then discretized with a sampling period T_e which is equal to the highest of all sensors sampling periods. This leads to the linear discrete-time state-space representations (4.21), (4.22) and (4.23):

• **Discretized subsystem 1:**

$$\left\{ \begin{array}{l} \begin{bmatrix} z_{k+1} \\ \psi_{k+1} \\ V_{z_{k+1}} \\ \omega_{z_{k+1}} \end{bmatrix} = \mathbf{A} \begin{bmatrix} z_k \\ \psi_k \\ V_{z_k} \\ \omega_{z_k} \end{bmatrix} + \begin{bmatrix} 0 & 0 \\ 0 & 0 \\ \frac{T_e}{m} & 0 \\ 0 & \frac{T_e}{I_{zz}} \end{bmatrix} \begin{bmatrix} F_{z_k}^R \\ \tau_{z_k}^R \end{bmatrix} + \mathbf{E}_1 \boldsymbol{\omega}_k, \\ \\ \begin{bmatrix} z_k \\ \psi_k \end{bmatrix} = \mathbf{C} \begin{bmatrix} z_k \\ \psi_k \\ V_{z_k} \\ \omega_{z_k} \end{bmatrix} + \mathbf{F}_1 \boldsymbol{\omega}_k, \end{array} \right. \quad (4.21)$$

• **Discretized subsystem 2:**

$$\left\{ \begin{array}{l} \begin{bmatrix} \phi_{k+1} \\ \theta_{k+1} \\ \omega_{x_{k+1}} \\ \omega_{y_{k+1}} \end{bmatrix} = \mathbf{A} \begin{bmatrix} \phi_k \\ \theta_k \\ \omega_{x_k} \\ \omega_{y_k} \end{bmatrix} + \begin{bmatrix} 0 & 0 \\ 0 & 0 \\ \frac{T_e}{I_{xx}} & 0 \\ 0 & \frac{T_e}{I_{yy}} \end{bmatrix} \begin{bmatrix} \tau_{x_k}^R \\ \tau_{y_k}^R \end{bmatrix} + \mathbf{E}_2 \boldsymbol{\omega}_k, \\ \\ \begin{bmatrix} \phi_k \\ \theta \end{bmatrix} = \mathbf{C} \begin{bmatrix} \phi_k \\ \theta_k \\ \omega_{x_k} \\ \omega_{y_k} \end{bmatrix} + \mathbf{F}_2 \boldsymbol{\omega}_k, \end{array} \right. \quad (4.22)$$

• **Discretized subsystem 3:**

$$\left\{ \begin{array}{l} \begin{bmatrix} x_{k+1} \\ y_{k+1} \\ V_{x_{k+1}} \\ V_{y_{k+1}} \end{bmatrix} = \mathbf{A} \begin{bmatrix} x_k \\ y_k \\ V_{x_k} \\ V_{y_k} \end{bmatrix} + \begin{bmatrix} 0 & 0 \\ 0 & 0 \\ \frac{T_e}{m} & 0 \\ 0 & \frac{T_e}{m} \end{bmatrix} \begin{bmatrix} F_{x_k}^R \\ F_{y_k}^R \end{bmatrix} + \mathbf{E}_3 \boldsymbol{\omega}_k, \\ \\ \begin{bmatrix} x_k \\ y_k \end{bmatrix} = \mathbf{C} \begin{bmatrix} x_k \\ y_k \\ V_{x_k} \\ V_{y_k} \end{bmatrix} + \mathbf{F}_3 \boldsymbol{\omega}_k. \end{array} \right. \quad (4.23)$$

The same matrices $\mathbf{A} = \begin{bmatrix} \mathbf{I}_2 & T_e \mathbf{I}_2 \\ \mathbf{0}_2 & \mathbf{I}_2 \end{bmatrix}$ and $\mathbf{C} = \begin{bmatrix} \mathbf{I}_2 & \mathbf{0}_2 \end{bmatrix}$ are obtained for the three subsystems. The perturbations and the measurement noises are considered to be modeled by the vector $\boldsymbol{\omega}_k$ which is bounded by the unitary box \mathbb{B}^6 and the matrices $\mathbf{E}_i = \epsilon_i \cdot \begin{bmatrix} \mathbf{I}_4 & \mathbf{0}_{4 \times 2} \end{bmatrix}$, $\mathbf{F}_i = \gamma_i \cdot \begin{bmatrix} \mathbf{0}_4 & \mathbf{I}_{4 \times 2} \end{bmatrix}$, for $i \in \{1, 2, 3\}$. The scalars ϵ_i and γ_i represent the accuracy precision provided by the sensors information. The reader will notice that the discretized subsystems (4.21),

(4.22) and (4.23) of the octorotor are written in the form (4.8). In the following, this octorotor is the application platform for a guaranteed ellipsoidal set-membership state estimation technique, used in the design of Synthetic Aperture Radar (SAR) detailed in the next section.

4.6.2 Application to the design of SAR

Synthetic Aperture Radar (SAR) has been proposed in the fifties to provide images of large areas with high resolution [Carrara et al., 1995]. Since then, airplanes and satellites have been the main carriers of SAR sensors [Moreira et al., 2013]. In recent years, due to reduction in their cost and weight, SAR sensors are being mounted and tested on small UAVs [Zaugg et al., 2006], [Yan et al., 2008], [Gonzalez-Partida et al., 2008]. Moreover, SAR images are formed using the phase evolution resulted from comparing (e.g. via match filtering) a SAR transmitted pulse signal (i.e. typically thousands of pulses per second, hence the term Pulse Repetition Frequency – PRF) with the received scattered signal of the illuminated scatterers of the scene under study [Carrara et al., 1995], [Moreira et al., 2013]. This is done while the SAR sensor is moving. A popular operating mode for SAR is the stripmap (side-looking), where ideally the SAR antenna points to a fixed direction (as illustrated in Figure 4.5) and the sensor is assumed to move in a perfect linear trajectory with a constant speed and orientation, which is not the case for the UAV used in this work. Indeed, and even under the best circumstances, perturbations will cause the drone’s path to deviate from its assumed coordinates. As a result, errors might occur in the formation of SAR images if the deviation (e.g. the difference between the ideal and the real UAV’s position) is not accurately taken into account. Errors on the estimation of the position of the SAR sensor (hence, the UAV’s position) lead to errors on the relative distance D_r between the SAR sensor and the scatterer (see Figure 4.5), which involve a phase error ϕ_e in the SAR data as shown in the next equation:

$$\phi_e = \frac{4\pi\delta_D f_0}{c_0}, \quad (4.24)$$

where δ_D is the error on the estimation of the relative distance D_r , with $D_r \in [D_{min}, D_{max}]$, f_0 is the working frequency and c_0 is the light speed in free-space (equation adapted from [Carrara et al., 1995], page 225) where the working wavelength has been replaced by:

$$\lambda = \frac{f_0}{c_0}. \quad (4.25)$$

In this work, the drone’s linear position is estimated using the ellipsoidal

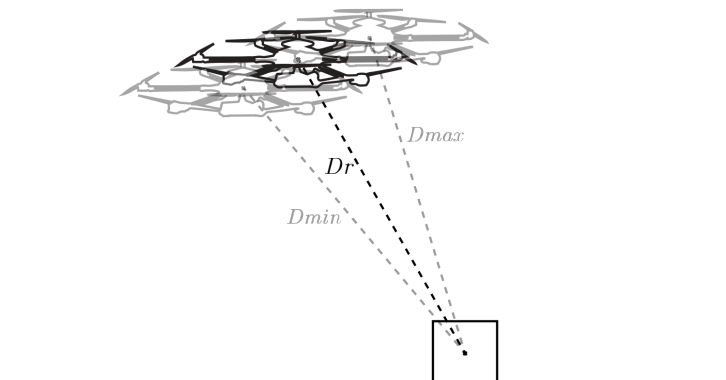


Figure 4.5 – Representation of the drone and the scatterer

state estimation technique detailed in Section 4.4. This method offers guaranteed estimation bounds for the coordinates at each iteration. Thus, the relative distance D_r between the drone and the scatterer can be computed and bounded by a maximal D_{max} and minimal D_{min} bounds. For instance, the estimation error of the drone's position on both axes induces a relative distance error between the UAV and the scatterer. The next two figures present examples of SAR images with an accurately estimated UAV position (Figure 4.6) and with an erroneous estimated UAV position (Figure 4.7). The SAR parameters for these examples are detailed in Table 4.1. As the Figure 4.7 shows, due to phase errors, the position of a single scatterer at 50m range and 2m azimuth with respect to the scanned region can be mistaken as being three scatterers.

Table 4.1 – SAR parameters

| | |
|---------------------|--------|
| PRF | 2kHz |
| Bandwidth | 200MHz |
| Operating frequency | 5GHz |
| Scatterer position | |
| Azimuth | 2m |
| Ground range | 50m |

It is common to use signal processing autofocus techniques to compensate these phase errors as long as they are inferior to about 60rad [Carrara et al., 1995]. Therefore, according to (4.24), knowing the maximum error amplitude

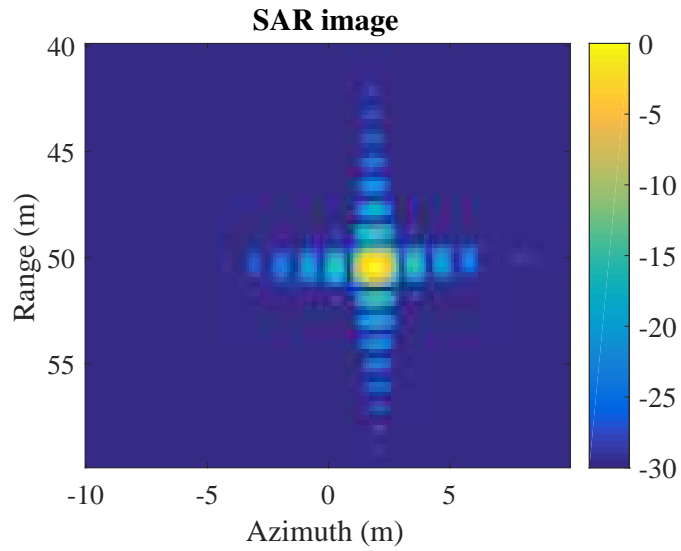


Figure 4.6 – SAR image obtained in the ideal case allowing to correctly identify the scatterer position

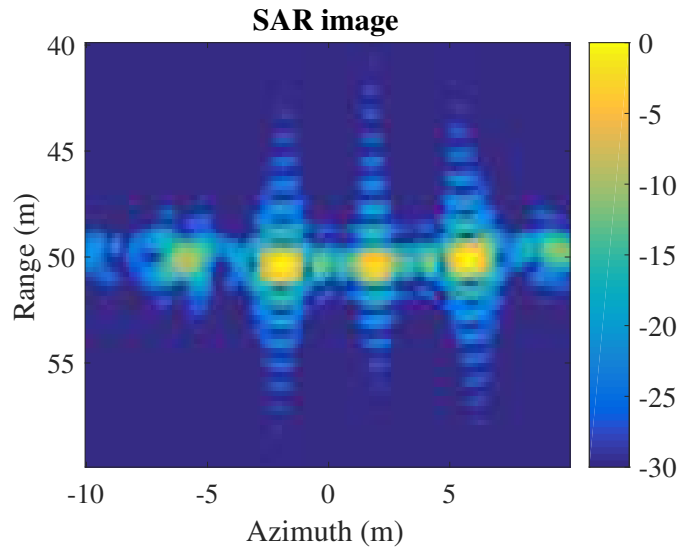


Figure 4.7 – SAR image obtained with an erroneous estimated position

in the position estimation of the UAV will let us know the maximum working frequency of the SAR sensor. Reciprocally, if the working frequency of the SAR sensor is imposed, this will specify the maximum acceptable error (in terms of guaranteed bounds) of the position estimation of the UAV to obtain SAR images with acceptable performance. In the next section, we will use the guaranteed ellipsoidal state estimation technique to estimate the position of the UAV where the SAR sensors are mounted. This step is followed by the computation of the maximum allowed error amplitude in estimation, in the goal of obtaining the suitable frequencies for which the SAR sensor can operate.

4.6.3 Simulation results

The three discretized subsystems (4.21), (4.22) and (4.23) presented in Section 4.6.1 are fully controllable and observable. Considering the presence of state perturbations and measurement noises, the complete numerical discrete-time model of the octorotor can be obtained with the drone parameters shown in Table 4.2 including payload. The sampling period $T_e = 0.1s$ is the highest of all sensors sampling period. An accuracy of $\pm 1m$ is assumed for both the GPS and the altimeter, and an accuracy of $\pm 0.01rad/s$ is considered for the gyroscope. Based on this information on the bounds of measurement noises and perturbations, the matrices $\mathbf{F}_1 = [\mathbf{0}_4 \quad \tilde{\mathbf{F}}_1]$, with $\tilde{\mathbf{F}}_1 = \begin{bmatrix} 1 & 0 \\ 0 & 0.01 \end{bmatrix}$, $\mathbf{F}_2 = 0.01 \cdot [\mathbf{0}_4 \quad \mathbf{I}_{4 \times 2}]$ and $\mathbf{F}_3 = [\mathbf{0}_4 \quad \mathbf{I}_{4 \times 2}]$ are chosen in (4.21), (4.22) and (4.23). For simplification, the state perturbations can be chosen as follows $\mathbf{E}_1 = \mathbf{E}_2 = \mathbf{E}_3 = 10^{-3} \cdot [\mathbf{I}_4 \quad \mathbf{0}_{4 \times 2}]$. The drone's behavior was simulated using a Matlab/Simulink simulator implementing the non-linear model. Additionally, a linear quadratic integral (LQI) controller, detailed in [Makarov et al., 2015] for this UAV is used for nominal input computations. These nominal control inputs are then fed into the linear designed system (4.21), (4.22) and (4.23).

Table 4.2 – Drone parameters

| | |
|--------------------|-------------------------|
| Total mass m | 3.69kg |
| Inertia components | |
| I_{xx} | 0.0869kg·m ² |
| I_{yy} | 0.0873kg·m ² |
| I_{zz} | 0.1683kg·m ² |

Two reference trajectories have been tested in the simulation:

- A circular trajectory in which the drone rotates around its z-axis at a constant tangential speed,
- A linear trajectory back and forth on the x-axis at a linear constant speed which allows the drone to scan the selected area and process the estimated positions for the radar application.

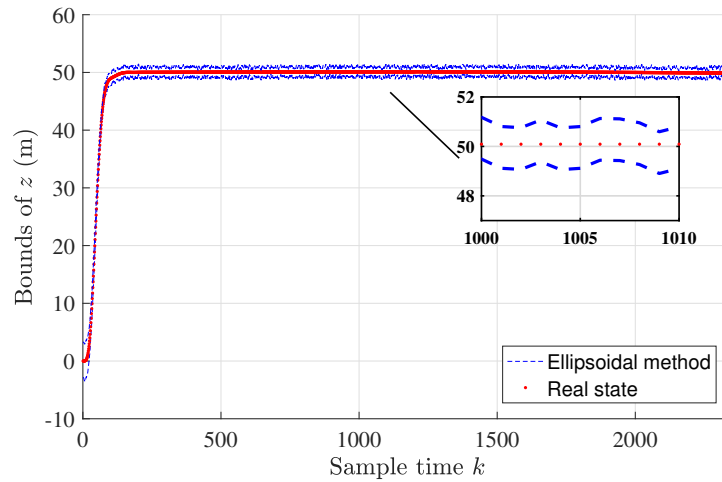


Figure 4.8 – Estimation bounds of the altitude z

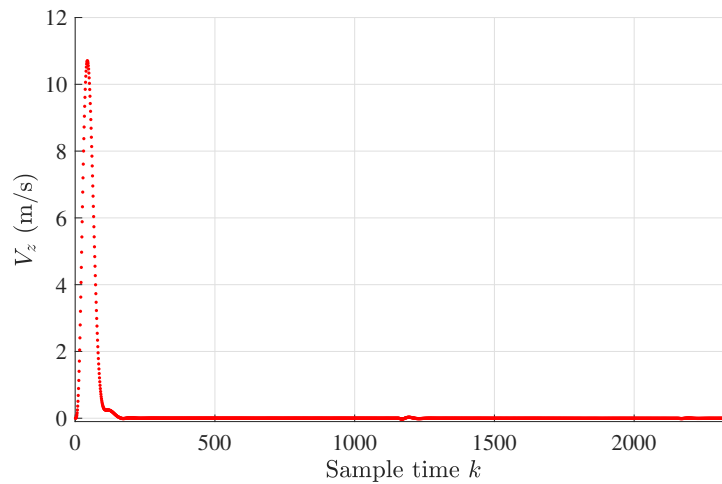


Figure 4.9 – Drone's velocity on the z-axis

The circular trajectory is used to validate the ellipsoidal set-membership estimation technique, whereas the aim of the linear trajectory is to estimate

the components of the state vector and test them in a radar imaging application. More precisely, the goal is to compute the frequencies for which the radar can operate; thus the need to compute the distance between the drone (i.e. the radar) and the target at each sample time. The guaranteed bounds for the relative distance provided by the set-membership state estimation technique are used to find the error on the estimation and the working frequency afterwards. The drone is initially, on the floor in an equilibrium state. The rotor's generated thrust compensates the weight.

The estimation results have been obtained with an Intel Core i7 processor-3770 3.40 GHz. The entire flight duration for both trajectories is 235s. Both trajectories correspond first to a take-off to an altitude of 50m. The results for the take-off of the drone are the same for both movements regardless of the trajectory type. Figure 4.8 presents the guaranteed estimation bounds (blue dashed lines) of the altitude z , calculated by the mean of the technique previously detailed in Section 3. It can be seen that the real state (the red dots in Figure 4.8) are guaranteed to remain inside the estimated bounds (see the zoom of Figure 4.8), despite the presence of perturbations and measurement noises. The velocity on the z -axis is shown in Figure 4.9.

In the next sections, the set-membership state estimation technique is validated through two different trajectories: a circular trajectory and a linear trajectory suitable for the radar application.

4.6.3.1 Case 1: Circular trajectory

After the take-off, the drone moves in a circular trajectory as shown in Figure 4.10.

Figures 4.11 and 4.13 show the bounds of x and y , respectively computed as detailed in (4.23) applying the ellipsoidal set-membership state estimation method for 2350 iterations. The real state is represented by red dots and it is found inside the estimated bounds. Notice that at $t = 0$, the position of the drone is $(x_0, y_0) = (0, 0)$ and the velocity on both axes is equal to 0. The velocity of the drone varies between -2m/s and 2m/s as shown in Figure 4.12 and Figure 4.14.

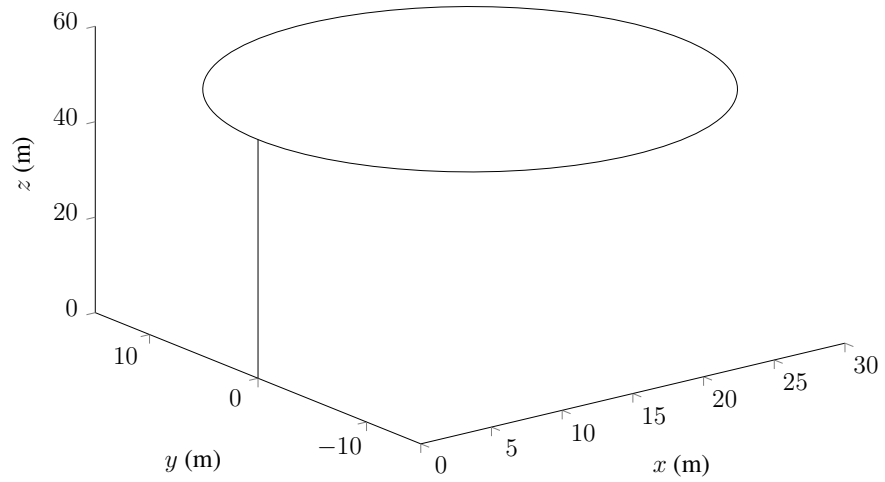


Figure 4.10 – Circular reference trajectory

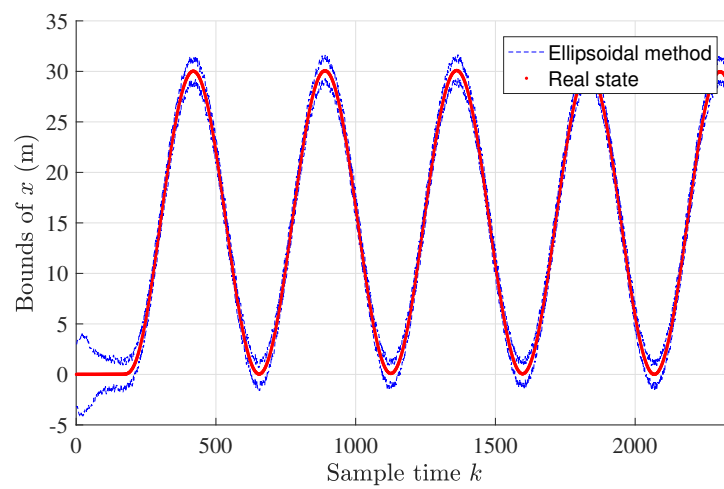


Figure 4.11 – Circular trajectory: estimation bounds of the linear position x

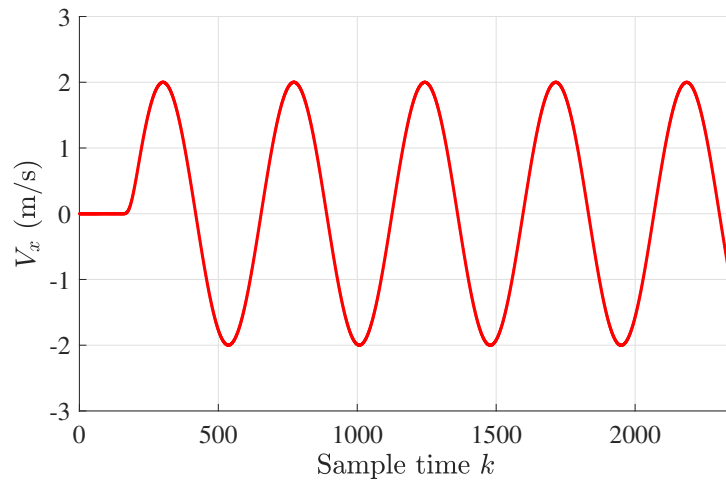


Figure 4.12 – Circular trajectory: drone’s velocity on the x-axis

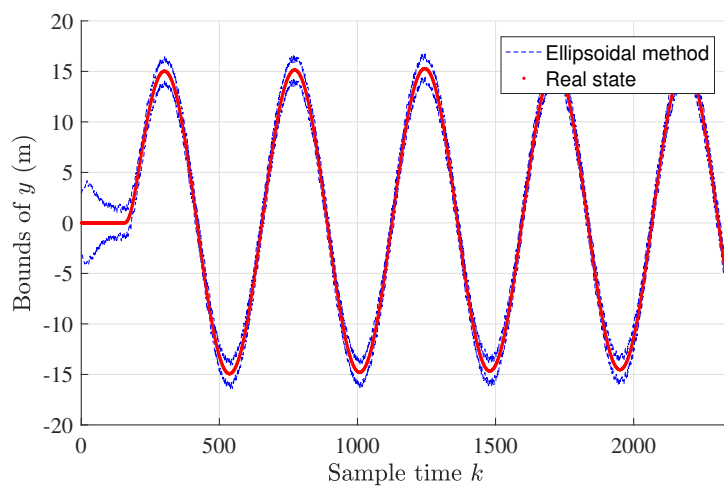


Figure 4.13 – Circular trajectory: estimation bounds of the linear position y

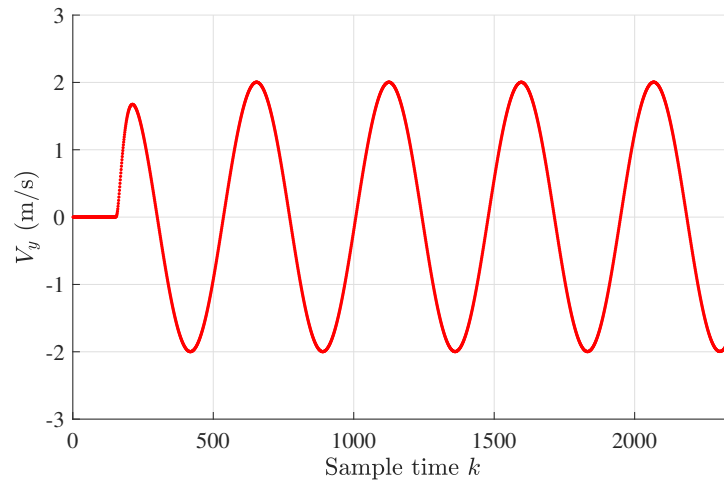


Figure 4.14 – Circular trajectory: drone’s velocity on the y-axis

4.6.3.2 Case 2: Linear trajectory for a SAR application

After the take-off, the reference trajectory shown in Figure 4.15 is composed of a movement on the x-axis from $x = 0$ to $x = 250\text{m}$ and then back to $x = 0$ at a constant speed of 2.5m/s , which is a relevant trajectory for the drone in a radar application.

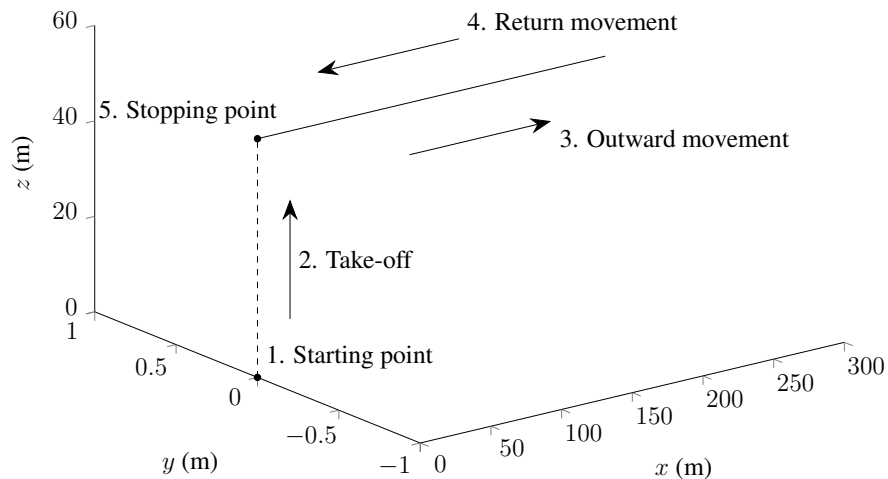


Figure 4.15 – Linear proposed trajectory

While the drone is moving, the radar scans a region where the potential target is expected. More precisely, the drone takes off from the initial starting

point to reach a certain altitude. Then, it goes in an outward movement along the x-axis where it can scan a certain region before returning to its stopping point. These movements are represented in Figure 4.15.

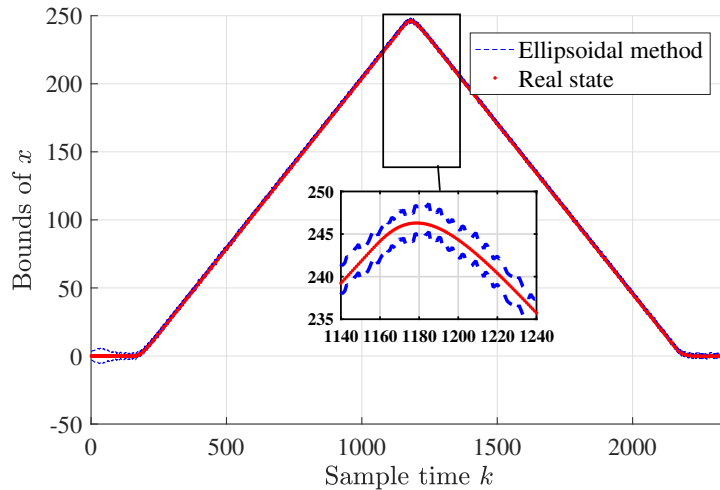


Figure 4.16 – Linear trajectory: estimation bounds of the linear position x

Figure 4.16 shows the estimation done on the drone’s movement, along the x-axis. A part of the figure has been zoomed in order to better exhibit the position on the x-axis which is guaranteed inside the estimation bounds. The UAV keeps moving forward with a constant speed until it reaches its destination ($x = 250\text{m}$), this is when it moves in the opposite direction to reach the stopping point (Figure 4.15) with the same speed as Figure 4.17 shows. By the end, the drone would have scanned the area and would have identified the targets, this is why the final velocity is equal to zero. It should be noticed that no movement is made on the y-axis, however (as shown in Figure 4.18), the real y position is found between the upper and lower bounds (blue dashed curve in Figure 4.18) estimated by the ellipsoidal technique (4.14).

While moving in its planned linear trajectory, the drone images a scatterer during 8s (which corresponds to 20m for a nominal speed of 2.5m/s) in the stripmap mode. An extreme case is considered here where the scatterer is at 50m range and 10m azimuth with respect to the scanned region (see Table 4.3).

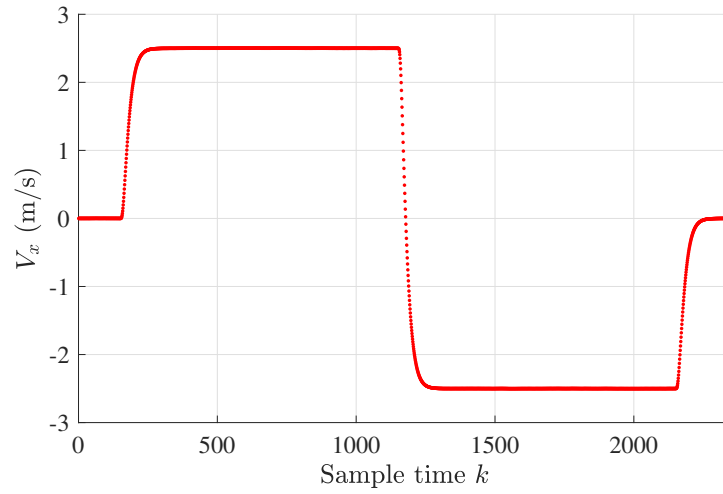


Figure 4.17 – Linear trajectory: drone’s velocity on the x-axis

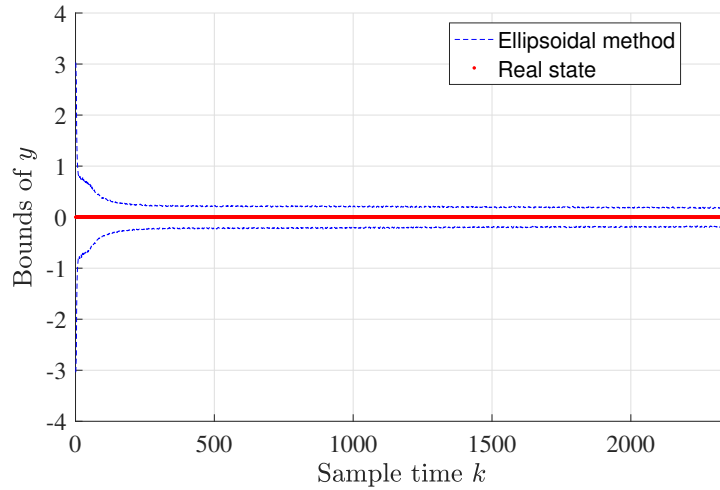


Figure 4.18 – Linear trajectory: estimation bounds of the linear position y

Table 4.3 – SAR parameters considered for the linear trajectory

| | |
|--------------------|------|
| PRF | 2kHz |
| Scatterer position | |
| Azimuth | 10m |
| Ground range | 50m |

Using the bounds found for the coordinates of the drone, the maximal,

real and minimal distances between the scatterer and UAV are calculated at each iteration. Afterwards, $|D_{min} - D_r|$ and $|D_{max} - D_r|$ are plotted in Figure 4.19, where δ_D is equal to $\max(\delta_{max}, \delta_{min})$. Since phase errors can be effectively compensated by autofocus techniques up to 60rad, and using (4.24) in Section 4 with $\delta_D \approx 2\text{m}$, the maximum operating frequency of the SAR sensor has to be less than 600MHz (very high frequency VHF and ultra high frequency UHF applications).

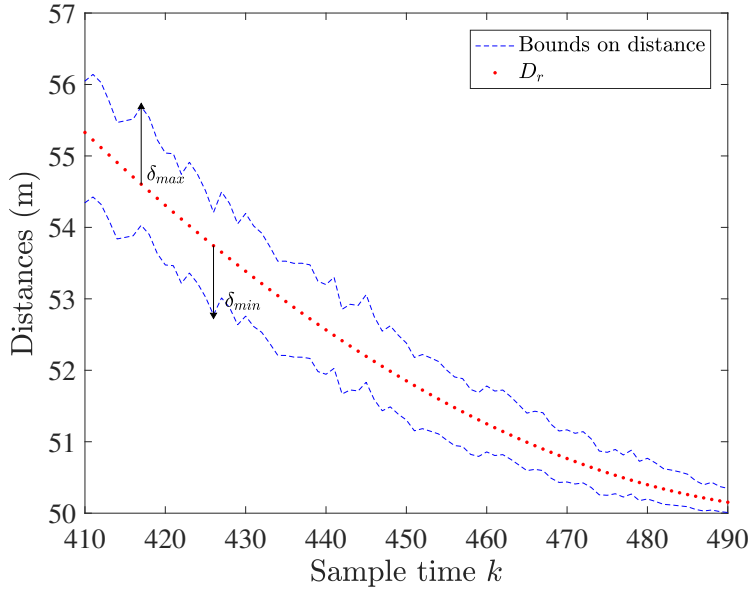


Figure 4.19 – Distance errors

4.7 Conclusion

This chapter discussed ellipsoidal set-membership state estimation for linear time invariant systems. First, a previously developed ellipsoidal set-membership state estimation technique for multi-variable systems has been improved to deal with a general case where control inputs are considered. Then, a brief comparison has been made between this technique and the classical Kalman filter for discrete-time linear time invariant systems, subject to perturbations and measurement noises. The guaranteed ellipsoidal set-membership estimation method is compared to the classical Kalman Filter, in terms of accuracy and complexity. The best estimation results (i.e. guaranteed bounds) are obtained with the improved estimation method. The main advantage of the Kalman filter is its simplicity and lower computational

complexity.

In a second part, this chapter illustrated an application of the detailed ellipsoidal guaranteed set-membership state estimation technique to an ocrotor's attitude and position used for radar applications. The considered technique minimizes an ellipsoidal set in the presence of bounded perturbations and measurement noises in order to improve the estimation accuracy at each sample time. The computed bounds are used in the context of radar applications to find the operating frequency of the synthetic aperture radar. The next chapter proposes an extension of this ellipsoidal set-membership state estimation approach to descriptor systems.

Chapter 5

Ellipsoidal state estimation for descriptor systems

Contents

| | | |
|------------|---|------------|
| 5.1 | Introduction | 96 |
| 5.2 | Overview of descriptor systems | 98 |
| 5.2.1 | Practical examples | 98 |
| 5.2.2 | Basic properties of descriptor systems | 99 |
| 5.3 | Problem formulation | 100 |
| 5.4 | Ellipsoidal state estimation technique for LTI descriptor systems | 102 |
| 5.4.1 | <i>Method 1</i> : Off-line state estimation approach with a constant observer gain | 102 |
| 5.4.2 | <i>Method 2</i> : Online ellipsoidal state estimation approach | 106 |
| 5.4.3 | <i>Method 3</i> : Online ellipsoidal state estimation approach with vector scaling technique | 107 |
| 5.5 | Ellipsoidal state estimation for LTV descriptor systems | 113 |
| 5.5.1 | Problem formulation | 113 |
| 5.5.2 | <i>Method 4</i> : Online flexible shape ellipsoidal state estimation approach | 114 |
| 5.5.3 | <i>Method 5</i> : Online flexible shape ellipsoidal state estimation approach with vector scaling technique | 117 |
| 5.6 | Conclusion | 121 |

5.1 Introduction

A mathematical model is in general required for the investigation of systems dynamics via analysis and simulation. Usually, the behavior of a dynamical system is described by differential equations. These differential equations result in discrete-time linear time invariant systems discussed in the previous chapters. However, many physical systems are modeled using differential equations coupled with algebraic equations to take into account the physical phenomena that standard differential equations can not completely describe. For instance, the algebraic equations allow us to take into consideration physical conservation laws such as energy, mass and volume.

Overall, the system can be modeled using a combination of differential and algebraic equations, i.e. by differential-algebraic equations (DAE). They represent simultaneously the behavior of the system and the set of constraints that the system is subject to. In control engineering, these systems are known as *descriptor systems* or *singular systems* [Dai, 1989]. The formulation of descriptor systems retains the physical meaning of the modeled system, e.g. mechanical systems taking into account constraints related to scientific phenomena [Varga, 2017]. It is therefore useful in electrical networks [Reis, 2010], power systems [Hill and Mareels, 1990], chemical plants [Biegler et al., 2012], biological processes [Liu et al., 2008], economic systems [Varga, 2017], aircraft modeling [Stevens et al., 2015] etc. In other terms, descriptor systems can be considered as a generalization of dynamical system. Descriptor systems were firstly introduced from a control theory point of view by Luenberger [Luenberger, 1977] and then became a powerful tool of system modeling [Lewis, 1985]. In the last few decades, the development of reliable studies for the stability [Han, 2004], controllability [Bender and Laub, 1987], [Bara, 2011], [Varga, 1995] and observability [Campbell et al., 1991], [Yip and Sincovec, 1981] of descriptor systems have been the center of attention for more and more researchers. The need of these studies arises from the fact that descriptor systems offer a more general overview of the system description than the standard state-space systems. Indeed, when the descriptor matrix is the identity matrix, the descriptor representation is equivalent to the standard state-space representation [Wang et al., 2012]. In order to make descriptor systems accessible to expert or non-specialist users, a descriptor system toolbox for Matlab has been introduced in [Varga, 2000] providing new tools to manipulate generalized state-space systems, both for the case of continuous- and discrete-time systems. In addition, this toolbox proposes numerous extensions for systems with singular descriptor matrix and provides robust tools for fault detection and isolation of descriptor systems. Among the work done in literature, state observers are designed for linear [Wang

et al., 2012], [Darouach and Boutayeb, 1995] and non-linear descriptor systems [Koenig et al., 2008], [Shields, 1997]. Moreover, a considerable amount of literature has been published on state estimation for discrete-time linear and non-linear descriptor systems [Wu et al., 2010]. Due to its simplicity and efficiency, the Kalman filter [Kalman, 1960] is a powerful tool widely used in stochastic state estimation for standard and descriptor systems [Ishihara et al., 2006], [Nikoukhah et al., 1999], [Nikoukhah et al., 1992] via its different versions. Similarly, the set-membership state estimation techniques were firstly introduced to standard linear time invariant systems, before inspiring similar approaches for descriptor systems. In this context, a zonotopic set-membership state estimation approach has been proposed in [Wang et al., 2018], [Wang et al., 2016] for discrete-time descriptor systems subject to uncertainties and unknown inputs. Despite the fact that set-membership state estimation techniques offer a good estimation accuracy, while maintaining a realistic aspect of the problem, there is a lack of set-membership state estimation approaches for descriptor systems. To fill this gap, in the present chapter, set-membership state estimation techniques are formulated as feasible optimization problems solved to compute guaranteed bounds for the components of the state vector of descriptor systems subject to bounded perturbations and measurement noises. The chapter starts with a brief overview of descriptor systems theory and applications and proceeds to extend the guaranteed ellipsoidal set-membership state estimation approaches from [Ben Chabane et al., 2014] for discrete-time linear time invariant descriptor systems. In this context, firstly, a constant observer gain matrix for the considered descriptor system is computed off-line via a linear matrix inequality (LMI) optimization problem. This result has been published to the 23rd International Conference on System Theory, Control and Computing, 2019. To the end of improving the accuracy of the method, the observer gain is computed online via an optimization problem. This approach is then further improved by deriving a scaling technique for descriptor system. The additional step reduces the computation load due to online calculation, while keeping an accurate estimation. Finally, the chapter introduces an ellipsoidal set-membership state estimation technique for discrete-time linear time variant (LTV) descriptor systems with bounded perturbations and measurement noises. This technique includes the scaling technique for LTI systems and considers, the measurement at the next time instant as well quadratic constraints on the perturbations. Additionally, it allows us to update at each time instant the size and shape of the ellipsoidal estimated set which leads to better accuracy. The results developed in this chapter will be submitted soon in form of a journal paper to Automatica.

5.2 Overview of descriptor systems

The class of systems addressed in this chapter corresponds to deterministic, discrete-time linear descriptor systems with finite dimension. This class of systems can cover a large number of systems encountered in practice. A state-space realization of this type of descriptor systems is the following:

$$\begin{cases} \mathbf{E}_d \mathbf{x}_{k+1} &= \mathbf{A} \mathbf{x}_k + \mathbf{B} \mathbf{u}_k + \mathbf{E} \boldsymbol{\omega}_k \\ \mathbf{y}_k &= \mathbf{C} \mathbf{x}_k + \mathbf{F} \boldsymbol{\omega}_k \end{cases} \quad (5.1)$$

where $\mathbf{x}_k \in \mathbb{R}^{n_x}$ is the state vector, $\mathbf{u}_k \in \mathbb{R}^{n_u}$ the input vector and $\mathbf{y}_k \in \mathbb{R}^{n_y}$ the output vector at time instant k . Here, the perturbations are unknown but bounded by unitary boxes such that $\boldsymbol{\omega}_k \in \mathbb{B}^{n_w}$. Moreover, appropriate dimensions are considered for the system matrices $\mathbf{E}_d \in \mathbb{R}^{n_x \times n_x}$, $\mathbf{A} \in \mathbb{R}^{n_x \times n_x}$, $\mathbf{B} \in \mathbb{R}^{n_x \times n_u}$, $\mathbf{C} \in \mathbb{R}^{n_y \times n_x}$, $\mathbf{E} \in \mathbb{R}^{n_x \times n_w}$ and $\mathbf{F} \in \mathbb{R}^{n_y \times n_w}$. The main difference with the standard state-space representation is a possible *singular matrix* \mathbf{E}_d in (5.1) which means that:

$$\text{rank}(\mathbf{E}_d) < n_x.$$

5.2.1 Practical examples

It is important to show with an example how a descriptor system in control engineering can model different systems from various fields of study. We consider the electrical system in Figure 5.1 with an inductor of inductance L , capacitor of capacitance C and charge q , a continuous voltage source V and the resistances R_1 , R_2 and R_3 .

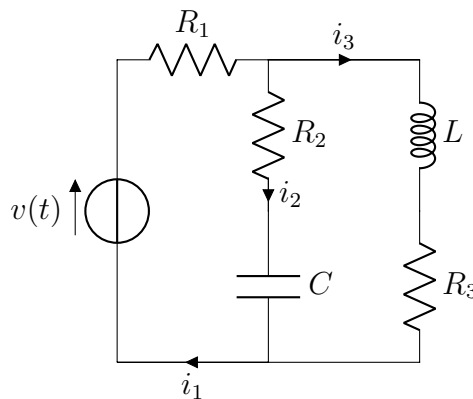


Figure 5.1 – Electrical circuit

The system can be mathematically modeled using differential equations obtained by using the current and voltage Kirchoff's laws:

$$\frac{dq}{dt} = i_2(t), \quad (5.2)$$

$$L \frac{di_3}{dt} + R_3 i_3(t) = \frac{1}{C} q(t) + R_2 i_2(t), \quad (5.3)$$

with an additional constraint due to the fact that in a series circuit, the voltage is the sum of the voltage drops of the individual components:

$$0 = (R_1 + R_2) i_2(t) + R_1 i_3(t) + \frac{1}{C} q(t) - v(t) \quad (5.4)$$

Transforming the system into the form (5.1) yields:

$$\begin{bmatrix} 1 & 0 & 0 \\ 0 & 0 & L \\ 0 & 0 & 0 \end{bmatrix} \begin{bmatrix} \frac{dq(t)}{dt} \\ \frac{di_2(t)}{dt} \\ \frac{di_3(t)}{dt} \end{bmatrix} = \begin{bmatrix} 0 & 1 & 0 \\ \frac{1}{C} & R_2 & -R_3 \\ \frac{1}{C} & (R_1 + R_2) & R_1 \end{bmatrix} \begin{bmatrix} q(t) \\ i_2(t) \\ i_3(t) \end{bmatrix} + \begin{bmatrix} 0 \\ 0 \\ -1 \end{bmatrix} v(t) \quad (5.5)$$

Notice that the state-space part has been singled out by the transformation.

Indeed the matrix $\mathbf{E}_d = \begin{bmatrix} 1 & 0 & 0 \\ 0 & 0 & L \\ 0 & 0 & 0 \end{bmatrix}$ is singular with $\text{rank}(\mathbf{E}_d) = 2 < 3$. This

is expected, because the internal variables of the system may depend directly on derivatives of the input or not. In this case, the only dynamic elements in the circuit are the inductor and the capacitor, the rest depend directly on the input voltage $v(t)$, which is a primordial constraint for the modeling of the system.

5.2.2 Basic properties of descriptor systems

Before detailing the proposed set-membership state estimation techniques for descriptor systems, it is useful to discuss some of the basic properties of these systems that we will further need in this chapter [Dai, 1989].

Definition 5.1. A descriptor system is *observable* if:

$$\text{rank} \begin{bmatrix} \mathbf{E}_d \\ \mathbf{C} \end{bmatrix} = n_x, \quad (5.6)$$

and

$$\text{rank} \begin{bmatrix} \lambda \mathbf{E}_d - \mathbf{A} \\ \mathbf{C} \end{bmatrix} = n_x, \forall \lambda \in \mathbb{C}. \quad (5.7)$$

Expressions (5.6) and (5.7), guaranteeing *infinite observability* and *finite observability*, respectively (see [Varga, 2017]), are needed to ensure the existence of Luenberger type observers for a descriptor system ([Dai, 1989], [Hou and Muller, 1995]).

Definition 5.2. If the descriptor system (7.1) is used for control purposes, it should be *controllable*. Its controllability is assumed if:

$$\text{rank} \begin{bmatrix} \mathbf{E}_d & \mathbf{B} \end{bmatrix} = n_x, \quad (5.8)$$

and

$$\text{rank} \begin{bmatrix} \lambda \mathbf{E}_d - \mathbf{A} & \mathbf{B} \end{bmatrix} = n_x, \forall \lambda \in \mathbb{C}. \quad (5.9)$$

Conditions (5.6)-(5.8) guarantees a weakly minimal descriptor realization. In the general case, a minimal descriptor realization can be considered by ensuring $\mathbf{AN}(\mathbf{E}_d) \subseteq \mathcal{R}(\mathbf{E}_d)$, where $\mathcal{N}(\mathbf{E}_d)$ and $\mathcal{R}(\mathbf{E}_d)$ are the kernel and the range of the descriptor matrix \mathbf{E}_d , respectively [Varga, 2017].

5.3 Problem formulation

Let us consider the following discrete-time linear time invariant descriptor system described by the following equations

$$\begin{cases} \mathbf{E}_d \mathbf{x}_{k+1} = \mathbf{A} \mathbf{x}_k + \mathbf{B} \mathbf{u}_k + \mathbf{E} \boldsymbol{\omega}_k \\ \mathbf{y}_k = \mathbf{C} \mathbf{x}_k + \mathbf{F} \boldsymbol{\omega}_k \end{cases} \quad (5.10)$$

where $\mathbf{x}_k \in \mathbb{R}^{n_x}$ is the state vector, $\mathbf{u}_k \in \mathbb{R}^{n_u}$ the input vector and $\mathbf{y}_k \in \mathbb{R}^{n_y}$ the output vector at time instant k . Here, the perturbations are unknown but bounded by unitary boxes such that $\boldsymbol{\omega}_k \in \mathbb{B}^{n_w}$. Moreover, appropriate dimensions are considered for the system matrices $\mathbf{E}_d \in \mathbb{R}^{n_x \times n_x}$, $\mathbf{A} \in \mathbb{R}^{n_x \times n_x}$, $\mathbf{B} \in \mathbb{R}^{n_x \times n_u}$, $\mathbf{C} \in \mathbb{R}^{n_y \times n_x}$, $\mathbf{E} \in \mathbb{R}^{n_x \times n_w}$ and $\mathbf{F} \in \mathbb{R}^{n_y \times n_w}$. Besides, the initial state belongs to the ellipsoid

$$\mathcal{E}(\mathbf{P}_0, \bar{\mathbf{x}}_0, \rho_0) = \{\mathbf{x} \in \mathbb{R}^{n_x} : (\mathbf{x} - \bar{\mathbf{x}}_0)^\top \mathbf{P}_0 (\mathbf{x} - \bar{\mathbf{x}}_0) \leq \rho_0\} \quad (5.11)$$

with $\mathbf{P}_0 = \mathbf{P}_0^\top \succ 0$ being the shape matrix, $\bar{\mathbf{x}}_0$ the center and ρ_0 the so called radius of $\mathcal{E}(\mathbf{P}_0, \bar{\mathbf{x}}_0, \rho_0)$. The matrix \mathbf{E}_d is a possible singular matrix with:

$$\text{rank}(\mathbf{E}_d) \leq n_x. \quad (5.12)$$

Based on Section 5.2.2, in order to guarantee the observability of the descriptor system (5.10), it is assumed that the observability conditions (5.6) and (5.7) hold. Moreover, the system (5.10) is used for control purposes, its

controllability (i.e. expressions (5.8) and (5.9)) has to be assumed.

Additionally, since (5.6) holds, there exist two matrices $\mathbf{T} \in \mathbb{R}^{n_x \times n_x}$ and $\mathbf{N} \in \mathbb{R}^{n_x \times n_y}$ such that [Wang et al., 2012]:

$$\mathbf{T}\mathbf{E}_d + \mathbf{N}\mathbf{C} = \mathbf{I}_{n_x}. \quad (5.13)$$

We now show that this equality allows us to compute \mathbf{x}_{k+1} from \mathbf{x}_k , \mathbf{u}_k , $\boldsymbol{\omega}_k$ and $\boldsymbol{\omega}_{k+1}$. Multiplying by \mathbf{T} the first equation of system (5.10) and by \mathbf{N} the second equation (evaluated at time instant $k + 1$), we obtain:

$$\begin{cases} \mathbf{T}\mathbf{E}_d\mathbf{x}_{k+1} &= \mathbf{T}\mathbf{A}\mathbf{x}_k + \mathbf{T}\mathbf{B}\mathbf{u}_k + \mathbf{T}\mathbf{E}\boldsymbol{\omega}_k, \\ \mathbf{N}\mathbf{y}_{k+1} &= \mathbf{N}\mathbf{C}\mathbf{x}_{k+1} + \mathbf{N}\mathbf{F}\boldsymbol{\omega}_{k+1}. \end{cases}$$

Equivalently, highlighting the term $\mathbf{N}\mathbf{C}\mathbf{x}_{k+1}$ in the second equation leads to:

$$\begin{cases} \mathbf{T}\mathbf{E}_d\mathbf{x}_{k+1} &= \mathbf{T}\mathbf{A}\mathbf{x}_k + \mathbf{T}\mathbf{B}\mathbf{u}_k + \mathbf{T}\mathbf{E}\boldsymbol{\omega}_k, \\ \mathbf{N}\mathbf{C}\mathbf{x}_{k+1} &= \mathbf{N}\mathbf{y}_{k+1} - \mathbf{N}\mathbf{F}\boldsymbol{\omega}_{k+1}. \end{cases}$$

Adding both equalities and taking into account the equality (5.13), we obtain:

$$\mathbf{x}_{k+1} = \mathbf{T}\mathbf{A}\mathbf{x}_k + \mathbf{T}\mathbf{B}\mathbf{u}_k + \mathbf{N}\mathbf{y}_{k+1} + \mathbf{T}\mathbf{E}\boldsymbol{\omega}_k - \mathbf{N}\mathbf{F}\boldsymbol{\omega}_{k+1}. \quad (5.14)$$

In this framework, we further investigate the set-membership state estimation problem based on ellipsoids for the descriptor system (5.10).

Goal: Given an ellipsoidal estimation $\mathcal{E}(\mathbf{P}, \bar{\mathbf{x}}_k, \rho_k)$ for the state \mathbf{x}_k from (5.10) at time instant k , the aim is to find an ellipsoidal estimation for the state \mathbf{x}_{k+1} at time instant $k + 1$ of the form $\mathcal{E}(\mathbf{P}, \bar{\mathbf{x}}_{k+1}, \rho_{k+1})$.

This problem is further addressed in the upcoming sections where we detail several guaranteed ellipsoidal state estimation techniques for LTI and LTV descriptor systems. An overview of these techniques is given in Figure 5.2.

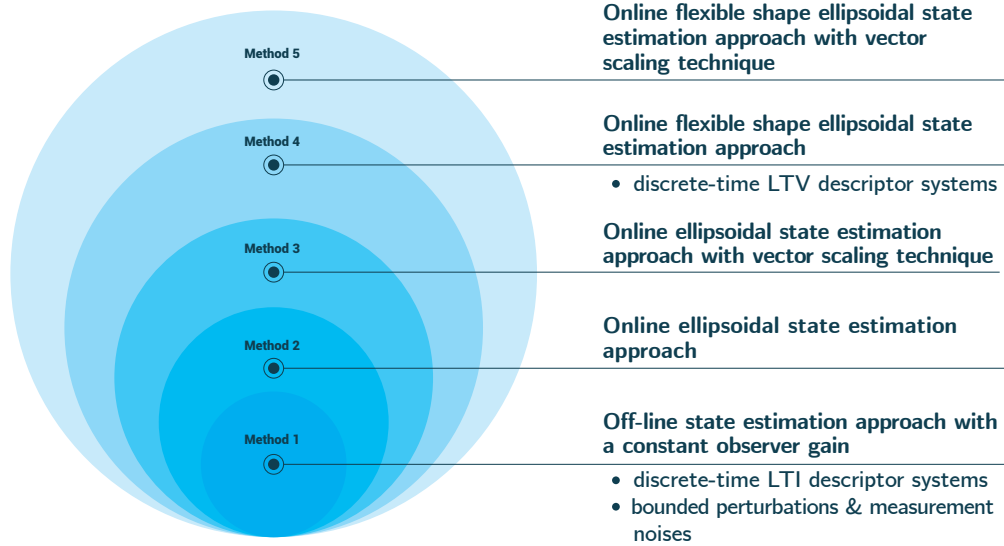


Figure 5.2 – An overview of the five methods developed in this chapter

5.4 Ellipsoidal state estimation technique for LTI descriptor systems

In this section, three approaches are extended for ellipsoidal set-membership state estimation of discrete-time linear time invariant descriptor systems. The first one (Method 1) computes off-line a constant observer matrix. The second one (Method 2) is an online technique where the observer gain is computed once per iteration via an optimization problem, which is computationally expensive. The third approach (Method 3) represents a trade-off between the first off-line fast approach, and the second online accurate approach.

5.4.1 *Method 1*: Off-line state estimation approach with a constant observer gain

This section details the guaranteed ellipsoidal state estimation for the LTI discrete-time descriptor systems (5.10). Knowing that the perturbations and noises are bounded, the proposed approach minimizes the radius of the ellipsoidal estimation in such way that, at each time instant k , the following

inequality is satisfied:

$$\rho_{k+1} \leq \beta\rho_k + \sigma, \quad (5.15)$$

where $\beta \in (0, 1)$ is a real bounded number and σ is a strictly positive scalar $\sigma > 0$. In fact, expression (5.15) formulates the non increasing property of the ellipsoidal radius. We notice that (5.15) is equivalent to:

$$\rho_{k+1} - \rho_k \leq (\beta - 1)\rho_k + \sigma, \quad (5.16)$$

Since $\beta - 1 < 0$, we infer that:

$$\rho_{k+1} \leq \rho_k,$$

for every

$$\rho_k \geq \frac{\sigma}{1 - \beta}.$$

With a pair of matrices \mathbf{T} and \mathbf{N} satisfying (5.13), a Luenberger observer of the following form [Wang et al., 2012] is designed for the descriptor system (5.10):

$$\bar{\mathbf{x}}_{k+1} = \mathbf{T}\mathbf{A}\bar{\mathbf{x}}_k + \mathbf{T}\mathbf{B}\mathbf{u}_k + \mathbf{L}(\mathbf{y}_k - \mathbf{C}\bar{\mathbf{x}}_k) + \mathbf{N}\mathbf{y}_{k+1}, \quad (5.17)$$

where \mathbf{L} is the observer gain to be determined such that the error between the real state and the nominal estimated state $\bar{\mathbf{x}}_k$ asymptotically converges to zero. Guaranteeing the ellipsoidal state estimation for the state vector \mathbf{x}_k at each time instant k is shown in the following theorem, allowing to extend the results from [Ben Chabane et al., 2014] to the considered descriptor system (5.10).

Theorem 5.1. Given a scalar $\beta \in (0, 1)$, the matrices \mathbf{T} and \mathbf{N} satisfying (5.13), and an initial state \mathbf{x}_0 , suppose that there exist a matrix $\mathbf{P} \in \mathbb{R}^{n_x \times n_x}$, with $\mathbf{P} = \mathbf{P}^\top \succ 0$ a matrix $\mathbf{Y} \in \mathbb{R}^{n_x \times n_y}$, and a scalar $\sigma > 0$ such that the linear matrix inequality:

$$\begin{bmatrix} \beta\mathbf{P} & * & * \\ \mathbf{0} & \sigma & * \\ \mathbf{P}\mathbf{T}\mathbf{A} - \mathbf{Y}\mathbf{C} & (\mathbf{P}\mathbf{T}\mathbf{E} - \mathbf{Y}\mathbf{F})\boldsymbol{\omega}_k - \mathbf{P}\mathbf{N}\mathbf{F}\boldsymbol{\omega}_{k+1} & \mathbf{P} \end{bmatrix} \succ 0, \quad (5.18)$$

holds for all $\boldsymbol{\omega}_k, \boldsymbol{\omega}_{k+1} \in \mathbb{B}^{n_w}$. Then, the system state \mathbf{x}_k of the descriptor system (5.10) satisfies:

$$\mathbf{x}_k \in \mathcal{E}(\mathbf{P}, \bar{\mathbf{x}}_k, \rho_k), \quad \forall k \geq 0,$$

where, defining $\mathbf{L} = \mathbf{P}^{-1}\mathbf{Y}$, $\bar{\mathbf{x}}_0 = \mathbf{x}_0$, $\rho_0 = \bar{\mathbf{x}}_0^\top \mathbf{P} \bar{\mathbf{x}}_0$, the sequence $\bar{\mathbf{x}}_{k+1}$ and ρ_{k+1} , $k \in \mathbb{N}$ can be obtained from the recursive expressions:

$$\bar{\mathbf{x}}_{k+1} = \mathbf{T}\mathbf{A}\bar{\mathbf{x}}_k + \mathbf{T}\mathbf{B}\mathbf{u}_k + \mathbf{N}\mathbf{y}_{k+1} + \mathbf{L}(\mathbf{y}_k - \mathbf{C}\bar{\mathbf{x}}_k), \quad (5.19)$$

$$\rho_{k+1} = \beta\rho_k + \sigma. \quad (5.20)$$

Proof. Since \mathbf{T} and \mathbf{N} satisfy (5.13), the state vector \mathbf{x}_{k+1} of the descriptor system (5.10) satisfies (5.14).

The estimation error \mathbf{z}_k is defined as the difference between the real value of the state \mathbf{x}_k and the nominal estimated state $\bar{\mathbf{x}}_k$ at time instant k , i.e.

$$\mathbf{z}_k = \mathbf{x}_k - \bar{\mathbf{x}}_k.$$

Using (5.19) and (5.14), the error dynamic equation is given by:

$$\begin{aligned} \mathbf{z}_{k+1} &= \mathbf{x}_{k+1} - \bar{\mathbf{x}}_{k+1} \\ &= \mathbf{T}\mathbf{A}\mathbf{z}_k + \mathbf{T}\mathbf{E}\mathbf{w}_k - \mathbf{N}\mathbf{F}\boldsymbol{\omega}_{k+1} - \mathbf{L}(\mathbf{y}_k - \mathbf{C}\bar{\mathbf{x}}_k) \\ &= (\mathbf{T}\mathbf{A} - \mathbf{L}\mathbf{C})\mathbf{z}_k + (\mathbf{T}\mathbf{E} - \mathbf{L}\mathbf{F})\boldsymbol{\omega}_k - \mathbf{N}\mathbf{F}\boldsymbol{\omega}_{k+1} \\ &= \mathbf{A}_L\mathbf{z}_k + \boldsymbol{\eta}_k, \end{aligned} \quad (5.21)$$

with

$$\mathbf{A}_L = \mathbf{T}\mathbf{A} - \mathbf{L}\mathbf{C}, \quad (5.22)$$

$$\boldsymbol{\eta}_k = (\mathbf{T}\mathbf{E} - \mathbf{L}\mathbf{F})\boldsymbol{\omega}_k - \mathbf{N}\mathbf{F}\boldsymbol{\omega}_{k+1}. \quad (5.23)$$

We notice that, for every k , the vector $\boldsymbol{\eta}_k$ belongs to the following set:

$$\boldsymbol{\eta}_k \in \Upsilon = \{ (\mathbf{T}\mathbf{E} - \mathbf{L}\mathbf{F})\boldsymbol{\omega}_a - \mathbf{N}\mathbf{F}\boldsymbol{\omega}_b : \boldsymbol{\omega}_a \in \mathbb{B}^{n_w}, \boldsymbol{\omega}_b \in \mathbb{B}^{n_w} \}$$

This allows us to take into consideration the evolution of the perturbation knowing that $\boldsymbol{\omega}_k$ and $\boldsymbol{\omega}_{k+1}$ are independent. To validate Theorem 5.1, we prove that if $\mathbf{z}_k^\top \mathbf{P} \mathbf{z}_k \leq \rho_k$, then the following expression is verified:

$$\mathbf{z}_{k+1}^\top \mathbf{P} \mathbf{z}_{k+1} = (\mathbf{A}_L \mathbf{z}_k + \boldsymbol{\eta}_k)^\top \mathbf{P} (\mathbf{A}_L \mathbf{z}_k + \boldsymbol{\eta}_k) \leq \beta \rho_k + \sigma, \quad \forall \boldsymbol{\eta}_k \in \Upsilon. \quad (5.24)$$

With the notation:

$$F_0(\mathbf{z}_k, \boldsymbol{\eta}_k) = \beta \rho_k + \sigma - (\mathbf{A}_L \mathbf{z}_k + \boldsymbol{\eta}_k)^\top \mathbf{P} (\mathbf{A}_L \mathbf{z}_k + \boldsymbol{\eta}_k), \quad (5.25)$$

$$F_1(\mathbf{z}_k) = \rho_k - \mathbf{z}_k^\top \mathbf{P} \mathbf{z}_k, \quad (5.26)$$

and using the S-Procedure [Boyd et al., 1994], we have that (5.24) holds if there exists $\mu > 0$ such that:

$$F_0(\mathbf{z}_k, \boldsymbol{\eta}_k) - \mu F_1(\mathbf{z}_k) \geq 0, \quad \forall \mathbf{z}_k \in \mathbb{R}^{n_x}, \forall \boldsymbol{\eta}_k \in \Upsilon. \quad (5.27)$$

Choosing $\mu = \beta$ and using the definitions of $F_0(\mathbf{z}_k, \boldsymbol{\eta}_k)$ and $F_1(\mathbf{z}_k)$, we obtain that (5.24) holds if for every $\mathbf{z}_k \in \mathbb{R}^{n_x}$ and every $\boldsymbol{\eta}_k \in \Upsilon$:

$$\sigma - (\mathbf{A}_L \mathbf{z}_k + \boldsymbol{\eta}_k)^\top \mathbf{P} (\mathbf{A}_L \mathbf{z}_k + \boldsymbol{\eta}_k) + \beta \mathbf{z}_k^\top \mathbf{P} \mathbf{z}_k \geq 0. \quad (5.28)$$

This can be rewritten in the matrix form as:

$$\begin{bmatrix} \mathbf{z}_k \\ 1 \end{bmatrix}^\top \begin{bmatrix} -\mathbf{A}_L^\top \mathbf{P} \mathbf{A}_L + \beta \mathbf{P} & -\mathbf{A}_L^\top \mathbf{P} \boldsymbol{\eta}_k \\ -\boldsymbol{\eta}_k^\top \mathbf{P} \mathbf{A}_L & \sigma - \boldsymbol{\eta}_k^\top \mathbf{P} \boldsymbol{\eta}_k \end{bmatrix} \begin{bmatrix} \mathbf{z}_k \\ 1 \end{bmatrix} \geq 0, \quad (5.29)$$

for every $\mathbf{z}_k \in \mathbb{R}^n$ and every $\boldsymbol{\eta}_k \in \Upsilon$. Expression (5.29) is satisfied if:

$$\begin{bmatrix} -\mathbf{A}_L^\top \mathbf{P} \mathbf{A}_L + \beta \mathbf{P} & -\mathbf{A}_L^\top \mathbf{P} \boldsymbol{\eta}_k \\ -\boldsymbol{\eta}_k^\top \mathbf{P} \mathbf{A}_L & \sigma - \boldsymbol{\eta}_k^\top \mathbf{P} \boldsymbol{\eta}_k \end{bmatrix} \succ 0, \quad \forall \boldsymbol{\eta}_k \in \Upsilon. \quad (5.30)$$

Equivalently, expression (5.30) can be rewritten as follows:

$$\begin{bmatrix} \beta \mathbf{P} & \mathbf{0} \\ \mathbf{0} & \sigma \end{bmatrix} - \begin{bmatrix} \mathbf{A}_L^\top \mathbf{P} \\ \boldsymbol{\eta}_k^\top \mathbf{P} \end{bmatrix} \mathbf{P}^{-1} \begin{bmatrix} \mathbf{P} \mathbf{A}_L & \mathbf{P} \boldsymbol{\eta}_k \end{bmatrix} \succ 0, \quad \forall \boldsymbol{\eta}_k \in \Upsilon. \quad (5.31)$$

The Schur complement [Boyd et al., 1994] applied to the previous equation leads to the following equivalent LMI:

$$\begin{bmatrix} \beta \mathbf{P} & \mathbf{0} & \mathbf{A}_L^\top \mathbf{P} \\ \mathbf{0} & \sigma & \boldsymbol{\eta}_k^\top \mathbf{P} \\ \mathbf{P} \mathbf{A}_L & \mathbf{P} \boldsymbol{\eta}_k & \mathbf{P} \end{bmatrix} \succ 0, \quad \forall \boldsymbol{\eta}_k \in \Upsilon. \quad (5.32)$$

From the equality $\mathbf{A}_L = \mathbf{T} \mathbf{A} - \mathbf{L} \mathbf{C}$ and the definition of Υ we obtain that (5.24) is satisfied if for every $\mathbf{w}_a \in \mathbb{B}^{n_w}$ and every $\mathbf{w}_b \in \mathbb{B}^{n_w}$:

$$\begin{bmatrix} \beta \mathbf{P} & * & * \\ \mathbf{0} & \sigma & * \\ \mathbf{P} \mathbf{T} \mathbf{A} - \mathbf{Y} \mathbf{C} & (\mathbf{P} \mathbf{T} \mathbf{E} - \mathbf{Y} \mathbf{F}) \boldsymbol{\omega}_k - \mathbf{P} \mathbf{N} \mathbf{F} \boldsymbol{\omega}_{k+1} & \mathbf{P} \end{bmatrix} \succ 0.$$

with

$$\mathbf{Y} = \mathbf{P} \mathbf{L}. \quad (5.33)$$

This proves the claim of the theorem. \square

The center of the ellipsoid is calculated using (5.17) which is a special form of the Luenberger observer for discrete-time descriptor systems LTI, with the gain $\mathbf{L} = \mathbf{P}^{-1} \mathbf{Y}$ found after solving the linear matrix inequality (5.18).

Considering the worst case where $\rho_{k+1} = \beta \rho_k + \sigma$ at each iteration is a sufficient condition to guarantee the convergence of the sequence. Reducing the size of the associated ellipsoid can be done by minimizing σ subject to the LMI (5.18). Solving this LMI off-line to get a constant matrix gain significantly reduces the computation time of the technique.

When we consider that the scalar β is a real variable, the expression (5.18) is a case of a bilinear matrix inequality (BMI). However, since $\beta \in (0, 1)$ is a

bounded scalar variable, the BMI is rewritten as a linear matrix inequality (LMI) problem by fixing the value of the scalar β successively using either the bisection algorithm or an available BMI solver, e.g. the `penbmi` solver, for example [Kočvara and Stingl, 2003].

5.4.2 Method 2: Online ellipsoidal state estimation approach

Similar to the previous technique, this approach aims to find the smallest ellipsoid in terms of accuracy that contains the state estimate. The main difference between the off-line and the online technique is the fact that the latter one minimizes the ellipsoidal radius ρ_{k+1} at each time instant [Ben Chabane et al., 2014]. Thus, the proof here is similar to the off-line method in the Theorem 5.1 substituting σ by $\rho_{k+1} - \beta\rho_k$ and \mathbf{L} by \mathbf{L}_k . In other words, considering that the system state \mathbf{x}_k belongs to the ellipsoid $\mathcal{E}(\mathbf{P}, \bar{\mathbf{x}}_k, \rho_k)$ at time instant k , with the matrix \mathbf{P} , the radius ρ_k and the scalar σ computed off-line (using the result of Theorem 5.1), the system state \mathbf{x}_{k+1} at time instant $k+1$ is guaranteed inside the ellipsoid of the form $\mathcal{E}(\mathbf{P}, \bar{\mathbf{x}}_{k+1}, \rho_{k+1})$, for all $\boldsymbol{\omega}_k, \boldsymbol{\omega}_{k+1} \in \mathbb{B}^{n_w}$, if the following optimization problem holds:

$$\begin{aligned} & \min_{\beta, \mathbf{Y}_k, \rho_{k+1}} \rho_{k+1} \\ & \text{subject to} \\ & \left\{ \begin{array}{l} \left[\begin{array}{ccc} \beta\mathbf{P} & * & * \\ \mathbf{0} & \rho_{k+1} - \beta\rho_k & * \\ \mathbf{P}\mathbf{T}\mathbf{A} - \mathbf{Y}_k\mathbf{C} & (\mathbf{P}\mathbf{T}\mathbf{E} - \mathbf{Y}_k\mathbf{F})\boldsymbol{\omega}_k - \mathbf{N}\mathbf{F}\boldsymbol{\omega}_{k+1} & \mathbf{P} \end{array} \right] \succ 0, \\ \rho_{k+1} \leq \beta\rho_k + \sigma \end{array} \right. \end{array} \quad (5.34)$$

with a scalar $\beta \in (0, 1)$,

$$\mathbf{Y}_k = \mathbf{P}\mathbf{L}_k \in \mathbb{R}^{n_x \times n_y} \quad (5.35)$$

and the center of the ellipsoid:

$$\bar{\mathbf{x}}_{k+1} = \mathbf{T}\mathbf{A}\bar{\mathbf{x}}_k + \mathbf{T}\mathbf{B}\mathbf{u}_k + \mathbf{N}\mathbf{y}_{k+1} + \mathbf{L}_k(\mathbf{y}_k - \mathbf{C}\bar{\mathbf{x}}_k). \quad (5.36)$$

Due to the fact that this estimation method updates the ellipsoidal radius online, the computational complexity can be high. The LMI problem presented in (5.34) has to be verified in 2^{2n_w} vertices. The second constraint $\rho_{k+1} \leq \beta\rho_k + \sigma$ guarantees the non increasing condition of the radius. This implies a reduction of the ellipsoidal radius only if the radius ρ_k is larger than $\rho_\infty = \frac{\sigma}{1-\beta}$. In order to reduce the computation time when solving the online optimization problem, the online technique can be extended to avoid vertex enumeration. This will be done by taking into account the structure of the perturbation vector $\boldsymbol{\omega}_k$ in the approach presented in the next section.

5.4.3 Method 3: Online ellipsoidal state estimation approach with vector scaling technique

To the aim of reducing the computation time when solving the online optimization problem, the online technique can be modified to avoid vertex enumeration by taking into account the structure of the perturbation vector $\boldsymbol{\omega}_k$. The proposed approach is based on the scaling technique previously introduced in [Ben Chabane et al., 2014] for standard systems, and based on the results developed by [Alamo et al., 2008b]. This scaling technique is applied to (5.34). An extended vector

$$\mathbf{w} = \begin{bmatrix} \boldsymbol{\omega}_k^\top & \boldsymbol{\omega}_{k+1}^\top \end{bmatrix}^\top \in \mathbb{B}^{2n_w}, \quad (5.37)$$

with $|\mathbf{w}| \leq 1$ can be formed. Moreover, we consider $\mathbf{w}^\top \mathbf{e}_i \mathbf{e}_i^\top \mathbf{w} \leq 1$, for $i = 1, \dots, 2n_w$, with \mathbf{e}_i being the columns of the identity matrix $\mathbf{I}_{2n_w} = \begin{bmatrix} \mathbf{e}_1 & \mathbf{e}_2 & \dots & \mathbf{e}_{2n_w} \end{bmatrix}$. Then, denoting by $\tilde{\mathbf{T}}_i = \mathbf{e}_i \mathbf{e}_i^\top$ the matrix having only the element (i, i) equal to 1, the following scalar inequalities hold:

$$\mathbf{w}^\top \tilde{\mathbf{T}}_i \mathbf{w} \leq 1, \quad i = 1, \dots, 2n_w. \quad (5.38)$$

This result will be exploited by the following property.

Property 5.1. (see Property 1 in [Ben Chabane et al., 2014]) Consider a positive definite matrix $\mathbf{S} = \mathbf{S}^\top \in \mathbb{R}^{2n_w \times 2n_w}$ and the positive real scalars $\rho > 0$ and $\tau_i \geq 0$ such that, for $i = 1, \dots, 2n_w$, all the three following inequalities hold:

$$\left\{ \begin{array}{l} \mathbf{w}^\top \tilde{\mathbf{T}}_i \mathbf{w} \leq 1, \end{array} \right. \quad (5.39a)$$

$$\left\{ \begin{array}{l} \sum_{i=1}^{2n_w} \tau_i < \rho, \end{array} \right. \quad (5.39b)$$

$$\left\{ \begin{array}{l} \sum_{i=1}^{2n_w} \tau_i \tilde{\mathbf{T}}_i \succ \mathbf{S}. \end{array} \right. \quad (5.39c)$$

Then, this implies:

$$\frac{1}{\rho} \cdot \mathbf{w} \mathbf{w}^\top \prec \mathbf{S}^{-1}. \quad (5.40)$$

Proof. Looking back at expression (5.39), it is trivial to say that:

$$\rho > \sum_{i=0}^{2n_w} \tau_i \geq 0. \quad (5.41)$$

Multiplying the left side of (5.39c) by \mathbf{w}^\top and then the right side of the new expression by \mathbf{w} yields:

$$\mathbf{w}^\top \left(\sum_{i=1}^{2n_w} \tau_i \tilde{\mathbf{T}}_i \right) \mathbf{w} \succ \mathbf{w}^\top \mathbf{S} \mathbf{w}. \quad (5.42)$$

Equivalently, manipulating expression (5.42), gives:

$$\sum_{i=1}^{2n_w} \tau_i (\mathbf{w}^\top \tilde{\mathbf{T}}_i \mathbf{w}) \succ \mathbf{w}^\top \mathbf{S} \mathbf{w}. \quad (5.43)$$

Using (5.39a), expression (5.43) becomes equivalent to:

$$\mathbf{w}^\top \mathbf{S} \mathbf{w} \prec \sum_{i=1}^{2n_w} \tau_i (\mathbf{w}^\top \tilde{\mathbf{T}}_i \mathbf{w}) \prec \sum_{i=0}^{2n_w} \tau_i \prec \rho. \quad (5.44)$$

To proceed with the proof, expression (5.44) can be rewritten under the following form:

$$\rho - \mathbf{w}^\top \mathbf{S} \mathbf{w} > 0, \mathbf{S} \succ 0, \quad (5.45)$$

Using the Schur complement to reformulate expression (5.45) yields:

$$\begin{bmatrix} \rho & \mathbf{w}^\top \\ \mathbf{w} & \mathbf{S}^{-1} \end{bmatrix} \succ 0, \mathbf{S} \succ 0 \quad (5.46)$$

and

$$\begin{bmatrix} \mathbf{S}^{-1} & \mathbf{w} \\ \mathbf{w}^\top & \rho \end{bmatrix} \succ 0, \rho > 0. \quad (5.47)$$

Applying again the Schur complement leads to another form of the expression (5.47) such that:

$$\mathbf{S}^{-1} - \mathbf{w} \rho^{-1} \mathbf{w}^\top \succ 0, \rho > 0. \quad (5.48)$$

which is another form of (5.40). \square

Furthermore, left and right multiplying the inequality (5.34) by the matrix $\begin{bmatrix} \mathbf{I} & \mathbf{0} & \mathbf{0} \\ \mathbf{0} & \mathbf{0} & \mathbf{I} \\ \mathbf{0} & \mathbf{I} & \mathbf{0} \end{bmatrix}$ leads to:

$$\begin{bmatrix} \beta \mathbf{P} & * & * \\ \mathbf{P} \mathbf{T} \mathbf{A} - \mathbf{Y}_k \mathbf{C} & \mathbf{P} & * \\ \mathbf{0} & ((\mathbf{P} \mathbf{T} \mathbf{E} - \mathbf{Y}_k \mathbf{F}) \boldsymbol{\omega}_k - \mathbf{P} \mathbf{N} \mathbf{F} \boldsymbol{\omega}_{k+1})^\top & \rho_{k+1} - \beta \rho_k \end{bmatrix} \succ 0 \quad (5.49)$$

with $\rho_{k+1} - \beta\rho_k > 0$. Using the notation:

$$\mathbf{H}_k = \begin{bmatrix} \mathbf{PTE} - \mathbf{Y}_k\mathbf{F} & -\mathbf{PNF} \end{bmatrix}, \quad (5.50)$$

a simplified expression of (5.49) can be obtained such that:

$$\begin{bmatrix} \beta\mathbf{P} & * & * \\ \mathbf{PTA} - \mathbf{Y}_k\mathbf{C} & \mathbf{P} & * \\ \mathbf{0} & (\mathbf{H}_k\mathbf{w})^\top & \rho_{k+1} - \beta\rho_k \end{bmatrix} \succ 0 \quad (5.51)$$

with \mathbf{w} given by (5.37). Applying the Schur complement on (5.51) leads us to the following equation:

$$\begin{bmatrix} \beta\mathbf{P} & * \\ \mathbf{PTA} - \mathbf{Y}_k\mathbf{C} & \mathbf{P} - \frac{1}{\rho_{k+1} - \beta\rho_k} \mathbf{H}_k\mathbf{w}\mathbf{w}^\top \mathbf{H}_k^\top \end{bmatrix} \succ 0, \quad (5.52)$$

with $\rho_{k+1} - \beta\rho_k > 0$. Applying (5.40) to the term:

$$\frac{1}{\rho_{k+1} - \beta\rho_k} \mathbf{w}\mathbf{w}^\top$$

with $\rho = \rho_{k+1} - \beta\rho_k$, means that $\exists \mathbf{S} = \mathbf{S}^\top \succ 0$ such that:

$$\frac{1}{\rho_{k+1} - \beta\rho_k} \mathbf{w}\mathbf{w}^\top \prec \mathbf{S}^{-1} \quad (5.53)$$

From (5.52) and (5.53) it can be inferred that:

$$\begin{bmatrix} \beta\mathbf{P} & * \\ \mathbf{PTA} - \mathbf{Y}_k\mathbf{C} & \mathbf{P} - \mathbf{H}_k\mathbf{S}^{-1}\mathbf{H}_k^\top \end{bmatrix} \succ 0, \text{ with } \mathbf{S} \succ 0. \quad (5.54)$$

Decomposing (5.54) and applying the Schur complement on it gives the following LMI:

$$\begin{bmatrix} \beta\mathbf{P} & * & * \\ \mathbf{PTA} - \mathbf{Y}_k\mathbf{C} & \mathbf{P} & * \\ \mathbf{0} & [\mathbf{PTE} - \mathbf{Y}_k\mathbf{F} \quad -\mathbf{PNF}]^\top & \mathbf{S} \end{bmatrix} \succ 0, \text{ with } \mathbf{S} \succ 0. \quad (5.55)$$

To summarize, if the online LMI constraint (5.34) is verified, then there exist a scalar $\beta \in (0, 1)$ and a matrix $\mathbf{S} = \mathbf{S}^\top \succ 0$, with $\mathbf{S} \in \mathbb{R}^{2n_w \times 2n_w}$ such that (5.55) together with $\rho_{k+1} - \beta\rho_k > 0$ hold. In a typical descriptor system, when considering both perturbation vectors $\boldsymbol{\omega}_k$ and $\boldsymbol{\omega}_{k+1}$, a large computation time is required since the LMI (5.34) has to be verified for all

the 2^{2n_w} vertices of the box \mathbb{B}^{2n_w} . The presented scaling technique permits avoiding the vertex enumeration used in the online approach (5.34).

Next, an illustrative example is considered to show the performance of the proposed ellipsoidal state estimation approaches: *Method 1* (5.18), *Method 2* (5.34) and *Method 3* (5.55).

Example 5.1. Let us consider the discrete-time linear time-invariant descriptor system (5.10) with the following matrices:

$$\mathbf{E}_d = \begin{bmatrix} 1 & 0 & 0 \\ 0 & 1 & 0 \\ 0 & 0 & 0 \end{bmatrix}, \mathbf{A} = \begin{bmatrix} 0.5 & 0 & 0 \\ 0.8 & 0.95 & 0 \\ -1 & 0.5 & 1 \end{bmatrix}, \mathbf{B} = \begin{bmatrix} 1 & 0 \\ 0 & 1 \\ 0 & 0 \end{bmatrix}, \mathbf{C} = \begin{bmatrix} 1 & 0 & 1 \\ 1 & -1 & 0 \end{bmatrix},$$

$$\mathbf{E} = \begin{bmatrix} 0.1 & 0 & 0 & 0 & 0 \\ 0 & 1.5 & 0 & 0 & 0 \\ 0 & 0 & 0.6 & 0 & 0 \end{bmatrix}, \mathbf{F} = \begin{bmatrix} 0 & 0 & 0 & 0.5 & 0 \\ 0 & 0 & 0 & 0 & 1.5 \end{bmatrix}.$$

The control signal is $\mathbf{u}(t) = [0.5 \sin(t) + 1 \quad -2 \cos(t)]^\top$, for $t \in [0 \quad 5\pi]$, with 50 sampling steps. The perturbation vector $\boldsymbol{\omega}_k$ is randomly generated with $\|\boldsymbol{\omega}_k\|_\infty \leq 1$. The matrices \mathbf{E} , \mathbf{A} , \mathbf{B} and \mathbf{C} satisfy the rank conditions (5.6), (5.7), (5.8), (5.9). A possible solution satisfying the condition (5.13) is:

$$\mathbf{T} = \begin{bmatrix} 0.6667 & 0.3333 & 0 \\ 0.3333 & 0.6667 & 0 \\ -0.6667 & -0.3333 & 0 \end{bmatrix} \text{ and } \mathbf{N} = \begin{bmatrix} 0 & 0.3333 \\ 0 & -0.3333 \\ 1 & -0.3333 \end{bmatrix}.$$

The initial state \mathbf{x}_0 is inside the ellipsoid $\mathcal{E}(\mathbf{P}_0, \bar{\mathbf{x}}_0, \rho_0)$, with $\mathbf{P}_0 = \mathbf{I}_3$, $\bar{\mathbf{x}}_0 = [0 \quad 0 \quad 0]^\top$ and $\rho_0 = 1$ as a random initialization choice. The three techniques are tested and analyzed on the considered descriptor system using `mincx`, a LMI solver of the Matlab Robust Control Toolbox, with an Intel Core i7-8750G 3.10 GHz.

Simulation results plotted in Figures 5.3-5.5 illustrate the bounds of each element x_1 , x_2 and x_3 of the state vector after 50 iterations of the ellipsoidal set-membership state estimation techniques. The black lines are obtained by the off-line technique when solving LMI (5.18), i.e. via Method 1. Moreover, the blue dashed lines represent the online technique (Method 2) solving LMI (5.34), while the green dashed lines are obtained using the online ellipsoidal approach with the scaling technique allowing (Method 3) to avoid the vertex enumeration (5.55). Figures 5.3 to 5.5 show that the real state represented by the red stars is guaranteed to belong to the bounds computed by the techniques at each time instant k . The bounds computed by the ellipsoidal off-line technique (Method 1) are larger than the bounds obtained by the online ellipsoidal estimation method with scaling technique (Method 3), which are also larger than the bounds computed by the online technique (Method 2).

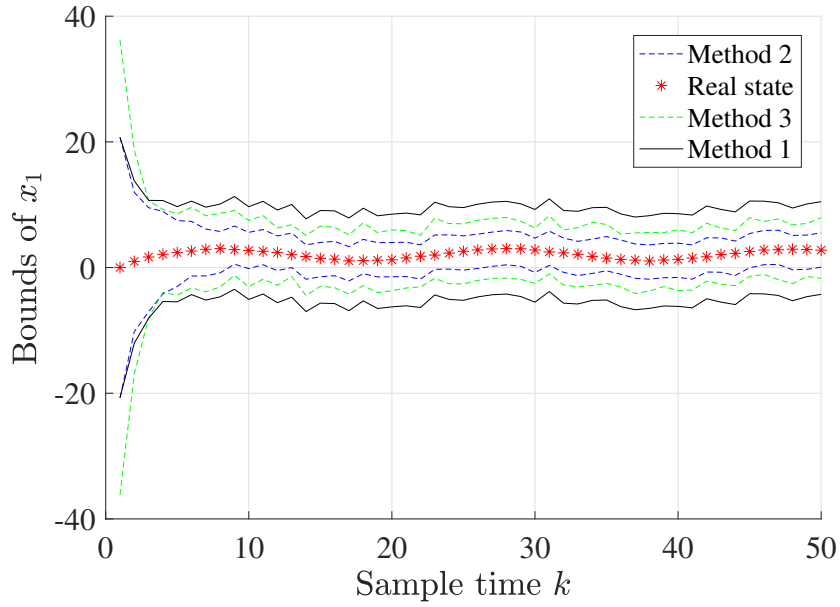


Figure 5.3 – Example 5.1: bounds of x_1

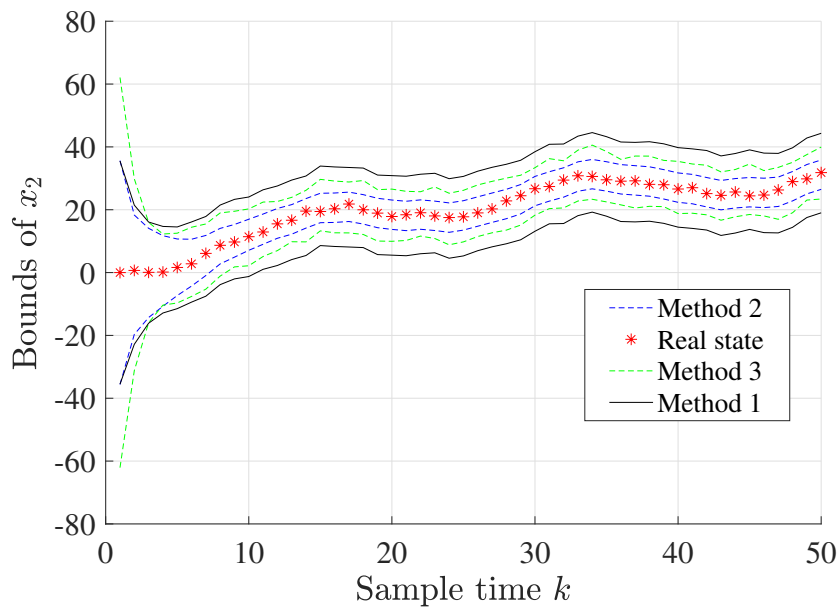


Figure 5.4 – Example 5.1: bounds of x_2

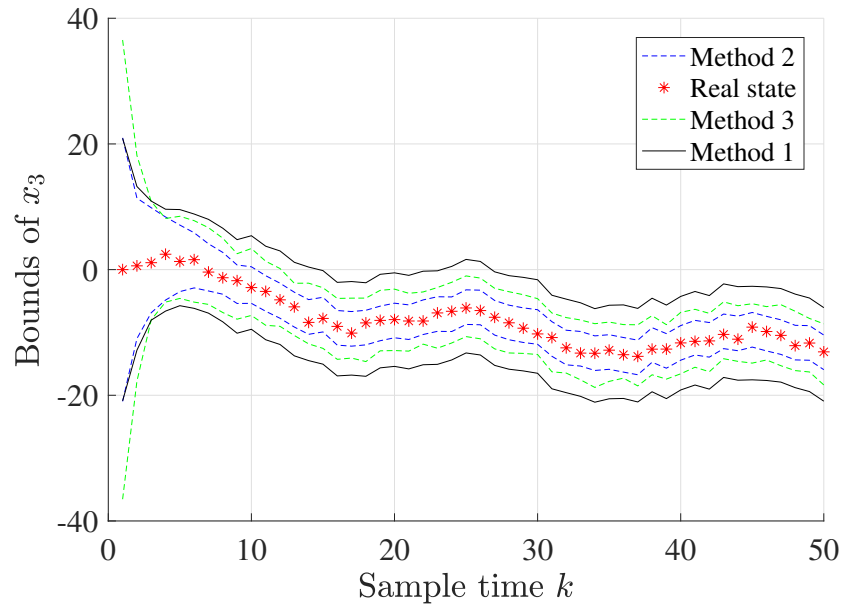
Figure 5.5 – Example 5.1: bounds of x_3

Table 5.1 – Example 5.1: total computation time

| Algorithm | Time (second) |
|-----------|---------------|
| Method 1 | 0.61 |
| Method 2 | 6.56 |
| Method 3 | 0.77 |

The low computation time of Method 1 is the fruit of the off-line computation of the feasible set of the state estimate. However, as the simulation shows, a good trade-off between accuracy and complexity is offered by Method 3. In this simulation test, the elapsed CPU time for Method 3 is 0.77 seconds. This is thanks to the scaling technique which avoids the vertex enumeration. Method 2 offers a faster convergence rate of state estimation than the other techniques but with increased complexity due to the online computation of the radius (see Table 5.1).

Furthermore, the accuracy of the state estimation approach inversely proportional to the volume of ellipsoidal set obtained at steady state. Table 5.2 showing the different volume obtained by the three techniques confirms the fact that Method 3 offers a better estimation accuracy compared to the Method 1 with a gain on simulation time compared to Method 2 accord-

ing to Table 5.1.

Table 5.2 – Example 5.1: volume of ellipsoidal sets at steady state

| Algorithm | Volume |
|-----------|--------|
| Method 1 | 44.69 |
| Method 2 | 2.24 |
| Method 3 | 8.31 |

5.5 Ellipsoidal state estimation for LTV descriptor systems

In this thesis, we assume unknown but bounded perturbations and measurement noises. In general, in control systems or model analysis, it is important to incorporate uncertainties in the considered model. The mathematical simplification in the modeling phase, the inevitable errors involved in engineering coming from different sources or from partial knowledge of the system can lead to uncertainties in the model.

The goal of this section is to extend the previous developed state estimation technique to the case of linear time variant descriptor systems with bounded noises and perturbations and interval uncertainties in the evolution matrix of the model.

5.5.1 Problem formulation

Consider the following discrete-time linear time variant descriptor system:

$$\begin{cases} \mathbf{E}_d \mathbf{x}_{k+1} = \mathbf{A}_k \mathbf{x}_k + \mathbf{B} \mathbf{u}_k + \mathbf{E} \boldsymbol{\omega}_k, \\ \mathbf{y}_k = \mathbf{C} \mathbf{x}_k + \mathbf{F} \boldsymbol{\omega}_k, \end{cases} \quad (5.56)$$

where $\mathbf{x}_k \in \mathbb{R}^{n_x}$ is the state vector of the system, $\mathbf{u}_k \in \mathbb{R}^{n_u}$ is the control input vector and $\mathbf{y}_k \in \mathbb{R}^{n_y}$ is the measured output vector at sample time k . The vector $\boldsymbol{\omega}_k \in \mathbb{R}^{n_w}$ contains both the state perturbations and the measurement perturbations (noise, offset, etc.), which are non-correlated. It is also assumed that the perturbations $\boldsymbol{\omega}_k$ are bounded by the unitary box \mathbb{B}^{n_w} , with $n_w = n_x + n_y$ and the initial state \mathbf{x}_0 is bounded by the ellipsoid:

$$\mathcal{E}(\mathbf{P}_0, \bar{\mathbf{x}}_0, \rho_0) = \{\mathbf{x} \in \mathbb{R}^{n_x} : (\mathbf{x} - \bar{\mathbf{x}}_0)^\top \mathbf{P}_0 (\mathbf{x} - \bar{\mathbf{x}}_0) \leq \rho_0\}.$$

Matrices \mathbf{A}_k , \mathbf{B} , \mathbf{C} , \mathbf{E} , \mathbf{E}_d and \mathbf{F} have the appropriate dimensions. The matrix \mathbf{A}_k is an unknown time-varying matrix belonging to interval matrix $[\mathbf{A}]$ (see Section 3.3.1 for more details on interval uncertainties).

Goal: Given an ellipsoidal estimation set $\mathcal{E}(\mathbf{P}, \bar{\mathbf{x}}_k, \rho_k)$ for the state \mathbf{x}_k from (5.56) at time instant k , the aim is to find an ellipsoidal estimation for the state \mathbf{x}_{k+1} at time instant $k+1$ of the form $\mathcal{E}(\mathbf{P}, \bar{\mathbf{x}}_{k+1}, \rho_{k+1})$ taking into consideration that the evolution matrix of the model is not constant. The next section presents an ellipsoidal technique to treat this problem.

5.5.2 Method 4: Online flexible shape ellipsoidal state estimation approach

This method minimizes the size of the ellipsoidal state estimation set of the linear time variant (LTV) descriptor system (5.56) by solving an online Linear Matrix Inequality (LMI) problem, while allowing to adjust the shape of the ellipsoid, which reduces the conservativeness of the estimation. Method 4 extends a previously developed ellipsoidal set-membership state estimation technique for LTV systems [Ben Chabane, 2015] to the case of descriptor systems. This method based on the use of the S-procedure for quadratic functions [Boyd et al., 1994] can be applied on linear time-varying systems with possible interval uncertainties, bounded perturbations and measurement noises. The following theorem formulates the solution to this problem.

Theorem 5.2. Let us consider an uncertain discrete-time descriptor system of the form (5.56), under the following assumptions:

- (i) At time k , the system state \mathbf{x}_k belongs to the ellipsoid $\mathcal{E}(\mathbf{P}_k, \bar{\mathbf{x}}_k, \rho_k)$,
- (ii) At time k , the uncertainties are bounded by a convex set Ω_k , i.e. $(\boldsymbol{\omega}_k, \mathbf{A}_k) \in \mathcal{V}_{\Omega_k}$, with \mathcal{V}_{Ω_k} denoting the vertices of Ω_k ,
- (iii) There exist two matrices \mathbf{T} and \mathbf{N} satisfying (5.13),
- (iv) There exist the matrices $\mathbf{P}_{k+1} = \mathbf{P}_{k+1}^\top \succ 0$, with $\mathbf{P}_{k+1} \in \mathbb{R}^{n_x \times n_x}$, $\mathbf{Y}_{k+1} \in \mathbb{R}^{n_x \times n_y}$, $\mathbf{G}_{k+1} \in \mathbb{R}^{n_x \times n_x}$, the vector $\mathbf{g}_{k+1} \in \mathbb{R}^{n_x}$ and the positive scalars $\beta_{k+1}, \rho_{k+1} > 0$ such that the following LMI is satisfied for every $(\boldsymbol{\omega}_k, \mathbf{A}_k) \in \mathcal{V}_{\Omega_k}$:

$$\begin{bmatrix} \beta_{k+1} \mathbf{P}_k & * & * \\ \mathbf{0} & \rho_{k+1} - \beta_{k+1} \rho_k & * \\ \mathbf{P}_{k+1} \mathbf{T} \mathbf{A}_k - \mathbf{Y}_{k+1} \mathbf{C} & \boldsymbol{\tau}_{k+1} & \mathbf{P}_{k+1} \end{bmatrix} \succ 0, \quad (5.57)$$

with $\boldsymbol{\tau}_{k+1} = (\mathbf{P}_{k+1} \mathbf{T} \mathbf{A}_k - \mathbf{Y}_{k+1} \mathbf{C} - \mathbf{G}_{k+1}) \bar{\mathbf{x}}_k + (\mathbf{P}_{k+1} \mathbf{T} \mathbf{E} - \mathbf{Y}_{k+1} \mathbf{F}) \boldsymbol{\omega}_k - \mathbf{g}_{k+1} + \mathbf{N}_k \mathbf{y}_{k+1} - \mathbf{N}_k \mathbf{F} \boldsymbol{\omega}_{k+1}$,

then, at time $k+1$, the system state \mathbf{x}_{k+1} belongs to the ellipsoid $\mathcal{E}(\mathbf{P}_{k+1}, \bar{\mathbf{x}}_{k+1}, \rho_{k+1})$, with $\bar{\mathbf{x}}_{k+1} = \mathbf{P}_{k+1}^{-1}(\mathbf{G}_{k+1}\bar{\mathbf{x}}_k + \mathbf{Y}_{k+1}\mathbf{y}_k + \mathbf{g}_{k+1})$.

Proof. Since \mathbf{T} and \mathbf{N} satisfy the condition (5.13), we have in virtue of equation (5.14) that the state vector \mathbf{x}_{k+1} of the descriptor system (5.56) satisfies:

$$\mathbf{x}_{k+1} = \mathbf{TA}_k\mathbf{x}_k + \mathbf{TB}\mathbf{u}_k + \mathbf{N}\mathbf{y}_{k+1} + \mathbf{TE}\boldsymbol{\omega}_k - \mathbf{NF}\boldsymbol{\omega}_{k+1}. \quad (5.58)$$

Let us define the error between the real state and the nominal estimated state at time instant k by:

$$\mathbf{z}_k = \mathbf{x}_k - \bar{\mathbf{x}}_k.$$

Therefore, the error dynamics at the next time instant:

$$\begin{aligned} \mathbf{z}_{k+1} &= \mathbf{x}_{k+1} - \bar{\mathbf{x}}_{k+1} \\ &= \mathbf{TA}_k\mathbf{x}_k + \mathbf{TE}\boldsymbol{\omega}_k + \mathbf{N}\mathbf{y}_{k+1} - \mathbf{NF}\boldsymbol{\omega}_{k+1} - \mathbf{P}_{k+1}^{-1}(\mathbf{G}_{k+1}\bar{\mathbf{x}}_k + \mathbf{Y}_{k+1}\mathbf{y}_k + \mathbf{g}_{k+1}) \end{aligned} \quad (5.59)$$

The notation $\mathbf{P}_{k+1}^{-1}\mathbf{Y}_{k+1} = \mathbf{L}_{k+1}$ yields:

$$\mathbf{z}_{k+1} = \mathbf{TA}_k\mathbf{x}_k + \mathbf{TE}\boldsymbol{\omega}_k - \mathbf{L}_{k+1}\mathbf{y}_k - \mathbf{P}_{k+1}^{-1}(\mathbf{G}_{k+1}\bar{\mathbf{x}}_k + \mathbf{g}_{k+1}) + \mathbf{N}\mathbf{y}_{k+1} - \mathbf{NF}\boldsymbol{\omega}_{k+1}. \quad (5.60)$$

Then, using the measurement equation in (5.56) to replace \mathbf{y}_k leads to:

$$\begin{aligned} \mathbf{z}_{k+1} &= \mathbf{TA}_k\mathbf{x}_k + \mathbf{TE}\boldsymbol{\omega}_k - \mathbf{L}_{k+1}\mathbf{C}\mathbf{x}_k - \mathbf{L}_{k+1}\mathbf{F}\boldsymbol{\omega}_k \\ &\quad - \mathbf{P}_{k+1}^{-1}(\mathbf{G}_{k+1}\bar{\mathbf{x}}_k + \mathbf{g}_{k+1}) + \mathbf{N}\mathbf{y}_{k+1} - \mathbf{NF}\boldsymbol{\omega}_{k+1}. \end{aligned} \quad (5.61)$$

Regrouping the terms in \mathbf{z}_k , $\bar{\mathbf{x}}_k$ and $\boldsymbol{\omega}_k$ gives:

$$\begin{aligned} \mathbf{z}_{k+1} &= (\mathbf{TA}_k - \mathbf{L}_{k+1}\mathbf{C})\mathbf{z}_k + (\mathbf{TA}_k - \mathbf{L}_{k+1}\mathbf{C})\bar{\mathbf{x}}_k + (\mathbf{TE} - \mathbf{L}_{k+1}\mathbf{F})\boldsymbol{\omega}_k \\ &\quad - \mathbf{P}_{k+1}^{-1}(\mathbf{G}_{k+1}\bar{\mathbf{x}}_k + \mathbf{g}_{k+1}) + \mathbf{N}\mathbf{y}_{k+1} - \mathbf{NF}\boldsymbol{\omega}_{k+1}. \end{aligned} \quad (5.62)$$

The error can be rewritten under the form of:

$$\mathbf{z}_{k+1} = \tilde{\mathbf{A}}_{L_{k+1}}\mathbf{z}_k + \tilde{\boldsymbol{\eta}}_{k+1}, \quad (5.63)$$

with

$$\tilde{\mathbf{A}}_{L_{k+1}} = \mathbf{TA}_k - \mathbf{L}_{k+1}\mathbf{C}, \quad (5.64)$$

$$\begin{aligned} \tilde{\boldsymbol{\eta}}_{k+1} &= (\mathbf{TA}_k - \mathbf{L}_{k+1}\mathbf{C})\bar{\mathbf{x}}_k + (\mathbf{TE} - \mathbf{L}_{k+1}\mathbf{F})\boldsymbol{\omega}_k \\ &\quad - \mathbf{P}_{k+1}^{-1}(\mathbf{G}_{k+1}\bar{\mathbf{x}}_k + \mathbf{g}_{k+1}) + \mathbf{N}\mathbf{y}_{k+1} - \mathbf{NF}\boldsymbol{\omega}_{k+1}. \end{aligned} \quad (5.65)$$

The next step in order to verify the result of the theorem is to prove that the following expression holds:

$$\mathbf{z}_k^\top \mathbf{P}_k \mathbf{z}_k \leq \rho_k \Rightarrow \mathbf{z}_{k+1}^\top \mathbf{P}_{k+1} \mathbf{z}_{k+1} \leq \rho_{k+1}. \quad (5.66)$$

Denote by:

$$F_0(\mathbf{z}_k) = \rho_{k+1} - \mathbf{z}_{k+1}^\top \mathbf{P}_{k+1} \mathbf{z}_{k+1} \quad (5.67)$$

and

$$F_1(\mathbf{z}_k) = \rho_k - \mathbf{z}_k^\top \mathbf{P}_k \mathbf{z}_k, \quad (5.68)$$

using the S-Procedure, the expression (5.66) is verified if there exists $\beta_{k+1} > 0$ such that:

$$F_0(\mathbf{z}_k) - \beta_{k+1} F_1(\mathbf{z}_k) \geq 0, \quad \forall (\boldsymbol{\omega}_k, \mathbf{A}_k) \in \Omega_k. \quad (5.69)$$

Expression (5.69) is equivalent to saying that:

$$\mathbf{z}_{k+1}^\top \mathbf{P}_{k+1} \mathbf{z}_{k+1} + \beta_{k+1} (\rho_k - \mathbf{z}_k^\top \mathbf{P}_k \mathbf{z}_k) \leq \rho_{k+1}, \quad \forall (\boldsymbol{\omega}_k, \mathbf{A}_k) \in \Omega_k. \quad (5.70)$$

Using expression (5.63) to substitute \mathbf{z}_{k+1} by its equivalent form yields:

$$\begin{aligned} \mathbf{z}_k^\top (\tilde{\mathbf{A}}_{L_{k+1}}^\top \mathbf{P}_{k+1} \tilde{\mathbf{A}}_{L_{k+1}} - \beta_{k+1} \mathbf{P}_k) \mathbf{z}_k + 2 \tilde{\boldsymbol{\eta}}_{k+1}^\top \mathbf{P}_{k+1} \tilde{\mathbf{A}}_{L_{k+1}} \mathbf{z}_k + \tilde{\boldsymbol{\eta}}_{k+1}^\top \mathbf{P}_{k+1} \tilde{\boldsymbol{\eta}}_{k+1} + \\ + \beta_{k+1} \rho_k - \rho_{k+1} \leq 0, \quad \forall (\boldsymbol{\omega}_k, \mathbf{A}_k) \in \Omega_k \end{aligned} \quad (5.71)$$

Expression (5.71) can be rewritten as:

$$\begin{bmatrix} \mathbf{z}_k \\ 1 \end{bmatrix}^\top \begin{bmatrix} \tilde{\mathbf{A}}_{L_{k+1}}^\top \mathbf{P}_{k+1} \tilde{\mathbf{A}}_{L_{k+1}} - \beta_{k+1} \mathbf{P}_k & * \\ \tilde{\boldsymbol{\eta}}_{k+1}^\top \mathbf{P}_{k+1} \tilde{\mathbf{A}}_{L_{k+1}} & \tilde{\boldsymbol{\eta}}_{k+1}^\top \mathbf{P}_{k+1} \tilde{\boldsymbol{\eta}}_{k+1} + \beta_{k+1} \rho_k - \rho_{k+1} \end{bmatrix} \begin{bmatrix} \mathbf{z}_k \\ 1 \end{bmatrix} \prec 0, \quad (5.72)$$

with $\forall (\boldsymbol{\omega}_k, \mathbf{A}_k) \in \Omega_k$ and $\forall \mathbf{z}_k \in \mathbb{R}^{n_x}$. The expression (5.72) is verified, $\forall \mathbf{z}_k \in \mathbb{R}^{n_x}$, if:

$$\begin{bmatrix} -\tilde{\mathbf{A}}_{L_{k+1}}^\top \mathbf{P}_{k+1} \tilde{\mathbf{A}}_{L_{k+1}} + \beta_{k+1} \mathbf{P}_k & * \\ -\tilde{\boldsymbol{\eta}}_{k+1}^\top \mathbf{P}_{k+1} \tilde{\mathbf{A}}_{L_{k+1}} & -\tilde{\boldsymbol{\eta}}_{k+1}^\top \mathbf{P}_{k+1} \tilde{\boldsymbol{\eta}}_{k+1} - \beta_{k+1} \rho_k + \rho_{k+1} \end{bmatrix} \succ 0, \quad (5.73)$$

$\forall (\boldsymbol{\omega}_k, \mathbf{A}_k) \in \Omega_k$, or equivalently if:

$$\begin{bmatrix} \beta_{k+1} \mathbf{P}_k & \mathbf{0} \\ \mathbf{0} & \rho_{k+1} - \beta_{k+1} \rho_k \end{bmatrix} - \begin{bmatrix} \tilde{\mathbf{A}}_{L_{k+1}}^\top \mathbf{P}_{k+1} \\ \tilde{\boldsymbol{\eta}}_{k+1}^\top \mathbf{P}_{k+1} \end{bmatrix} \mathbf{P}_{k+1}^{-1} \begin{bmatrix} \mathbf{P}_{k+1} \tilde{\mathbf{A}}_{L_{k+1}} & \mathbf{P}_{k+1} \tilde{\boldsymbol{\eta}}_{k+1} \end{bmatrix} \succ 0, \quad (5.74)$$

$\forall (\boldsymbol{\omega}_k, \mathbf{A}_k) \in \Omega_k$. Using the Schur complement, (5.74) becomes:

$$\begin{bmatrix} \beta_{k+1} \mathbf{P}_k & * & * \\ \mathbf{0} & \rho_{k+1} - \beta_{k+1} \rho_k & * \\ \mathbf{P}_{k+1} \tilde{\mathbf{A}}_{L_{k+1}} & \mathbf{P}_{k+1} \tilde{\boldsymbol{\eta}}_{k+1} & \mathbf{P}_{k+1} \end{bmatrix} \succ 0, \quad \forall (\boldsymbol{\omega}_k, \mathbf{A}_k) \in \Omega_k. \quad (5.75)$$

Taking into account that $\mathbf{P}_{k+1}\tilde{\mathbf{A}}_{L_{k+1}} = \mathbf{P}_{k+1}\mathbf{TA}_k - \mathbf{Y}_{k+1}\mathbf{C}$ and that:

$$\begin{aligned} \mathbf{P}_{k+1}\tilde{\boldsymbol{\eta}}_{k+1} &= (\mathbf{P}_{k+1}\mathbf{TA}_k - \mathbf{Y}_{k+1}\mathbf{C})\bar{\mathbf{x}}_k + (\mathbf{P}_{k+1}\mathbf{TE} - \mathbf{Y}_{k+1}\mathbf{F})\boldsymbol{\omega}_k \\ &\quad - \mathbf{G}_{k+1}\bar{\mathbf{x}}_k - \mathbf{g}_{k+1} + \mathbf{P}_{k+1}\mathbf{N}\mathbf{y}_{k+1} - \mathbf{NF}\boldsymbol{\omega}_{k+1}, \end{aligned} \quad (5.76)$$

the linear matrix inequality (5.57) is found. This proves the claim of Theorem 5.2. \square

Remark 5.1. The vector $\boldsymbol{\omega}_k$ and the matrix \mathbf{A}_k appear in an affine way in the LMI (5.57), therefore the inequality should be verified for all the vertices of Ω_k .

In the next section, Method 4 is improved by adding the vector scaling technique [Ben Chabane, 2015]. As proven in Section 5.4.3, the vector scaling technique improves the accuracy of the state estimation but requires higher computational complexity since it solves an additional LMI problem.

5.5.3 Method 5: Online flexible shape ellipsoidal state estimation approach with vector scaling technique

The state estimation in the previous subsection computes the ellipsoidal set $\mathcal{E}(\mathbf{P}_{k+1}, \bar{\mathbf{x}}_{k+1}, \rho_{k+1})$ using the measurements \mathbf{y}_k . To adjust the ellipsoidal estimation set, a convenient technique is to use the measurement \mathbf{y}_{k+1} at time $k+1$. In this context, additional quadratic constraints on the output measurement taking into account the structure of the perturbations and the measurement noise allow to improve the accuracy of the estimation. Starting from the ellipsoidal state estimation computed by Theorem 5.2, the idea is to consider supplementary quadratic constraints on the measurement \mathbf{y}_{k+1} and on the perturbations $\boldsymbol{\omega}_{k+1}$ in order to compute the new ellipsoidal state estimation set. This is similar to a correction step based on the measurements at time $k+1$. Consider the ellipsoidal estimation set $\mathcal{E}(\mathbf{P}_{k+1}, \bar{\mathbf{x}}_{k+1}, \rho_{k+1})$ obtained at sample time $k+1$ by the ellipsoidal estimation method (Theorem 5.2) and the following measurements:

$$\mathbf{y}_{k+1} - \mathbf{C}\mathbf{x}_{k+1} = \mathbf{F}\boldsymbol{\omega}_{k+1}. \quad (5.77)$$

Similar to Method 3, an extended vector:

$$\mathbf{w} = \begin{bmatrix} \boldsymbol{\omega}_k^\top & \boldsymbol{\omega}_{k+1}^\top \end{bmatrix}^\top \in \mathbb{B}^{2n_w},$$

with $|\mathbf{w}| \leq 1$ is formed. Thus, the vector \mathbf{w}_k satisfies:

$$\mathbf{w}^\top \tilde{\mathbf{T}}_i \mathbf{w} \leq 1, \quad i = 1, \dots, 2n_w, \quad (5.78)$$

with $\tilde{\mathbf{T}}_i = \mathbf{e}_i \mathbf{e}_i^\top$, for $i = 1, \dots, 2n_w$, and \mathbf{e}_i being the columns of the identity matrix $\mathbf{I}_{2n_w} = [\mathbf{e}_1 \ \mathbf{e}_2 \ \dots \ \mathbf{e}_{2n_w}]$. The matrix $\tilde{\mathbf{T}}_i$ has only the element (i, i) equal to 1.

The objective is to find $\mathcal{E}'(\mathbf{P}'_{k+1}, \bar{\mathbf{x}}'_{k+1}, \rho'_{k+1})$, an updated ellipsoidal estimation set, such that the equations (5.77) and (5.78) hold. The following proposition summarizes the result of this problem.

Proposition 5.1. Consider the state estimation described by the ellipsoid $\mathcal{E}(\mathbf{P}_{k+1}, \bar{\mathbf{x}}_{k+1}, \rho_{k+1})$ after solving the optimization problem in Theorem 5.2 for system (5.56) at time $k + 1$, based on the information available at time k . If there exist a matrix $\mathbf{P}'_{k+1} = \mathbf{P}'_{k+1} \succ 0$ in $\mathbb{R}^{n_x \times n_x}$, a matrix $\mathbf{H} = \mathbf{H}^\top \succ 0$ in $\mathbb{R}^{n_y \times n_y}$, a vector $\bar{\mathbf{x}}'_{k+1} \in \mathbb{R}^{n_x}$ and a real positive scalar $\rho'_{k+1} > 0$ such that the following LMI constraints are verified:

$$\left\{ \begin{array}{l} \left[\begin{array}{ccc} \boldsymbol{\eta}_1 & * & * \\ \boldsymbol{\eta}_2 & \eta_3 - \sum_{i=1}^{n_x+n_y} \mu_i & * \\ \mathbf{P}'_{k+1} & -\mathbf{b}_{k+1} & \mathbf{P}'_{k+1} \end{array} \right] \succ 0, \\ \mathbf{F}^\top \mathbf{H} \mathbf{F} < \sum_{i=1}^{n_x+n_y} \mu_i \tilde{\mathbf{T}}_i, \\ \mathbf{P}' \succ 0, \mathbf{P}'_{k+1} \geq \mathbf{P}_{k+1}, \theta \geq 0, \theta < 1, \gamma > 0, \\ \rho'_{k+1} > \theta \rho_{k+1}, \rho_{k+1} \leq \alpha \rho_k + \gamma, \\ \mu_i \geq 0, \quad i = 1, \dots, n_x + n_y, \end{array} \right. \quad (5.79)$$

with:

$$\begin{aligned} \mathbf{b}_{k+1} &= \mathbf{P}'_{k+1} \bar{\mathbf{x}}'_{k+1}, \\ \boldsymbol{\eta}_1 &= \theta \mathbf{P}_{k+1} + \mathbf{C}^\top \mathbf{H} \mathbf{C}, \\ \boldsymbol{\eta}_2 &= -\theta \bar{\mathbf{x}}_{k+1}^\top \mathbf{P}_{k+1} - \mathbf{y}_{k+1}^\top \mathbf{H} \mathbf{C}, \\ \eta_3 &= \rho'_{k+1} - \theta \rho_{k+1} + \theta \|\bar{\mathbf{x}}_{k+1}\|_{\mathbf{P}_{k+1}}^2 + \|\mathbf{y}_{k+1}\|_{\mathbf{H}}^2, \end{aligned} \quad (5.80)$$

then the updated ellipsoidal state estimation set is $\mathcal{E}'(\mathbf{P}'_{k+1}, \bar{\mathbf{x}}'_{k+1}, \rho'_{k+1})$.

Method 5 is an extension of a previously developed technique for linear time variant standard systems proposed in [Ben Chabane, 2015]. It is improved in this thesis by considering linear time variant descriptor systems.

Example 5.2 shows the performance of the proposed ellipsoidal state estimation approach when solving LMIs (5.57) and (5.1), i.e. Method 5.

Example 5.2. Consider the following discrete-time linear time variant descriptor system:

$$\begin{cases} \mathbf{E}_d \mathbf{x}_{k+1} &= \mathbf{A}_k \mathbf{x}_k + \mathbf{B} \mathbf{u}_k + \mathbf{E} \boldsymbol{\omega}_k, \\ \mathbf{y}_k &= \mathbf{C} \mathbf{x}_k + \mathbf{F} \boldsymbol{\omega}_k, \end{cases} \quad (5.81)$$

$$\text{with } \mathbf{E}_d = \begin{bmatrix} 1 & 0 & 0 \\ 0 & 1 & 0 \\ 0 & 0 & 0 \end{bmatrix}, \mathbf{A}_k = \begin{bmatrix} -0.4 & 0 & 0 \\ 0.01\delta_{1k} & 0.1 & 2 \\ -1 & \delta_{2k} & 0.2\delta_{3k} \end{bmatrix}, \mathbf{B} = \mathbf{0}_2,$$

$$\mathbf{C} = \begin{bmatrix} 1 & 0 & 1 \\ 1 & -1 & 0 \end{bmatrix}, \mathbf{E} = 10^{-3} \cdot \begin{bmatrix} 5 & 0 & 0 & 0 & 0 \\ 0 & 5 & 0 & 0 & 0 \\ 0 & 0 & 6 & 0 & 0 \end{bmatrix}, \mathbf{F} = 5 \cdot 10^{-3} [\mathbf{0}_{2 \times 3} \quad \mathbf{I}_{2 \times 2}].$$

The vector $\boldsymbol{\omega}_k \in \mathbb{B}^5$ and the uncertainty parameters are randomly generated with $\|\boldsymbol{\omega}_k\|_\infty \leq 1$ and $|\delta_{i_k}| < 1$, $i = 1, 2, 3$. We consider constant matrices \mathbf{T} and \mathbf{N} satisfying (5.13) such that:

$$\mathbf{T} = \begin{bmatrix} 0.6667 & 0.3333 & 0 \\ 0.3333 & 0.6667 & 0 \\ -0.6667 & -0.3333 & 0 \end{bmatrix} \text{ and } \mathbf{N} = \begin{bmatrix} 0 & 0.3333 \\ 0 & -0.3333 \\ 1 & -0.3333 \end{bmatrix}.$$

Randomly chosen, the initial state \mathbf{x}_0 is inside the ellipsoid $\mathcal{E}(\mathbf{P}_0, \bar{\mathbf{x}}_0, \rho_0)$, with $\mathbf{P}_0 = 10 \cdot \mathbf{I}_3$, $\bar{\mathbf{x}}_0 = 10 \cdot [1 \ 1 \ 1]^\top$, and $\rho_0 = 50$. In this example, the results obtained by Method 5 for descriptor systems are analyzed. Figures 5.6 to 5.8 illustrate the bounds of the signal \mathbf{x}_k after 10 iterations obtained by the *improved ellipsoidal estimation method* in blue dashed lines. The real state represented by red asterisks is inside the blue bounds at each time instant k which proved the accuracy and efficiency of this technique. Additionally, it is shown that this technique offers a high rate of convergence of the components of the state vector.

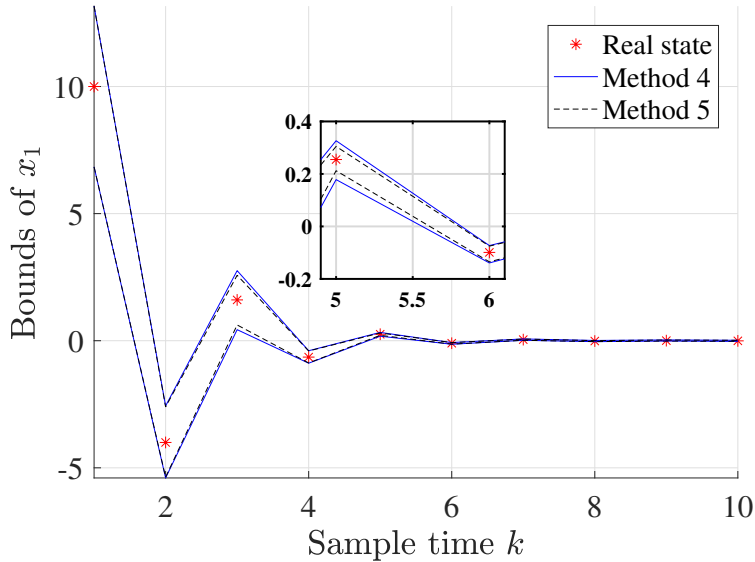


Figure 5.6 – Example 5.2: bounds of x_1

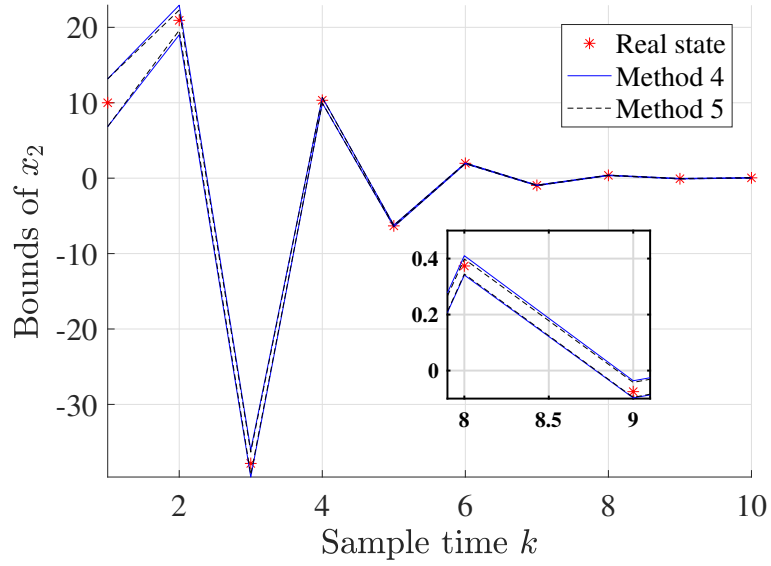


Figure 5.7 – Example 5.2: bounds of x_2

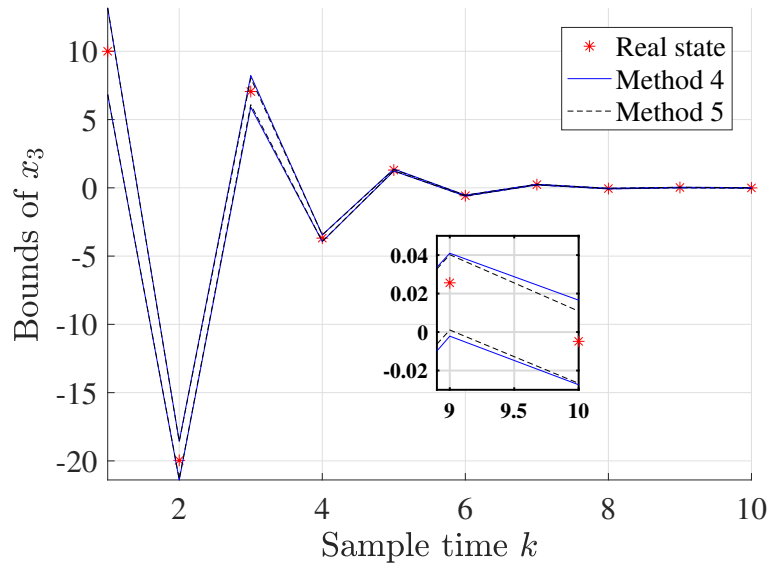


Figure 5.8 – Example 5.2: bounds of x_3

5.6 Conclusion

A new guaranteed ellipsoidal state estimation approach for linear descriptor systems with bounded perturbations and measurement noises has been proposed in this chapter. The methods represent an extension of previously developed techniques in [Ben Chabane, 2015] for standard systems. Successive improvements are elaborated in the five proposed methods. *Method 1* is developed for discrete-time Linear Time Invariant (LTI) descriptor systems. In this method, the radius of the ellipsoidal set is minimized by off-line solving an LMI problem once, leading to compute a constant observer matrix gain. In *Method 2*, the observer gain is updated at each time instant by solving an online LMI problem. This leads to a better estimation accuracy compared to *Method 1*, but with higher complexity due to the vertex enumeration related to the considered perturbations bounds. Applying a new vector scaling technique for *Method 2*, the computation time is significantly reduced in *Method 3*, while keeping an acceptable level of the estimation accuracy.

Finally, this ellipsoidal state estimation method is extended to the case of discrete-time Linear Time Variant (LTV) systems (*Method 4*) with interval uncertainties in the evolution matrix. This method is based on the online minimization of the size of the ellipsoidal state estimation set by solving a Linear Matrix Inequality optimization problem. Not only the size, but also the shape of the ellipsoidal set is adjusted at each time instant allowing to reduce the conservatism in comparison to the previous methods. An improvement of the accuracy of the proposed ellipsoidal estimation method has been presented in *Method 5* by adding quadratic constraints on both measurements and perturbations. This allows us to reduce the bounds of the estimation domain, offering a better estimation accuracy.

In the next chapter, set-membership state estimation approaches are developed using zonotopic sets for the accuracy they provide compared to ellipsoids. These approaches are developed for standard systems and their extension to descriptor systems will be considered as a potential perspective for this PhD thesis.

Part II

Zonotopic set-membership state estimation

Chapter 6

Zonotopic set-membership state estimation

Contents

| | | |
|------------|---|------------|
| 6.1 | Introduction | 125 |
| 6.2 | Zonotopic state estimation | 126 |
| 6.3 | Zonotopic set-membership estimation technique based on a Luenberger observer | 128 |
| 6.4 | Overview of piecewise affine systems | 133 |
| 6.4.1 | Practical example | 133 |
| 6.4.2 | State estimation for PWA systems | 134 |
| 6.5 | Zonotopic state estimation for PWA systems | 136 |
| 6.6 | Conclusion | 140 |

6.1 Introduction

In the last decades, the problem of state estimation has been studied by many researchers, leading to different state estimation methods such as Kalman filter [Kalman, 1960], Luenberger observer [Luenberger, 1964], set-membership estimation [Witsenhausen, 1968], [Schweppe, 1968], functional observer [Murdoch, 1973], [Moore and Ledwich, 1975], moving-horizon estimation [Grizzle and Moraal, 1990], [Michalska and Mayne, 1991], [Mare and De Dona, 2006], [Alamir, 2007]. In the previous chapters, we discussed in details several set-membership state estimation techniques based on ellipsoids for linear time invariant standard and descriptor systems. Here, the uncertainties of the

system are modeled using zonotopes [Puig et al., 2001], [Combastel, 2003], [Alamo et al., 2005], [Alamo et al., 2008a], [Le et al., 2011]. The estimator computes at each sample time a zonotopic set containing all the possible system states that are consistent with the perturbations, the uncertainties and the measurement noise. These techniques are mainly based on a prediction step followed by a correction step. Zonotopes offer a good compromise between flexibility and complexity; therefore they have been used in several topics in automatic control applications that include but not limited to reachability analysis [Althoff et al., 2007], [Girard, 2005], [Girard and Le Guernic, 2008], collision detection [Guibas et al., 2005], identification [Bravo et al., 2006], state estimation [Puig et al., 2001], [Combastel, 2003], [Alamo et al., 2005], [Alamo et al., 2008a], fault detection [Guerra et al., 2008], [Ingimundarson et al., 2008], [Stoican, 2011] and fault diagnosis [Combastel et al., 2008]. Moreover, when using zonotopes, the wrapping effect is reduced (compared to boxes) leading to a more precise result of the estimation [Kühn, 1998]. In this chapter, zonotopes are chosen to solve the set-membership state estimation problem due to their advantages. The chapter starts with a brief summary of zonotopic set-membership state estimation techniques in literature. A particular zonotopic set-membership state estimation technique based on a Luenberger observer is applied to the model of the octorotor detailed in Chapter 4. This result has been presented to the 12th Summer Workshop on Interval Methods 2019. The considered zonotopic set-membership state estimation is further analyzed and extended to deal with a new class of systems called piecewise affine systems. PWA systems are linear systems whose dynamics are governed by multiple linear time invariant equations. Extensively, the state-space of a piecewise affine system is partitioned into two or more regions, in each of which the dynamics are governed by a linear time invariant system equations. Even though the behavior of PWA systems can be complex, they share many properties with a standard LTI system. Here, we consider a particular class of PWA systems: a bi-modal PWA system which can be interesting to study from theoretical and practical points of view.

6.2 Zonotopic state estimation

This chapter focuses on a two-step zonotopic set-membership state estimation technique. In the prediction step, a zonotopic set consistent with the model is found, and then, in a second step, a strip consistent with the measurements is computed. The difference between existing different techniques relies in the correction step where the construction of the final state estimation set

is computed. It is indeed the intersection between the two previously found sets consistent with the predictions and the measurements. In the zonotopic state estimation case, several methods are used in literature: segments minimization method [Alamo et al., 2005], volume minimization method [Alamo et al., 2005], Singular Value Decomposition-based method [Combastel, 2003] and the \mathbf{P} -radius minimization method [Le et al., 2013b]. In the following, we will give an overview of these techniques. However, a detailed synthesis of some of these methods can be found in [Le, 2012].

Using the representation of the intersection between the zonotope and a strip [Alamo et al., 2005], the following techniques are the one mainly used in zonotopic set-membership state estimation:

- *Segments minimization method* [Alamo et al., 2005]: In this technique, the goal is to improve the accuracy of the state estimation by minimizing the size of the segments that generate the zonotopic estimation set.
- *Volume minimization method* [Alamo et al., 2005]: The goal of this technique is to minimize the volume of the zonotopic estimation set to improve the accuracy of the estimation technique, however this technique could lead to very narrow zonotopes.
- *\mathbf{P} -radius minimization method* [Le et al., 2013b]: The \mathbf{P} -radius provides a criterion to evaluate the size of the zonotope, thus the accuracy of the estimation. For the same matrix \mathbf{P} , a smaller value of the \mathbf{P} -radius means a smaller zonotope.
- *Singular Value Decomposition-based method* [Combastel, 2003]: In this technique, the consistent state set with the measurement is not explicitly used. However, the extended space of the predicted zonotopic set, called *abstract space*, is decomposed into two complementary subspaces: one influenced by the measurements, while the other is not affected.

The \mathbf{P} -radius minimization of the zonotope leads to a trade-off between the accuracy of the estimation offered by the volume minimization of a zonotope and the rapidity of the segments minimization technique. The SVD method and \mathbf{P} -radius minimization zonotopic method offer quite similar results [Le, 2012]. However, the \mathbf{P} -radius based method imposes a fixed gain to construct the zonotopic estimation set which is parametrized by a vector/matrix computed off-line. In order to take advantage of this result, the next section considers the \mathbf{P} -radius in a zonotopic set-membership state estimation technique.

6.3 Zonotopic set-membership estimation technique based on a Luenberger observer

Consider the following standard discrete-time Linear Time Invariant (LTI) system:

$$\begin{cases} \mathbf{x}_{k+1} = \mathbf{A}\mathbf{x}_k + \mathbf{B}\mathbf{u}_k + \mathbf{E}\boldsymbol{\omega}_k \\ \mathbf{y}_k = \mathbf{C}\mathbf{x}_k + \mathbf{F}\boldsymbol{\omega}_k \end{cases} \quad (6.1)$$

where $\mathbf{x}_k \in \mathbb{R}^{n_x}$ is the state vector of the system, $\mathbf{u}_k \in \mathbb{R}^{n_u}$ is the control input vector and $\mathbf{y}_k \in \mathbb{R}^{n_y}$ is the measured output vector at sample time k . The vector $\boldsymbol{\omega}_k \in \mathbb{B}^{n_w}$ contains the state perturbations and measurement noises.

Theorem 6.1. (based on [Wang et al., 2018]) Consider \mathbf{x}_0 the initial state and assume that the state \mathbf{x}_k belongs to the zonotope $\mathcal{Z}(\mathbf{p}_k, \mathbf{H}_k) = \mathbf{p}_k \oplus \mathbf{H}_k \mathbb{B}^m$. Given a scalar $\beta \in (0, 1)$, if there exist a positive definite matrix $\mathbf{P} = \mathbf{P}^\top \succ 0$ in $\mathbb{R}^{n_x \times n_x}$, a matrix $\mathbf{Y} \in \mathbb{R}^{n_x \times n_y}$ for which the following LMI holds:

$$\begin{bmatrix} \beta\mathbf{P} & \mathbf{0} & \mathbf{A}^\top\mathbf{P} - \mathbf{C}^\top\mathbf{Y}^\top \\ * & \boldsymbol{\Theta}^\top\boldsymbol{\Theta} & \mathbf{E}^\top\mathbf{P} - \mathbf{F}^\top\mathbf{Y}^\top \\ * & * & \mathbf{P} \end{bmatrix} \succeq 0, \quad (6.2)$$

then it is guaranteed that $\mathbf{x}_{k+1} \in \mathcal{Z}(\bar{\mathbf{x}}_{k+1}, \mathbf{H}_{k+1})$, $\forall \boldsymbol{\omega}_k \in \mathbb{B}^{n_x+n_y}$, where:

$$\bar{\mathbf{x}}_{k+1} = \mathbf{A}\bar{\mathbf{x}}_k + \mathbf{B}\mathbf{u}_k + \mathbf{L}(\mathbf{y}_k - \mathbf{C}\bar{\mathbf{x}}_k), \quad (6.3)$$

$$\mathbf{H}_{k+1} = [\mathbf{A}_L\mathbf{H}_k \quad \boldsymbol{\eta}], \quad (6.4)$$

with $\mathbf{Y} = \mathbf{P}\mathbf{L}$, $\boldsymbol{\Theta} = [\mathbf{E}^\top \quad \mathbf{F}^\top]^\top$, $\mathbf{A}_L = \mathbf{A} - \mathbf{L}\mathbf{C}$ and $\boldsymbol{\eta} = \mathbf{E} - \mathbf{L}\mathbf{F}$.

Proof. The error $\mathbf{z}_k = \mathbf{x}_k - \bar{\mathbf{x}}_k$ between the real state and the nominal estimated state at time k belongs to centered zonotope $\mathbf{H}_k \mathbb{B}^m$. At time $k+1$, one has:

$$\mathbf{z}_{k+1} = \mathbf{A}_L\mathbf{z}_k + \boldsymbol{\eta}\boldsymbol{\omega}_k \in \mathbf{A}_L\mathbf{p}_k \oplus \mathbf{H}_{k+1}. \quad (6.5)$$

Denote the \mathbf{P} -radius of the zonotopic set at the time instant k by:

$$r_k = \max_{\mathbf{x}_k \in \hat{\mathcal{X}}_k} (\|\mathbf{x}_k - \bar{\mathbf{x}}_k\|_{\mathbf{P}}^2). \quad (6.6)$$

This can be rewritten like:

$$r_k = \max_{\hat{\mathbf{z}}} \|\hat{\mathbf{H}}_k \hat{\mathbf{z}}\|_{\mathbf{P}}^2, \quad (6.7)$$

with $\hat{\mathbf{z}} \in \mathbb{B}^{r+n_x+n_y}$. The non increase of the \mathbf{P} -radius [Le, 2012] of the zonotopic error at each time instant can be expressed by:

$$r_{k+1} \leq \beta r_k + \max_{\boldsymbol{\theta}} \|\boldsymbol{\Theta}\boldsymbol{\theta}\|_2^2. \quad (6.8)$$

The expression:

$$r_{k+1} < \beta r_k, \quad (6.9)$$

with $\beta \in (0, 1)$, ensures the contraction of the \mathbf{P} -radius. However, this is difficult to verify in the presence of perturbations and measurement noises. Equation (6.8) represents a relaxation of this condition, where the term:

$$\max_{\boldsymbol{\theta}} \|\boldsymbol{\Theta}\boldsymbol{\theta}\|_2^2$$

is a positive constant that bounds the influence of the set of disturbances. This inequality can be rewritten under the form of:

$$\max_{\hat{\mathbf{z}}} \|\mathbf{H}_{k+1}\hat{\mathbf{z}}\|_{\mathbf{P}}^2 \leq \beta \max_{\mathbf{z}} \|\mathbf{H}_k\mathbf{z}\|_{\mathbf{P}}^2 + \max_{\boldsymbol{\theta}} \|\boldsymbol{\Theta}\boldsymbol{\theta}\|_2^2 \quad (6.10)$$

with the notations $\hat{\mathbf{z}} = \begin{bmatrix} \mathbf{z}^\top & \boldsymbol{\theta}^\top \end{bmatrix}^\top \in \mathbb{B}^{m+n_x+n_y}$, $\mathbf{z} \in \mathbb{B}^m$ and $\boldsymbol{\theta} \in \mathbb{B}^{n_x+n_y}$. Using the reverse triangle inequality leads to a sufficient condition for:

$$\max_{\hat{\mathbf{z}}} (\|\mathbf{H}_{k+1}\hat{\mathbf{z}}\|_{\mathbf{P}}^2 - \beta \|\mathbf{H}_k\mathbf{z}\|_{\mathbf{P}}^2 - \|\boldsymbol{\Theta}\boldsymbol{\theta}\|_2^2) \leq 0. \quad (6.11)$$

Extensively, $\forall \mathbf{z}, \boldsymbol{\theta}$, the next expression is verified:

$$\hat{\mathbf{z}}^\top \mathbf{H}_{k+1}^\top \mathbf{P} \mathbf{H}_{k+1} \hat{\mathbf{z}} - \beta \mathbf{z}^\top \mathbf{H}_k \mathbf{P} \mathbf{H}_k \mathbf{z} - \boldsymbol{\theta}^\top \boldsymbol{\Theta}^\top \boldsymbol{\Theta} \boldsymbol{\theta} \leq 0. \quad (6.12)$$

Thus now we can write the following equation:

$$\mathbf{H}_{k+1}\hat{\mathbf{z}} = (\mathbf{A} - \mathbf{LC})\mathbf{H}_k\mathbf{z} + (\mathbf{E} - \mathbf{LF})\boldsymbol{\theta}. \quad (6.13)$$

Moreover, replacing $\mathbf{H}_{k+1}\hat{\mathbf{z}}$ in (6.12) gives:

$$\begin{aligned} & (\mathbf{H}_k^\top \mathbf{z}^\top (\mathbf{A} - \mathbf{LC})^\top + \boldsymbol{\theta}^\top (\mathbf{E} - \mathbf{LF})^\top) \mathbf{P} ((\mathbf{A} - \mathbf{LC})\mathbf{H}_k\mathbf{z} + (\mathbf{E} - \mathbf{LF})\boldsymbol{\theta}) - \\ & - \beta \mathbf{z}^\top \mathbf{H}_k \mathbf{P} \mathbf{H}_k \mathbf{z} - \boldsymbol{\theta}^\top \boldsymbol{\Theta}^\top \boldsymbol{\Theta} \boldsymbol{\theta} \leq 0 \quad \forall \mathbf{z}, \boldsymbol{\theta} \end{aligned} \quad (6.14)$$

Regrouping the terms of (6.14) and applying the Schur complement leads to:

$$\begin{bmatrix} \mathbf{H}_k\mathbf{z} \\ \boldsymbol{\theta} \end{bmatrix}^\top \begin{bmatrix} (\mathbf{A} - \mathbf{LC})^\top \mathbf{P} (\mathbf{A} - \mathbf{LC}) - \beta \mathbf{P} & * \\ (\mathbf{E} - \mathbf{LF})^\top \mathbf{P} (\mathbf{A} - \mathbf{LC}) & (\mathbf{E} - \mathbf{LF})^\top \mathbf{P} (\mathbf{E} - \mathbf{LF}) - \boldsymbol{\Theta}^\top \boldsymbol{\Theta} \end{bmatrix} \begin{bmatrix} \mathbf{H}_k\mathbf{z} \\ \boldsymbol{\theta} \end{bmatrix} \preceq 0 \quad (6.15)$$

Doing some manipulations with (6.15), the following matrix inequality is derived:

$$\begin{bmatrix} \beta \mathbf{P} & \mathbf{0} \\ \mathbf{0} & \Theta^\top \Theta \end{bmatrix} - \begin{bmatrix} (\mathbf{A} - \mathbf{LC})^\top \mathbf{P} \\ (\mathbf{E} - \mathbf{LF})^\top \mathbf{P} \end{bmatrix} \mathbf{P}^{-1} \begin{bmatrix} (\mathbf{A} - \mathbf{LC})^\top \mathbf{P} \\ (\mathbf{E} - \mathbf{LF})^\top \mathbf{P} \end{bmatrix}^\top \succeq 0 \quad (6.16)$$

Using the Schur complement definition, this expression is equivalent to the following matrix inequality:

$$\begin{bmatrix} \beta \mathbf{P} & \mathbf{0} & (\mathbf{A} - \mathbf{LC})^\top \mathbf{P} \\ * & \Theta^\top \Theta & (\mathbf{E} - \mathbf{LF})^\top \mathbf{P} \\ * & * & \mathbf{P} \end{bmatrix} \succeq 0. \quad (6.17)$$

The change of variables $\mathbf{Y} = \mathbf{P}\mathbf{L}$ leads us to (6.2). \square

The center of the zonotope \mathbf{p}_{k+1} (which is the nominal state estimation at time instant $k+1$) is computed like a Luenberger observer which is motivated by the fact that the system is linear. The gain $\mathbf{L} = \mathbf{P}^{-1}\mathbf{Y}$ is obtained after solving the LMI (6.2). Notice that when β is a free variable in the interval $(0, 1)$, the expression (6.2) becomes a very simple case of Bilinear Matrix Inequality (BMI). As $\beta \in (0, 1)$ is a bounded scalar, this expression can be rewritten as a LMI problem by successively fixing the value of β via the bisection algorithm.

Example 6.1. The Mikrokopter ARF Okto-XL

We recall the example of the octorotor employed in the context of radar applications that we used in Chapter 4. As mentioned earlier, the Mikrokopter ARF Okto-XL is equipped with a micro-controller that provides fused and filtered information from the sensors about the drone's position.

A non-linear dynamical model together with a linearized model around the static hovering equilibrium with null translational and rotational velocities and null roll, pitch and yaw angles exist [Chevet et al., 2017]. The linear discretized model with a sampling period T_e has been detailed in Chapter 4 through (4.21)- (4.23). However, for linear position estimation problems, we only need the two subsystems describing the longitudinal and the altitude dynamics, respectively, reminded below:

$$\begin{aligned} \mathbf{x}_{1_{k+1}} &= \mathbf{A}\mathbf{x}_{1_k} + \mathbf{B}_1\mathbf{u}_{1_k} + \mathbf{E}_1\boldsymbol{\omega}_k, \\ \mathbf{y}_{1_k} &= \mathbf{C}\mathbf{x}_{1_k} + \mathbf{F}_1\boldsymbol{\omega}_k, \\ \\ \mathbf{x}_{3_{k+1}} &= \mathbf{A}\mathbf{x}_{3_k} + \mathbf{B}_3\mathbf{u}_{3_k} + \mathbf{E}_3\boldsymbol{\omega}_k, \\ \mathbf{y}_{3_k} &= \mathbf{C}\mathbf{x}_{3_k} + \mathbf{F}_3\boldsymbol{\omega}_k, \end{aligned}$$

$$\text{with } \mathbf{x}_{1_k} = [z_k \ \psi_k \ V_{z_k} \ \omega_{z_k}]^\top, \mathbf{x}_{3_k} = [x_k \ y_k \ V_{x_k} \ V_{y_k}]^\top, \mathbf{u}_{1_k} = [F_{z_k}^R \ \tau_{z_k}^R]^\top,$$

$$\mathbf{u}_{3_k} = [F_{x_k}^R \ F_{y_k}^R]^\top, \mathbf{y}_{1_k} = [z_k \ \psi_k]^\top, \mathbf{y}_{3_k} = [x_k \ y_k]^\top, \mathbf{A} = \begin{bmatrix} \mathbf{I}_2 & T_e \mathbf{I}_2 \\ \mathbf{0}_2 & \mathbf{I}_2 \end{bmatrix},$$

$$\mathbf{B}_1 = \begin{bmatrix} 0 & 0 \\ 0 & 0 \\ \frac{T_e}{m} & 0 \\ 0 & \frac{T_e}{I_{zz}} \end{bmatrix}, \mathbf{B}_3 = \begin{bmatrix} 0 & 0 \\ 0 & 0 \\ \frac{T_s}{m} & 0 \\ 0 & \frac{T_e}{m} \end{bmatrix}, \mathbf{C} = [\mathbf{I}_2 \ \mathbf{0}_2].$$

tions and the measurement noises $\boldsymbol{\omega}_k$ are bounded by the unitary box \mathbb{B}^6 . Additionally, the same assumptions on state perturbations and measurement noises considered in Chapter 4 are used here. The control inputs F_x^R , F_y^R and F_z^R are the components of the resulting propeller's force, whereas τ_z^R is the component of the resulting propeller's torque expressed in the drone's frame denoted by the superscript R .

A sampling period $T_e = 0.02\text{s}$ of all sensors is considered. A linear trajectory is simulated to validate the efficiency of the zonotopic set-membership estimation technique. It corresponds to a take-off to an altitude of 50m and then to a flight on the x-axis with a linear constant speed as presented in Figure 6.1. The flight duration is 235s.

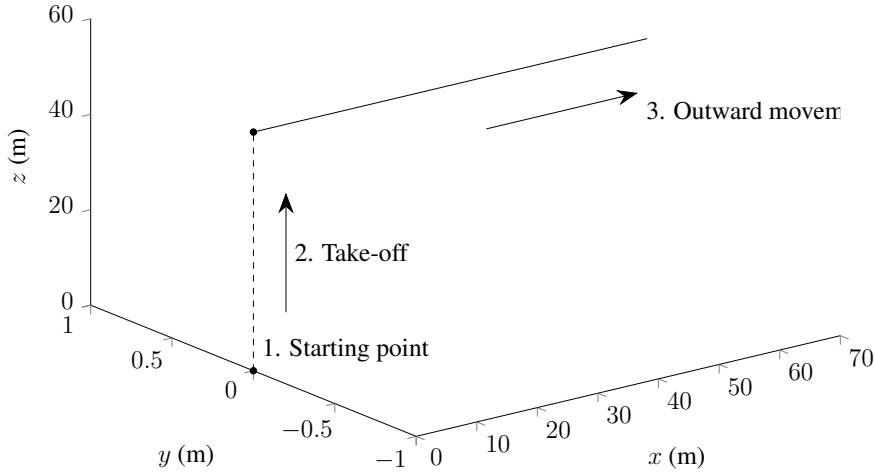


Figure 6.1 – Linear proposed trajectory

Figure 6.2 shows the guaranteed bounds of the linear position x of the drone, whereas Figure 6.3 presents the guaranteed estimation bounds of the altitude z . The example compares the state estimation between the off-line ellipsoidal method (Method 1) presented in Chapter 5 and the off-line

zonotopic method in this chapter.

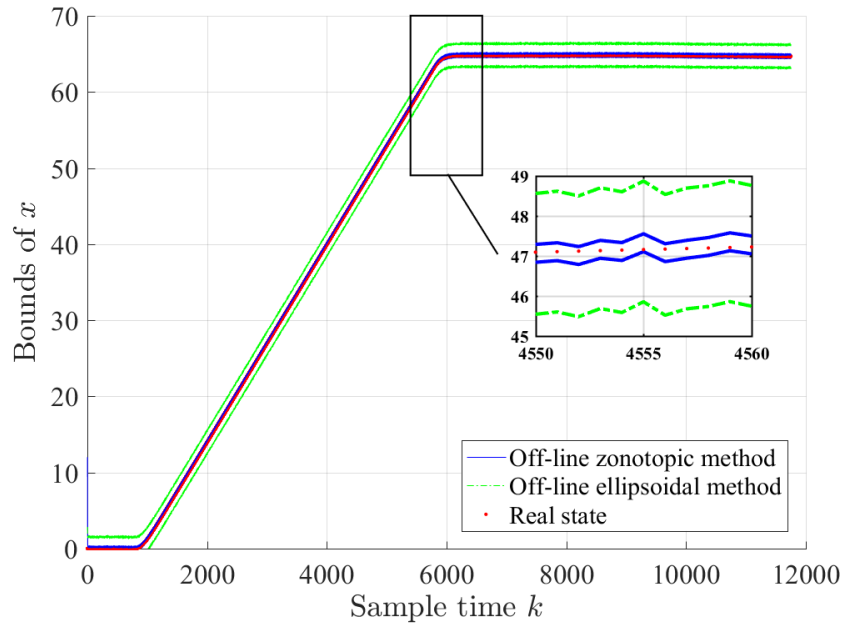


Figure 6.2 – Example 6.1: bounds of the linear position x

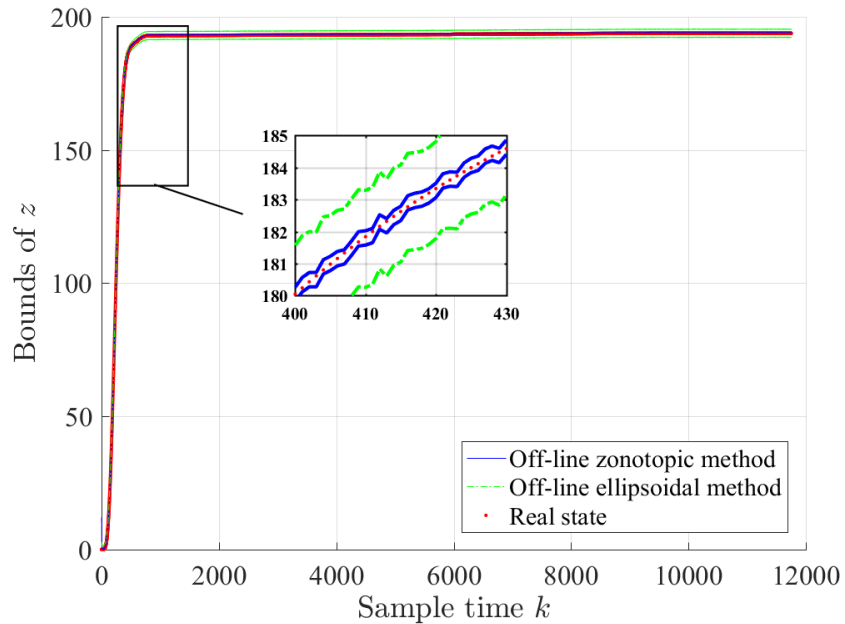


Figure 6.3 – Example 6.1: bounds of the altitude z

It is shown in Figures 6.2 and 6.3 that the real state (red dots) is guaranteed to remain inside of the bounds computed by the two techniques despite of the considered measurement noises and state perturbations. The off-line ellipsoidal method has larger bounds (green dashes) than the off-line zonotopic off-line method represented by the blue line. This means that the zonotopic method offers a higher accuracy than the ellipsoidal method with a similar computation time since they both compute the observer's gain by off-line solving a LMI.

6.4 Overview of piecewise affine systems

Piecewise affine systems (PWA) can be seen as a special class of linear time invariant systems whose state evolution is not limited to one equation. The dynamical behavior of a system is governed by a set of affine equations, each valid in one particular region out of different regions of the state-space. This class of systems can cover a large number of systems encountered in practice, specifically those that consider relays, dead-zones and saturation [Feng, 2002]. The PWA systems description is similar to the LTI models, a possible state-space representation of PWA systems being the following:

$$\begin{cases} \mathbf{x}_{k+1} = \mathbf{A}_i \mathbf{x}_k + \mathbf{B}_i \mathbf{u}_k + \mathbf{E} \boldsymbol{\omega}_k, \\ \mathbf{y}_k = \mathbf{C}_i \mathbf{x}_k + \mathbf{F} \boldsymbol{\omega}_k, \end{cases} \quad (6.18)$$

where $\mathbf{x}_k \in \mathbb{R}^{n_x}$, $\mathbf{y}_k \in \mathbb{R}^{n_y}$, $\mathbf{u}_k \in \mathbb{R}^{n_u}$ are respectively the state vector, the measured output vector and the control input vector of the system at time instant k . The vector $\boldsymbol{\omega}_k \in \mathbb{B}^{n_x+n_y}$ contains the state perturbations and measurement noises.

6.4.1 Practical example

It is important to show with an example how a PWA system in control engineering can model different systems. Therefore before elaborating on the state estimation problem of PWA systems, we provide an example of a particular system called a bi-modal piecewise affine system based on the partitioning of the state-space into only two regions. We consider the two-tank benchmark [Thuan and Camlibel, 2014] depicted in Figure 6.4 and used in the context of water regulating systems with u the constant water flow into the first tank. The variables x_1 and x_2 designate the deviations of the water level from the bottom of the first and the second tank, respectively. The valve is closed when the amount of water in the second tank exceeds 11 i.e. $x_2 \geq 1$.

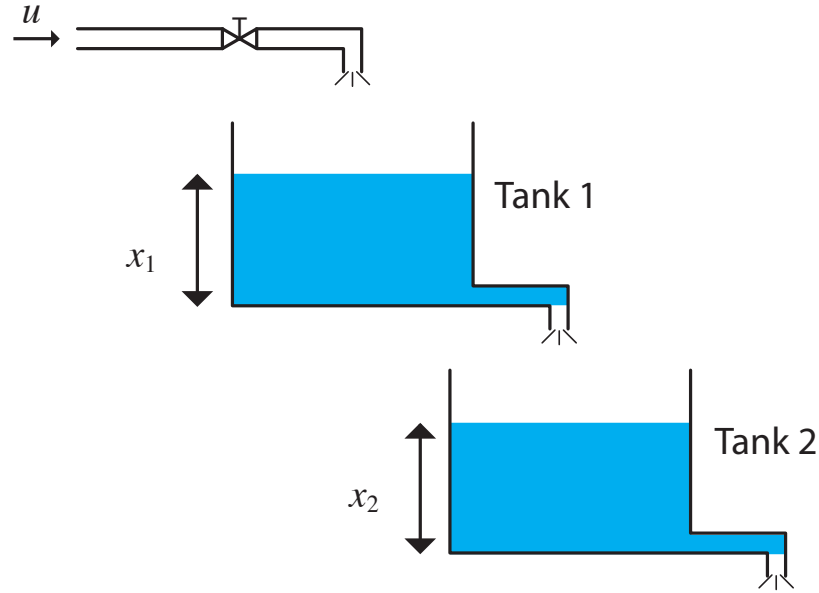


Figure 6.4 – Two-tank system

The system can be mathematically modeled by considering a state vector of the water levels in tanks 1 and 2 resulting in the following continuous-time formulation:

$$\begin{bmatrix} \dot{x}_1(t) \\ \dot{x}_2(t) \end{bmatrix} = \begin{bmatrix} -1 & 0 \\ 1 & -1 \end{bmatrix} \begin{bmatrix} x_1(t) \\ x_2(t) \end{bmatrix} + \begin{bmatrix} 0 \\ 0 \end{bmatrix} u(t) \quad \text{if } x_2 \geq 1 \quad (6.19)$$

$$\begin{bmatrix} \dot{x}_1(t) \\ \dot{x}_2(t) \end{bmatrix} = \begin{bmatrix} -1 & 0 \\ 1 & -1 \end{bmatrix} \begin{bmatrix} x_1(t) \\ x_2(t) \end{bmatrix} + \begin{bmatrix} 1 \\ 0 \end{bmatrix} u(t) \quad \text{if } x_2 < 1 \quad (6.20)$$

As such, this system is an example of a bi-modal piecewise affine system. In the rest of this chapter, the zonotopic set-membership state estimation technique will be presented for a bi-modal piecewise affine system. This approach is a first step towards the long term goal of dealing with a general representation of a piecewise affine systems and hybrid systems.

6.4.2 State estimation for PWA systems

PWA systems have been studied for a long time. Kalman presented in one of his works a concrete qualitative understanding of these systems, by treating a saturated system by a series of polyhedral regions in the state-space. These polyhedral regions were separated by switching boundaries [Kalman, 1955]. Recently, an increasing interest has been given to these systems due

to their wide applications and promising aspects [Xu and Xie, 2014]. Indeed, PWA systems are used to model a large class of systems, mainly hybrid and switched systems. In this context, many contributions ranging from the modeling [Johansson, 2003], [Johansson and Rantzer, 1997] to controllers elaboration [Feng, 2003a], [Rodrigues and How, 2003] were done on PWA systems, even though some of the characteristics and properties can be conservative. Here, we only focus on the state estimation of piecewise affine systems. In this context, various approaches have been proposed in the literature for the state estimation problem of PWA systems [Juloski et al., 2003], [Juloski et al., 2002]. However most of these results can be classified as conservative [Alessandri and Coletta, 2001a], [Alessandri and Coletta, 2001b] considering the fact that they don't take into consideration some of the characteristics of these systems, for instance the partition information. More recent studies integrated the partition information in the design of observers [Juloski et al., 2003], [Juloski et al., 2002] for bi-modal systems. More precisely, [Alessandri and Coletta, 2001a] developed a Luenberger type observer for both continuous-time and discrete-time piecewise affine systems. Moreover, in [Alessandri and Coletta, 2001b], a state estimation approach for linear systems based on the use of switching observers (switching between different observer gains) is proposed. An observer design [Feng, 2003b] as well as several filter design methods [Feng, 2005] are proposed for discrete-time piecewise affine linear systems. The paper [Feng, 2005] makes the assumption that the real model and the state estimator always switch to the same partition at the same time. This is possible by partitioning the output not the state-space which does not apply on most of the PWA systems. In a general case, no guarantee exists that the estimated state and the real system state are in the same partition at every time instant. The estimation errors can lead to cases where the estimated system state operates in a different region than the real state. For this case, a design procedure for the Luenberger type of observer, which does not require information on currently active dynamics of a bi-modal PWA system is proposed in [Juloski et al., 2003], [Juloski et al., 2002]. Additionally, other studies focused on different approaches for state estimation of PWA systems, such as the moving-horizon estimation (MHE) [Ferrari-Trecate et al., 2002], H_∞ and H_2 estimators [Xu and Xie, 2014]. Nevertheless, to our knowledge, few researchers have addressed the problem of set-membership state estimation for PWA systems [Bemporad et al., 2005]. The papers [Rakovic and Mayne, 2004] and [Rakovic et al., 2004] address the problem of set-membership state estimation for discrete time piecewise affine systems subject to additive but bounded disturbances. Indeed, a recursive filtering algorithm for piecewise affine systems using polygons is provided. Furthermore, [Tabatabaeipour

and Stoustrup, 2013] presents a zonotopic set-membership state estimation technique for piecewise affine systems. At each iteration, the technique computes via analytic method the intersection between the zonotope estimating the state with each of the polyhedral partitions of the piecewise affine system and then minimize it. Nevertheless, this technique remains computationally expensive and the result of approximation can be sometimes conservative since the method is based on the minimization of the segments of zonotopes [Alamo et al., 2005]. Moreover, set-membership state estimation techniques were developed for hybrid systems [Ramdani et al., 2009], [Meslem et al., 2010], [Heemels et al., 2001]. However, hybrid systems are beyond the scope of this thesis.

6.5 Zonotopic state estimation for PWA systems

Consider the following discrete-time bi-modal piecewise affine system:

$$\mathbf{x}_{k+1} = \begin{cases} \mathbf{A}_1 \mathbf{x}_k + \mathbf{B} \mathbf{u}_k + \mathbf{E} \boldsymbol{\omega}_k & \text{if } \mathbf{r}^\top \mathbf{x}_k \leq d, \\ \mathbf{A}_2 \mathbf{x}_k + \mathbf{B} \mathbf{u}_k + \mathbf{E} \boldsymbol{\omega}_k & \text{if } \mathbf{r}^\top \mathbf{x}_k > d, \end{cases} \quad (6.21a)$$

$$\mathbf{y}_k = \mathbf{C} \mathbf{x}_k + \mathbf{F} \boldsymbol{\omega}_k, \quad (6.21b)$$

where $\mathbf{x}_k \in \mathbb{R}^{n_x}$ is the state vector of the system, $\mathbf{u}_k \in \mathbb{R}^{n_u}$ is the control input vector, and $\mathbf{y}_k \in \mathbb{R}^{n_y}$ is the measured output vector at sample time k . The vector $\boldsymbol{\omega}_k \in \mathbb{B}^{n_x+n_y}$ contains the state perturbations and measurement noises (offset, noise etc.). It is bounded by the unitary interval, therefore the matrices \mathbf{E} and \mathbf{F} represent the weights for the normalized perturbations. The hyperplane defined by the switching condition $\mathbf{r}^\top \mathbf{x}_k = d$ separates the state-space system into two different half-spaces in which, at each time instant k , one of the two dynamics is active. This is clearly represented in Figure 6.5. The system (6.21) is a standard bi-modal piecewise affine system, with the same observation matrix \mathbf{C} , perturbations weight matrix \mathbf{E} , and measurement noises weight matrix \mathbf{F} . Moreover, depending on the switching condition, we distinguish two model matrices \mathbf{A}_1 and \mathbf{A}_2 . All these matrices, have appropriate dimensions, with the pairs $(\mathbf{C}, \mathbf{A}_1)$ and $(\mathbf{C}, \mathbf{A}_2)$ detectable and the pairs $(\mathbf{A}_1, \mathbf{B})$ and $(\mathbf{A}_2, \mathbf{B})$ stabilizable. The initial state is assumed to belong to the zonotope $\mathcal{Z}(\mathbf{p}_0, \mathbf{H}_0)$, where \mathbf{p}_0 is the center of the zonotope and \mathbf{H}_0 the matrix of its generators.

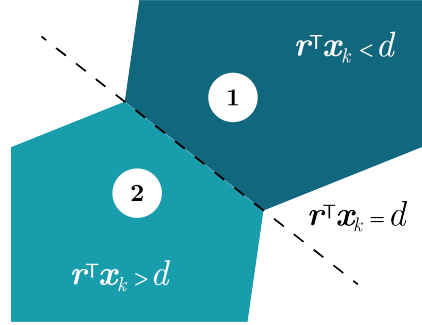


Figure 6.5 – Partitions of the state-space

Goal: Given a zonotopic estimation set for \mathbf{x}_k of the form $\mathcal{Z}(\mathbf{p}_k, \mathbf{H}_k)$, with $\bar{\mathbf{x}}_k = \mathbf{p}_k$ the nominal estimated state, the aim of this technique is to provide a zonotopic state estimation set for \mathbf{x}_{k+1} of the form $\mathcal{Z}(\mathbf{p}_{k+1}, \mathbf{H}_{k+1})$.

As a Luenberger observer for the system (6.21), we propose the following bi-modal structure [Juloski et al., 2003]:

$$\bar{\mathbf{x}}_{k+1} = \begin{cases} \mathbf{A}_1 \bar{\mathbf{x}}_k + \mathbf{B} \mathbf{u}_k + \mathbf{L}_1 (\mathbf{y}_k - \mathbf{C} \bar{\mathbf{x}}_k) & \text{if } \mathbf{r}^\top \bar{\mathbf{x}} \leq d, \\ \mathbf{A}_2 \bar{\mathbf{x}}_k + \mathbf{B} \mathbf{u}_k + \mathbf{L}_2 (\mathbf{y}_k - \mathbf{C} \bar{\mathbf{x}}_k) & \text{if } \mathbf{r}^\top \bar{\mathbf{x}} > d. \end{cases} \quad (6.22)$$

The observer is designed (i.e. \mathbf{L}_1 and \mathbf{L}_2 are determined) such that the state estimate $\bar{\mathbf{x}}$ converges asymptotically to \mathbf{x} . Denote by $\mathbf{z}_k = \mathbf{x}_k - \bar{\mathbf{x}}_k$ the error between the real state and the nominal estimated state. Assuming the knowledge of the partition to which the real state of the system belongs and considering that the state estimation belongs to the same partition, the error dynamics of the state estimation is described by:

$$\mathbf{z}_{k+1} = \begin{cases} (\mathbf{A}_1 - \mathbf{L}_1 \mathbf{C}) \mathbf{z}_k + (\mathbf{E} - \mathbf{L}_1 \mathbf{F}) \mathbf{w}_k & \text{if condition ①} \\ (\mathbf{A}_2 - \mathbf{L}_2 \mathbf{C}) \mathbf{z}_k + (\mathbf{E} - \mathbf{L}_2 \mathbf{F}) \mathbf{w}_k & \text{if condition ②} \end{cases} \quad (6.23)$$

with the following conditions:

- Condition ①: $\mathbf{r}^\top \bar{\mathbf{x}} \leq d$ and $\mathbf{r}^\top \mathbf{x} \leq d$,
- Condition ②: $\mathbf{r}^\top \bar{\mathbf{x}} > d$ and $\mathbf{r}^\top \mathbf{x} > d$.

Conditions ① and ② mean that the real state and the nominal estimated state are in the same region considering the knowledge of the position of the real state.

In details, expression (6.23) is obtained starting from:

$$\mathbf{z}_{k+1} = \mathbf{x}_{k+1} - \bar{\mathbf{x}}_{k+1}. \quad (6.24)$$

In the following we consider the two conditions. If the condition ① $\mathbf{r}^\top \bar{\mathbf{x}} \leq d$ and $\mathbf{r}^\top \mathbf{x} \leq d$ holds or the condition ② $\mathbf{r}^\top \bar{\mathbf{x}} > d$ and $\mathbf{r}^\top \mathbf{x} > d$ holds, the computation leads to:

$$\mathbf{z}_{k+1} = (\mathbf{A}_i - \mathbf{L}_i \mathbf{C}) \mathbf{z}_k + (\mathbf{E} - \mathbf{L}_i \mathbf{F}) \boldsymbol{\omega}_k, \quad (6.25)$$

for $i = 1, 2$. Moving to set computations, the error \mathbf{z}_k belongs to:

$$\mathbf{z}_k = \mathbf{x}_k - \bar{\mathbf{x}}_k \in \mathbf{p}_k \oplus \mathbf{H}_k \mathbb{B}^m \oplus \{-\mathbf{p}_k\}. \quad (6.26)$$

Thus, the error belongs to the centered zonotope:

$$\mathbf{z}_k \in \mathbf{H}_k \mathbb{B}^m. \quad (6.27)$$

Using equation (6.27), the error at the next time instant belongs to:

$$\mathbf{z}_{k+1} \in \begin{cases} [(\mathbf{A}_1 - \mathbf{L}_1 \mathbf{C}) \mathbf{H}_k & \mathbf{E} - \mathbf{L}_1 \mathbf{F}] \mathbb{B}^{m+n_x+n_y} & \text{if ①,} \\ [(\mathbf{A}_2 - \mathbf{L}_2 \mathbf{C}) \mathbf{H}_k & \mathbf{E} - \mathbf{L}_2 \mathbf{F}] \mathbb{B}^{m+n_x+n_y} & \text{if ②.} \end{cases} \quad (6.28)$$

Next, the idea is to compute a matrix $\mathbf{P} = \mathbf{P}^\top$ such that, the \mathbf{P} -radius of the zonotopic state estimation set is not increased at each iteration. Similar to the previous approach applied to the octorotor model, the \mathbf{P} -radius can be expressed as $r_k = \max_{\hat{\mathbf{z}}} \|\hat{\mathbf{H}}_k \hat{\mathbf{z}}\|_{\mathbf{P}}^2$. Theorem 6.1 can be applied here to each of the two cases we have. Therefore, there exist the matrices \mathbf{L}_1 , \mathbf{L}_2 and \mathbf{P} such that two LMIs are verified in the same time.

Cases ① and ② are similar to the work done in the previous sections. Thus, with a change of variables $\mathbf{Y}_i = \mathbf{P} \mathbf{L}_i$ with $\mathbf{P} \in \mathbb{R}^{n_x \times n_x}$, $\mathbf{L}_i \in \mathbb{R}^{n_x \times n_x}$ and $\mathbf{Y}_i \in \mathbb{R}^{n_x \times n_x}$ leads to:

$$\begin{bmatrix} \beta \mathbf{P} & \mathbf{0} & \mathbf{A}_i^\top \mathbf{P} - \mathbf{C}^\top \mathbf{Y}_i^\top \\ * & \boldsymbol{\Theta}^\top \boldsymbol{\Theta} & \mathbf{E}^\top \mathbf{P} - \mathbf{F}^\top \mathbf{Y}_i^\top \\ * & * & \mathbf{P} \end{bmatrix} \succeq 0, \quad (6.29)$$

for $i = 1, 2$.

Remark 6.1. These results for the zonotopic set-membership state estimation techniques are preliminary. The extension of this technique considering a bi-modal observation matrix \mathbf{C} or input matrix \mathbf{B} along with the model matrix \mathbf{A}_i is possible.

Remark 6.2. The results in this chapter are considered for bi-modal PWA systems. However, they can be extended for a general representation of PWA systems, with $i > 2$.

To validate this extension to PWA bi-modal systems, we consider the following example.

Example 6.2. Consider the system (6.21) with the following notations:
 $\mathbf{A}_1 = \begin{bmatrix} 0.7969 & -0.227 \\ 0.1798 & 0.9767 \end{bmatrix}$, $\mathbf{A}_2 = \begin{bmatrix} 0.4969 & -0.2247 \\ 0.0798 & 0.9767 \end{bmatrix}$, $\mathbf{C} = \begin{bmatrix} 0.5 & 0 \end{bmatrix}$,
 $\mathbf{E} = \begin{bmatrix} 0.02 & 0 & 0 \\ 0 & 0.02 & 0 \end{bmatrix}$, $\mathbf{F} = \begin{bmatrix} 0 & 0 & 0.03 \end{bmatrix}$. The perturbations vector is randomly generated and the input vector is neglected ($\mathbf{B} = \mathbf{0}$) such that the evolution of the system is only governed by the initial state $\mathbf{x}_0 = \begin{bmatrix} 5 & 5 \end{bmatrix}^\top$ belonging to the zonotope $\mathcal{Z}(\mathbf{x}_0, \mathbf{H}_0)$, with $\mathbf{H}_0 = \begin{bmatrix} 1 & 2 \\ 2 & 1 \end{bmatrix}$. The switching condition is given such that $\mathbf{r}^\top = \begin{bmatrix} 1 & 1 \end{bmatrix}$ and $d = 2$.

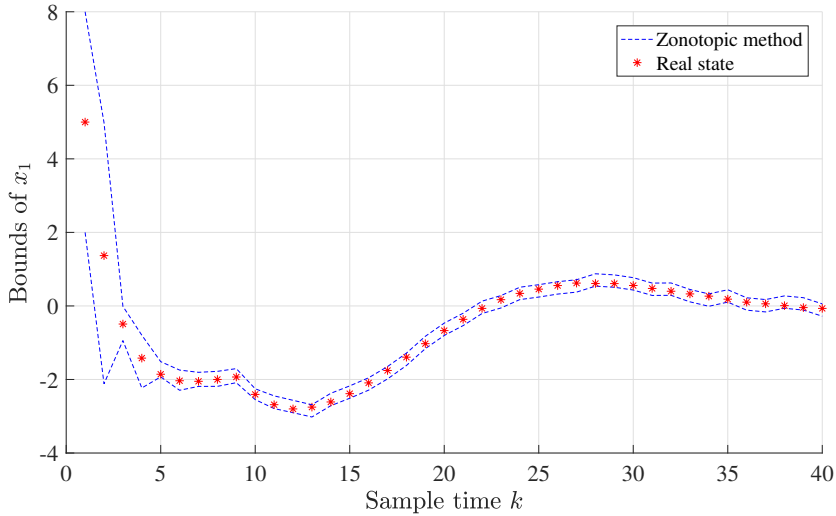
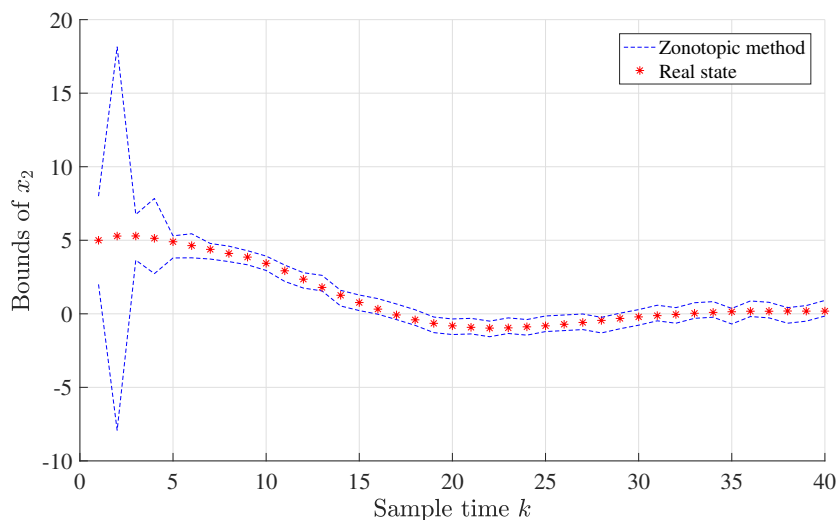


Figure 6.6 – Example 6.2: bounds of x_1

The state estimation simulation is depicted in Figures 6.6 and 6.7 where we can see that the real state (red asterisks) is guaranteed to belong to the bounds computed by our zonotopic state estimator (blue dashes) at each time instant. The guaranteed bounds were obtained by solving simultaneously the LMIs (6.29) corresponding the two considered cases.

Figure 6.7 – Example 6.2: bounds of x_2

6.6 Conclusion

As an alternative to ellipsoidal set-membership state estimation, the results proposed in this chapter rely on zonotopic set-membership state estimation.

After an overview of the zonotopic set-membership state estimation in literature, we introduce a technique based on a Luenberger observer and the \mathbf{P} -radius minimization method. Solving a linear matrix inequality (LMI) problem guarantees that the state belongs to a zonotope and the estimation error decreases at each time instant. An application to an octorotor model has been also proposed and presented to the 12th Summer Workshop on Interval Methods, 2019.

Furthermore, the main contribution of this chapter is the introduction of a new guaranteed zonotopic state estimation approach for a particular class of bi-modal piecewise affine systems with bounded perturbations and measurement noises. The technique computes the Luenberger observer gains off-line which makes the approach simple and easy to implement, while guaranteeing that the state belongs to a zonotope at each time instant. These are preliminary results and they will be submitted as a journal paper.

The main line of reasoning of the zonotopic state estimation for piecewise affine systems can be used to extend this technique to a general case of a standard PWA system. Additionally, it can be interesting to compare this technique to the ellipsoidal state estimation techniques extended for PWA systems.

In the next chapter, a different perspective of the set-membership state

estimation problem is presented. The new approach combines both deterministic and stochastic approaches considering zonotopic constraints on the system state. Indeed, we introduce a new Zonotopic Constrained Kalman Filter (ZCKF) that guarantees that the system state belongs to a zonotope representing the set of constraints that the state is subject to.

Chapter 7

Zonotopic constrained Kalman filter

Contents

| | | |
|------------|---|------------|
| 7.1 | Introduction | 143 |
| 7.2 | Constrained Kalman filter | 145 |
| 7.3 | Zonotopic Constrained Kalman Filter (ZCKF) | 147 |
| 7.3.1 | Preliminary work | 147 |
| 7.3.2 | Algorithmic solution for ZCKF | 149 |
| 7.3.3 | Computation details | 150 |
| 7.3.4 | Iterative Shrinkage Thresholding Algorithm (ISTA) | 152 |
| 7.3.5 | Fast Iterative Shrinkage Thresholding Algorithm (FISTA) | 153 |
| 7.4 | Extended Zonotopic Constrained Kalman Filter (EZCKF) | 158 |
| 7.5 | Conclusion | 163 |

7.1 Introduction

In the previous chapters, we discussed two major approaches for set-membership state estimation with a focus on ellipsoidal or zonotopic set-based techniques. As it is obvious by now, in the state estimation theory, the Kalman filter [Kalman, 1960] is well known to be suitable for the state estimation of linear systems assuming the knowledge of the characteristics (covariance, average, etc.) of perturbations and noises governing the state and measurements.

Moreover, many extensions of the Kalman filter have been developed through time to deal with real time systems (e.g. Extended Kalman filter [Schmidt, 1966], unscented Kalman filter [Wan and Merwe, 2000], Kalman-Bucy filter [Kalman and Bucy, 1961] etc.). Due to its accuracy and easy implementation, the Kalman filter is widely used in industrial fields. As an alternative, the deterministic approach, particularly the set-membership state estimation became subject of research interest since it considers bounded perturbations and measurement noises. Additionally, the estimated state belongs to a geometrical set such as ellipsoids and zonotopes that we detailed through this thesis. With the intention of mixing the advantages of both approaches, in [Combastel, 2015b], the classic Kalman filter and the zonotopic state estimation are combined in a zonotopic Kalman filter (ZKF) based on the introduction of a new notion of covariation connecting the two approaches. Even though the Kalman filter is a powerful tool in state estimation, some of the known information about the system state can not be integrated. For example, distances and speeds are always positive, and these information should be treated as state constraints during the state estimation. A possible solution is to use descriptor systems introducing differential algebraic equations that are considered as a generalization of dynamical systems. Indeed, as shown in Chapter 5, algebraic equations, representing equality constraints of the systems, can be added to describe physical phenomena that a standard dynamical model can not describe. In this chapter, we address inequality constraints that can be applied on the state of the system. There has been a wide use of systems with state constraints in state estimation applications that include but are not limited to biomedical systems [Quintana et al., 1987], camera tracking [Julier and LaViola, 2007] and others. An overview of the techniques to incorporate equality and inequality constraints from the literature is given in Section 7.2. Then, Section 7.3 proposes a new approach for a constrained Kalman filter guaranteeing that the estimated state, at each time instant, belongs to a given zonotope, which is the envelope of the constraints applied on the system state. Indeed, the unconstrained Kalman estimation is projected onto the zonotope; an optimization problem is solved at each iteration such that the state belongs to this zonotope. Unlike the common deterministic approaches dealing with zonotopes, this technique requires no intersection between two geometrical sets allowing us to reduce the computation time. The main contribution of this chapter (which is also the major contribution of this thesis) is the development of a new approach for a zonotopic constrained Kalman filter (ZCKF) for systems subject to a potentially large number of linear inequality constraints on the state, with reduced complexity due to the use of an efficient optimization strategy. Indeed, the novelty is the design of a dual algorithm taking advantage of the particular

structure of the problem. The complexity of the optimization problem will no longer be affected by the potentially large number of constraints defining the zonotope. Within the algorithm, a particularization of the iterative shrinkage-thresholding algorithm (ISTA) is presented in Section 7.3.4 to take advantage of its simplicity. Then, an improvement of the convergence rate is considered by using the fast ISTA algorithm, known as FISTA [Nesterov, 1983], [Beck and Teboulle, 2009], in Section 7.3.5. These results have been presented at the 57th IEEE Conference on Decision and Control, 2018. An extension of the ZCKF strategy is proposed in Section 7.4 and is part of a future submission to Automatica.

7.2 Constrained Kalman filter

When the system is subject to equality constraints, different approaches can be applied to incorporate them. One approach focuses, for instance, on the system model reduction [Wen and Durrant-Whyte, 1992], decreasing the number of computations of the Kalman filter even though it might lead to the loss of the physical meaning of the state variables. Another technique is to consider the constraints as perfect measurements with zero measurement noise [Porrill, 1988], but this will provide a new augmented measurement equation leading to a singular measurement noise covariance. In addition, increasing the dimension of the problem leads to larger computational complexity of the Kalman gain. A third approach is to project the unconstrained estimation onto the constraint surface at each time iteration [Simon and Chia, 2002]. These three different approaches result in the same final optimal state estimation as proven in [Simon, 2010], in which a comparison of Kalman filters results in case of equality and inequality constraints, for the different methods, has been made. The advantage of the third approach lies in its capacity to be extended to inequality constraints. Another method to use for inequality constraints is the probability density function (PDF) truncation in which the constrained state estimate equals the mean of the truncated PDF [Simon and Simon, 2010], [Shimada et al., 1998]. In parallel, the same problem has been treated differently in [Scott et al., 2016]: a set-based state estimation problem has been considered using constrained zonotopes to take into account linear equality constraints on the unit hypercube within its generators polytopes, zonotopes or even ellipsoids. Nevertheless, if the problem of state estimation is addressed using zonotopes, the complexity grows considerably due to set operations (e.g. intersection).

Goal: Given an estimation for the real state \mathbf{x}_k subject to known linear constraints, the objective of this chapter is to provide a zonotopic constrained

estimation for the state at the next time instant \mathbf{x}_{k+1} . In other terms, the envelope of the constraints is a zonotope of the form $\mathcal{Z} = (\mathbf{p}, \mathbf{H})$. Before going into details, we start by presenting the structure of the constrained Kalman filter.

Let us consider the following standard discrete-time LTI system:

$$\begin{cases} \mathbf{x}_{k+1} = \mathbf{A}\mathbf{x}_k + \mathbf{B}\mathbf{u}_k + \mathbf{w}_k, \\ \mathbf{y}_k = \mathbf{C}\mathbf{x}_k + \mathbf{v}_k, \end{cases} \quad (7.1)$$

where $\mathbf{x}_k \in \mathbb{R}^{n_x}$, $\mathbf{u}_k \in \mathbb{R}^{n_u}$ and $\mathbf{y}_k \in \mathbb{R}^{n_y}$ are respectively the state vector of the system, the input vector, and the measured output vector at sample time k . The matrices $\mathbf{A} \in \mathbb{R}^{n_x \times n_x}$, $\mathbf{B} \in \mathbb{R}^{n_x \times n_u}$ and $\mathbf{C} \in \mathbb{R}^{n_y \times n_x}$ are respectively the system, control and output matrices. Here, $\mathbf{w}_k \in \mathbb{R}^{n_x}$ and $\mathbf{v}_k \in \mathbb{R}^{n_y}$ are random, independent white Gaussian noises with zero mean and covariances \mathbf{G}_w and \mathbf{G}_v respectively, i.e. $\mathbf{w}_k \sim N(0, \mathbf{G}_w)$, $\mathbf{v}_k \sim N(0, \mathbf{G}_v)$. Notice that the state is a random Gaussian vector and the initial state is chosen $\mathbf{x}_0 \sim N(\mathbf{x}_{0|-1}, \mathbf{G}_{0|-1})$. The Kalman filter is a recursive estimator, conceptualized in two phases: prediction and correction. The first phase uses the estimation from a previous time instant $\hat{\mathbf{x}}_{k-1|k-1}$ to produce a new estimate of the state at the current instant $\hat{\mathbf{x}}_{k|k-1}$. In the second phase, the prediction is combined with the measurement information \mathbf{y}_k to refine the estimation $\hat{\mathbf{x}}_{k|k}$. An overview of the standard Kalman filter¹ along with its equation can be found in Chapter 4. Unavailable in the classical filter, constrained filtering consists on correcting the estimation by considering constraints on the state vector [Simon, 2010]. Suppose that the system state verifies the inequality constraints:

$$\tilde{\mathbf{K}}\mathbf{x}_k \leq \tilde{\mathbf{c}},$$

with the matrix $\tilde{\mathbf{K}}$ and the vector $\tilde{\mathbf{c}}$ of appropriate dimensions. The constrained estimate is obtained solving the following optimization problem:

$$\begin{aligned} \min_{\mathbf{x}_k \in \mathbb{R}^{n_x}} \quad & \|\mathbf{x}_k - \hat{\mathbf{x}}_{k|k}\|_{\mathbf{W}}^2 \\ \text{s.t.} \quad & \tilde{\mathbf{K}}\mathbf{x}_k \leq \tilde{\mathbf{c}}, \end{aligned} \quad (7.2)$$

where \mathbf{W} is a symmetric positive-definite weighting matrix $\mathbf{W} = \mathbf{W}^\top \succ 0$. If $\mathbf{W} = \mathbf{G}_{k|k}^{-1}$, then the maximum probability estimate of the state with respect to constraints is obtained [Simon and Chia, 2002]. The unconstrained state estimation is directly projected onto the constrained subspace. The

¹For simplicity reasons, we chose to work with a classical Kalman filter in this chapter. However, the proposed algorithms in this chapter can also work with the different extensions of the Kalman filter.

constrained state estimate is then the solution of a quadratic programming (QP) problem. For general quadratic optimization problems, various methods are commonly used. For example, the interior point method [McShane et al., 1989] solves inequality constrained convex problems in polynomial time, whereas the active set method [Panier, 1987] proceeds by solving equality subproblems and verifying if the original constraints are satisfied. The algorithm in this chapter is based on a dual formulation of the (primal) problem of obtaining the minimum weighted distance of the unconstrained Kalman estimation to a zonotopic constraint. The designed algorithm belongs to the class of accelerated gradient methods [Nesterov, 2018], [Beck and Teboulle, 2009]. It allows us to address zonotopic constraints, in the context of the Kalman filter, with a simple implementation that is well suited for real time applications. The presented algorithm inherits the convergence properties of accelerated methods. The proposed zonotopic constrained Kalman filter will be presented in the next section.

7.3 Zonotopic Constrained Kalman Filter (ZCKF)

Motivated by the above discussion, we recall the fact that a zonotope is a symmetric convex polytope that can also be represented by the half-space representation (see Chapter 3). The conversion between the two representations is studied in [Fukuda, 2004], [Seymour, 1994]. Notice that solving a convex optimization problem constrained by a zonotope is equivalent to solving an optimization problem with linear inequalities. Obtaining the optimal solution based on classical optimization strategies, specially when the zonotope has a large number of generators, can be quite time consuming and not well suited for online implementations. The following subsections show how to implement a dual formulation of the original problem that takes into consideration the specific structure of the zonotopic constraint. In the dual formulation the number of decision variables grows with the dimension of the state-space and not with the number of generators required to define the zonotopic constraint.

7.3.1 Preliminary work

In the context of the duality principle explained in Chapter 3, optimization problems can be seen from two perspectives: the primal and the dual problem. In a convex problem, the primal and dual optimal objective values are equal under rather general assumptions [Boyd and Vandenberghe, 2004]. In

this work, we address an optimization problem of the form:

$$\begin{aligned} J^* = \min_{\mathbf{u} \in \mathcal{U}} J_u(\mathbf{u}) \\ \text{s.t. } \mathbf{R}\mathbf{u} - \mathbf{p} = \mathbf{0}, \end{aligned} \quad (7.3)$$

with $\mathbf{u} \in \mathbb{R}^m$, $\mathbf{R} \in \mathbb{R}^{n \times m}$, and $\mathbf{p} \in \mathbb{R}^n$. It is assumed that $\mathcal{U} \subseteq \mathbb{R}^m$ is a convex set. Following the dual approach proposed in Nesterov's work [Nesterov, 2005], a formal definition of the dual cost is provided.

Definition 7.1. Given the matrix $\mathbf{R} \in \mathbb{R}^{n \times m}$, the vector $\mathbf{p} \in \mathbb{R}^n$, and the primal function $J_u: \mathcal{U} \rightarrow \mathbb{R}$ from (7.3), let us define the smooth function called *dual function*:

$$f(\boldsymbol{\alpha}) = \max_{\mathbf{u} \in \mathcal{U}} \langle \boldsymbol{\alpha}, \mathbf{R}\mathbf{u} - \mathbf{p} \rangle - J_u(\mathbf{u}) \quad (7.4)$$

and

$$\mathbf{u}(\boldsymbol{\alpha}) = \arg \max_{\mathbf{u} \in \mathcal{U}} \langle \boldsymbol{\alpha}, \mathbf{R}\mathbf{u} - \mathbf{p} \rangle - J_u(\mathbf{u}). \quad (7.5)$$

Following the results in [Nesterov, 2005], given that:

$$-J^* \leq \max_{\mathbf{u} \in \mathcal{U}} \langle \boldsymbol{\alpha}, \mathbf{R}\mathbf{u} - \mathbf{p} \rangle - J_u(\mathbf{u}), \quad (7.6)$$

with J^* defined by (7.3), the solution of the original problem is obtained by minimizing $f(\boldsymbol{\alpha})$ with respect to $\boldsymbol{\alpha}$, with an inner maximization problem to find the optimal value of $\mathbf{u}(\boldsymbol{\alpha})$. For this formulation, the following property holds.

Property 7.1. [Nesterov, 2005] Suppose that $J_u(\cdot)$ is a smooth strictly convex function with the hessian:

$$\frac{\partial^2 J_u(\mathbf{u})}{\partial \mathbf{u}^2} \succeq \mathbf{S} \succ 0 \quad (7.7)$$

and suppose that \mathcal{U} is a convex set. Then, using the notation:

$$\bar{\mathbf{u}} = \mathbf{u}(\bar{\boldsymbol{\alpha}}) = \arg \max_{\mathbf{u} \in \mathcal{U}} \langle \bar{\boldsymbol{\alpha}}, \mathbf{R}\mathbf{u} - \mathbf{p} \rangle - J_u(\mathbf{u}), \quad (7.8)$$

we have:

$$f(\boldsymbol{\alpha}) \leq f(\bar{\boldsymbol{\alpha}}) + \langle \mathbf{R}\bar{\mathbf{u}} - \mathbf{p}, \Delta\boldsymbol{\alpha} \rangle + \frac{1}{2} \Delta\boldsymbol{\alpha}^\top \mathbf{R}\mathbf{S}^{-1} \mathbf{R}^\top \Delta\boldsymbol{\alpha}, \quad (7.9)$$

with $\Delta\boldsymbol{\alpha} = \boldsymbol{\alpha} - \bar{\boldsymbol{\alpha}}$.

This property states that in order to compute an increment $\Delta\boldsymbol{\alpha}$ leading to an improvement of the dual function (i.e. $f(\boldsymbol{\alpha} + \Delta\boldsymbol{\alpha}) \leq f(\boldsymbol{\alpha})$) it suffices to obtain $\Delta\boldsymbol{\alpha}$ in such a way that:

$$\langle \mathbf{R}\bar{\mathbf{u}} - \mathbf{p}, \Delta\boldsymbol{\alpha} \rangle + \frac{1}{2} \Delta\boldsymbol{\alpha}^\top \mathbf{R}\mathbf{S}^{-1} \mathbf{R}^\top \Delta\boldsymbol{\alpha} \quad (7.10)$$

is minimized. The optimal value for $\Delta\boldsymbol{\alpha}$ has an explicit solution because the function to be minimized is a quadratic convex function of $\Delta\boldsymbol{\alpha}$.

7.3.2 Algorithmic solution for ZCKF

The state estimation of the system (7.1) at each time instant k is subject to a system of inequality constraints that can be rewritten as a zonotopic constraint of the form $\mathbf{x}_k \in \mathbf{p} \oplus \mathbf{H}\mathbb{B}^m$. This constraint is equivalent to the existence of $\mathbf{w} \in \mathbb{R}^m$ such that $\|\mathbf{w}\|_\infty \leq 1$ and $\mathbf{x}_k = \mathbf{p} + \mathbf{H}\mathbf{w}$, with $\mathbf{p} \in \mathbb{R}^{n_x}$ the center and $\mathbf{H} = [\mathbf{h}_1 \ \mathbf{h}_2 \ \dots \ \mathbf{h}_m] \in \mathbb{R}^{n_x \times m}$ the generators matrix of the zonotope. Hence, we are faced to the problem of computing the minimum distance from the unconstrained Kalman estimate $\hat{\mathbf{x}}_{k|k}$ to the zonotope. This distance is zero if $\hat{\mathbf{x}}_{k|k}$ is included in the zonotope. The constrained Kalman filter optimization problem is:

$$\begin{aligned} \min_{\mathbf{z}, \mathbf{w}} \quad & J_{z,w}(\mathbf{z}, \mathbf{w}) \\ \text{s.t.} \quad & \mathbf{z} = \mathbf{p} + \mathbf{H}\mathbf{w} \\ & \|\mathbf{w}\|_\infty \leq 1, \end{aligned} \quad (7.11)$$

where the cost function is defined such as:

$$\begin{aligned} J_{z,w}(\mathbf{z}, \mathbf{w}) &= J_z(\mathbf{z}) + \frac{\epsilon}{2} \mathbf{w}^\top \mathbf{w} \\ &= \frac{1}{2} \|\mathbf{z} - \hat{\mathbf{x}}_{k|k}\|_{\mathbf{G}_{k|k}^{-1}}^2 + \frac{\epsilon}{2} \mathbf{w}^\top \mathbf{w}. \end{aligned} \quad (7.12)$$

In this setting, the scalar $\epsilon > 0$ is an arbitrarily small regularization parameter that guarantees that the quadratic function $J_{z,w}(\mathbf{z}, \mathbf{w})$ meets the strict convexity assumption of the Property 7.1. From the inspection of the quadratic function $J_{z,w}(\mathbf{z}, \mathbf{w})$ we have that the hessian is given by the following block diagonal matrix:

$$\mathbf{S} = \text{diag}(\mathbf{G}_{k|k}^{-1}, \epsilon \mathbf{I}_m). \quad (7.13)$$

Notice that $\mathbf{z} = \mathbf{p} + \mathbf{H}\mathbf{w}$ is equivalent to:

$$[\mathbf{I} \quad -\mathbf{H}] \begin{bmatrix} \mathbf{z}^\top & \mathbf{w}^\top \end{bmatrix}^\top = \mathbf{p}.$$

This allows us to rewrite the problem (7.11) in the form of (7.3), with:

$$\begin{aligned} \mathbf{u} &= \begin{bmatrix} \mathbf{z}^\top & \mathbf{w}^\top \end{bmatrix}^\top, \\ \mathbf{R} &= [\mathbf{I} \quad -\mathbf{H}], \\ J_u(\mathbf{u}) &= J_u \left(\begin{bmatrix} \mathbf{z} \\ \mathbf{w} \end{bmatrix} \right) = J_{z,w}(\mathbf{z}, \mathbf{w}). \end{aligned}$$

The function $\mathbf{u}(\boldsymbol{\alpha})$, as defined in Property 7.1, is given by:

$$\mathbf{u}(\boldsymbol{\alpha}) = \arg \max_{\|\mathbf{w}\|_\infty \leq 1, \mathbf{z} \in \mathbb{R}^{n_x}} \langle \boldsymbol{\alpha}, \mathbf{z} - \mathbf{p} - \mathbf{H}\mathbf{w} \rangle - J_z(\mathbf{z}) - \frac{\epsilon}{2} \mathbf{w}^\top \mathbf{w}. \quad (7.14)$$

We notice that the previous optimization problem can be decomposed in two independent ones as shown in (7.15):

$$\mathbf{u}(\boldsymbol{\alpha}) = \begin{bmatrix} \mathbf{z}(\boldsymbol{\alpha}) \\ \mathbf{w}(\boldsymbol{\alpha}) \end{bmatrix} = \begin{bmatrix} \arg \max_{\mathbf{z} \in \mathbb{R}^{n_z}} \langle \boldsymbol{\alpha}, \mathbf{z} \rangle - J_z(\mathbf{z}) \\ \arg \max_{\|\mathbf{w}\|_\infty \leq 1} -\langle \boldsymbol{\alpha}, \mathbf{H}\mathbf{w} \rangle - \frac{\epsilon}{2} \mathbf{w}^\top \mathbf{w} \end{bmatrix}. \quad (7.15)$$

As noticed, the variable \mathbf{z} , constrained by the linear inequalities forming the zonotope in the primal mode, belongs to the set of real numbers in the dual mode. In other terms, the number of decision variables in the optimization problem no longer depends on the number of linear constraints, but on the dimension of the state-space, which is generally smaller.

7.3.3 Computation details

This subsection details how to obtain the explicit expressions for \mathbf{z}_j , \mathbf{w}_j and $\Delta \boldsymbol{\alpha}_j$, required to implement both ISTA and FISTA algorithms at the j th iteration.

7.3.3.1 Expression for $\mathbf{z}(\boldsymbol{\alpha}_j)$

Based on expression (7.15), we recall here the definition of $\mathbf{z}_j = \mathbf{z}(\boldsymbol{\alpha}_j)$:

$$\mathbf{z}_j = \arg \max_{\mathbf{z} \in \mathbb{R}^{n_z}} \langle \boldsymbol{\alpha}, \mathbf{z} \rangle - J_z(\mathbf{z}), \quad (7.16)$$

where $J_z(\mathbf{z}) = \frac{1}{2} \|\mathbf{z} - \hat{\mathbf{x}}_{k|k}\|_{\mathbf{G}_{k|k}^{-1}}^2$. With the notation:

$$\Delta \mathbf{z}_j = \mathbf{z}_j - \hat{\mathbf{x}}_{k|k},$$

equation (7.16) becomes:

$$\mathbf{z}_j = \hat{\mathbf{x}}_{k|k} + \Delta \mathbf{z}_j,$$

where

$$\Delta \mathbf{z}_j = \arg \max_{\Delta \mathbf{z} \in \mathbb{R}^{n_z}} \boldsymbol{\alpha}_j^\top \Delta \mathbf{z} - \frac{1}{2} \Delta \mathbf{z}^\top \mathbf{G}_{k|k}^{-1} \Delta \mathbf{z}. \quad (7.17)$$

In order to obtain $\Delta \mathbf{z}_j$ we have to determine the value for $\Delta \mathbf{z}$ that cancels the gradient, i.e. $\Delta \mathbf{z}_j$ is given by:

$$\boldsymbol{\alpha}_k - \mathbf{G}_{k|k}^{-1} \Delta \mathbf{z}_j = 0.$$

Thus, $\Delta \mathbf{z}_j = \mathbf{G}_{k|k} \boldsymbol{\alpha}_j$ and then \mathbf{z}_j is obtained by (7.18):

$$\mathbf{z}_j = \mathbf{G}_{k|k} \boldsymbol{\alpha}_j + \hat{\mathbf{x}}_{k|k}. \quad (7.18)$$

7.3.3.2 Expression for $\mathbf{w}(\alpha_j)$

We recall from (7.15) that:

$$\mathbf{w}(\alpha_j) = \arg \max_{\|\mathbf{w}\|_\infty \leq 1} -\langle \alpha_j, \mathbf{H}\mathbf{w} \rangle - \frac{\epsilon}{2} \mathbf{w}^\top \mathbf{w}. \quad (7.19)$$

Consider the following notation:

$$\mathbf{w}_j = \mathbf{w}(\alpha_j) = \begin{bmatrix} w_j(1) & w_j(2) & \dots & w_j(m) \end{bmatrix}^\top. \quad (7.20)$$

We show in what follows that it is possible to obtain each component of \mathbf{w}_j from the solution of a 1-dimensional optimization problem. Since $\mathbf{H} = \begin{bmatrix} \mathbf{h}_1 & \mathbf{h}_2 & \dots & \mathbf{h}_m \end{bmatrix}$, we have from (7.19) that:

$$\begin{aligned} \mathbf{w}_j &= \arg \max_{w_j(i), i=1, \dots, m} - \sum_{i=1}^m (\alpha_j^\top \mathbf{h}_i) w_j(i) - \sum_{i=1}^m \frac{\epsilon}{2} w_j^2(i) \\ &\text{s.t. } |w_j(i)| \leq 1, \quad i = 1, \dots, m. \end{aligned}$$

We notice that this is a separable optimization problem in which each component $w_j(i)$ can be obtained from:

$$w_j(i) = \arg \max_{w_j(i) \in \mathbb{R}, |w_j(i)| \leq 1} -(\alpha_j^\top \mathbf{h}_i) w_j(i) - \frac{\epsilon}{2} w_j^2(i), \quad i = 1, \dots, m. \quad (7.21)$$

We remark that the gradient of $-(\alpha_j^\top \mathbf{h}_i) w_j(i) - \frac{\epsilon}{2} w_j^2(i)$ vanishes at $-\frac{1}{\epsilon} \alpha_j^\top \mathbf{h}_i$. This, along with the constraint $|w_j(i)| \leq 1$, gives the expression:

$$w_j(i) = \begin{cases} -\frac{1}{\epsilon} \alpha_j^\top \mathbf{h}_i, & \text{if } |\frac{1}{\epsilon} \alpha_j^\top \mathbf{h}_i| \leq 1 \\ 1, & \text{if } -\frac{1}{\epsilon} \alpha_j^\top \mathbf{h}_i > 1 \\ -1 & \text{if } -\frac{1}{\epsilon} \alpha_j^\top \mathbf{h}_i < -1 \end{cases} \quad (7.22)$$

for each component $w_j(i)$ with $i = 1, \dots, m$.

7.3.3.3 Expression for $\Delta \alpha_j$

In view of Property 7.1 we have that the gradient of the dual cost for a given α_j is given by $\mathbf{R}\mathbf{u}_j - \mathbf{p} = \mathbf{z}_j - \mathbf{p} - \mathbf{H}\mathbf{w}_j$. Moreover, Property 7.1 also states that an optimal local improvement with respect to the value obtained for α_j is given by $\alpha_j + \Delta \alpha_j$. The optimal local increment $\Delta \alpha_j$ is obtained from the minimization of:

$$\langle \mathbf{R}\mathbf{u}(\alpha_j) - \mathbf{p}, \Delta \alpha_j \rangle + \frac{1}{2} \alpha_j^\top \mathbf{R} \mathbf{S}^{-1} \mathbf{R}^\top \Delta \alpha_j.$$

By deriving with respect to $\Delta\boldsymbol{\alpha}_j$ and setting the derivative equal to 0, we obtain that the value of $\Delta\boldsymbol{\alpha}_j$ at each iteration j is given by the expression:

$$\Delta\boldsymbol{\alpha}_j = (\mathbf{R}\mathbf{S}^{-1}\mathbf{R}^\top)^{-1}(\mathbf{p} + \mathbf{H}\mathbf{w}_j - \mathbf{z}_j). \quad (7.23)$$

Notice that this last expression provides an exit condition for an algorithm based on the gradient information. If the norm of $\mathbf{p} + \mathbf{H}\mathbf{w}_{j-1} - \mathbf{z}_{j-1}$ is small, the pair $(\mathbf{w}_{j-1}, \mathbf{z}_{j-1})$ is close to optimality because the gradient at $\boldsymbol{\alpha}_{j-1}$ is close to zero. Therefore, the norm of $\|\mathbf{p} + \mathbf{H}\mathbf{w}_{j-1} - \mathbf{z}_{j-1}\|$ could be used as exit condition for a numerical algorithm computing the solution of the zonotopic constrained Kalman estimation.

7.3.4 Iterative Shrinkage Thresholding Algorithm (ISTA)

The particularization of the iterative shrinkage-thresholding algorithm (ISTA) to the specific dual formulation adopted in this chapter is illustrated by Algorithm 4.

Algorithm 4 ISTA method applied to (7.11)

Input: $\hat{\mathbf{x}}_{k|k}, \mathbf{H}, \mathbf{p}$.

Output: $\mathbf{p} + \mathbf{H}\mathbf{w}_{j-1}$.

- 1: **Initialization:** $j = 1, \boldsymbol{\alpha}_1 = \mathbf{0}, \mathbf{z}_0 = \hat{\mathbf{x}}_{k|k}, \mathbf{w}_0 = \mathbf{0}$.
 - 2: **while** $\|\mathbf{z}_{j-1} - \mathbf{p} - \mathbf{H}\mathbf{w}_{j-1}\| > \mu$ **do**
 - 3: Compute \mathbf{z}_j and \mathbf{w}_j , with (7.18) and (7.22), respectively.
 - 4: Compute $\Delta\boldsymbol{\alpha}_j$ from (7.23).
 - 5: $\boldsymbol{\alpha}_{j+1} = \boldsymbol{\alpha}_j + \Delta\boldsymbol{\alpha}_j$.
 - 6: $j = j + 1$.
 - 7: **return** $\mathbf{p} + \mathbf{H}\mathbf{w}_{j-1}$.
-

The scalar variable μ denotes the desired tolerance for which the solution is finally reached. Notice that the output $\mathbf{p} + \mathbf{H}\mathbf{w}_{j-1}$ belongs, by construction, to the zonotope $\mathbf{p} \oplus \mathbf{H}\mathbb{B}^m$. Moreover, $\mathbf{p} + \mathbf{H}\mathbf{w}_{j-1}$ provides, up to a numeric accuracy controlled by the exit parameter μ , the closest point, according to the weighted norm $\|\cdot\|_{\mathbf{G}_{k|k}^{-1}}$, to the original unconstrained Kalman estimation $\hat{\mathbf{x}}_{k|k}$. We conclude that the output of the algorithm provides the numerical solution to the zonotopic Kalman filter estimation problem. The convex optimization problem (7.11) could be solved via classical methods. However, with high order zonotopes, the problem can involve a large number of constraints, which motivates the use of our approach.

One of the advantages of the algorithm above is its simplicity. However, the ISTA algorithm is recognized as a slow method [Nesterov, 2018], [Beck

and Teboulle, 2009]. In fact, it is guaranteed to converge with a convergence rate of $\mathcal{O}(\frac{1}{j})$. A faster algorithm, called fast iterative shrinkage-thresholding algorithm (FISTA) provides a better convergence rate: the difference with the optimal solution decreases with $\mathcal{O}(\frac{1}{j^2})$, see [Nesterov, 2018], [Beck and Teboulle, 2009]. The speed of convergence and simplicity of both algorithms make them well suited for online applications [Richter et al., 2012].

7.3.5 Fast Iterative Shrinkage Thresholding Algorithm (FISTA)

In what follows, we present how to adapt the FISTA algorithm to the optimization problem considered here (see Algorithm 5).

Algorithm 5 FISTA method applied to (7.11)

Input: $\hat{\mathbf{x}}_{k|k}, \mathbf{H}, \mathbf{p}$.
Output: $\mathbf{p} + \mathbf{H}\mathbf{w}_{j-1}$.

- 1: **Initialization:** $j = 1, \boldsymbol{\alpha}_1 = \mathbf{0}, \mathbf{z}_0 = \hat{\mathbf{x}}_{k|k}, \mathbf{w}_0 = \mathbf{0}, \boldsymbol{\eta}_0 = \mathbf{0}, t_j = 1$.
- 2: **while** $\|\mathbf{z}_{j-1} - \mathbf{p} - \mathbf{H}\mathbf{w}_{j-1}\| > \mu$ **do**
- 3: Compute \mathbf{z}_j and \mathbf{w}_j using (7.18) and (7.22), respectively.
- 4: Compute $\Delta\boldsymbol{\alpha}_j$ from (7.23).
- 5: $\boldsymbol{\eta}_j = \boldsymbol{\alpha}_j + \Delta\boldsymbol{\alpha}_j$.
- 6: $t_{j+1} = 0.5(1 + \sqrt{1 + 4t_j^2})$.
- 7: $\boldsymbol{\alpha}_{j+1} = \boldsymbol{\eta}_j + \frac{t_j - 1}{t_{j+1}}(\boldsymbol{\eta}_j - \boldsymbol{\eta}_{j-1})$.
- 8: $j = j + 1$.
- 9: **return** $\mathbf{p} + \mathbf{H}\mathbf{w}_{j-1}$.

The main difference between the two algorithms relies in the fact that in FISTA, the gradient of the dual function is evaluated as a linear combination of the last two values of an auxiliary variable $\boldsymbol{\eta}_j$ [Beck and Teboulle, 2009]. This means that $\boldsymbol{\alpha}_{j+1}$ is obtained by interpolation between the two previous points of the auxiliary variable ($\boldsymbol{\eta}_j$ and $\boldsymbol{\eta}_{j-1}$). The computational time per iteration for FISTA is basically the same as for ISTA. However, as commented before, the convergence rate of FISTA is much better.

The convergence analysis of both algorithms is extensively detailed in [Beck and Teboulle, 2009]. To test the algorithm and the assumption that the FISTA algorithm has a better convergence rate than the ISTA algorithm [Beck and Teboulle, 2009], three examples are further presented.

Example 7.1. Given a zonotope $\mathcal{Z}(\mathbf{p}_1, \mathbf{H}_1)$ with normalized random values $\mathbf{p}_1 = \text{randn}(n_x, 1)$ and $\mathbf{H}_1 = \frac{1}{m}\text{randn}(n_x, m)$, with $n_x = 2$ and $m = 15$, the idea is to find the closest point to the state estimate that belongs to the zonotope. The exact values of \mathbf{p}_1 and \mathbf{H}_1 are $\mathbf{p}_1 = [0.0423 \quad -0.0403]^\top$ and $\mathbf{H}_1 = [\mathbf{H}_a \quad \mathbf{H}_b \quad \mathbf{H}_c]$, with:

$$\mathbf{H}_a = \begin{bmatrix} -0.0434 & 0.0381 & -0.1089 & 0.0431 & 0.0640 \\ 0.0260 & -0.0768 & 0.0338 & 0.0086 & 0.0777 \end{bmatrix},$$

$$\mathbf{H}_b = \begin{bmatrix} -0.1026 & 0.0081 & 0.0253 & 0.0524 & 0.0248 \\ -0.0480 & 0.0519 & 0.0451 & -0.0098 & -0.0081 \end{bmatrix},$$

$$\mathbf{H}_c = \begin{bmatrix} -0.0299 & -0.1230 & -0.0699 & 0.0499 & -0.0972 \\ -0.0708 & 0.0315 & 0.0630 & 0.0703 & -0.0277 \end{bmatrix}.$$

For verification and validation purposes, we assume the prior knowledge of the optimal solution z^* of the problem (7.11). Therefore, let us consider the Kalman state estimation to be $\hat{\mathbf{x}}_{k|k} = [-1.5639 \quad 0.2457]^\top$, the covariance of estimation $\mathbf{G}_{k|k} = \mathbf{I}_{n_x}$ at the time instant k , with $\epsilon = 10^{-4}$ in (7.12) and the optimal solution that should be reached $\mathbf{z}^* = [-0.8148 \quad -0.0702]^\top$.

Figure 7.1 shows that starting with the unconstrained state estimate represented by the black asterisk (sub-figure 7.1a), the algorithm offers a new feasible point (denoted by a red circle) at each iteration, with a decreased value of the original objective function (7.11), which means a closer point to the blue zonotope (see sub-figures 7.1b to 7.1f). This was done by taking one step in the direction of the gradient of the objective function. By adopting the estimate projection method, we are computing the minimum distance from the unconstrained estimate to the zonotope. At the end of the algorithm, the last red circle reaches the pre-calculated optimal solution represented by the green asterisk.

The algorithm is expected to find better and better solution until the convergence criterion is met (see Figure 7.1).

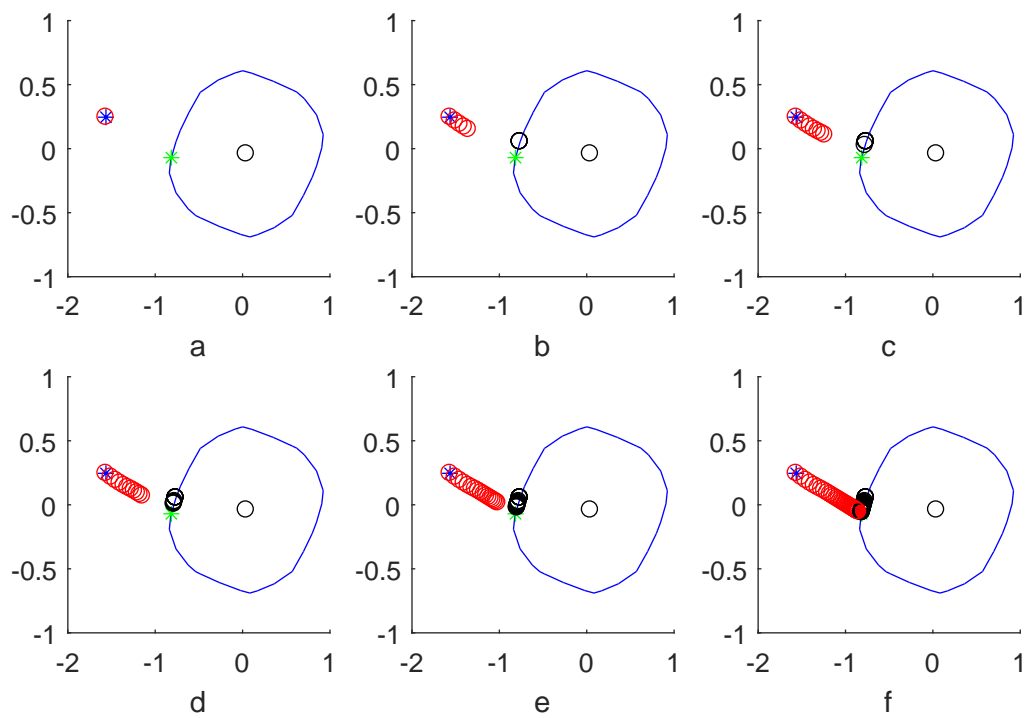


Figure 7.1 – Illustration of the proposed zonotopic constrained algorithm

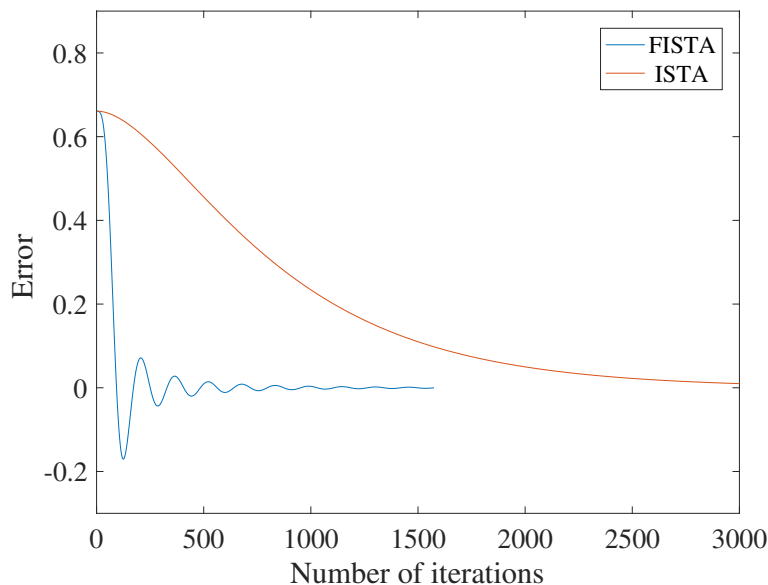


Figure 7.2 – Comparison of estimation errors obtained with ISTA and FISTA

The exit criterion is the norm of the deviation of \mathbf{z}_j from the closest vertex of the zonotope $\mathbf{p} + \mathbf{H}\mathbf{w}_j$ (black circle at each iteration) that is $\|\mathbf{z}_j - \mathbf{p} - \mathbf{H}\mathbf{w}_j\|$. This norm is measured at each iteration and the algorithm terminates when it is less or equal to $\mu = 10^{-8}$.

In order to expose the advantages of FISTA over ISTA, the algorithms were tested on the same example 7.1. Figure 7.2 shows a comparison of the function value error $J(\mathbf{z}_j) - J(\mathbf{z}^*)$. Clearly, the results provided by FISTA are much better than the ones provided by the ISTA algorithm in means of convergence rate. In fact, it can be seen that after 500 iterations, FISTA reaches an accuracy of 10^{-4} , which is more precise than ISTA by several orders of magnitude, and demonstrates its efficiency. Moreover, ISTA needed more than 3000 iterations to reach the optimal value which was equivalent to 0.08s that FISTA obtained after less than 1000 iterations (0.02s) with an accuracy of 10^{-7} .

Example 7.2. Consider the system (7.1) with:

$$\mathbf{A} = \begin{bmatrix} 1 & 0.3 \\ -0.225 & 0.925 \end{bmatrix},$$

$$\mathbf{B} = \begin{bmatrix} 1 & 1 \end{bmatrix}^T,$$

$$\mathbf{C} = \begin{bmatrix} 1 & 0 \end{bmatrix}.$$

The system state is estimated using a classical Kalman filter with $\mathbf{x}_0 \sim N(\mathbf{x}_{0|-1}, \mathbf{G}_{0|-1})$, $\mathbf{u}_k = 5$, $\mathbf{w}_k \sim N(0, 0.02)$, $\mathbf{v}_k \sim N(0, 0.01)$, $\mathbf{x}_{0|-1} = [0 \ 2]^\top$ and $\mathbf{G}_{0|-1} = \mathbf{I}_2$. The constraints envelope $\mathcal{Z}(\mathbf{p}_2, \mathbf{H}_2)$, with:

$$\mathbf{p}_2 = [2 \ -0.5]^\top,$$

$$\mathbf{H}_2 = \begin{bmatrix} -2 & 1 & -0.6 \\ 0.8 & -0.8 & 1.6 \end{bmatrix},$$

is chosen randomly, on the basis of knowledge of the trajectory of the system for illustration purposes.

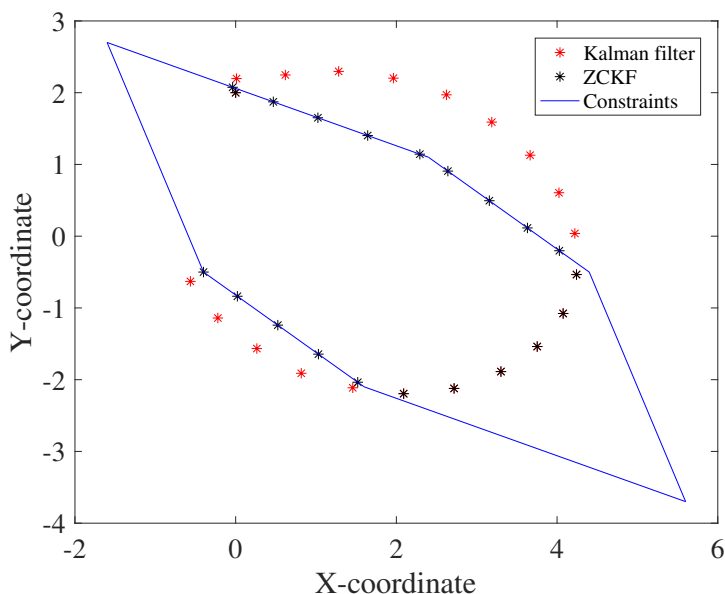


Figure 7.3 – Classical Kalman filter versus zonotopic constrained Kalman filter

Example 7.3. The chosen constraints are not too loose to prove the efficiency of the algorithm no matter where the estimate is located, and not too tight to keep a realistic problem, allowing variations on the state variables and trajectory. The regularization parameter is $\epsilon = 10^{-4}$. Figure 7.3 shows the plot of the system trajectory, along with the zonotope representing the constraints envelope, the unconstrained estimates and the constrained estimates. The red asterisks obtained by applying the classical Kalman filter, are the input for the constraints algorithm. It can be noticed that the unconstrained estimates remain the same if they already belong to the zonotope

(blue lines). If not, the constrained estimates (black asterisks) are obtained using the proposed algorithm. The constrained estimates, then, belong to the zonotope.

Set-membership state estimation approaches, that consist mainly in computing the intersection between the predicted uncertain set and the measurement set, usually require a large computation time. Therefore, it is interesting to study the computational time of the proposed approach, once applied to state estimation problems subject to a large number of linear constraints. Table 7.1 shows the simulation time in seconds, for both algorithms ISTA and FISTA when dealing with large scale zonotopes up to an order of $m = 10000$. The simulation results have been obtained with an Intel Core *i7 - 4790* 3.60 GHz, for random generated zonotopes with $n_x = 2$ and a desired tolerance of $\mu = 0.01$. Clearly it can be shown that the computation time is significantly reduced when using the proposed approach with FISTA.

Table 7.1 – Computation time of the considered algorithms with large-scale zonotopes

| Parameter | Computation time (s) | |
|-----------|----------------------|---------------------|
| | ZCKF based on ISTA | ZCKF based on FISTA |
| m | | |
| 10 | 1.4 | 0.02 |
| 100 | 5.35 | 0.04 |
| 1000 | 125.35 | 0.12 |
| 10000 | 762 | 3.2 |

7.4 Extended Zonotopic Constrained Kalman Filter (EZCKF)

When the convex optimization problem (7.11) is applied to a large scale system, the number of decision variables can reach thousands when dealing with high order zonotopes. This motivated the use of the approach based on FISTA, where most of the computational effort is limited to simple equations of multiplications and additions. Furthermore, the use of the generator representation of a zonotope $\mathcal{Z}(\mathbf{p}, \mathbf{H})$ presents significant advantages in research. In fact, being able to represent a complex geometrical form using a "simple" matrix, leads to easier and simpler computations. When the order of the zonotope defined by the number of its generators increases, the complexity of the algorithm grows up. The goal of this section is to compute a reduced order zonotope, approximating a high order zonotope. This problem is tackled in the literature, by using reduction techniques, more precisely the

reduction of the number of generators of a zonotope. Concisely, it consists of replacing a subset of generators by a lower number that form an interval [Combastel, 2006] or a parallelotope [M. Althoff and Buss, 2010]. The choice of the subset and the quality of the approximation depend generally on the criterion used to split the zonotope. Here, a complexity reduction technique is integrated on what was done in the previous algorithms, to limit the number of generators defining the zonotope at each iteration. It is more convenient time-wise to iterate on a smaller zonotope rather than on the original one.

In this context, the algorithm should be able to find a smaller zonotope that we will refer to by the *non fixed zonotope*. More precisely, the generators forming the matrix \mathbf{H} are sorted in a way that:

$$\mathbf{H} = \begin{bmatrix} \mathbf{h}_1 & \mathbf{h}_2 & \dots & \mathbf{h}_m \end{bmatrix}$$

such that:

$$\left| \frac{1}{\epsilon} \boldsymbol{\alpha}_j^\top \mathbf{h}_1 \right| \leq \left| \frac{1}{\epsilon} \boldsymbol{\alpha}_j^\top \mathbf{h}_2 \right| \leq \dots \leq \left| \frac{1}{\epsilon} \boldsymbol{\alpha}_j^\top \mathbf{h}_m \right|$$

The choice of the active generators is critical to solve the dual problem as it determines the set of generators that influence the final result the most. The new *non fixed zonotope* is $\mathcal{Z}(\mathbf{p}_{new}, \mathbf{H}_{nf})$ with:

$$\mathbf{H}_{nf} = \begin{bmatrix} \mathbf{h}_1 & \mathbf{h}_2 & \dots & \mathbf{h}_l \end{bmatrix}, \quad (7.24)$$

$$\mathbf{w}_{nf} = \begin{bmatrix} \mathbf{w}_1 & \mathbf{w}_2 & \dots & \mathbf{w}_l \end{bmatrix}, \quad (7.25)$$

formed of the first l generators of m ($l < m$), with a new center \mathbf{p}_{new} , obtained by a simple translation of the previous zonotope center such that

$$\mathbf{p}_{new} = \mathbf{p} + \mathbf{H}_f \mathbf{w}_f, \quad (7.26)$$

with

$$\mathbf{H}_f = \begin{bmatrix} \mathbf{h}_{l+1} & \mathbf{h}_{l+2} & \dots & \mathbf{h}_m \end{bmatrix}, \quad (7.27)$$

$$\mathbf{w}_f = \begin{bmatrix} \mathbf{w}_{l+1} & \mathbf{w}_{l+2} & \dots & \mathbf{w}_m \end{bmatrix}. \quad (7.28)$$

Once the smaller zonotope is chosen, the algorithm is expected to find a feasible solution with respect to the zonotope $\mathcal{Z}(\mathbf{p}_{new}, \mathbf{H}_{nf})$.

Briefly, and similar to the previous FISTA algorithm, Algorithm 6 takes as input the zonotope forming the constraints along with the unconstrained Kalman filter. Mainly, each iteration of the algorithm consists of a gradient step of the smooth part followed by a shrinkage operation.

Algorithm 6 Reduced FISTA method applied to (7.11)

Input: $\mathbf{z}_{Kalman}, \mathbf{H}, \mathbf{p}$ **Output:** α_k

- 1: **Initialization:** $k = 1, \alpha_1 = \mathbf{0}$
 - 2: Split the initial zonotope $\mathcal{Z}(\mathbf{p}, \mathbf{H})$ and find $\mathbf{H}_f, \mathbf{w}_f, \mathbf{H}_{nf}, \mathbf{w}_{nf}$, with (7.27), (7.28), (7.24), (7.25), respectively.
 - 3: **if** \mathbf{H}_f is not empty **then**
 - 4: $\mathbf{p}_{new} = \mathbf{p} + \mathbf{H}_f \mathbf{w}_f$
 - 5: **while** $\|\mathbf{z}_{j-1} - \mathbf{p}_{new} - \mathbf{H} \mathbf{w}_{j-1}\| > \mu$ **do**
 - 6: Compute \mathbf{z}_j and \mathbf{w}_j using (7.18) and (7.22), respectively.
 - 7: Compute $\Delta \alpha_j$ from (7.23).
 - 8: $\boldsymbol{\eta}_j = \alpha_j + \Delta \alpha_j$.
 - 9: $t_{j+1} = 0.5(1 + \sqrt{1 + 4t_j^2})$.
 - 10: $\alpha_{j+1} = \boldsymbol{\eta}_j + \frac{t_j - 1}{t_{j+1}}(\boldsymbol{\eta}_j - \boldsymbol{\eta}_{j-1})$.
 - 11: $j = j + 1$.
 - 12: **return** $\mathbf{p} + \mathbf{H} \mathbf{w}_{j-1}$.
-

The main difference with the previous algorithm is the newly added reduction step of zonotopes, that makes the computations more efficient. Indeed, the complexity of Algorithm 6 strongly depends on the number of constraints, thus on the order of zonotopes represented by their number of generators and dimensions. The foremost advantage then of the additional zonotope reduction step in the algorithm is a reduced complexity, therefore reduced computation time. Actually, at each iteration, the algorithm finds a solution with a decreased value of the original objective function (7.11) with respect to the reduced zonotope. This output is close enough to the optimal solution of the algorithm. However, reaching the optimal solution using one or more reduced zonotopes is faster than considering the original zonotope, with a potentially large number of constraints in computations.

Example 7.4. To prove the effectiveness of the proposed EZCKF, we consider a randomly generated zonotope $\mathcal{Z}(\mathbf{p}, \mathbf{H})$, with $\mathbf{p} = \text{randn}(n_x, 1)$ and a normalized form of the matrix $\mathbf{H} = \frac{1}{m} \text{randn}(n_x, m)$ that forms the constraints for the system state with $n_x = 2$ and $m = 20$. The exact values of \mathbf{p} and \mathbf{H} are:

$$\mathbf{p} = \begin{bmatrix} 0.0185 & -0.0035 \end{bmatrix}^\top,$$

$$\mathbf{H} = [\mathbf{H}_a \quad \mathbf{H}_b \quad \mathbf{H}_c \quad \mathbf{H}_d],$$

such that:

$$\begin{aligned}\mathbf{H}_a &= \begin{bmatrix} -0.0884 & -0.0623 & 0.0576 & -0.0107 & -0.1191 \\ 0.0149 & 0.0348 & -0.0380 & 0.0584 & 0.1042 \end{bmatrix}, \\ \mathbf{H}_b &= \begin{bmatrix} 0.0426 & -0.0672 & 0.0255 & -0.0366 & 0.0329 \\ 0.0352 & -0.0575 & -0.0052 & 0.0414 & 0.0154 \end{bmatrix}, \\ \mathbf{H}_c &= \begin{bmatrix} 0.0262 & -0.0751 & -0.0351 & 0.0080 & 0.0156 \\ -0.0273 & -0.0333 & 0.0529 & 0.0651 & 0.0050 \end{bmatrix}, \\ \mathbf{H}_d &= \begin{bmatrix} 0.0716 & 0.0834 & 0.0025 & 0.0567 & -0.0110 \\ 0.0017 & -0.0205 & 0.0098 & 0.0186 & -0.0619 \end{bmatrix}.\end{aligned}$$

A prior knowledge of the optimal solution is assumed for verification purposes such that $\mathbf{z}_{sol} = [0.3382 \quad -0.6963]^\top$. The unconstrained Kalman estimate is $\mathbf{z}_{Kalman} = [0.4070 \quad -0.9123]^\top$ and the covariance of estimation equals to \mathbf{I}_{n_x} .

Figures 7.4, 7.5 and 7.6 show the zonotopic constrained algorithm in details. Instead of iterating on the entire zonotope shown in Figure 7.4, the algorithm chooses at the beginning a smaller zonotope (See Figure 7.5), in terms of the number of generators ($m_1 = 5$). The algorithm iterates until finding the best solution coherent with the chosen zonotope which is the projection of the unconstrained estimate on the smaller zonotope. This solution is feasible and clearly closer to the optimal solution. For more accuracy, the algorithm iterates next with a larger zonotope ($m_2 = 10$) as shown in Figure 7.6, keeping the generators that affect the most the shape of the zonotope. Starting with the previously obtained solution, the algorithm iterates until reaching a better solution. The convergence criterion is met when the error the variable \mathbf{z} represented by the red circles, and $\mathbf{z}_{zon} = \mathbf{p}_{new} + \mathbf{H}_{nf}\mathbf{w}_{nf}$ represented by the black circles is relatively small ($< 10^{-4}$). The new zonotope and the original zonotope have the same side where the optimal solution is located. The algorithm is guaranteed to converge at the end to the pre-calculated solution represented by the green asterisk. When the number of generators is relatively high, using the EZCKF multiple times on small zonotopes is better in terms of time complexity than solving the algorithm on a large scale zonotope. More precisely, in this example for $m = 20$, the ZCKF reaches the optimal solution in 0.02s while the EZCKF reaches the optimal solution slightly faster (0.019s). The speed is improved when we consider larger zonotopes.

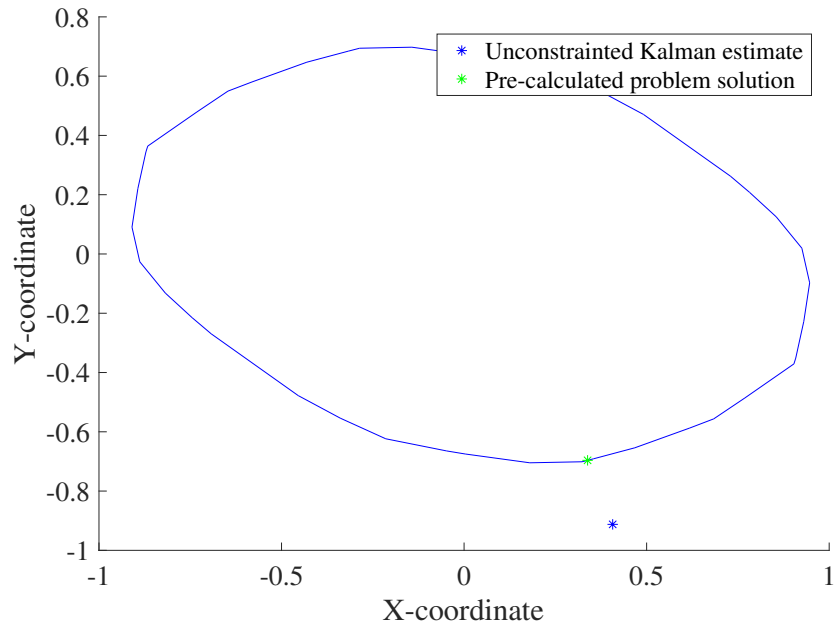


Figure 7.4 – Original setup

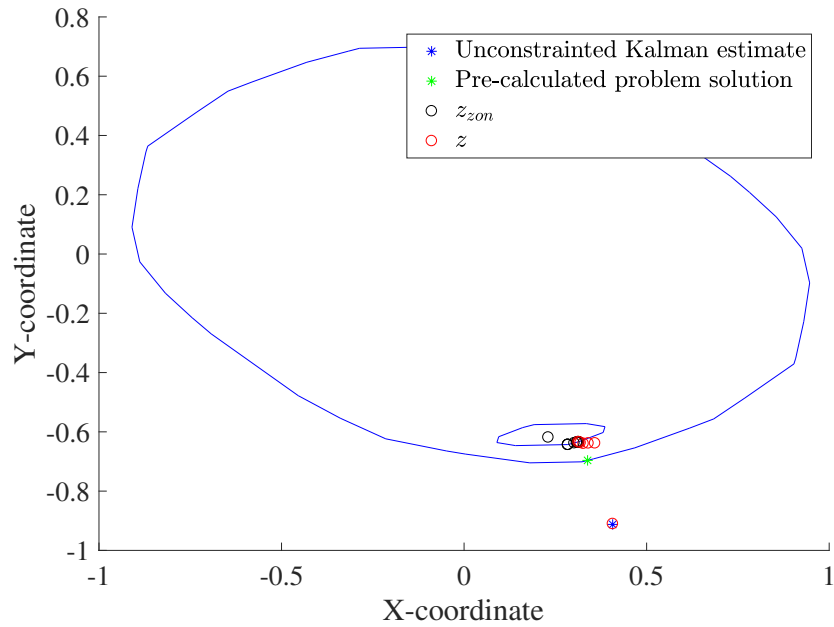


Figure 7.5 – Example 7.4: first zonotope

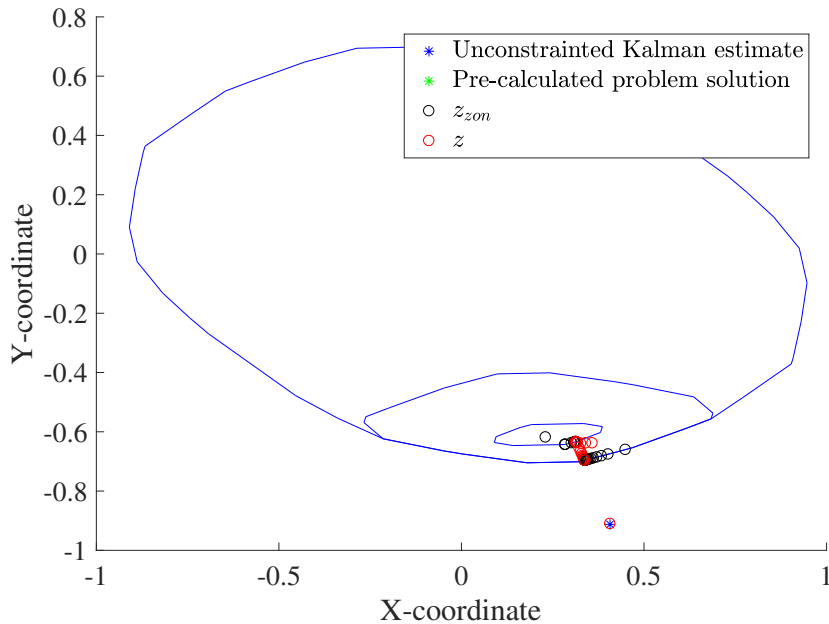


Figure 7.6 – Example 7.4: second zonotope

7.5 Conclusion

This chapter presents a new approach to design a zonotopic constrained Kalman filter (ZCKF) combining the advantages of stochastic and deterministic approaches. The proposed technique guarantees that the system state at each time instant belongs to a given zonotope. Using the duality principle, the unconstrained estimated state is projected on a zonotope via a convex optimization problem taking advantage of the particular structure of the problem. The optimal solution of the problem can be obtained either through the simple and efficient iterative shrinkage-thresholding algorithm ISTA or FISTA, the faster version of ISTA.

The second contribution of the chapter is to consider an additional step of zonotope order reduction in order to improve the overall performance of the algorithm in terms of speed of convergence and computational complexity. This is done by limiting the number of generators of the zonotope, thus the number of computations per iteration. The simplicity and reduced complexity of the approach makes it a promising method to use in set-membership state estimation for large scale systems possibly subject to a large number of constraints. This could also be an advantage, if the approach is applied to large scale real systems.

Chapter 8

Conclusion and perspectives

This chapter summarizes all the contributions presented in this thesis and discusses our future research directions in the field of set-membership state estimation.

8.1 Conclusion

This thesis discusses the advances of state estimation, particularly set-membership state estimation, and proposes new ellipsoidal and zonotopic state estimation techniques in the presence of bounded disturbances and measurement noises for different classes of linear systems. The main contributions of this thesis are divided into two parts:

- The first part builds upon previous results developed in the literature and applies an ellipsoidal set-membership state estimation technique to an octorotor in the context of radar applications. An extension to discrete-time both linear time invariant (LTI) and linear time variant (LTV) descriptor systems in the presence of bounded perturbations and measurement noises is proposed.
- In the second part, a new zonotopic state estimation approach using a Luenberger observer and based on the minimization of \mathbf{P} -radius is applied to the same model of an octorotor in a first step. In a second step, this approach has been further extended to deal with a new class of systems: the bi-modal piecewise affine systems. Furthermore, the problem of set-membership state estimation has been treated differently, combining deterministic and stochastic approaches. A new zonotopic constrained Kalman filter (ZCKF) which combines the good

accuracy of the zonotopic set-membership state estimation and the reduced complexity of the classical Kalman filter is presented.

The first part deals with the set-membership state estimation problem for standard discrete-time linear time invariant systems with bounded perturbations and bounded measurement noises. An existing ellipsoidal set-membership state estimation technique is exposed, then compared to the classical Kalman filter in terms of accuracy and complexity. The ellipsoidal technique offers high precision but higher complexity compared to the Kalman filter. Then, the method is extended to include control inputs in order to apply it on a model of an octorotor in a radar application context where the goal is to compute its operating frequency. Additionally, this technique inspired the development of several ellipsoidal set-membership state estimation techniques for discrete-time descriptor systems:

- *Method 1* computes a fixed observer gain by off-line solving a LMI problem,
- *Method 2* updates the observer gain at each time instant aiming for better accuracy but with higher complexity compared to *Method 1*,
- *Method 3* aims to avoid the vertex enumeration problem in *Method 2* by using a vector scaling technique.

Finally, an extension is proposed for LTV descriptor systems. Thus, *Method 4* computes at each time instant an updated observer gain and a flexible shape of the estimated ellipsoidal set. Quadratic constraints on both perturbations and measurements are considered in *Method 5* to reduce the estimation bounds.

In the second part, the set-membership state estimation problem is solved using zonotopes as an alternative for ellipsoids. A guaranteed zonotopic set-membership estimation technique based on a typical Luenberger observer and on the minimization of the \mathbf{P} -radius of a zonotope for linear discrete time LTI standard systems. This technique is then compared to the off-line ellipsoidal approach provided by *Method 1* in Chapter 5 and applied to the same octorotor model used in synthetic aperture radar. Another contribution of this thesis is the extension of this off-line zonotopic state-estimation to deal with a particular class of bi-modal piecewise affine systems by considering some additional LMI constraints in the optimization problem.

Moreover, taking into consideration the previous contributions, a new approach for a zonotopic constrained Kalman filter (ZCKF) is proposed in Chapter 7 guaranteeing that the estimated state, at each time instant, belongs to a given zonotope, which is the envelope of the inequality constraints

applied on the system state via an optimization problem. Unlike the common deterministic approaches dealing with zonotopes, this technique requires no intersection between two geometrical sets allowing to reduce the computation complexity. The novelty of this part (which is the major contribution of this thesis) is the design of a dual algorithm taking advantage of the particular structure of the problem. The complexity of the optimization problem will no longer be affected by the potentially large number of constraints defining the zonotope. Within the algorithm, a particularization of the iterative shrinkage-thresholding algorithm (ISTA) is presented to take advantage of its simplicity. An improvement of the convergence rate is considered by using the fast ISTA algorithm, known as FISTA [Nesterov, 1983], [Beck and Teboulle, 2009]. Then, we introduce in a second part, within the FISTA algorithm, a new extended zonotopic Kalman filter (EZCKF) reducing the complexity of the zonotopic constraints. EZCKF approximates the given zonotope by a lower order one, by limiting the number of generators at each time instant. This step reduces the computational time of the FISTA algorithm.

8.2 Future directions

Several mid-term and long-term directions are proposed below.

This thesis mainly focused on considering that the perturbations belongs to a box. An interesting perspective would be to consider that the perturbations vector belong as well to an ellipsoid in Part I which allows us to avoid the vertex enumeration without compromising on the accuracy of the online ellipsoidal set-membership state estimation technique for descriptor systems. Another interesting idea is to work with interval uncertainties in the model, both for the standard and the descriptor systems. Additionally, it is important to compare the ellipsoidal set-membership state estimation techniques for descriptor systems with existing techniques in literature in particular those using zonotopes.

As stated in Chapter 6, the off-line zonotopic technique has been developed for bi-modal piecewise systems. This could potentially lead to a zonotopic state estimation technique for a general standard representation of piecewise affine systems. To further our research, we intend to develop ellipsoidal set-membership state estimation techniques for PWA systems to take advantage of their simplicity in state estimation and compare them in terms of accuracy and complexity with the developed zonotopic techniques.

In addition, we believe that the new results of Chapter 7 represent an initial step toward a promising approach for state estimation of large scale systems that combines the advantages of deterministic and stochastic ap-

proaches. Future work on this topic should address the application of the presented contributions (ZCKF and EZCKF) on a more complex system with experimental validation. Moreover, another way to extend these results is to update the state covariance matrix in the Kalman filter. Indeed, at the end of the execution of the ZCKF algorithm we have more confidence in the system's state estimation meaning that the covariance matrix could be updated to improve the state estimation at the next time instant. Notice that the ZCKF and EZCKF approaches have been developed starting from a classical Kalman filter. Further improvements can be done by using several extensions of the Kalman filter.

Finally, on a wider level, it is important to further use the developed state estimation methods (using zonotopes and ellipsoids) in the context of fault detection and fault tolerant control.

Bibliography

- Abdolhosseini, M., Zhang, Y. M., and Rabbath, C. A. (2013). An efficient model predictive control scheme for an unmanned quadrotor helicopter. *Journal of Intelligent & Robotic Systems*, 70(1-4):27–38.
- Alamir, M. (2007). Nonlinear moving horizon observers: theory and real-time implementation. *Lecture Notes in Control and Information Sciences*, 363:139–179.
- Alamo, T., Bravo, J. M., and Camacho, E. F. (2005). Guaranteed state estimation by zonotopes. *Automatica*, 41:1035–1043.
- Alamo, T., Bravo, J. M., Redondo, M. J., and Camacho, E. F. (2008a). A set-membership state estimation algorithm based on DC programming. *Automatica*, 44(1):216–224.
- Alamo, T., Tempo, R., Ramírez, D. R., and Camacho, E. F. (2008b). A new vertex result for robustness problems with interval matrix uncertainty. *Systems and Control Letters*, 57:474–481.
- Alessandri, A. and Coletta, P. (2001a). Design of Luenberger observers for a class of hybrid linear systems. In *Proc. of International Workshop on Hybrid Systems: Computation and Control*, pages 7–18.
- Alessandri, A. and Coletta, P. (2001b). Switching observers for continuous-time and discrete-time linear systems. In *In Proc. of the American Control Conference*, volume 3, pages 2516–2521, Arlington, VA, USA.
- Althoff, M., Stursberg, O., and Buss, M. (2007). Reachability analysis of linear systems with uncertain parameters and inputs. In *Proc. of the 46th IEEE Conference on Decision and Control*, volume 41, pages 726–732. New Orleans, LA, USA.
- Althoff, M., Stursberg, O., and Buss, M. (2010). Computing reachable sets of hybrid systems using a combination of zonotopes and polytopes. *Nonlinear Analysis: Hybrid Systems*, 4(2):233–249.

- Bara, G. I. (2011). Robust analysis and control of parameter-dependent uncertain descriptor systems. *Systems & Control Letters*, 60(5):356–364.
- Barmish, B. and Sankaran, J. (1979). The propagation of parametric uncertainty via polytopes. *IEEE Transactions on Automatic Control*, 24(2):346–349.
- Beck, A. and Teboulle, M. (2009). A fast iterative shrinkage-thresholding algorithm for linear inverse problems. *SIAM Journal on Imaging Sciences*, 2(1):183–202.
- Bemporad, A., Garulli, A., Paoletti, S., and Vicino, A. (2005). A bounded-error approach to piecewise affine system identification. *IEEE Transactions on Automatic Control*, 50(10):1567–1580.
- Ben Chabane, S. (2015). *Techniques de detection de défauts à base d'estimation d'état ensembliste pour systemes incertains*. PhD thesis, Thèse de doctorat Paris Saclay.
- Ben Chabane, S., Stoica Maniu, C., Alamo, T., Camacho, E., and Dumur, D. (2014.). A new approach for guaranteed ellipsoidal state estimation. In *Proc. of 19th IFAC World Congress*, pages 6533 – 6538, Cape Town, South Africa.
- Ben Chabane, S., Stoica Maniu, C., Alamo, T., Camacho, E. F., and Dumur, D. (2014a). Ellipsoidal state estimation for systems with interval uncertainties. In *Proc. of 53rd IEEE Conference on Decision and Control*, pages 2603–2608, Los Angeles, United States.
- Ben Chabane, S., Stoica Maniu, C., Alamo, T., Camacho, E. F., and Dumur, D. (2014b). Improved set-membership estimation approach based on zonotopes and ellipsoids. In *Proc. of European Control Conference*, pages 993–998, Strasbourg, France.
- Bender, D. and Laub, A. (1987). The linear-quadratic optimal regulator for descriptor systems. *IEEE Transactions on Automatic Control*, 32(8):672–688.
- Bertsekas, D. and Rhodes, I. (1971a). Recursive state estimation for a set-membership description of uncertainty. *IEEE Transactions on Automatic Control*, 16(2):117–128.
- Bertsekas, D. P. and Rhodes, I. B. (1971b). Recursive state estimation for a set-membership description of uncertainty. *IEEE Transaction on Automatic Control*, 16(2):117–128.

- Biegler, L. T., Campbell, S. L., and Mehrmann, V. (2012). *Control and optimization with differential-algebraic constraints*. SIAM.
- Boyd, S., El Ghaoui, L., Feron, E., and Balakrishnan, V. (1994). *Linear matrix inequalities in system and control theory*. SIAM.
- Boyd, S. and Vandenberghe, L. (2004). *Convex optimization*. Cambridge University Press, New York, NY, USA.
- Bravo, J. M., Alamo, T., and Camacho, E. F. (2006). Bounded error identification of systems with time-varying parameters. *IEEE Transactions on Automatic Control*, 51(7):1144–1150.
- Bronstein, E. M. (2008). Approximation of convex sets by polytopes. *Journal of Mathematical Sciences*, 153(6):727–762.
- Campbell, S. L., Nichols, N. K., and Terrell, W. J. (1991). Duality, observability, and controllability for linear time-varying descriptor systems. *Circuits, Systems and Signal Processing*, 10(4):455–470.
- Carrara, W., Goodman, R., and Majewski, R. (1995). *Spotlight synthetic aperture radar: signal processing algorithms*. Artech House Inc.
- Casbeer, D. W., Beard, R. W., McLain, T. W., Li, S.-M., and Mehra, R. K. (2005). Forest fire monitoring with multiple small UAVs. *In Proc. of American Control Conference*, pages 3530–3535.
- Cauchy, A. (1847). Méthode générale pour la résolution des systèmes d'équations simultanées. *Comp. Rend. Sci. Paris*, 25(1847):536–538.
- Chernousko, F. L. (1994). *State estimation for dynamic systems*. CRC Press, Boca Raton.
- Chevet, T., Makarov, M., Stoica Maniu, C., Hinostroza, I., and Tarascon, P. (2017). State estimation of an octorotor with unknown inputs. application to radar imaging. *In Proc. of 21st International Conference on System Theory, Control and Computing*, pages 723–728.
- Chisci, L., Garulli, A., and Zappa, G. (1996). Recursive state bounding by parallelotopes. *Automatica*, 32(7):1049–1055.
- Combastel, C. (2003). A state bounding observer based on zonotopes. *In Proc. of 2003 European Control Conference*, pages 2589–2594, Cambridge, United Kingdom.

- Combastel, C. (2006). A state bounding observer for uncertain non-linear continuous-time systems based on zonotopes. *In Proc. of the 44th Decision and Control, European Control Conference*, 2005:7228–7234.
- Combastel, C. (2015a). Merging Kalman filtering and zonotopic state bounding for robust fault detection under noisy environment. *IFAC-PapersOnLine*, 48(21):289–295.
- Combastel, C. (2015b). Zonotopes and Kalman observers: gain optimality under distinct uncertainty paradigms and robust convergence. *Automatica*, 55:265–273.
- Combastel, C., Zhang, Q., and Lalami, A. (2008). Fault diagnosis based on the enclosure of parameters estimated with an adaptive observer. *In Proc. of the 17th World Congress IFAC*, pages 7314–7319, Seoul, Korea.
- Dai, L. (1989). *Singular control systems*. Springer-Verlag, Berlin, Heidelberg.
- Dantzig, G. B. (1972). Fourier-Motzkin elimination and its dual. Technical report, DTIC document.
- Darouach, M. and Boutayeb, M. (1995). Design of observers for descriptor systems. *IEEE Transactions on Automatic Control*, 40(7):1323–1327.
- Daryin, A. N. and Kurzhanski, A. B. (2012). Estimation of reachability sets for large-scale uncertain systems: from theory to computation. *In Proceedings of 51st IEEE Conference on Decision and Control, Maui, Hawaii, USA*, pages 7401–7406.
- Daryin, A. N., Kurzhanski, A. B., and Vostrikov, I. V. (2006). Reachability approaches and ellipsoidal techniques for closed-loop control of oscillating systems under uncertainty. *In Proc. of 45th IEEE Conference on Decision and Control, San Diego, United States*, pages 6390–6395.
- De Marina, H. G., Pereda, F. J., Giron-Sierra, J. M., and Espinosa, F. (2011). UAV attitude estimation using unscented Kalman filter and TRIAD. *IEEE Transactions on Industrial Electronics*, 59(11):4465–4474.
- Durieu, C., Walter, E., and Polyak, B. (2001). Multi-Input Multi-Output ellipsoidal state bounding. *Journal of Optimization Theory and Applications*, 111(2):273–303.
- Efimov, D., Raïssi, T., Chebotarev, S., and Zolghadri, A. (2013). Interval state observer for nonlinear time varying systems. *Automatica*, 49(1):200–205.

- El Ghaoui, L. and Calafiore, G. (2001). Robust filtering for discrete time systems with bounded noise and parametric uncertainty. *IEEE Transactions on Automatic Control*, 46(7).
- Feng, G. (2002). Stability analysis of piecewise discrete-time linear systems. *IEEE Transactions on Automatic Control*, 47(7):1108–1112.
- Feng, G. (2003a). Controller synthesis of fuzzy dynamic systems based on piecewise Lyapunov functions and bilinear matrix inequalities. In *Proc. of the 12th IEEE International Conference on Fuzzy Systems*, volume 2, pages 1327–1332.
- Feng, G. (2003b). Observer-based output feedback controller design of piecewise discrete-time linear systems. *IEEE Transactions on Circuits and Systems I: Fundamental Theory and Applications*, 50(3):448–451.
- Feng, G. (2005). Robust filtering design of piecewise discrete time linear systems. *IEEE Transactions on signal processing*, 53(2):599–605.
- Ferrari-Trecate, G., Mignone, D., and Morari, M. (2002). Moving horizon estimation for hybrid systems. *IEEE Transactions on Automatic Control*, 47(10):1663–1676.
- Fletcher, R. (1976). Conjugate gradient methods for indefinite systems. In *Numerical analysis*, pages 73–89. Springer.
- Fogel, E. and Huang, Y. F. (1982). On the value of information in system identification-bounded noise case. *Automatica*, 18:229–238.
- Fukuda, K. (1997). cdd/cdd+ reference manual. *Institute for Operations Research, ETH-Zentrum*, pages 91–111.
- Fukuda, K. (2004). From the zonotope construction to the Minkowski addition of convex polytopes. *Journal of Symbolic Computation*, 38(4):1261–1272.
- Garcia, R. A., Raffo, G. V., Ortega, M. G., and Rubio, F. R. (2015). Guaranteed quadrotor position estimation based on GPS refreshing measurements. In *Proc. of IFAC Workshop on Advanced Control and Navigation for Autonomous Aerospace Vehicles*, 48(9):67–72.
- Gauss, C. F. (1857). *Theory of the motion of the heavenly bodies moving about the Sun in conic sections: A translation of Gauss's "Theoria Motus." with an Appendix*. Little, Brown and Company.

- Girard, A. (2005). Reachability of uncertain linear systems using zonotopes. In *Proc. of the International Workshop on Hybrid Systems: Computation and Control*, pages 291–305. Springer.
- Girard, A. and Le Guernic, C. (2008). Zonotope/hyperplane intersection for hybrid systems reachability analysis. In *International Workshop on Hybrid Systems: Computation and Control*, pages 215–228. Springer.
- Gonzalez-Partida, J.-T., Almorox-Gonzalez, P., Burgos-Garcia, M., and Dorta-Naranjo, B.-P. (2008). SAR system for UAV operation with motion error compensation beyond the resolution cell. *Sensors, vol. 8, no. 5*, pages 3384–3405.
- Grant, M. and Boyd, S. (2014). CVX: Matlab software for disciplined convex programming, version 2.1.
- Gritzmann, P. and Sturmfels, B. (1993). Minkowski addition of polytopes: Computational complexity and applications to Gröbner bases. *SIAM Journal on Discrete Mathematics*, 6(2):246–269.
- Grizzle, J. W. and Moraal, P. E. (1990). Observer based control of nonlinear discrete-time systems. In *Proc. of the 29th IEEE Conference on Decision and Control*, pages 760–767, Honolulu, USA.
- Guerra, P., Puig, V., and Witczak, M. (2008). Robust fault detection with unknown-input interval observers using zonotopes. In *Proc. of the 17th World Congress IFAC*, pages 5557–5562, Seoul, Korea.
- Guibas, L. J., Nguyen, A., and Zhang, L. (2005). Zonotopes as bounding volume. In *Proc. of the Symposium on Discrete Algorithm*, pages 803–812.
- Haar, A. (1924). *Über lineare ungleichungen*. A. M. Kir. Ferencz Jozsef Tudományegyetem Baratai Egyesületének.
- Han, Q.-L. (2004). A descriptor system approach to robust stability of uncertain neutral systems with discrete and distributed delays. *Automatica*, 40(10):1791–1796.
- Hansen, E. R. (1965). Interval arithmetic in matrix computations. *SIAM Journal on Numerical Analysis: Series B*, 2(2):308–320.
- Hassan, H., Barsoum, B., and Habib, I. (1999). Simultaneous spectrophotometric determination of rutin, quercetin and ascorbic acid in drugs using a Kalman filter approach. *Journal of Pharmaceutical and Biomedical Analysis*, 20(1):315 – 320.

- Hausamann, D., Zirnig, W., Schreier, G., and Strobl, P. (2005). Monitoring of gas pipelines – A civil UAV application. *Aircraft Engineering and Aerospace Technology*, 77(5):352–360.
- Heemels, W. P., De Schutter, B., and Bemporad, A. (2001). Equivalence of hybrid dynamical models. *Automatica*, 37(7):1085–1091.
- Herceg, M., Kvasnica, M., Jones, C., and Morari, M. (2013). Multi-Parametric Toolbox 3.0. In *Proc. of the European Control Conference*, pages 502–510, Zürich, Switzerland.
- Hill, D. J. and Mareels, I. M. (1990). Stability theory for differential/algebraic systems with application to power systems. *IEEE Transactions on Circuits and Systems*, 37(11):1416–1423.
- Hoshino, M., Gunji, Y., Oho, S., and Takano, K. (1996). A Kalman filter to estimate direction for automotive navigation. In *IEEE/SICE/RSJ International Conference on Multisensor Fusion and Integration for Intelligent Systems*, pages 145–150.
- Hou, M. and Muller, P. C. (1995). Design of a class of Luenberger observers for descriptor systems. *IEEE Transactions on Automatic Control*, 40(1):133–136.
- Hu, T. and Lin, Z. (2003). Composite quadratic Lyapunov functions for constrained control systems. *IEEE Transaction on Automatic Control*, 48:440–450.
- Ingimundarson, A., Bravo, J. M., Puig, V., Alamo, T., and Guerra, P. (2008). Robust fault detection using zonotope-based set-membership consistency. *International journal of Adaptive Control and Signal Processing*, 23(4):311–330.
- Ishihara, J. Y., Terra, M. H., and Campos, J. C. (2006). Robust Kalman filter for descriptor systems. *IEEE Transactions on Automatic Control*, 51(8):1354–1354.
- Jaulin, L., Kieffer, M., Didrit, O., and Walter, E. (2001). *Interval analysis*. Springer.
- Johansson, M. and Rantzer, A. (1997). Computation of piecewise quadratic Lyapunov functions for hybrid systems. In *Proc. of the European Control Conference*, pages 2005–2010.

-
- Johansson, M. K.-J. (2003). *Piecewise linear control systems: a computational approach*, volume 284. Springer.
- Julier, S. J. and LaViola, J. J. (2007). On Kalman filtering with nonlinear equality constraints. *IEEE Transactions on Signal Processing*, 55(6):2774–2784.
- Juloski, A. L., Heemels, W., and Weiland, S. (2002). Observer design for a class of piece-wise affine systems. In *Proc. of the 41st IEEE Conference on Decision and Control*, volume 3, pages 2606–2611, Las Vegas, NV, USA.
- Juloski, A. L., Heemels, W. P. M. H., Boers, Y., and Verschure, F. (2003). Two approaches to state estimation for a class of piecewise affine systems. In *Proc. of the 42nd IEEE International Conference on Decision and Control*, pages 143–148 Vol.1.
- Kada, B., Munawar, K., Shaikh, M., Hussaini, M., and Al-Saggaf, U. (2016). UAV attitude estimation using nonlinear filtering and low-cost mems sensors. In *Proc. of the 7th IFAC Symposium on Mechatronic Systems*, 49:521–528.
- Kalman, E. R. (1955). Phase-plane analysis of automatic control systems with nonlinear gain elements. *Transactions of the American Institute of Electrical Engineers, Part II: Applications and Industry*, 73(6):383–390.
- Kalman, R. E. (1960). A new approach to linear filtering and prediction problems. *Transactions of the ASME—Journal of Basic Engineering*, 82(Series D):35–45.
- Kalman, R. E. and Bucy, R. S. (1961). New results in linear filtering and prediction theory. *Transactions of the ASME, Ser. D, J. Basic Eng*, page 109.
- Kingston, D. and Beard, R. (2004). Real-time attitude and position estimation for small UAVs using low-cost sensors. In *Proc. of the AIAA 3rd Unmanned Unlimited Technical Conference, Workshop and Exhibit*, page 6488.
- Koenig, D., Marx, B., and Jacquet, D. (2008). Unknown input observers for switched nonlinear discrete time descriptor systems. *IEEE Transactions on Automatic Control*, 53(1):373.
- Koustousova, E. K. (2011). State estimation for control systems with a multiplicative uncertainty through polyhedral techniques. In *Proc. of the*

- IFIP Conference on System Modeling and Optimization*, pages 165–176. Springer.
- Kočvara, M. and Stingl, S. (2003). PENNON: A code for convex nonlinear and semidefinite programming. *Optimization methods and software*, 18(3):317–333.
- Kühn, W. (1998). Rigorously computed orbits of dynamical systems without the wrapping effect. *Computing*, 61:47–67.
- Kurzhanski, A. B. and Vályi, I. (1996). *Ellipsoidal calculus for estimation and control*. Birkhäuser Boston.
- Kurzhanskiy, A. A. and Varaiya, P. (2006-2007). Ellipsoidal toolbox manual.
- Laliberte, A. S. and Rango, A. (2009). Texture and scale in object-based analysis of subdecimeter resolution unmanned aerial vehicle (UAV) imagery. *IEEE Transactions on Geoscience and Remote Sensing*, 47(3):761–770.
- Le, V. T. H. (2012). *Commande prédictive robuste par des techniques d’observateurs à base d’ensembles zonotopiques*. PhD thesis, Supélec, France.
- Le, V. T. H., Alamo, T., Camacho, E. F., Stoica, C., and Dumur, D. (2011). A new approach for guaranteed state estimation by zonotopes. In *Proc. the 18th World Congress IFAC*, pages 9242–9247, Milan, Italy.
- Le, V. T. H., Stoica, C., Alamo, T., Camacho, E. F., and Dumur, D. (2013a). *Zonotopes: From guaranteed state-estimation to control*. John Wiley & Sons.
- Le, V. T. H., Stoica, C., Alamo, T., Camacho, E. F., and Dumur, D. (2013b). Zonotopic guaranteed state estimation for uncertain systems. *Automatica*, 49(1):3418–3424.
- Lewis, F. (1985). Fundamental, reachability, and observability matrices for discrete descriptor systems. *IEEE Transactions on automatic control*, 30(5):502–505.
- Liu, P., Zhang, Q., Yang, X., and Yang, L. (2008). Passivity and optimal control of descriptor biological complex systems. *IEEE Transactions on Automatic Control*, 53:122–125.

-
- Lofberg, J. (2004). YALMIP: a toolbox for modeling and optimization in Matlab. In *Proc. of the IEEE International Conference on Robotics and Automation*, pages 284–289, New Orleans, United States.
- Luenberger, D. (1977). Dynamic equations in descriptor form. *IEEE Transactions on Automatic Control*, 22(3):312–321.
- Luenberger, D. G. (1964). Observing the state of a linear system. *IEEE Transactions on Military Electronics*, 8:74 – 80.
- M. Althoff, O. S. and Buss, M. (2010). Computing reachable sets of hybrid systems using a combination of zonotopes and polytopes. *Nonlinear Analysis: Hybrid Systems*, 4(2):233–249.
- Makarov, M., Stoica Maniu, C., Tebbani, S., and Hinostroza, I. (2016). In proc. of the control design for an octorotor for radar applications, Lacanau, France. *SONDRA 4th Workshop*.
- Makarov, M., Stoica Maniu, C., Tebbani, S., Hinostroza, I., Beltrami, M. M., Kienitz, J., Menegazzi, R., Moreno, C. S., Rocheron, T., and Lombarte, J. R. (2015). Octorotor UAVs for radar applications: modeling and analysis for control design. In *Proc. of the Workshop on Research, Education and Development of Unmanned Aerial Systems, Cancun, Mexico*.
- Manoliu, M. and Tompaidis, S. (2002). Energy futures prices: term structure models with Kalman filter estimation. *Applied Mathematical Finance*, 9(1):21–43.
- Mare, J. B. and De Dona, J. A. (2006). Moving horizon estimation of constrained nonlinear systems by carleman approximations. In *Proc. of the 45th IEEE Conference on Decision and Control*, pages 2147–2152, San Diego, USA.
- McElhoe, B. A. (1966). An assessment of the navigation and course corrections for a manned flyby of Mars or Venus. *IEEE Transactions on Aerospace and Electronic Systems*, AES-2(4):613–623.
- McShane, K. A., Monma, C. L., and Shanno, D. (1989). An implementation of a primal-dual interior point method for linear programming. *ORSA Journal on Computing*, 1(2):70–83.
- Meslem, N., Ramdani, N., and Candau, Y. (2010). Using hybrid automata for set-membership state estimation with uncertain nonlinear continuous-time systems. *Journal of Process Control*, 20(4):481–489.

- Michalska, H. and Mayne, D. Q. (1991). Moving horizon observers. In *Proc. of the IFAC Symposium Nonlinear Control System Design*, pages 576–581, Bordeaux, France.
- Moore, J. B. and Ledwich, G. F. (1975). Minimal order observers for estimating linear functions of a state vector. *IEEE Transactions on Automatic Control*, 20(5):623–632.
- Moore, R. E. (1966). *Interval analysis*, volume 4. Prentice-Hall Englewood Cliffs, NJ.
- Moore, R. E. (1979). *Methods and applications of interval analysis*. SIAM.
- Moreira, A., Prats-Iraola, P., Younis, M., Krieger, G., Hajnesk, I., and Papathanassiou, K. P. (2013). A tutorial on synthetic aperture radar. *IEEE Geoscience and Remote Sensing Magazine*, pages 6–43.
- Murdoch, P. (1973). Observer design for a linear functional of the state vector. *IEEE Transactions on Automatic Control*, 18(3):308–310.
- Nesterov, Y. (1983). A method for unconstrained convex minimization problem with the rate of convergence $O(1/k^2)$. *Doklady AN USSR*, 269:543–547.
- Nesterov, Y. (2005). Smooth minimization of non-smooth functions. *Mathematical Programming*, 103(1):127–152.
- Nesterov, Y. (2013). Gradient methods for minimizing composite functions. *Mathematical Programming*, 140(1):125–161.
- Nesterov, Y. (2018). *Lectures on convex optimization*, volume 137. Springer.
- Nesterov, Y. and Nemirovski, A. (1994). Interior point polynomial methods in convex programming: Theory and applications. *Society for Industrial and Applied Mathematics*.
- Nex, F. and Remondino, F. (2014). UAV for 3D mapping applications: A review. *Applied Geomatics*, 6(1):1–15.
- Nikoukhah, R., Campbell, S. L., and Delebecque, F. (1999). Kalman filtering for general discrete-time linear systems. *IEEE Transactions on Automatic Control*, 44(10):1829–1839.
- Nikoukhah, R., Willsky, A. S., and Levy, B. C. (1992). Kalman filtering and Riccati equations for descriptor systems. *IEEE Transactions on Automatic Control*, 37(9):1325–1342.

- Norton, J. (1987). Identification and application of bounded-parameter models. *Automatica*, 23(4):497 – 507.
- Panier, E. R. (1987). An active set method for solving linearly constrained nonsmooth optimization problems. *Mathematical Programming*, 37(3):269–292.
- Petre, E., Tebbani, S., and Selişteanu, D. (2015). Robust-adaptive control strategies for a time delay bioelectrochemical process using interval observers. *Asian Journal of Control*, 17(5):1767–1778.
- Polyak, B., Nazin, S. A., Durieu, C., and Walter, E. (2004). Ellipsoidal parameter or state estimation under model uncertainty. *Automatica*, 40:1171–1179.
- Porrill, J. (1988). Optimal combination and constraints for geometrical sensor data. *International Journal of Robotics Research*, 7(6):66–77.
- Pourasghar, M., Puig, V., and Ocampo-Martinez, C. (2016). Comparison of set-membership and interval observer approaches for state estimation of uncertain systems. In *Proc. of the European Control Conference*, pages 1111–1116, Aalborg, Denmark.
- Puig, V., Cugueró, P., and Quevedo, J. (2001). Worst-case estimation and simulation of uncertain discrete-time systems using zonotopes. In *Proc. of the European Control Conference*, Porto, Portugal.
- Quintana, V., Scott, B., and Chikhani, A. (1987). Constrained power system state estimation. *10th IFAC Triennial World Congress on Automatic Control, Germany*, 20:7–12.
- Raïssi, T., Efimov, D., and Zolghadri, A. (2011). Interval state estimation for a class of nonlinear systems. *IEEE Transactions on Automatic Control*, 57(1):260–265.
- Rakovic, S. and Mayne, D. (2004). State estimation for piecewise affine, discrete time systems with bounded disturbances. In *Proc. of the 43rd IEEE Conference on Decision and Control, Nassau, Bahamas*, 4:3557–3562.
- Rakovic, S. V., Grieder, P., Kvasnica, M., Mayne, D. Q., and Morari, M. (2004). Computation of invariant sets for piecewise affine discrete time systems subject to bounded disturbances. In *Proc. of the 43rd IEEE Conference on Decision and Control, Nassau, Bahamas*, 2:1418–1423 Vol.2.

- Ramdani, N., Meslem, N., and Candau, Y. (2009). A hybrid bounding method for computing an over-approximation for the reachable set of uncertain nonlinear systems. *IEEE Transactions on Automatic Control*, 54(10):2352–2364.
- Reis, T. (2010). Circuit synthesis of passive descriptor systems—a modified nodal approach. *International Journal of Circuit Theory and Applications*, 38(1):44–68.
- Richter, S., Jones, C. N., and Morari, M. (2012). Computational complexity certification for real-time MPC with input constraints based on the fast gradient method. *IEEE Transactions on Automatic Control*, 57(6):1391–1403.
- Rodrigues, L. and How, J. P. (2003). Observer-based control of piecewise-affine systems. *International Journal of Control*, 76(5):459–477.
- Salameh, J. P., Cauet, S., Etien, E., Sakout, A., and Rambault, L. (2018). Enhanced Kalman filter through modified empirical mode decomposition for wind profile exogenous disturbance extraction isolation in wind turbines. In *Proc. of the 7th International Conference on Systems and Control (ICSC)*, pages 51–58.
- Scherer, C. S. and Weiland, S. (2007). Linear matrix inequalities in control.
- Schmidt, S. F. (1966). Application of state-space methods to navigation problems. *Advances in Control Systems*, 3:293–340.
- Schön, S. and Kutterer, H. (2005). Using zonotopes for overestimation-free interval least-squares-some geodetic applications. *Reliable Computing Springer*, 11:137–155.
- Schweppe, F. (1968). Recursive state estimation: Unknown but bounded errors and system inputs. *IEEE Transactions on Automatic Control*, 13(1):22–28.
- Scott, J. K., Raimondo, D. M., Marseglia, G. R., and Braatz, R. D. (2016). Constrained zonotopes. *Automatica*, 69(C):126–136.
- Seymour, P. (1994). A note on hyperplane generation. *Journal of Combinatorial Theory, Series B*, 61(1):88–91.
- Shields, D. N. (1997). Observer design and detection for nonlinear descriptor systems. *International Journal of Control*, 67(2):153–168.

-
- Shimada, N., Shirai, Y., Kuno, Y., and Miura, J. (1998). Hand gesture estimation and model refinement using monocular camera-ambiguity limitation by inequality constraints. In *Proc. of the 3rd IEEE International Conference on Automatic Face and Gesture Recognition*, pages 268–273.
- Simon, D. (2010). Kalman filtering with state constraints: a survey of linear and nonlinear algorithms. *IET Control Theory Applications*, 4(8):1303–1318.
- Simon, D. and Chia, T. L. (2002). Kalman filtering with state equality constraints. *IEEE Transactions on Aerospace and Electronic Systems*, 38(1):128–136.
- Simon, D. and Simon, D. L. (2010). Constrained Kalman filtering via density function truncation for turbofan engine health estimation. *International Journal of Systems Science*, 41(2):159–171.
- Smith, G. L. and Schmidt, S. F. (1961). The application of statistical filter theory to optimal trajectory determination onboard a circumlunar vehicle. In *AAS meeting*.
- Sorenson, H. W. (1970). Least-squares estimation: from Gauss to Kalman. *IEEE Spectrum Magazine*, 7(7):63–68.
- Stevens, B. L., Lewis, F. L., and Johnson, E. N. (2015). *Aircraft control and simulation: dynamics, controls design, and autonomous systems*. John Wiley & Sons.
- Stoican, F. (2011). *Fault tolerant control based on set-theoretic methods*. PhD thesis, Université de Paris Sud-Supélec.
- Tabatabaeipour, S. M. and Stoustrup, J. (2013). Set-membership state estimation for discrete time piecewise affine systems using zonotopes. In *Proc. of the European Control Conference*, pages 3143–3148, Zurich, Switzerland.
- Teixeira, B. O., Tôrres, L. A., Iscold, P., and Aguirre, L. A. (2011). Flight path reconstruction—A comparison of nonlinear Kalman filter and smoother algorithms. *Aerospace Science and Technology*, 15(1):60–71.
- Thuan, L. Q. and Camlibel, M. K. (2014). On the existence, uniqueness and nature of Carathéodory and Filippov solutions for bimodal piecewise affine dynamical systems. *Systems & Control Letters*, 68:76–85.
- Vandenberghe, L. and Boyd, S. (1994). Positive definite programming. *Mathematical Programming: State of the Art*, pages 276–308.

- Varga, A. (1995). On stabilization methods of descriptor systems. *Systems and Control Letters*, 24(2):133–138.
- Varga, A. (2000). A descriptor systems toolbox for MATLAB. In *Proc of the IEEE International Symposium on Computer-Aided Control System Design*, pages 150–155.
- Varga, A. (2017). *Solving Fault Diagnosis Problems - Linear Synthesis Techniques*. Springer.
- Walter, E. and Piet-Lahanier, H. (1989). Exact recursive polyhedral description of the feasible parameter set for bounded-error models. *IEEE Transaction on Automatic Control*, 34(8):911–915.
- Wan, E. A. and Merwe, R. V. D. (2000). The unscented Kalman filter for nonlinear estimation. In *Proc. of the IEEE Adaptive Systems for Signal Processing, Communications, and Control Symposium*, pages 153–158.
- Wang, Y. and Puig, V. (2016). Zonotopic extended Kalman filter and fault detection of discrete-time nonlinear systems applied to a quadrotor helicopter. In *Proc. of the 3rd Conference on Control and Fault-Tolerant Systems, Barcelona, Spain*, pages 367–372.
- Wang, Y., Puig, V., and Cembrano, G. (2018). Set-membership approach and Kalman observer based on zonotopes for discrete-time descriptor systems. *Automatica*, 93:435–443.
- Wang, Y., Puig, V., Cembrano, G., and Alamo, T. (2016). Guaranteed state estimation and fault detection based on zonotopes for differential-algebraic-equation systems. In *Proc. of the 3rd Conference on Control and Fault-Tolerant Systems, Barcelona, Spain*, pages 478–484.
- Wang, Z., Shen, Y., Zhang, X., and Wang, Q. (2012). Observer design for discrete-time descriptor systems: an LMI approach. *Systems & Control Letters*, 61(6):683–687.
- Wen, W. and Durrant-Whyte, H. F. (1992). Model-based multi-sensor data fusion. In *IEEE International Conference on Robotics and Automation*, pages 1720–1726 vol.2.
- Witsenhausen, S. H. (1968). Sets of possible states of linear systems given perturbed observations. *IEEE Transactions on Automatic Control*, 13:556–558.

- Wu, L., Shi, P., and Gao, H. (2010). State estimation and sliding-mode control of markovian jump singular systems. *IEEE Transactions on Automatic Control*, 55(5):1213–1219.
- Xu, J. and Xie, L. (2014). *Control and estimation of piecewise affine systems*. Elsevier.
- Yan, J., Guo, J., Wang, Q. L. K., and Liu, X. (2008). X-band mini SAR radar on eight-rotor mini-UAV. *In Proc. of the IEEE Geoscience and Remote Sensing Symposium*, pages 6702–6705.
- Yip, E. and Sincovec, R. (1981). Solvability, controllability, and observability of continuous descriptor systems. *IEEE Transactions on Automatic Control*, 26(3):702–707.
- Zaugg, E., Hudson, D., and Long, D. (2006). The BYU SAR: A small, student-built SAR for UAV operation. *In Proc. of the IEEE Geoscience and Remote Sensing Symposium, Denver, Colorado, USA*, pages 411–414.
- Ziegler, G. M. (1995). *Lecture on polytopes*. Springer.

Titre : Contribution à l'estimation d'état par méthodes ensemblistes ellipsoïdales et zonotopiques

Mots clés : Estimation d'état ensembliste, inégalité matricielle linéaire, ellipsoïdes, zonotopes.

Résumé : Dans le contexte des systèmes dynamiques, cette thèse développe des techniques d'estimation d'état ensemblistes pour différentes classes de systèmes. On considère pour cela le cas d'un système standard linéaire invariant dans le temps soumis à des perturbations, des bruits de mesure et des incertitudes inconnus, mais bornés.

Dans une première étape, une technique d'estimation d'état ellipsoïdale est étendue, puis appliquée sur un modèle d'ocrotor utilisé dans un contexte radar. Une extension de cette approche ellipsoïdale d'estimation d'état est proposée pour des systèmes descripteurs.

Dans la deuxième partie, nous proposons une

méthode fondée sur la minimisation du \mathbf{P} -rayon d'un zonotope, appliquée à un modèle d'ocrotor. Cette méthode est ensuite étendue pour traiter un cas particulier de systèmes affines par morceaux.

Dans la continuité des approches précédentes, un nouveau filtre de Kalman sous contraintes zonotopiques est proposé dans la dernière partie de cette thèse. En utilisant la forme duale d'un problème d'optimisation, l'algorithme projette l'état sur un zonotope qui forme l'enveloppe de l'ensemble des contraintes auxquelles l'état est soumis. La complexité de l'algorithme est ensuite améliorée en remplaçant le zonotope initial par une forme réduite en limitant son nombre de générateurs.

Title: Contribution to ellipsoidal and zonotopic set-membership state estimation

Keywords: Set-membership state estimation, linear matrix inequality, ellipsoids, zonotopes.

Abstract: In the context of dynamical systems, this thesis focuses on the development of robust set-membership state estimation procedures for different classes of systems. We consider the case of standard linear time-invariant systems, subject to unknown but bounded perturbations and measurement noises.

The first part of this thesis builds upon previous results on ellipsoidal set-membership approaches. An extended ellipsoidal set-membership state estimation technique is applied to a model of an octorotor used for radar applications. Then, an extension of this ellipsoidal state estimation approach is proposed for descriptor systems. In the second part, we pro-

pose a state estimation technique based on the minimization of the \mathbf{P} -radius of a zonotope, applied to the same model of the octorotor. This approach is further extended to deal with a particular class of piecewise affine systems.

In the continuity of the previous approaches, a new zonotopic constrained Kalman filter is proposed in the last part of this thesis. By solving a dual form of an optimization problem, the algorithm projects the state on a zonotope forming the envelope of the set of constraints that the state is subject to. Then, the computational complexity of the algorithm is improved by replacing the original possibly large-scale zonotope with a reduced form, by limiting its number of generators.



